Defining a small molecules differentiation cocktail for generation of Dopaminergic Neurons from Wharton's Jelly Mesenchymal Stem Cells

A dissertation presented to the Faculty of Medicine and Surgery in part fulfilment of the requirements for the degree of Master of Science in Biochemistry at the University of Malta

Supervisor: Dr Byron Baron

Deborah Warrington

21/09/2022

ACKNOWLEDGMENTS

First of all, I would like to thank the University of Malta and the Department of Medicine and Surgery for enabling students in Malta to further their knowledge and gain proficiency in their field.

I would like to thank Prof. Richard Muscat for permitting me to conduct this study at the Centre of Molecular Medicine and Biobanking, and Prof. Anthony Fenech for consenting the use of the laboratories of the Department of Clinical Pharmacology and Therapeutics for the duration of this project.

Furthermore, I would like to thank the Endeavour Scholarship Scheme (Malta) for the funding awarded for this study.

I would like to express my deep gratitude for the support and guidance given to me by my supervisor Dr Byron Baron, as well as Dr Vanessa Zammit, and Isaac Micallef, throughout this research project. Finally, I would like to thank those closest to me for their ongoing support.

The research work disclosed in this publication is partially funded by the Endeavour Scholarship Scheme (Malta). Scholarships are part-financed by the European Union - European Social Fund (ESF) - Operational Programme II – Cohesion Policy 2014-2020 “Investing in human capital to create more opportunities and promote the well-being of society”.

Operational Programme II - European Structural and Investment Funds 2014-2020
“Investing in human capital to create more opportunities and promote the well-being of society”
Project part-financed by the European Social Fund
Co-financing rate: 80% European Union; 20% National Funds

ABSTRACT

The incidence of neurodegenerative diseases is on the rise, and yet patients remain without a cure. A suitable disease model could be applied for drug development, disease progression modelling and regenerative therapy. The study's primary aim was to define a fully-characterised dopaminergic neuronal transdifferentiation protocol for research and therapeutic purposes, with the principal objective being the treatment of Mesenchymal Stem Cells (MSCs) with a 3-stage small molecule strategy. Using RT-qPCR, RNA transcript levels for neural markers were assessed in differentiating cells. Changes in protein lysine and arginine methylation and dopamine-release in differentiating cells were explored using Western blotting, and ELISA respectively. Changes in cell structure towards a neuronal morphology and neurite outgrowth increased considerably with each stage of differentiation. RNA transcript levels suggested that Stage 2 cells had differentiated into immature neuronal cells. Substantial changes in protein methylation levels of cells at different treatment stages were found, and dopamine release increased in Stages 2- and 3-treated cells. ELISA results suggest that the protocol was successful at specifying a dopaminergic fate, though the cells might require further maturation in culture. Mass Spectrometry results revealed hundreds of unique proteins between MSCs and Stage 3 induced neurons, with expression of many neuron-associated proteins in the final neuronal cells. More experiments are required to conclude on the cellular differentiation extent achieved, cell fate, and functionality, and to fully optimise the

Operational Programme II - European Structural and Investment Funds 2014-2020
"Investing in human capital to create more opportunities and promote the well-being of society"
Project part-financed by the European Social Fund
Co-financing rate: 80% European Union; 20% National Funds

protocol for dopaminergic differentiation of MSCs. The results produced in this study reveal the potential of this research and warrant the study's further investigation.

Word count: 250 words

Keywords: Mesenchymal Stem Cells, Dopaminergic neurons, Reprogramming and Transdifferentiation strategy, small molecules, Parkinson's disease.

Operational Programme II - European Structural and Investment Funds 2014-2020
"Investing in human capital to create more opportunities and promote the well-being of society"
Project part-financed by the European Social Fund
Co-financing rate: 80% European Union; 20% National Funds

TABLE OF CONTENTS

LIST OF TABLES

LIST OF FIGURES

LIST OF ABBREVIATIONS

The following abbreviations have been used within this dissertation:

5-HT – serotonin,

ACN – Acetonitrile,

AD – Alzheimer's disease,

ADHD – Attention-deficit hyperactivity disorder,

ANOVA - analysis of variance,

APS - ammonium persulfate,

ASCL or MASH1– achaete-scute family bHLH transcription factor 1,

AT - adipose tissue,

ATP – adenosine triphosphate,

BDNF – brain derived neurotrophic factor,

bFGF – fibroblast growth factor basic,

bHLH – basic helix-loop-helix,

BLBP – brain lipid binding protein,

BMP – bone morphogenetic protein,

BMP4 – bone morphogenetic protein 4,

BMPRI/IIs - BMP receptors type I and II,

BSA – Bovine serum albumin,

cAMP – cyclic adenosine monophosphate,

CD – cluster of differentiation,

cDNA – complimentary DNA,

CM – Conditioned media,

CPP - cryo poor plasma,

CREB - cAMP response element binding protein,

CYCA – cyclin A,

DA – dopaminergic,

DAPT - [N-(3,5-Difluorophenacetyl)-L-alanyl]-S-phenylglycine t-butyl ester,

DAT - dopamine transporter,

db-cAMP - dibutyryl cyclic-AMP,

DMEM - Dulbecco's Modified Eagle Medium,

DMSO - Dimethyl Sulfoxide,

DNA – deoxyribonucleic acid,

DTT - 1,4-Dithio-DL-thriethol,

ECM - extracellular matrix,

EDTA - Ethylenediaminetetraacetic acid disodium salt dyhydrate,

ELISA - Enzyme-linked immunosorbent assay,

ERK1/2 - extracellular signal-regulated kinase,

FGF4/8 – fibroblast growth factor 4 and 8,

FGF8 – fibroblast growth factor 8,

FOXA1/2 - forkhead box A 1/2,

FP – floor plate,

FSK – Forskolin,

GAPDH – glyceraldehyde-3-phosphate dehydrogenase,

GDNF – Glial cell line derived neurotrophic factor,

GFAP – glial fibrillary acidic protein,

GFLs - GDNF family ligands,

GFR- GDNF Family Receptor,

GFRα - GDNF Family Receptor alpha,

GSK-3β - glycogen synthetase kinase-3β,

H – histone,

HDMs - histone demethylases,

HMTs - histone methyltransferases,

IAA – Iodoacetamide,

IPCs – intermediate progenitor cells,

iPSCs - induced pluripotent stem cells,

K – lysine,

LEF/TCF - lymphoid enhancer-binding factor 1/T cell-specific transcription factor,

LMX1A/B - LIM homeobox transcription factor 1 alpha/beta,

LSD1 - Lysine-specific demethylase 1,

LUHMES - Lund Human Mesencephalic,

MAML - Mastermind-like,

MAPK - mitogen-activated protein kinase,

mDA – midbrain dopaminergic,

MLC - myosin light chain,

MS - Mass spectrometry,

MSCs – mesenchymal stem cells,

NECs – neuroepithelial cells,

NeuN – Neuronal nuclei,

NEUROD1 – neuronal differentiation 1,

NGF - nerve growth factor,

NGN2 – neurgenin 2,

NICD - Notch intracellular domain,

NPCs – neural progenitor cells,

NSCs – neural stem cells,

NTC – no template control,

NTFs – neurotrophic factors,

NTs – neurotrophins,

NURR1 - nuclear receptor subfamily 4 group A member 2,

OTX2 – orthodenticle homeobox 2,

p75NTR – p75 neurotrophin receptor,

PAGE – Polyacrylamide Gel Electrophoresis

PBS - Phosphate Buffered Saline,

PcG – Polycomb-group,

PD – Parkinson's disease,

PI3K/AKT - phosphoinositide-3-kinase/protein kinase B,

PITX3 - paired-like homeodomain 3,

PKA - protein kinase A,

PLCγ - phospholipase C gamma,

PPIA - Peptidylprolyl Isomerase A,

PSD95 – postsynaptic density protein 95,

Ptc – patched,

PTM - post-translational modification,

RA – retinoic acid,

RGCs – radial glial cells,

RNA – Ribonucleic Acid,

ROCK - Rho-associated kinase,

RPL13A - Ribosomal Protein L13a,

RPLP0 - Ribosomal Protein Lateral Stalk Subunit P0,

RT - room temperature,

RTKs - Receptor Tyrosine Kinases,

RT-qPCR – Reverse transcription quantitative Polymerase Chain Reaction,

SDS - Sodium Dodecyl Sulphate,

SGZ – subgranular zone,

SHH – sonic hedgehog,

SM1/2/3 – small molecules stages 1, 2, and 3,

Smo – smoothened,

SN – Substantia Nigra,

SNc – Substantia Nigra pars compacta,

STAT3 - signal transducer and activator of transcription 3,

SVZ – subventricular zone,

TAE - Tris-acetate-EDTA,

TBS - tris buffered saline,

TFA - Trifluoroacetic Acid,

TFs – transcription factors,

TGF-β - transforming growth factor beta,

TH – tyrosine hydroxylase,

Tm - melting temperatures,

TrxG – Trithorax-group,

UC – umbilical cord,

USCs - urine-derived stem cells ,

VMAT2 - vesicular monoamine transporter 2

VTA – ventral tegmental area,

VZ – ventricular zone,

WJ - Wharton's jelly,

WJ-MSCs – Wharton's jelly mesenchymal stem cells,

WNT – wingless.

Chapter 1 Literature Review

1.1. Dopaminergic neuron dysfunction and current treatments

Disorders of protein homeostasis with characteristic loss of neuronal structure and function result in paralysis, diminished cognition and sensation (Sivandzade & Cucullo, 2021). This pathology occurs in several neurodegenerative diseases, such as Parkinson's disease (PD), Alzhemier's disease (AD), Amyotrophic Lateral Sclerosis and Huntington's disease (HD).

There are 4 main dopaminergic (DA) networks within the brain that are salient in many cognitive, behavioural, and physiological process in humans. These include: the nigrostriatal pathway, whose degeneration is involved in PD; the mesolimbic pathway that is mostly involved in reward processing; the mesocortical network, involved in cognitive function and motivation; and the tuberofundibular pathway mainly involved in neuroendocrine regulation (Botticelli *et al.*, 2020). Changes occurring in brain circuits in which dopamine plays a central role as well as an imbalance in dopamine neurotransmission have been implicated in many neurological and neuropsychiatric diseases (Franco, Reyes-Resina & Navarro, 2021) such as drug addiction (Le Foll *et al.*, 2009; Botticelli *et al.*,2020;) and schizophrenia (Sonnenchein, Gomes & Grace, 2020; Brisch *et al.*, 2014).

PD is one of the most common chronic neurodegenerative disorders (Gordon *et al.*, 2022), affecting around 2-3% of people above age 60 (Mao *et al.*, 2021). It is defined by tremor, rigidity, bradykinesia and cognitive impairment (Karimi *et al.*, 2021). This malady is pathologically characterised by the progressive loss of DA neurons in the substantia nigra pars compacta (SNc) and the accumulation of α-synuclein-enriched intraneuronal aggregates known as Lewy bodies (Mao *et al.*, 2020). Loss of DA neurons results in decreased striatal dopamine production which brings about PD motor

symptoms, which present in such patients once they have already lost around 60% of SNc DA neurons (Mao *et al.,* 2020). At later stages of PD progression, nondopaminergic brain regions are also affected resulting in nonmotor symptoms including psychiatric symptoms, and dementia.

Although current treatments are able to manage disease symptoms and thus improve the quality of life of affected individuals for some time, such treatments are not able to stop disease progression (Mao *et al.,* 2020). Pharmaceutical treatments mainly involve the use of dopamine medications, such as Levodopa (Karimi *et al.,* 2021). This treatment functions to compensate for the lack of dopamine by enhancing its synthesis in midbrain DA neurons (Iarkov *et al.,* 2020). Their long-term use brings about adverse effects including aggravation of dyskinesia, drug resistance (Karimi *et al.,* 2021), and psychiatric problems (Iarkov *et al.,* 2020). Despite these side-effects and their inability to stop disease progression, L-DOPA is still the gold standard medication for PD after around 60 years (Iarkov *et al.,* 2020). Deep brain stimulation (DBS) is an alternative surgical approach presently used to treat PD patients (Karimi *et al.,* 2021). In DBS, the subthalamic nucleus and globus pallidus are stimulated with implanted electrodes. DBS is an expensive treatment and is associated with several risks, such as infection from the implanted device. Importantly, such surgical or pharmaceutical treatment strategies only temporarily manage the symptoms and do not target the underlying cause or diminish neuronal cell loss (Karimi *et al.,* 2021).

The significantly diminished quality of life of affected individuals and the curative inadequacy of current treatments for neurodegenerative disorders brings about a substantial burden on society and an increasingly high economic impact (Sivandzade & Cucullo, 2021). The fact that these diseases have complex physiological causes and mechanisms of ongoing neuronal loss, has hampered insight into their pathogenic

processes and thus the development of effective treatments. Furthermore, the limited regenerative capacity of the central nervous system (CNS) and the restricted ability of drugs to cross the blood-brain-barrier further compounds the issue.

An innovative approach to treatment of such diseases is regenerative (or stem) cell therapy. This therapy aims to ameliorate the repair response of dysfunctional or damaged neural tissue through the use of stem cells (Sivandzade & Cucullo, 2021). This approach is based on replacing lost or damaged cells or by providing an enriched and ideal environment that favours regeneration or protects existing healthy neurons and glial cells from injury (Sivandzade & Cucullo, 2021).

Many candidate drug treatments fail during the last steps of human clinical trials (Pandey *et al.*, 2022). A reason for this may be that animal disease models are not ideal predictors of human pathology, and their use has hampered scientific progress in producing new therapeutic drug treatments. Consequently, there is a great need for development of a suitable and accurate disease model for pre-clinical testing (Pandey *et al.*, 2022). DA neuronal cells produced from patient stem cells may be applied for precision medicine, so that a patient's genome and PD subtypes can be studied, and treatment can be tailored to patient disease aetiology (Iarkov *et al.*, 2020). Thus, induced neuronal cells may also be applied as an *ex vivo* disease model, to study disease aetiology and progression, and for drug screening and assessment (Nolbrant *et al.*, 2017).

1.2. Stem cells

Stem cells are cells within the body that are in an unspecialised state, and thus may differentiate into any cell type of a given organism (Zakrzewski, Dobrzynski, Szymonowicz & Rybak, 2019). Additionally, stem cells maintain a capacity for self-renewal (Poliwoda *et al.*, 2022). These cell types arise both within the embryo and the adult organism, depending on their degree of specialisation. Stem cell potency, that is the

differentiation power of a stem cell, decreases upon increased specialisation (Zakrzewski, Dobrzynski, Szymonowicz & Rybak, 2019). Thus, stem cells may be classified based on their potency, but also based on their origin (Poliwoda *et al.*, 2022).

Totipotent or omnipotent stem cells have the greatest potency (Poliwoda *et al.*, 2022). They can differentiate into cells of the entire organism; that is both embryonic (germ-line) and extra-embryonic structures (Charitos *et al.*, 2021). Zygote cells are totipotent because they can differentiate into cells of the placenta or progress into any of the three germ layers. Next, pluripotent cells exist in a state of lesser differentiation potential. Pluripotent cells can differentiate into any of the three germ layers, however not into cells of extra-embryonic structures (Poliwoda *et al.*, 2022). Embryonic stem cells (ESCs) are pluripotent stem cells since they can differentiate into cells of the embryo and not of the placenta (Zakrzewski, Dobrzynski, Szymonowicz & Rybak, 2019). Multipotent stem cells, such as a haematopoietic stem cell, are a step further in terms of specialisation, such that they can differentiate within only one of the three cell lineages (Kimbrel & Lanza, 2020). Further down the line, an oligopotent stem cell may specialise into a few cell types pertaining to one tissue, whilst a unipotent stem cell holds the most limited differentiation potential, as it can only form one cell type (Charitos *et al.*, 2019). Nevertheless, unipotent stem cells have a high capacity for self-renewal.

Somatic or adult stem cells are also undifferentiated cells; however, they are found within the developed organism (Nadig, 2009) in most mammalian organs and tissues (Charitos *et al.*, 2021). Adult stem cells are involved in growth and regeneration of lost or damaged cells, and can be multipotent or unipotent (Zakrzewski, Dobrzynski, Szymonowicz & Rybak, 2019). Neural stem cells (NSCs) are an example; they can generate nerve cells, oligodendrocytes, and astrocytes.

1.3. Mesenchymal Stem Cells

Mesenchymal stem cells (MSC) are a type of adult stem cell (Jiménez-Acosta *et al.,* 2022). MSCs are interchangeably referred to as multipotential stromal cells, mesenchymal stromal cells, or mesenchymal progenitor cells (Pittenger *et al.,* 2019).

1.3.1. Origin

MSCs were originally isolated from bone marrow, and since, have been found within various tissue types, including foetal, perinatal, and adult tissues. Specifically, MSCs can be isolated from peripheral blood, UC, foetal liver, foetal lung, adipose tissue, skeletal muscle, amniotic fluid and membrane, synovium, and the circulatory system (Neirinckx, Coste, Rogister, & Wislet-Gendebien, 2013); and also, dental tissues, endometrium, limb bud, placenta, salivary glands, and skin (Ullah, Subbarao, & Rho, 2015). The fact that MSCs occur in many tissues in the body and can be isolated easily is one of their many advantages (Han *et al.,* 2019).

1.3.2. Characteristics of MSCs

MSCs are typically spindle-shaped with elongated nuclei having two to three nucleoli (Jiménez-Acosta *et al.,* 2022). In culture they have been found to occur as two differing structures: fibroblastic or rhomboid. These cells are plastic-adherent, and mostly fibroblastic, whose typical differentiation power lies within the mesodermal lineage (Neirinckx, Coste, Rogister, & Wislet-Gendebien, 2013). Although MSCs are considered multipotent adult stem cells, they can differentiate into cell types within other lineages and not just within the mesoderm (Zakrzewski, Dobrzynski, Szymonowicz & Rybak, 2019; Poliwoda *et al.,* 2022). Thus, MSCs have a high plasticity, making them a good choice as the starting cells for transdifferentiation experiments (Jiménez-Acosta *et al.,* 2022).

Despite the myriad of studies on MSCs, there is no quantitative assay to identify these cells within a mixed population (Ullah, Subbarao & Rho, 2015). Nevertheless, the International Society for Cellular Therapy (ISCT) established the minimal criteria required for MSC identification. To begin with, MSCs can be distinguished by their characteristic of plastic adherence. Secondly, these cells exhibit a unique set of cell surface markers, including expression of cluster of differentiation (CD) markers, CD73, CD90, and CD105, with a lack of expression of CD14, CD34, CD45, CD11b, CD79a, CD19 and human leukocyte antigen Class II (Jiménez-Acosta *et al.*, 2022). Lastly, MSCs should possess an ability for their typical *in vitro* trilineage differentiation into adipocytes, chondrocytes, and osteoblasts. Such properties are applicable to all MSCs, although there may be some variations between MSCs isolated from different sources (Ullah, Subbarao, & Rho, 2015). MSCs have also been found positive for expression of CD29, CD44, CD146, and CD140b depending on the tissue they were isolated from.

1.3.3. Relation of Properties of MSCs To Their Therapeutic Application

Due to several advantageous characteristics, MSCs have been the subject of many studies and of over 900 US clinical trials (Kimbrel & Lanza, 2019). The application of MSCs for transplantation into patients was initiated as early as 1993 and since then their clinical use has been further addressed (Pittenger *et al.*, 2019). MSCs have many properties that make them a good fit as starting cells for transdifferentiation research and regenerative medicine (Choudhary, Gupta, & Singh, 2021; Han *et al.*, 2019). MSCs have a high degree of plasticity, but do not possess tumorigenic potential (Jiménez-Acosta *et al.*, 2022). They can be easily sourced from a large variety of tissues and their use presents no ethical apprehension (Jiménez-Acosta *et al.*, 2022). MSCs generate and release growth factors and cytokines (Pittenger *et al.*, 2019), anti-inflammatory molecules (Ullah *et al.*, 2015), and trophic factors at sites of injury for tissue regeneration (Urrutia *et al.*, 2019).

Additionally, MSCs have been shown to repair tissue damage by means of anti-apoptotic and cytoprotective signals, and their capacity for inducing angiogenesis (Zhang *et al.,* 2015; Kimbrel & Lanza, 2019).

One very crucial aspect of MSCs is their combined immunosuppressive properties and low immunogenicity (Zhang *et al.,* 2015). MSCs exhibit a low immunogenicity due to a lack of expression of HLA-DR and its co-stimulatory molecules, which enables MSCs to evade immunosurveillance, thus preventing an immune response in patients who receive cell transplants (Han e*t al.,* 2019; Zhang *et al.,* 2015). Furthermore, MSCs exert immunosuppressive properties, meaning they can inhibit the activity of a number of immune cells, such as T cells, B cells, or natural killer cells, due to low-level expression of HLA class I; as well as, via cell-cell contact and soluble factors (Choudhary, Gupta, & Singh, 2021; Zhang *et al.,* 2015).

Such properties provide a good rationale for MSCs to be employed as universal donor stem cells (Choudhary, Gupta, & Singh, 2020). This is important to note, since autologous MSC transplantation, i.e., the transplantation of MSCs sourced from within the patient themselves (Charitos *et al.*, 2021), poses several issues (Zhang *et al.,* 2015). Specifically, MSCs might be difficult to obtain from some patients or may exhibit a diminished biological activity (such as limited differentiation or regenerative potential) when taken from people of a certain age or with a particular disease. Therefore, it is sometimes challenging to obtain good quantities of healthy autologous MSCs with appropriate biological activity levels from certain individuals (Zhang *et al.,* 2015). This is why it is so advantageous that MSCs can be used in an allogenic manner, i.e., using MSCs from a donor for transplantation into a different recipient.

1.3.4. MSCs application in neural therapy

The mammalian adult CNS has a very poor capacity for repairing neural deterioration, thus any damage to the CNS is irreversible (Han *et al.*, 2019; Wang *et al.*, 2022; Jiménez -Acosta *et al.*, 2022). Several neurodegenerative diseases, such as AD and PD, amyotrophic lateral sclerosis, epilepsy, stroke and trauma, manifest with neuronal cell loss (Krabbe, Zimmer, & Meyer, 2005). As these diseases progress, significant neuronal harm is incurred, alongside neuronal cell death (Mollinari *et al.*, 2018). This destruction, in turn, prompts the loss of cognitive and physical capacities. Therefore, neurodegenerative diseases are highly incapacitating; yet they are currently still incurable. Several treatments exist; however, they only help to relieve some of the symptoms caused by the disease, and they do not hinder disease progress (Choudhary, Gupta & Singh, 2020).

With increasing life expectancy, there are now almost 100 million people in the world suffering from neurodegenerative diseases (Mollinari *et al.*, 2018). This has caused a strain on society as well as the economy. A decent human disease model is highly sought after in the scientific community. A suitable disease model, such as patient-specific neuronal cells, could be applied for drug development, disease progression modelling and regenerative therapy (Mollinari *et al.*, 2018). AD and PD are two of the most common neurodegenerative diseases; both still incurable (Tüshaus *et al.*, 2020). Having an appropriate disease cellular model would enable researchers to investigate the disease mechanism, identify risk genes, and screen for potential drug treatments.

Conversely to MSCs, NSCs have demonstrated a reduced capacity to differentiate into neuroglia when transplanted into adult mammalian brain and given ideal conditions for development (Choudhary, Gupta, & Singh, 2020). Considering this, MSCs are a more ideal starting cell type, since they are easily sourced, and can be certainly directed towards

neuronal and glial cell differentiation with chemical manipulation (Choudhary, Gupta, & Singh, 2020). The treatment of MSCs with neural inducing composites, can induce expression of neuron-specific markers, such as glial fibrillary acidic protein (GFAP), neuron-specific enolase (NSE) and neuronal nuclei (NEUN) (Choudhary, Gupta, & Singh, 2020).

MSCs have several unique characteristics that further convey their suitability as the starting cells in transdifferentiation towards neural cells (Jiménez-Acosta *et al.*, 2022). One such characteristic is the ability of MSCs to release signalling molecules that yield paracrine and autocrine effects that substitute for a multitude of genes and proteins that are aberrant in various neurodegenerative disorders (George, Hamblin & Abrahamse, 2019). Moreover, MSC paracrine secretions serve to protect neuronal cells from oxidative stress and apoptosis (Choudhary, Gupta, & Singh, 2020). Their on-site delivery of cytokines and growth factors supports angiogenesis, neurogenesis, synaptogenesis, and remyelination, for reconstruction of the damaged CNS (Han *et al.,* 2019). Additionally, MSCs are able to induce T cell tolerance and even release anti-inflammatory biomolecules, such as Transforming growth factor beta (TGF-β), which exerts neuroprotective effects (de Araújo Farias *et al.*, 2018).

Currently, most studies have produced functional DA neurons from either ESCs or iPSCs (Gaggi et al 2020; Gantner *et al.,* 2020; Nolbrant *et al.,* 2017). The use of ESC as the starting cells to derive neurons poses several issues since for their isolation, the embryo is destroyed in the process, and thus they are an ethically debated stem cell source (Zakrezewski *et al.,* 2019). iPSCs pose a risk for tumourigenicity because they have a greater risk of expressing oncogenes during their development (Zakrzewski *et al.*, 2019). Additionally, reprogramming patient somatic cells to iPSCs is a demanding procedure, and during their reprogramming, their somatic epigenetic memory is altered so that their

epigenetic signature is lost (Chabrat *et al.,* 2019). This is a significant limitation if the ensuing induced neuronal cells are to be used as models for patient disease. For these reasons, somatic stem cells have come to light as another possible source in which these issues are mostly avoided and patient-specific disease models may also be developed (Chabrat *et al.,* 2019; Gaggi *et al.,* 2020).

1.4. Neurons

Human neurogenesis is most deeply manifested during embryonic development rather than postnatally, although this still occurs in the adult brain (Vieira *et al.,* 2018). It is essential to consider both embryonic and adult neurogenesis in order to fully comprehend the mechanisms underlying the path from neural progenitors towards mature neurons. Embryonic neurogenesis shapes the brain's structure and function, whilst postnatal neurogenesis, although limited, is involved in neural regeneration, memory, cognition and emotion (Vieira *et al.,* 2018). Thus, the following sections discuss the current literature on both embryonic and adult neurogenesis.

1.4.1. The development of neurons – standard neuronal progenitor pathways

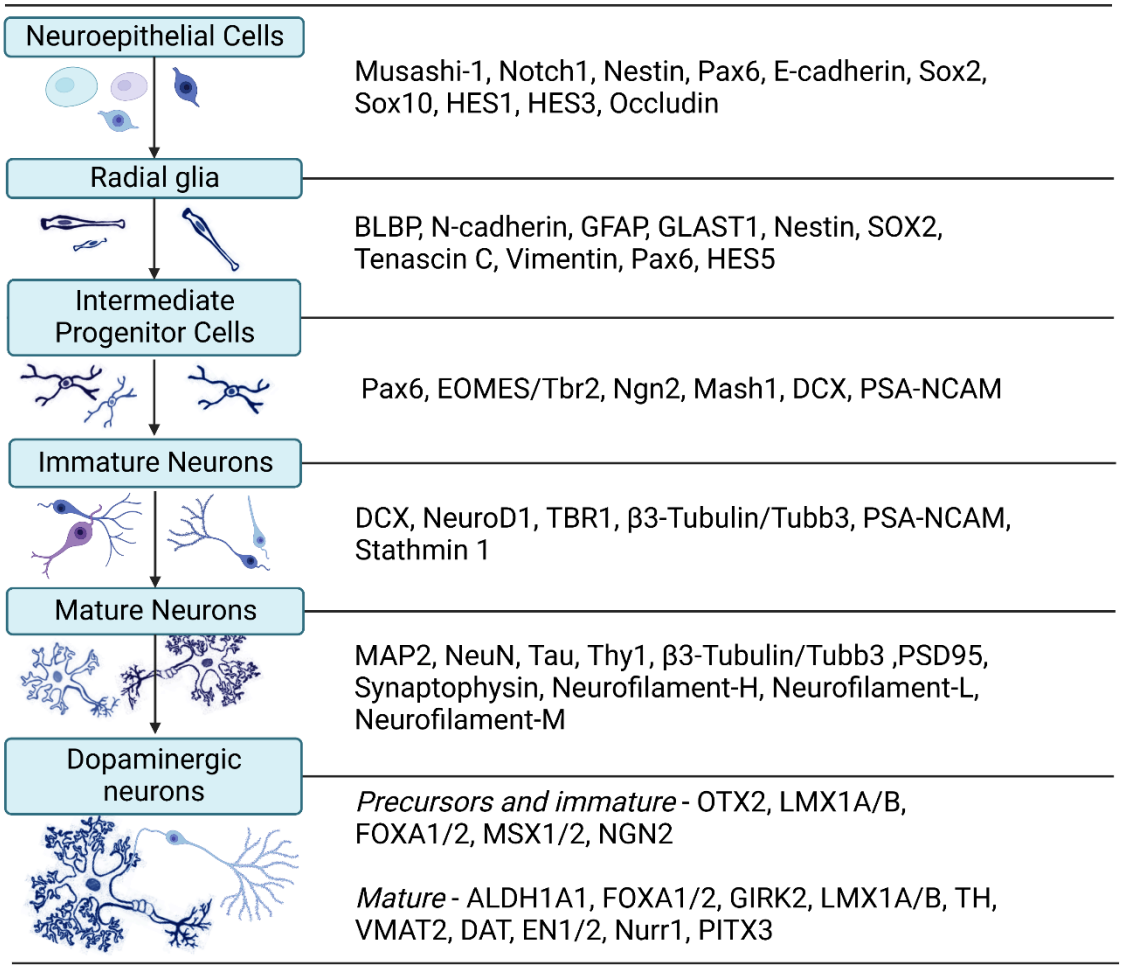

Figure 1.1. A flowchart showing the stages of neuronal differentiation, from neuroepithelial cells towards DA neurons. In addition, the names of various common neural markers can be found for each stage of neuronal differentiation. Adapted from Abcam, 2021; Cell Signalling Technology, 2022, and produced using Biorender.com.

1.4.1.1. Embryonic neurogenesis

The intricacy of human brain structure arises via several organised and distinct pools of neurons and glia that originate from a modest number of neural progenitors produced during embryonic development (Belmonte-Mateos & Pujades, 2022). Two proliferative regions of the developing brain are central to embryonic neurogenesis: the ventricular zone (VZ) and the subventricular zone (SVZ) (Zhang & Jiao, 2015).

NSCs are multipotent, unspecialised cells that are competent in self-renewal and in the generation of all neurons, oligodendrocytes and astroglia (Galiakberova & Dashinimaev, 2020; Zhang & Jiao, 2015). These cells are crucial for both embryonic and adult neurogenesis. Various cell types occurring in the developing embryonic brain can be considered as NSCs; these include neuroepithelial stem cells (NECs), radial glial cells (RGCs) and basal (or intermediate) progenitor cells. NECs proliferate to form the neural tube (Zhang & Jiao, 2015). These cells gain a neurogenic potential upon their development into RGCs (Martynoga, Drechsel & Guillemot, 2012). RGCs first proliferate to expand the progenitor cell pool (Belmonte-Mateos & Pujades, 2022) and then divide asymmetrically to produce more specialised cells (Galiakberova & Dashinimaev, 2020). These are the intermediate (basal) progenitor cells (IPCs), and these cells are in a neuronal progenitor state that is committed to producing neurons (Galiakberova & Dashinimaev, 2020).

1.4.1.2. Adult neurogenesis

Adult neurogenesis takes places in two brain regions maintained as neurogenic niches: the SVZ of the lateral ventricle and the subgranular zone (SGZ) of the hippocampal dentate gyrus (DG) (Bond, Ming, & Song, 2015; Galiakberova & Dashinimaev, 2020). A neurogenic niche is a region in the brain, which previously formed a part of the embryonic germinal layer, that boasts a unique microenvironment that maintains NSCs; hence, serving as a site for adult neurogenesis (Leal-Galicia *et al.*, 2021). In the SVZ, DA, GABAergic and glutamatergic neuronal cells are produced, whilst the SGZ generates granular cells that are involved in cognition, memory, and learning (Leal-Galicia *et al.*, 2021). The NSCs of the adult brain, known as radial glia-like cells, are contained within these two regions (Galiakberova & Dashinimaev, 2020).

Adult SVZ NSCs (or type B cells) divide asymmetrically for self-renewal and to generate neuronal precursor type C cells (transit amplifying progenitors) (Jurkowski *et al.,* 2020; Bond, Ming & Song, 2015). Type C cells divide symmetrically several times before progressing into type A cells (neuroblasts) (Galiakberova & Dashinimaev, 2020). Type A cells are the most differentiated cell state occurring within the SVZ (Jurkowski *et al.,* 2020). These type A cells divide a few times and then assemble sequentially, as they migrate towards the olfactory bulb where they eventually differentiate into various subcategories of interneurons or granule cells (Bond, Ming & Song, 2015; Jurkowski *et al.,* 2020).

In the adult SGZ, quiescent radial glia-like neural progenitor cells (NPCs) evolve into mature neurons by advancing through four individual phases; the progenitor cell phase, the early survival phase, the postmitotic maturation phase and lastly the late survival/maturation phase (Jurkowski *et al.,* 2020; Kempermann, Song & Gage, 2015, Hourigan *et al.,* 2021). These neurogenic phases span six to eight weeks in which the cells progress through six distinct cellular states which may be distinguished based on morphology and marker expression. These six cellular states include RGL cells, type 2a IPCs, type 2b IPCs, neuroblasts, immature neurons and mature neurons (Hourigan *et al.,* 2021).

1.4.2. Dopaminergic neuron development

The literature reviewed here will focus on DA neurogenesis occurring within the midbrain, since the majority of mammalian DA neurons are contained in this region (Gaggi *et al.,* 2020). During embryogenesis, midbrain floor plate (FP) precursors generate midbrain DA (mDA) neurons of the substantia nigra (SN), that project towards the dorsal striatum, forming the nigrostriatal pathway (Volpicelli *et al.,* 2020). This pathway functions to control voluntary movement. The FP DA precursors also produce other mDA

neuron groups; namely those in the ventral tegmental area (VTA) and the retrorubral field. These two mDA nuclei play a significant role in mood, emotion, and reward regulation by use of the meso-cortico-limbic system (Volpicelli *et al.,* 2020). In PD, it is degeneration of the nigrostriatal pathway that is behind the development of the disease (Wang *et al.,* 2020). On the other hand, schizophrenia, drug addiction, Attention-deficit hyperactivity disorder (ADHD), depression and chronic pain, are all associated with a dysfunctional meso-cortico-limbic pathway (Volpicelli *et al.,* 2020).

DA neurons characteristically synthesise and release the neurotransmitter dopamine (Arenas, Denham & Villaescusa, 2015). DA neurons can be identified by their expression of genes required for dopamine synthesis and neurotransmission, including tyrosine hydroxylase (TH) for generation of dopamine, the vesicular monoamine transporter 2 (VMAT2), dopamine transporter (DAT) and paired-like homeodomain 3 (PITX3) (Mesman & Smidt, 2020). The concerted effects of a multitude of morphogens and transcription factors (TFs) bring about the ensuing differentiation of precursor cells into neural progenitors, immature and finally mature DA neurons (Volpicelli *et al.,* 2020; Gaggi *et al.,* 2020). Specifically, the combined and timely activation of Sonic hedgehog (SHH), Fibroblast growth factor (FGF) 8 , Wingless 1 (WNT1), and TGF-β signalling pathways, enable expression of numerous TFs involved in DA neuronal development (Gaggi *et al.,* 2020). These TFs exert different functions and can be compiled accordingly (Brodksi *et al.,* 2019). Orthodenticle homeobox 2 (OTX2), LIM homeobox transcription factor 1 alpha/beta (LMX1A/B), and forkhead box A 1/2 (FOXA1/2) regulate the response of progenitor cells to signalling morphogens (SHH, FGFs, WNTs and BMPs – bone morphogenetic proteins), MSX1/2 and Neurogenin 2 (NGN2) regulate neurogenesis, and EN1/2, nuclear receptor subfamily 4 group A member 2 (NURR1), and PITX3 are involved in mDA neuron differentiation and survival (Brodski *et al.,* 2019).

The following subsections review the current literature on the *in vivo* development of specifically DA neurons.

1.4.2.1. Early development of the Midbrain

The FP, where mDA neurons originate (Mesman & Smidt, 2020) and the isthmus, are two signalling centres important during early midbrain development (Arenas, Denham & Villaescusa, 2015). The isthmus is also known as the mid-hindbrain border, since it distinguishes the midbrain from the hindbrain, in which serotonergic neurons develop. The isthmus develops when the transcription factor OTX2 starts to be expressed in the midbrain, and gastrulation brain homeobox 2 expression begins in the hindbrain (Arenas, Denham & Villaescusa, 2015; Volpicelli *et al.*, 2020). The isthmus is marked by expression of FGF8 that occurs within, and WNT1 expression that progresses out into the midbrain region and is centrally engaged in mDA neuron development (Mesman & Smidt, 2020).

Once the isthmus has formed, FP specification may take place (Mesman & Smidt, 2020). SHH signalling is critical for patterning of the FP. The findings of several studies contribute to the premise that SHH inhibits FP neurogenesis and that in turn, WNT signalling inhibits SHH in the FP to initiate FP neurogenesis, DA progenitor expansion and to induce expression of DA progenitor-specific genes (Bodea & Blaess, 2015; Brodski *et al.*, 2019; Nouri *et al.*, 2015).

Several other genes are expressed in the midbrain FP and play a central role in the start of mDA neuronal specification, such as the LIM-homeodomain transcription factor LMX1A and the basic helix-loop-helix (bHLH) factors NGN2 and Achaete-Scute Family BHLH Transcription Factor 1 (MASH1) (Mesman & Smidt, 2020). Expression of these two pro-neural genes, NGN2 and MASH1, in proliferating mDA progenitors is supported by OTX2 (Volpicelli *et al.*, 2020), which was previously defined as an important gene for

organisation of the Isthmus. FOXA2 is another essential TF; one of the first to be expressed in the ventral midbrain (Volpicelli *et al.,* 2020; Kim *et al.,* 2017). FOXA2 is responsible for the activation of an array of genes required for mDA neuron specification (Kim *et al.,* 2017). Evidently, a complex web of TFs and morphogens orchestrate an accurate FP patterning and specification, which is essential for the generation of a large NPC pool that will serve as the foundation for DA progenitors and their mdDA neuronal progeny later on (Mesman Smidt, 2020).

1.4.2.2. Progression of NPCs towards mature mdDA neurons

1.4.2.2.1. Lineage commitment and early differentiation of DA progenitors

Interestingly, several factors involved in the early stages of FP patterning and expansion of the NPC pool are also involved in the subsequent crucial phase of DA neuronal fate commitment. One such patterning factor with this dual role is OTX2 (Mesman & Smidt, 2020). It has been posited that OTX2 contributes to mdDA neuronal fate specification and pushes progenitor cells towards a DA progenitor fate (Puelles *et al.,* 2004; Simeone, 2005). OTX2 downregulates expression of Nkx2.2 to deter serotonergic neurons from being developed, indicating that this TF plays a role in repressing the generation of non-DA cell fates (Volpicelli *et al.,* 2020).

The sequential activation of a group of genes is necessary to stimulate the expression of other genes and TFs that are required to finalise the DA program in neural precursors already committed to the DA fate (Volpicelli *et al.,* 2020). These mDA differentiation genes include NURR1, PITX3, EN1, EN2, and LMX1A/B. These crucial genes must operate in a concerted manner in order for an mDA neuron to reach maturity correctly (Volpicelli *et al.,* 2020). Naturally, there are also cell-extrinsic factors that play a significant role in preparing and stimulating NPCs to advance towards a DA progenitor state and later towards mdDA neuronal cells, such as the aforementioned SHH and WNT

signalling (Bodea & Blaess, 2015; Brodski *et al.*, 2019). As has already been disclosed, SHH signalling is primarily involved in the early stages of development, specifically in the process of launching the mDA progenitor pool, whereas WNT signalling is more involved in inducing differentiation in mDA progenitors (Mesman, von Oerthel, & Smidt, 2014; Joksimovic *et al.*, 2009; Zhou *et al.*, 2016).

The earliest WNT family member to be expressed in midbrain NPCs is WNT1, which is expressed within the isthmus (Joyner & Miller, 2000; Prakash *et al.*, 2006; Wurst & Bally-Cuif, 2001). WNT1 is associated with the start of mDA neurogenesis, as well as the accurate pattering of the FP (Mesman & Smidt, 2020). WNT1, WNT2 and WNT3A stimulate the canonical WNT pathway, which plays a role in the proliferation and maturation of post-mitotic DA precursors towards mature mDA neurons (Bryja *et al.*, 2009; Castelo-Branco *et al.*, 2003; Sousa *et al.*, 2010; Castelo-Branco *et al.*, 2010).

1.4.2.2.2. Late differentiation and maturation

The maturation and survival of mDA neurons is coordinated by numerous factors including brain derived neurotrophic factor (BDNF) and glial cell line derived neurotrophic factor (GDNF) (Volpicelli *et al.*, 2020). Silencing of GDNF and BDNF in adult mice results in mDA neuronal loss (Pascual *et al.*, 2008), which suggests that GDNF and BDNF are vital for the survival of mDA neurons. Interestingly, a study proposed that GDNF is involved in the regulation of BDNF expression through a GDNF-PITX3-BDNF trophic loop (Peng *et al.*, 2011). In another study, the treatment of an animal model with BDNF before the induction of PD hindered the loss of SN DA neurons and their striatal projections (Palasz *et al.*, 2020). When BDNF was used in treatment after the induction of PD, it did not result in increased DA neurons, however, it did increase DA levels, synaptic plasticity, and DA axon growth (Palasz *et al.*, 2020).

FOXA2 expression in maintained in adult DA neurons, thus it has been proposed to be involved in assisting mature neurons in their survival (Domanskyi *et al.,* 2014). FOXA2, along with FOXA1, EN1 and EN2, have been implicated in cell fate determination, differentiation, and in sustaining mature mDA neurons and preventing their death by apoptosis (Ferri *et al.,* 2007; Alvarez-Fischer *et al.*, 2011). PITX3 has been demonstrated as a vital factor in differentiation and survival of mDA neurons (Maxwell *et al.,* 2005; Smidt *et al.,* 2004). Expression of PITX3 begins halfway through DA neuronal differentiation (Maxwell *et al.,* 2005). PITX3 is expressed in all SN and VTA neurons, however loss of its expression mostly impacts DA neurons of the SN.

Two other factors that have been implicated to interact with PITX3 with regards to mDA neuronal maturation are NURR1 and EN1 (Mesman & Smidt, 2020). Through the interaction of NURR1 and PITX3, the repressive effects of SMRT-HDAC complexes on NURR1 expression are halted so that NURR1 target genes may be expressed (Jacobs *et al.,* 2009). Moreover, it has been shown that loss of PITX3 expression brought about an increased EN1 expression, and the study proposed that these two genes might function to regulate one another's expression (Veenvliet *et al.,* 2013). NURR1 also plays a role in regulating the response to NTFs which are needed for maturation and survival of mDA neurons, such as GDNF (Volpicelli *et al.,* 2020). This function is carried out through controlling expression of GDNF receptor Ret and GDNF Family Receptor (GFR) alpha (GFRα) (Wallén et al., 2001; Galleguillos *et al.,* 2010). Additionally, NURR1 was found to be in control of expression of BDNF which is involved in neuroprotection of mDA neurons (Volpicelli *et al.,* 2007).

1.4.3. *In vitro* differentiation into neurons from different sources

1.4.3.1. Differentiation of ESCs to neurons

Neural differentiation of ESCs has been performed using neural inducers that control endogenous signalling pathways (Chambers *et al.*, 2009; Tropepe *et al.*, 2001). Various pathways have been targeted for the neural induction of ESCs. One of the main pathways targeted for inducing ESCs to form NSCs is the retinoic acid (RA) pathway (Vieira *et al.*, 2018). A study by Tonge and Andrews found that neural differentiation of hESCs requires an extended period of RA treatment and a high cell density, which resulted in increased expression of NEUROD1, PAX6 and SOX2 (2010). Another study found that ESCs required extracellular signal-regulated kinase (ERK1/2) phosphorylation for survival and neural differentiation (Li *et al.*, 2006). Furthermore, they found that NEUROD1, signal transducer and activator of transcription 3 (STAT3), nerve growth factor (NGF), BDNF and GDNF were also vital for neuronal differentiation of ESCs. In a study by Kunath *et al.*, ERK1/2 signalling was activated by FGF4 addition, which caused ESCs to exit the self-renewal state and start differentiating (2007). Furthermore, they described how FGF8 acts endogenously to elicit embryonic neural differentiation and support a temporary period of self-renewal of neural precursors (Kunath *et al.*, 2007).

In 2012, Kirkeby *et al.*, reported a neural induction protocol which successfully generated subtype-specific DA neural progenitors from ESCs based on embryoid body formation and dual SMAD inhibition. For neural induction, embryoid bodies were cultured in SB431542, SHH, and a glycogen synthetase kinase-3β (GSK-3β) inhibitor (CT99021) for 9 days and then BDNF, GDNF, and ascorbic acid from day 11 onwards with the addition of dibutyryl-cAMP and N-[N-(3,5-Difluorophenacetyl)-L-alanyl]-S-phenylglycine t-butyl ester (DAPT) from day 14 (Kirkeby *et al*., 2012).

1.4.3.2. Transdifferentiation of MSCs to neurons

As previously stated, typically, MSCs differentiate within their mesodermal lineage towards chondrocytes, adipocytes, and osteoblasts. However, given the presentation of ideal conditions, MSCs possess the capacity for differentiation within the remaining germ layers, i.e., the ectoderm, and endoderm (Ullah, Subbarao, & Rho, 2015; Choudhary, Gupta, & Singh, 2021). In the case that the MSCs are differentiating towards cells of ectodermal or endodermal lineages, the term transdifferentiation describes this process.

Transdifferentiation refers to the process by which adult stem cells may differentiate into cell types within a cell lineage that differs from that in which the somatic stem cell originally occurred (Krabbe, Zimmer, & Meyer, 2005). Transdifferentiation involves genetic reprogramming, whereby certain genes, those originally expressed in the cell, are deactivated, whilst activating others that correspond to characteristics of the new cell type. This can only be considered to have occurred once it is established that the cells have adopted a characteristic cellular phenotype (Krabbe, Zimmer & Meyer, 2005).

Overall, transdifferentiation is considered the safer option compared to transgene expression for production of iPSCs (Vieira *et al.*, 2018). This is because transdifferentiation produces fully-differentiated cells that have a low probability of taking up another cell phenotype or even the formation of tumours (Vieira *et al.*, 2018). Reprogramming of MSCs towards neuronal cell types *in vitro* has been achieved through several distinct routes (Jiménez-Acosta *et al.*, 2022). These include the use of growth factors, coculture with cells of the neural lineage, gene transfection, miRNAs, chemical compounds, and small molecules.

1.4.3.3. Differentiation of iPSCs to neurons

Pluripotent stem cells can differentiate into all cell types of the three germ layers and have an unlimited self-renewal ability (Hong & Do, 2019). iPSCs can be created

using differentiated cells from a donor, by inserting several reprogramming factors (Takahashi & Yamanaka, 2006). Their main advantages are that their use is not constrained by lack of donor availability, and they avoid ethical concerns that are posed when using ESCs (Hong & Do, 2019). For these reasons they are often used for differentiation studies and disease modelling. iPSCs have been differentiated into NSCs using both 2D and 3D culture as both neurospheres and neural rosettes (Elkabetz *et al.,* 2008) and primitive NSCs (Shin *et al.,* 2019).

Several studies have been performed in which iPSCs were differentiated into DA neurons (Hong & Do, 2019). In a study by Perrier *et al.,* iPSCs were cocultured with MS5 stromal cells which was found to increase the efficiency of their conversion into NECs (2004). Furthermore, they treated the induced NECs with FGF8 and SHH and achieved their differentiation into DA neurons. In another study, iPSCs were differentiated into functional DA neurons in a phase-guided 3D cell culture microfluidic bioreactor system (Moreno *et al.,* 2015). The induced neurons were found to express TH at a rate of 91%.

1.4.3.4. Other sources

Several research studies have adopted use of other kinds of stem cells for their neural induction and differentiation. One interesting example is the use of human nasal olfactory stem cells in a study conducted by Chabrat *et al.* (2019). These cells are a type of MSC, and what makes them ideal for neural induction is the fact that nasal olfactory tissue originates from the neural crest and is maintained in an embryo-like developmental state (Chabrat *et al.,* 2019). Several research groups have conducted differentiation studies starting with NSCs (Roybon *et al.,* 2008; Westerlund *et al.,* 2003). However, this is not so common in current literature, considering that there are significant challenges to obtaining NSCs and other issues that affect their suitability for clinical application (Wang *et al.,* 2020).

1.4.4. Dopaminergic neuron application in therapy

Due to medical and technological advancements, we have seen a dramatic increase in the world's population, together with an increase in life expectancy and thus an increase in the number of seniors (G7 National Academies, 2017). The major cause of death in older populations is cardiovascular disease and cancer, however neurodegenerative diseases such as AD, PD, and amyotrophic lateral sclerosis are within the top ten diseases and causes of death in the elderly. Neurodegenerative diseases, as of yet, do not have a cure, and their incidence greatly increases with age (Choudhary, Gupta & Singh, 2020). Tackling the lack of cures or means by which to slow disease progression in neurodegenerative disease is of paramount importance considering that the number of elderly people is projected to increase in the coming decades (G7 National Academies, 2017). Since life expectancy is expected to increase even more, so will the number of people affected by such diseases, as well as the individual, social and financial burden experienced due to providing help to patients. This warrants the search for more efficient therapies to subdue symptoms, to delay disease progression and hopefully, cure the disease (Vieira *et al.*, 2018). Cell-based regenerative therapy is an auspicious candidate for such a goal.

DA neurons are involved in numerous brain functions including motor control, and various behavioural and cognitive processes, including addiction, attention, motivation, reward, decision-making, and response to stress (Volpicelli et al., 2020: Mesman & Smidt, 2020). The degeneration of a portion of the mDA neuronal population in the SN is accountable for the development of PD (Surmeier, 2017; Mesman & Smidt, 2020), and brings about both motor and non-motor symptoms associated with PD (Mesman & Smidt, 2020). The degeneration of DA neurons was recently also implicated in the development of Alzheimer's disease (Krashia et al., 2019). Moreover, the dysfunction of DA neurons

has been associated with schizophrenia, drug addiction, ADHD, and depression (Volpicelli et al., 2020).

Transplantation of human foetal nigral tissue has been investigated as a therapeutic strategy for PD (Di Santo & Widmer, 2018). Investigations have demonstrated its safety and found that it reinnervates the dopamine-depleted striatum in PD patients (Hauser *et al.,* 1999; Hallett *et al.,* 2014; Kordower *et al.,* 2017). One issue that prevails is the limited survival of DA neurons after transplantation (Di Santo & Widmer, 2018). Hence, research efforts have been devoted to the search for non-foetal sources of DA neurons to boost DA survival.

The therapeutic utility of stem cell-derived neurons and NSCs has been explored by transplantation studies using animal models of degeneration, including models of HD AD and PD (Ghosh, 2019). In a primate PD model, transplanted undifferentiated NSCs migrated to the site of damage, where they survived and successfully enhanced the performance of the nigrostriatal system (Redmond *et al.,* 2007). Furthermore, some of the implanted NSCs started expressing TH and DAT. The brains of primates transplanted with these undeveloped NSCs were found to exhibit increased neuronal numbers, neuron size, and dopamine levels, with a decline in alpha-synuclein aggregation (Redmond *et al.,* 2007).

Stem cell differentiation protocols have the potential to be applied for clinical therapy, drug screening and disease modelling of neurodegenerative and neurodevelopmental diseases (Nolbrant *et al.*, 2017). Despite the promise held by stem cell therapy, there are still a number of issues to be addressed, and a lot more research to be done (Zakrzewki *et al.,* 2019). A critical issue that impedes such applications of stem cells, is the need for protocols that dictate accurate patterning and maintenance features for the generation of each individual neuronal subtype. In order for stem cells and the

deduced differentiation protocols to allow for such applications, these protocols must produce correct and genuine neuronal subtypes, in a controlled and reproducible manner so that there is low batch-to-batch variation (Nolbrant *et al.,* 2017). Importantly, the cells derived for therapy and transplantation into patients, must be able to completely replace lost or faulty cells (Zakrzewksi *et al.,* 2019).

1.5. Modulating biochemical pathways

Specific morphogens are of utmost importance for neural patterning and specification during embryonic development, and for regulation of adult NSCs (Bond, Ming & Song, 2015). Such morphogens include BMPs, TGF-β family proteins, Notch, WNTs, and SHH. These pathways may be manipulated through use of small molecules to direct MSCs toward neurons in culture.

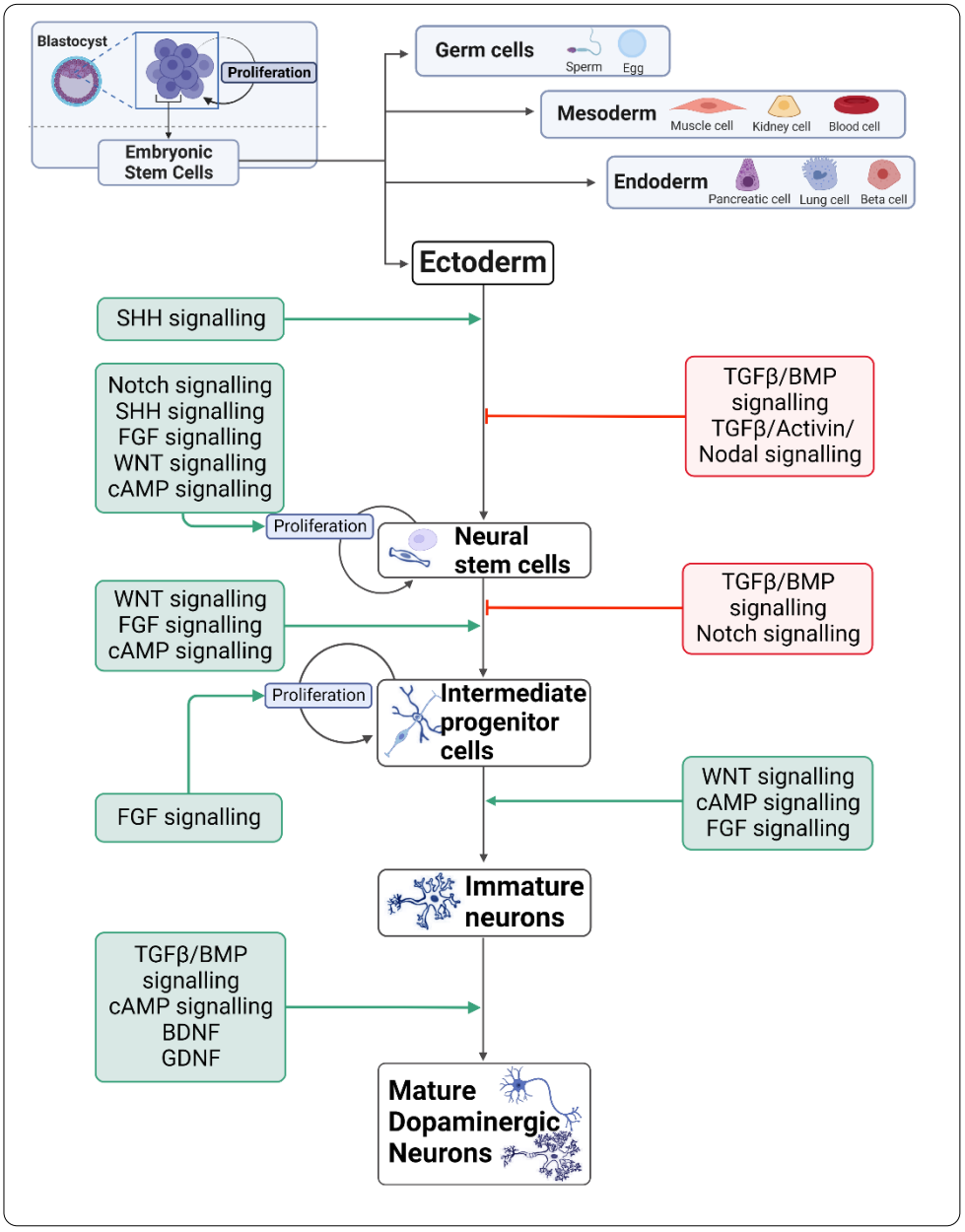

Figure 1.2. A flowchart that provides a summary of the main signalling pathways that influence neural differentiation of the Ectoderm. Inhibition is shown in red, and activation in green. Whether this inhibition or activation is exerted on differentiation or proliferation can be deduced from where the sharp arrow (green) or blunt arrow (red) ends. At the top of the image, the diagram shows ESCs from the inner cell mass of the blastocyst, that are totipotent, and can produce germ cells, and cells from within the 3 germ layers: the mesoderm, the endoderm and finally the ectoderm. From the ectoderm lineage, the main differentiation stages for production of DA neurons can be observed. Created using Biorender.com

1.5.1. WNT/β -catenin pathway

WNT ligands are a family of autocrine and paracrine-secreted glycoproteins (Navarro Quiroz *et al.*, 2018). If no WNT ligands are present, GSK-3β activates β-catenin, a primary regulator of the WNT pathway, to form a degradation complex comprising of GSK-3β/APC/Axin (Logan & Nusse, 2004), so that β-catenin is phosphorylated and ubiquitinated for its degradation by the proteasome (Navarro Quiroz *et al.*, 2018). Via this persistent degradation of β-catenin, in the absence of WNT ligand, existing levels of intracellular β-catenin are kept low so that transcription of WNT target genes is averted.

In the presence of a WNT ligand, it will interact with the G protein-coupled receptor Frizzled, to form a complex with low-density lipoprotein receptor 5/6 at the cell surface (Volpicelli *et al.*, 2020; Navarro Quiroz *et al.*, 2018). The activated receptor complex transmits a signal to activate the Dishevelled phosphoprotein, which inhibits glucose synthetase kinase 3 so that it cannot phosphorylate β-catenin. As a result, the β-catenin degradation pathway is terminated, so that β-catenin collects in the cell and may enter the nucleus to exert its effects (Logan & Nusse, 2004; Volpicelli *et al.*, 2020). In the nucleus, β-catenin interacts with several TFs, including the lymphoid enhancer-binding factor 1/T cell-specific transcription factor (LEF/TCF) and cell factor T, to initiate transcription of WNT target genes (Navarro Quiroz *et al.*, 2018; Logan & Nusse, 2004).

This highly conserved pathway is frequently involved in nervous system development, namely, neural tube formation, and development of the dorsal root ganglia and the midbrain (Navarro Quiroz *et al*., 2018). Firstly, WNT family proteins play a role in early caudalisation of the cells of the neural plate (Kirkeby *et al.*, 2012). The canonical WNT pathway promotes neuronal differentiation via upregulating expression of NGN1 and NGN2, which are pro-neural bHLH proteins (Wen, Li, & Liu, 2009). This upregulation occurs due to activation of their promoters by the β-catenin/TCF complex.

WNT/β-catenin signalling also exerts proliferative effects through increasing cyclin D1, cyclin D2, and c-Myc expression. Additionally, the canonical WNT pathway endorses the self-renewal of RGCs so that the radial glial population is maintained (Galiakberova & Dashinimaev, 2020). When it comes to mDA differentiation, several WNT proteins have been found to exert a significant influence (Volpicelli *et al.,* 2020). WNT1 has been found to stimulate proliferation in mDA precursors and thus amplifies the mDA precursor pool, whereas WNT5a enhances mDA differentiation (MacDonald, Tamai & He 2009).

1.5.2. Cyclic AMP Signalling

Interaction of specific ligands with membrane-bound G protein coupled receptors results in activation of the adenylyl cyclase enzyme that subsequently converts Adenosine Triphosphate (ATP) into cyclic adenosine monophosphate (cAMP) (George, Hamblin & Abrahamse, 2019). Activated and elevated cAMP intracellular levels bring about activation of protein kinase A (PKA), which is involved in multiple cell processes, such as stem cell proliferation and differentiation (George, Hamblin & Abrahamse, 2019). The cAMP pathway is involved in many cellular mechanisms including cell differentiation, metabolism, and apoptosis (Singh *et al.,* 2020).

cAMP production in the cell may also stimulate cAMP response element binding protein (CREB) to be activated by phosphorylation (Lepski *et al.*,2013). Increased cAMP and CREB levels have been shown to contribute to NPC proliferation and differentiation (Dworkin & Mantamadiotis, 2010), since CREB can bind to promoter regions of genes containing the cAMP response element (Lepski *et al.,* 2013). In a study by Fujioka, Fujioka & Duman, sustained cAMP levels enhanced formation of dendritic branches, and increased MAP2 expression within two weeks of differentiation treatment (2004). In a study conducted by Hulley, Hartikka & Lübbert, it was found that elevated cAMP levels prevent degeneration of DA neurons treated with toxic molecules, and it was thus found

to serve as a neuroprotective additive in DA neuronal culture (1995). It has been postulated that the beneficial effects of cAMP on neural induction and differentiation are related to CREB activation through the phosphorylation of PKA (Jagasia *et al.,* 2009). In fact, Merz, Herold, & Lie, discovered that phosphorylated CREB is elevated in NPCs and immature neurons during their differentiation (2011).

1.5.3. Fibroblast Growth Factor signalling

The FGFs are a family of secreted signalling growth factors and vital mitogens involved in the neural development in the embryo (Galiakberova & Dashinimaev, 2020). FGFs conduct their effects by interacting with cell surface receptors within the tyrosine kinase family (fibroblast growth factor receptor 1-4) (Brodski *et al.,* 2019). This interaction brings about activation of several downstream signal transduction cascades, including the mitogen-activated protein kinase (MAPK), phosphoinositide-3-kinase/protein kinase B (PI3K/AKT), phospholipase C gamma (PLCγ), and STAT pathways. FGF signal transduction brings about upregulated expression of genes usually within the ETS TF family, such as ETV4/5 (Brodski *et al.,* 2019). FGFs have been implicated to play a role in cell survival, proliferation, differentiation, migration, axon guidance and synaptogenesis.

Importantly, FGF family members are directly involved in development of the embryonic midbrain (Brodski *et al.,* 2019). FGF8 expression and signalling is crucial for the formation of the isthmus and for its maintenance. However, FGF signalling continues to be important even once the isthmus has formed, after which it is involved in sustaining NPC viability. Studies have shown that FGF8 or FGF receptor inactivation brings about increased apoptosis of NECs in the midbrain (Saarimäki-Vire *et al.,* 2007; Chi *et al.,* 2003). In embryogenesis, FGF signalling is critically involved in patterning and compartmentalisation of the midbrain, where it plays a role in establishing regional

identities of neuronal cells. However, it has also been found to be involved in support of both NPC maintenance and cell cycle exit for neural differentiation in mDA neurons (Lahti *et al.*, 2011; McGowan, Alaama, & Strieder, 2013). Later in embryonic production of mDA neurons, FGFs are involved in axon guidance and survival (Brodski *et al.*, 2019).

1.5.4. TGF-β signalling family

The TGF-β signalling family consists of the Activin/Nodal and BMP pathways (Zirra, Wiethoff, & Patani. 2016). When a ligand binds, receptor dimerization is triggered, which in turn prompts a signalling transduction pathway to phosphorylate and activate a family of cytoplasmic proteins known as the Smads (Zirra, Wiethoff, & Patani, 2016). In embryogenesis, the TGF-β family plays a central role in regulating the primary stages of nervous system development, dorsalisation, patterning of the CNS, stem cell lineage commitment, cell migration, axon guidance, synaptogenesis, and cell survival (Meyers & Kessler, 2017).

Several TGF-β superfamily members are expressed in the neural plate: including both BMP and Activin proteins (Timmer *et al.*, 2005). BMP signalling regulates the commitment to proliferation or differentiation through interacting with the WNT pathway. WNT1 and WNT3 upregulate proliferation of neuronal precursors and decrease differentiation. Since greater BMP signalling causes increased WNT1/3 expression, this results in a decreased neuronal differentiation. In the embryo, BMP signalling downregulates neurogenesis and instead boosts astroglial cell commitment of SVZ NSCs, or NSC quiescence in the SGZ (Bond, Ming, & Song, 2015). It is important to note that Activin receptors have different downstream effectors Smads from BMPs, whereby Activin/Nodal receptors use Smad2 and Smad3 ligands and BMPs use Smads 1, 5 and 8 (Timmer *et al.*, 2005; Zirra, Wiethoff, & Patani, 2016). This implies that the Activin receptors would elicit different biological effects to the BMPs.

The TGF-β/Activin/Nodal pathway is vital for ESCs proliferation, preserves their pluripotency, and thus it discourages differentiation of the neuroectoderm (Galiakberova & Dashinimaev, 2020). In fact, endogenous nodal antagonists, Lefty1 and Cerberus-1 are needed for anterior neural patterning. Inhibition of TGF-β signalling has been found to prompt the neural induction of ESCs towards the ectoderm, and bring about production of embryonic NSCs (Temple, 2001).

1.5.4.1. Activin A

Being members of the TGF-β superfamily, Activins comprise of either a homo- or hetero-dimer of two β-Activin subunits (Rodríguez-Martínez, Molina-Hernández, & Velasco, 2012). This means that one out of three proteins may be biologically produced: Activin A (βA/βA), Activin B (βB/βB) and Activin AB (βA/βB). Mature Activin proteins may bind to a complex of type I (ALK2/4/7) and type II (ACVR2A/B) transmembrane receptors having serine/threonine kinase activity. Once the appropriate ligand is bound, the type II receptor phosphorylates the type I receptor (ALK4) which becomes activated. The activated type I receptor then enables the phosphorylation and activation of Smad 2/3 proteins. Active Smad 2/3 proteins can form a complex with Smad 4 which migrates into the nucleus, binds to the relevant deoxyribonucleic acid (DNA) regions or associates with TFs for target gene expression (Rodríguez-Martínez, Molina-Hernández, & Velasco, 2012).

1.5.4.2. Bone Morphogenic Protein signalling

The BMP family is the largest subgroup of the TGF-β signalling family (Quiroz *et al.,* 2018). BMPs act as growth factors and are expressed in both embryonic and adult nervous systems (Galiakberova & Dashinimaev, 2020). BMP signal transduction occurs through two different receptor types: serine-threonine kinases and BMP receptors type I (BMPRIs including ALK1/2/3/6) and type II (BMPRIIs including BMPR2, ACVR2A/B)

(Quiroz *et al.,* 2018). Canonical BMP signalling is one kind of BMP signalling in which Smad proteins are employed as messengers (Galiakberova & Dashinimaev, 2020). Ligand binding results in formation of a tetramer complex composed of two BMP type I receptors and two BMP type II receptors (Quiroz *et al.,* 2018). This complex formation activates an intracellular signalling cascade that requires phosphorylated Smad proteins. Smad 1, Smad 5, and Smad 8 are phosphorylated and activated via type I BMP receptor kinases, and once activated, form a heteromeric complex with Co-Smad (Smad 4). These activated complexes translocate to the nucleus to activate transcription of target genes (Quiroz *et al.,* 2018).

BMPs are activated at different stages and within different brain regions to regulate progenitor proliferation, cell fate, differentiation, and apoptosis (Jovanovic *et al.,* 2018; Bond, Bhalala & Kessler, 2012; Brodski *et al.,* 2019). Whether BMPs will impede or promote such cell processes, depends on the cell type, its developmental stage, and the extracellular environment (Brodski *et al.,* 2019). Importantly, in embryogenesis, BMP signalling inhibits transformation from the primitive ectoderm to neural ectoderm (Galiakberova & Dashinimaev, 2020; Bond, Bhalala & Kessler, 2012). Thus, suppression of BMP-Smad signalling is critical for the initial neural induction of the ectoderm in embryonic neurogenesis. Noggin is the major endogenous inhibitor of BMP signalling and functions to regulate it (Galiakberova & Dashinimaev, 2020). Later, BMP-Smad1/5/8 signalling participates in the progression of neuronal differentiation, maturation, and specification of the CNS in embryogenesis. However, in early stages of embryogenesis, BMP-Smad-signalling works to maintain the dormant state of NSCs through temporarily boosting their quiescence, so that they are maintained as undifferentiated precursors (Galiakberova & Dashinimaev, 2020). BMPs exhibit cross-talk with several other critical developmental pathways; namely, WNT and SHH pathways (Brodski *et al.,* 2019).

In the adult nervous system, BMPs foster glial differentiation but inhibit neuronal specification (Quiroz *et al.*, 2018; Watabe & Miyazono, 2009). In the adult SVZ, BMP ligands and receptors are expressed within stem cells and neural progenitors, where they function as inhibitors of type B and type C neuronal cell differentiation. Hence, BMP signalling is important for maintenance of stemness properties (Quiroz *et al.*, 2018). Additionally, BMP proteins have been found to encourage the differentiation of MSCs towards chondroblast or osteoblast fates (Roelen & Dijke, 2003).

1.5.5. Hedgehog signalling

SHH is a soluble extracellular signalling protein that was initially found to support differentiation in the neural tube and limb bud (Faigle & Song, 2013). The SHH signalling protein is a major morphogen involved in patterning of the CNS during embryogenesis, and in control of the cell cycle of NSCs and NPCs (Galiakberova & Dashinimaev, 2020). It is now known that SHH is highly involved in regulation of multiple aspects of nervous system development, including the differentiation of the ventral forebrain, midbrain DA differentiation, and cerebellar neuronal precursor proliferation (Ericson *et al.*, 1995; Wechsler-Reya & Scott, 1999; Quiroz *et al.*, 2018).

SHH exerts its functions through interacting in a receptor complex comprised of the receptor Patched (Ptc), and its G-protein-coupled receptor Smoothened (Smo) (Faigle & Song, 2013). When the SHH ligand is present, via signal transduction of Smo, activated Ptc brings about the transcription of Gli-proteins amongst other SHH target genes. It has also been demonstrated that SHH plays a significant role in neurogenesis in adult neurogenic regions, such that SHH receptors Ptc and Smo are both expressed in adult hippocampus and progenitor cells obtained from this brain region (Traiffort *et al.*, 1998; Lai *et al.*, 2003). Ahn & Joyner, demonstrated that quiescent NSCs and progenitors in the adult SVZ and SGZ, responded to SHH signalling by committing to neurogenesis (2005).

Other than its function in boosting self-renewal, proliferation, and neurogenesis in adult NSCs, SHH has also been implicated in regulation of cellular migration in the adult brain (Faigle & Song, 2013).

1.5.6. Rho Kinase pathway

Rho is a small GTP-binding protein involved in multiple cellular functions (Labandeira-Garcia et al., 2015). RhoA, a member of the Rho family, conducts through a downstream effector Rho-associated kinase (ROCK). The ROCKs are a family of GTPases that modify actin cytoskeletal arrangements (Jia *et al.,* 2016). Two genes, ROCK I and ROCK II encode the two isoforms of this protein, of which ROCK II is expressed in the brain (Labandeira-Garcia et al., 2015). ROCK proteins phosphorylate a multitude of substrates, of which the myosin light chain (MLC) and the myosin binding subunit of the MLC phosphatase, were the first substrates discovered (Labandeira-Garcia et al., 2015). The majority of ROCK substrates are proteins involved in regulation of the actin cytoskeleton. ROCK is also implicated as a central effector of morphological changes occurring during apoptosis including cell contraction, membrane blebbing and fragmentation of apoptotic cells (Labandeira-Garcia et al., 2015).

In their study, Compagnucci *et al.,* found that ROCK inhibition enhanced a neuronal morphology in iPSC-derived neurons (2016). Furthermore, ROCK inhibition in these cells also brought about increased expression of NR4A1, which is a nuclear receptor that acts as an inducer of neurite outgrowth. Hence, ROCK signalling causes an inhibition of neurite outgrowth. Tonges *et al.,* investigated ROCK signalling and its effects on DA neurons in a cell culture model and *in vivo* mouse model of PD (2012). Their study found that inhibition of ROCK signalling rescued DA neuronal cell loss in both models. Moreover, they showed that ROCK inhibition in these models protected and conserved DA terminals. Tonges *et al.,* proposed that the AKT survival pathway is a central player

in the neuroprotective effects brought about by ROCK inhibition (2012). Furthermore, Labandeira-Garcia *et al.,* described how ROCK inhibition safeguards DA neurons from death (2014). ROCK inhibitors have axon-stabilising effects that enable neuroprotection and regeneration of DA neurons (Labandeira-Garcia et al., 2015).

1.5.7. Neurotrophic Factor Signalling

NTFs are proteins that are involved in regulation of survival, growth, morphological plasticity, and the synthesis of proteins necessary to conduct specific functions pertaining to mature neurons (Leal-Galicia *et al.,* 2021). NTFs are classified into three individual subset families: neurotrophins (NTs), GDNF family ligands (GFLs), and neuropoietic cytokines. Each family stimulates different pathways, although the various pathways' effects on cells are similar (Leal-Galicia *et al.,* 2021). Both NTs and GFLs are highly involved in regulation of adult neurogenesis within the SVZ and SGZ of the DG, the SN, striatum, habenula and cerebellum.

The NT family is highly involved in regulation of neuronal differentiation and survival, axonal and dendritic growth, synaptic transmission, and adult neural plasticity (Ribeiro & Xapelli, 2021). These NTs are also vital in the processes of memory and learning. Examples of NTs include NGF, BDNF, and NT3/4/5 (Leal-Galicia *et al.,* 2021). These proteins are primarily produced as proneurotrophins, after which they are either secreted from cells or are subjected to proteolytic cleavage to produce the final NT. NTs may interact with two types of receptors: either the p75 neurotrophin receptor (p75NTR) or the receptor tyrosine kinase (RTK) family (Leal-Galicia *et al.,* 2021). All NTs and proneurotrophins interact with p75NTRs, whereas only mature NTs bind to Trk receptors.

GFLs are activated in various tissues and bind to receptors on target cells to regulate development, survival, and differentiation (Leal-Galicia *et al.,* 2021). GFLs are also initially produced in a precursor form that undergoes proteolytic cleavage. Examples of

GFLs include GDNF, neurturin, artemin, and persephin. GFLs conduct their signals via binding to RTKs, however they are only activated if they are initially bound to GFRα receptors, which include four types (GFRα1-4). GDNF binds to GFRα1 and subsequently forms a complex which includes RET. GFLs are involved in the survival, differentiation, and migration of cells within various tissues. Importantly, GDNF is crucial for survival of DA neurons in the adult brain (Leal-Galicia *et al.,* 2021).

1.5.8. Notch signalling

The Notch signalling pathway can provoke both the maintenance and differentiation of NSCs (Delgado-Garcia & Amorim, 2016). When the Notch receptor Delta is activated, the Notch intracellular domain (NICD) transports to the nucleus and forms a complex with the DNA-binding protein RBPJK and coactivator Mastermind-like (MAML). In the adult neurogenic regions, RBPJK inhibition augments cell proliferation, as adult quiescent NSCs progress into rapidly-dividing transit-amplifying progenitor cells. The study proposed that the NICD-RBPJK-MAML complex enables expression of several bHLH transcriptional repressors such as HES1/5/3 (Imayoshi *et al..*, 2010). Such HES factors have been found to bind specific DNA regions to restrict the expression of several pro-neural genes, including ASCL1/MASH1, and NGN2 (Imayoshi *et al.,* 2010; Imayoshi *et al.,* 2013; Kageyama, Shimojo, & Imayoshi, 2015). Interestingly, the activation of these genes causes an activation of Notch in neighbouring cells, which halts their neuronal differentiation. This *lateral inhibition* occurs so that the simultaneous differentiation of NSCs is repressed, and the adult neurogenic niche is maintained (Imayoshi *et al.,* 2010). Hence, Notch signalling activation in early phases is important to inhibit expression of pro-neural genes to allow the neural population to proliferate and expand to sufficient numbers (Wen, Li & Liu, 2009).

A coordinated activation of Notch and WNT signalling supports the maintenance of the NSC population for effective neurogenesis, whereas inactivation of Notch causes a premature neuronal differentiation, thus diminishing the NSC population (Delgado-Garcia & Amorim, 2016). In a study by Das *et al.*, ESCs were prompted with activation of Notch signalling for six hours on day 3 of their neural induction, which led to significantly increased proliferation (2010). This effect is postulated to come about because Notch signalling activates cyclin D1 expression. In fact, a decreased cyclin D1 expression was found when Notch signalling was inhibited (Das *et al.*, 2010).

1.6. Small Molecules

Several naturally-occurring small molecules selectively act on developmental pathways to elicit specific cellular responses (Liu *et al.,* 2018). Thus, they can be used to bring about differentiation of stem cells within a chosen cell lineage and towards the cellular stages so desired. By changing the applied concentrations of small molecules, one can effectively manage their effects on cells to control their fate and differentiation (Liu *et al.,* 2018). Small molecules are permeable to the cell membrane, their effects are reversible, and their concentrations may be easily adapted to alter their effects in a practical manner (Qin *et al.,* 2020). Additionally, small molecules can be chemically synthesised, making them a cost-effective treatment. Such advantageous characteristics make them a favourable choice for small molecule cellular reprogramming strategies to be adopted into clinical therapy.

Name	Pathway interactions	Function
Activin A	Homodimer TGF-β superfamily cytokine	Neuroprotective agent, promotes neurite outgrowth and neuronal differentiation.
BDNF	Neurotrophin signalling through various pathways	Supports migration of neuronal cells, dendritic complexity, synaptogenesis, maturation, and plasticity of mature neurons, and serves a neuroprotective role. Specifically enhances survival of DA neurons.
CHIR99021	GSK-3β inhibitor and WNT pathway activator	Induces reprogramming of stem cells and specifies a DA progenitor cell fate. Promotes DA neuronal differentiation.
DAPT	γ-secretase inhibitor which inhibits Notch signalling	Inducer of neural differentiation and supports electrophysiological maturation.
Dibutyryl cyclic-AMP (db-cAMP)	Membrane permeable analogue of cAMP, PKA and CREB signalling	Inducer of neuronal differentiation, neurite outgrowth and neuron survival. Increases dopamine uptake and TH expression in DA neurons and encourages commitment to the DA fate.
FGF8	FGF signalling induces several downstream signalling including MAPK and PI3K/AKT pathways	Promotes specification of midbrain progenitors, and proliferation and differentiation of midbrain NSCs
Forskolin (FSK)	Adenylyl cyclase activator, increases cAMP and activity of protein kinases A/B	Inducer of neuronal differentiation, neuronal fate specification, neuronal morphology and axonal regeneration

GDNF	Neurotrophin signalling through various pathways	Enhances DA neuron survival and differentiation, neurite outgrowth, morphological maturation, and synaptogenesis.
Purmorphamine	Smo receptor agonist/SHH activator	Same as SHH
SB431542/A8301	Inhibitor of TGF-βRI/ALK5, ALK4 and ALK7	Induces reprogramming in stem cells and enhances commitment to neuroectoderm.
SHH	SHH pathway	Promotes proliferation of progenitor cells, DA neural induction of NSCs, and axon path-finding in differentiating DA neuronal cells.
TGF-β3	TGF-β family signalling	NTFs involved in DA neuron survival, neurite outgrowth and neuronal migration. Plays a role in regulating excitatory/inhibitory synaptic balance in DA neurons.
Y27632	ROCK inhibitor	Axon-stabilising, support of neurite outgrowth and neuron survival along neural induction treatment

Table 1.1. A summary table for the effects and pathway interactions of the small molecules and proteins used in the neural differentiation treatments in this study.

1.6.1. N2 and B27

N2 supplement is used in cultures to stimulate neuronal differentiation and morphogenesis, whereas B27 is a cytoprotective supplement that promotes neuronal cell maturation (Morii, Katayama & Inazu, 2020).

1.6.2. SB431542

This small molecule is an inhibitor of ALK4, 5, and 7 (Liu *et al.*, 2018). It inhibits the Activin/TGF-β pathways through preventing phosphorylation of the ALK4, ALK5

and ALK7 receptors (Chambers *et al.,* 2009). This compound has been found and employed in neural induction protocols to enhance reprogramming in stem cells (Liu *et al.,* 2018; Qin, Zhao, & Fu, 2017).

In amphibian models, BMP has been shown to inhibit neural differentiation of the ectoderm, instead promoting epidermal differentiation (Wilson & Hemmati-Brivanlou, 1995; Sasai *et al.,* 1995). In mouse ESCs, BMP signalling was found to inhibit neural induction instead enabling conversion into epidermis cells (Kawasaki *et al.,* 2000; Tropepe *et al.,* 2001; Ying *et al.,* 2003). Overall, such research studies suggest that TGF-β family signalling elicits the mesoderm and endoderm lineages (Vasan *et al.,* 2021). Moreover, as aforementioned, TGF-β/Activin/Nodal signalling perpetuates ESCs pluripotency, in turn preventing them from entering the neuroectoderm lineage (Galiakberova & Dashinimaev, 2020). Thus, this needs to be inhibited in order to allow for induction of the neuroectodermal fate (Vasan *et al.,* 2021). Studies have shown that inhibition of the TGF-β/Activin/Nodal pathway using the SB431542 inhibitor resulted in significant neural conversion of various stem cell types (Chambers *et al.,* 2009; Patani *et al.,* 2009). In another study, inhibition of TGF-β signalling was combined with activation of WNT signalling at early stages of neural induction and brought about considerable neural conversion of fibroblasts (Ladewig *et al.,* 2012).

1.6.3. CHIR99021

The WNT signalling pathway plays a central role in self-renewal and pluripotency reprogramming in pluripotent stem cells through activating expression of WNT target genes (Qin, Zhao, & Fu, 2017). A transcriptional repressor, TCF-3, acts to suppress expression of WNT target genes by binding to DNA at promoter regions of WNT-activated pluripotency genes. CHIR99021 is applied as a potent GSK-3β inhibitor (Wang *et al.,* 2020) that inhibits TCF-3, stopping it from blocking transcription of WNT

pluripotency genes (Qin, Zhao & Fu, 2017). Thus, it is employed to induce reprogramming of stem cells. WNT signalling also regulates expression of TFs related to neuronal differentiation, including neuronal differentiation 1 (NEUROD1) and prospero-related homeobox 1 (Jurkowski *et al.,* 2020). These factors encourage neurite development and dendritic branching. The WNT1 protein has been found to bring about proliferation of mDA progenitors, whilst WNT5a enhances their differentiation (Volpicelli *et al.,* 2020).

In a study by Kriks *et al.,* CHIR99021 was used to produce FP progenitors expressing LMX1a and FOXA2 (2011). The research study found that CHIR99021 treatment was able to stimulate patterning of neural progenitors, and propelled iPSCs to commit to DA neuronal fate. Another study by Xi *et al.,* also found that CHIR99021 treatment in early stages of iPSC differentiation was essential for inducing the midbrain fate (2012). Interestingly, their production of midbrain FP progenitors that were capable of developing into TH-positive DA neurons, was dependent on treatment of the neuronally-induced cells with FGF8 later on in the protocol. This implied that FGF8 is also necessary in pushing mDA neuronal progenitor differentiation (Wang *et al.,* 2020).

1.6.4. SHH and Purmorphamine

SHH is a soluble extracellular signalling protein that has been implicated in several aspect of nervous system development; namely, neuronal differentiation of the ventral forebrain, DA differentiation of the mesencephalon, and proliferation of neuronal precursors contained within the cerebellum (Navarro Quiroz *et al.,* 2018). SHH is one of the main factors in neural patterning of the midbrain FP during embryogenesis (Brodski *et al.,* 2019). In fact, all the factors required to activate SHH signalling are highly expressed in mDA progenitor regions during early neural development (Brodski *et al.,* 2019).

A study demonstrated how addition of exogenous SHH *in vitro* or its overexpression *in vivo*, augmented proliferation of progenitor cells (Lai *et al.,* 2003). In another study, conditional knock-out of *Smo* resulted in significantly diminished production of mDA progenitors and mDA neurons (Blaess, Corrales, & Joyner, 2006). SHH signalling is critical for DA neural induction of NSCs in the beginning stages of neurogenesis, and then later on, contributes to axon pathfinding in differentiated mDA neurons (Brodski *et al.,* 2019). The addition of SHH in neural induction treatments is vital for production of true mDA neurons *in vitro* (Brodski *et al.,* 2019). Purmorphamine is a small molecule Smo receptor agonist (Kim, Jeong, & Choi, 2020), and the Smo receptor is the signal transducer of SHH signalling (Faigle & Song, 2013). Thus, this can be used interchangeably with SHH.

1.6.5. Y27632

ROCK signalling activation has been found in neuroinflammatory processes, in axonal collapse and retraction and thus its inhibition has axon-stabilising effects and endorses neurite outgrowth (Labandeira-Garcia *et al.,* 2019). Furthermore, ROCK inhibition averts DA cell death caused by DA neurotoxins (Labandeira-Garcia *et al.,* 2019). It has been postulated that the neuroprotective and regenerating effects of ROCK inhibitors on DA neurons are manifested through activation of neuroprotective survival cascades and axon-stabilising effects. Y27632 is a ROCK inhibitor small molecule (Liu *et al.,* 2018) and can thus be used to protect stem cells and neurons from apoptosis during their neural differentiation and enhance their survival and neurite outgrowth (Labandeira-Garcia *et al.,* 2019).

1.6.6. FGF8

FGF8, which is an endogenous inducer of embryonic neural differentiation, was found to enhance neural induction of early neural cells along with their self-renewal (Chen *et al.,* 2010). Importantly, and as has been previously delineated, FGF8 is crucial in patterning of the midbrain area; specifically in establishment of the isthmus (Mesman & Smidt, 2020). FGF signalling may exert different effects depending on which stage of differentiation they are applied (Chuang, Tung, & Lin, 2015).

In vitro FGF signalling has been shown to promote proliferation and differentiation of midbrain NSCs (Murphy, Drago, & Bartlett, 1990; Tropepe *et al.,* 1999). Treatment of neural explants with FGF8 was found to elicit mDA neuron differentiation (Ye *et al.,* 1998). FGF treatment of cells in culture can simulate the signalling cascades that occur in embryonic neurogenic development and has thus been applied in mDA neuron differentiation protocols using neural progenitors, ESCs, iPSCs and somatic cells (Kim *et al.,* 2011; Friling *et al.,* 2009; Sánchez-Pernaute *et al.,* 2001). Studies have produced posterior mDA neuronal precursors from ESC-derived ventral midbrain progenitors via the scheduled administration of FGF8, and these mDA precursors produced dopamine-rich grafts that relieved PD symptoms when transplanted in an animal model (Kirkeby *et al.* 2017; Jaeger *et al.,* 2011; Nolbrant *et al.,* 2017). FGF signalling may be incorporated with other signalling morphogens known to be vital in embryonic mDA neurogenesis, such as SHH and WNT, in order to produce cultures of authentic mDA neurons, with diminished numbers of other cell subtypes (Brodski *et al.,* 2019).

1.6.7. Forskolin

FSK is a plant extract (George, Hamblin & Abrahamse, 2019), and an adenylate cyclase activator that is employed to increase cAMP concentrations in the cell (Singh *et al.,* 2020). FSK has been found to enhance neuronal specification and axonal

regeneration. In their study, Singh *et al.*, found that FSK treatment of MSCs augmented neurite length, axonal development, and induced morphological changes towards a neuronal morphology including presence of a distinct nucleus (2020). Moreover, a combination of FSK and bFGF (FGF basic) treatment brought about expression of TFs involved in the survival of DA neurons including NGN2, PITX3 as well as of neuronal and DA genes such as TUJ1, MAP2, DAT and TH (Singh *et al.*,2020).

When FSK brings about increased cAMP levels, it results in the phosphorylation of PKA and B-raf in MSCs (George, Hamblin & Abrahamse, 2019). The MAPK pathway utilises a protein chain which comprises Ras-Raf-MEK-ERK, that conduct signals from RTKs. This MAPK signalling plays a role in stem cell proliferation and differentiation via downstream regulators of cAMP signalling (George, Hamblin & Abrahamse, 2019). The sustained treatment with FSK and growth factors has been found to elevate cAMP and MAPK signalling, and the combination of FSK with bFGF has been proposed as an effective strategy for activating B-Raf and MAPK signalling for neuronal differentiation (George, Hamblin & Abrahamse, 2019).

1.6.8. Activin A

Activins possess a broad spectrum of roles in differing cell types, such that they may regulate cell death, cell proliferation, and cell differentiation (Rodríguez-Martínez, Molina-Hernández, & Velasco, 2012). Activin A is a homodimer TGF-β superfamily cytokine which is involved in neurogenesis in the CNS (Park *et al.*, 2016). This cytokine has been found to promote neuronal differentiation through several pathways (Timmer *et al.*, 2005; Fang *et al.*, 2012). Activin A was found to serve as a NTF in the culture of hippocampal neurons (Iwahori *et al.*, 1997), or as a neuroprotective agent, when it protected hippocampal cells from death in mice exposed to an excitotoxic compound (Tretter *et al.*, 2000). Treatment of the neuroblastoma cell line SK-N-SH with Activin A

prompted significant neurite outgrowth and augmented neuronal marker expression (Suzuki *et al.,* 2010). In their study, Rodríguez-Martínez, Molina-Hernández, & Velasco found that treatment of NPCs with Activin A significantly augmented their neuronal differentiation and expression of β-III Tubulin and MAP2 (2012).

1.6.9. DAPT

DAPT is a γ-secretase inhibitor that functions to indirectly inhibit Notch signalling (Qin, Zhao, & Fu, 2017). Activation of Notch signalling stimulates glial cell differentiation, whereas its deactivation brings about neuronal cell differentiation (Crawford & Roelink, 2007). Thus, DAPT has augmenting effects on neural differentiation. In a study by Zhang *et al.*, out of several other small molecules, DAPT was found to be the most effective, at inducing neuronal conversion of astrocytes to neurons (2015). Additionally, DAPT has been found to aid in electrophysiological maturation of iPSC-derived neurons (Abranches *et al.,* 2009; Borghese *et al.,* 2010).

Activation of Notch signalling prevents differentiation of NSCs by repressing expression of pro-neural TFs, such as NGNs and ASCL1 (Mukhtar & Taylor, 2018). It has been recognised that an activation of SHH signalling and restriction of Notch signalling together, brings about neural differentiation at the neural tube *in vivo*. Thus, Notch signalling must occur for proliferation and expansion of NSC pool in early stages of neural induction, however, this must be inhibited later on to enable expression of pro-neural genes and urge neuronal differentiation (Chuang, Tung & Lin, 2015).

1.6.10. Db-cAMP

Db-cAMP is a membrane-permeable analogue of cyclic-AMP (Kim *et al.,* 2011). It has been shown to have an inductive effect on neuronal differentiation after one week of treatment of adult rat SVZ NSCs (Zahir *et al.,* 2009). Other research studies have

employed db-cAMP for neuronal differentiation of neural stem and progenitor cells towards neurons (Kume *et al.,* 2008; Tojima, Koboyashi, & Ito, 2003). db-cAMP is postulated to conduct its neural effects via the PKA pathway, whose signalling activation brings about increased CREB expression (Kim *et al.*, 2011). The CREB protein is a salient factor in neuronal differentiation, whose effects resemble those of NEUROD1 and include enhancing neurite development and dendritic branching (Jurkowski *et al.,* 2020). Moreover, db-cAMP is a downstream effector of neurotrophin signalling, and is involved in enhancement of axonal regeneration, and neurite outgrowth (Kim *et al.,* 2011).

Db-cAMP has been found to decrease proliferation of human neuroblastoma cells whilst boosting TH activity, increasing cell size, and dendritic arborisation (Mena *et al.,* 1995). Furthermore, db-cAMP treatment of rat midbrain neurons augmented dopamine and TH levels. Their study proposed that db-cAMP treatment protects DA neurons from death, promotes DA differentiation of progenitor cells, as well as enhancing the DA phenotype in immature neurons (Mena *et al.,* 1995).

1.6.11. BDNF and GDNF

Neurotrophic pathways are paramount in the survival of DA neurons (Di Santo & Widmer, 2018). In a study by Di Santo & Widmer, treatment of DA neurons with NTFs increases survival and differentiation of NPCs (2018). GDNF enhances DA neuron survival and differentiation via activation of the RET-receptor complex and the GFRs. Studies have shown that GDNF increases dopamine uptake in foetal midbrain cultures, enhances DA differentiation and increases DA neuronal viability (Lin *et al.,* 1993; Widmer *et al.,* 2000). GDNF is also heavily involved in hippocampal neurogenesis (Oakes *et al.,* 2019), and has been shown to enhance neurite outgrowth, cell survival, and differentiation and maturation of several neuronal populations (Paratcha & Ledda, 2008). A study by Bonafina *et al.,* demonstrated that GDNF is crucial in morphological

maturation and synaptic integration of new neurons in the adult DG (Bonafina *et al.*, 2019).

BDNF is involved in migration of neuronal cells, dendritic complexity, synaptogenesis, maturation, and plasticity of mature neurons (Leal-Galicia *et al.*, 2021). This factor exerts its effects through activation of several pathways, including MAPK, and it brings about an increase in CREB protein (Sun, Qi, & Gao, 2018; Syal *et al.*, 2018). The activation of BDNF-TrkB in immature DG cells has been shown to promote their maturation, demonstrating the crucial role of BDNF in adult hippocampal neurogenesis (Badurek *et al.*, 2020). Moreover, BDNF is central to the early survival phase in the adult SGZ as it prompts proteins engaged in cell survival and migration through its effects on protein kinase C (Jurkowski *et al.*, 2020).

1.6.12. TGF-β3

Survival of mDA neurons *in vitro* and in PD animal models has been found to be significantly regulated by multiple NTFs, including TGF-β2 and TGF-β3 (Arenas, Denham, & Villaescusa, 2015; Meyers & Kessler, 2017). TGF-β2 and TGF-β3 interact with GDNF to enable its signalling (Peterziel, Unsicker, & Krieglstein, 2002). TGF-β and GDNF deficient mice suffered a significant loss of mDA neurons, indicating that these two work in concert together (Roussa *et al.*, 2009; Rahhal *et al.*, 2009). All three TGF-β isoforms have been found to enhance survival of mesencephalic DA neurons, whereby neutralising antibodies against TGF-β impeded their survival (Krieglstein & Unsicker, 1994; Poulsen *et al.*, 1994; Roussa, Farkas, & Krieglstein, 2004).

When both TGF-β2 and TGF-β3 were knocked out in mice embryos, a significant loss of DA neurons was observed (Roussa *et al.*, 2006). Several TGF-β isoforms have been found necessary for induction of axon formation and neuronal migration (Yi *et al.*, 2010) and have been shown to augment neurite outgrowth and numbers (Unsicker *et al.*,

1996). In another study, a loss of TGFβ Receptor 2 in DA neurons was found to reduce axonal growth, and TGF-β signalling was found to encourage dendritic growth and spine formation in DA neurons (Luo *et al.*, 2016). Moreover, TGF-β signalling was found to be pertinent for regulation of excitatory/inhibitory synaptic balance in DA neurons.

1.7. The outcome in terms of cell fate

The neural induction and differentiation protocol assessed in this study is intended to produce mature and authentic DA neuronal cells. The final goal is to define a robust protocol which has the potential to be employed to produce genuine DA neuronal cells as a cell model. Such a protocol could be used on patient-derived MSCs for *in vitro* disease modelling involving drug screening, transcriptomic and proteomic analyses, and gene therapy assessment. Small molecules have been chosen depending on the pathways they affect in order to attempt to direct the MSCs to enter the neuroectoderm lineage, to specify a DA progenitor cell fate, and then differentiate and mature into DA neurons.

1.8. Aims

Primary Aim – To define a fully-characterised DA neuronal differentiation protocol for research and therapeutic purposes. This will entail using small molecule concoctions that modulate cellular pathways involved in the development of DA neurons. In addition, to determine the functionality of the resulting induced-neuronal cells.

Secondary Aims – To explore the post-translational modification (PTM) changes brought about by the neural transdifferentiation treatment.

1.8.1. Objectives

1.8.1.1. Pertaining to fulfilment of the Primary Aim

1. Cell culture and treatment of MSCs along a DA neuronal differentiation protocol comprised of treatment with cocktails of small molecules and proteins.
2. Establish the effects induced by the small molecule treatments on MSCs through Reverse transcription quantitative Polymerase Chain Reaction (RT-qPCR) and Mass Spectrometry (MS) to determine cellular transdifferentiation extent.
3. Assess the functionality of the induced-neuronal cells produced using Enzyme-linked immunosorbent assay (ELISA) to measure dopamine released by the induced neurons in culture.

1.8.1.2. Pertaining to fulfilment of Secondary Aims

1. Investigation of PTMs by means of Western blot.

Chapter 2 Methodology

2.1. Materials

Name	Brand	Catalogue Number
Materials for cell culture and treatments		
Phosphate Buffered Saline (PBS)	Sigma Aldrich	P3813
Dulbecco's Modified Eagle Medium:Nutrient Mixture F-12 (DMEM:F-12)powder		D5523
Ethylenediaminetetraacetic acid disodium salt dihydrate (EDTA)		E5134
PenStrep		P0781
50x B27		17504044
Dimethyl Sulfoxide (DMSO)		276855-2L
Calcium Chloride	Anatar	10241
100x N2 supplement	Thermofisher Scientific	17502048
TrypLE Select		12563-011
100x Glutamax		A1286001
0.2µm filter		564-0020
Y27632	Peprotech	1293823
FSK		6652995
CHIR99021		2520691
A8301		9094360
TGF-β3		100-36E-10UG
Activin A		120-14E-10UG
SHH		100-45
FGF8		100-25A
GDNF		450-10
BDNF		450-02
bFGF		100-18B
SB431542		616464
db-cAMP	Biogems	1698950-50MG
DAPT		2088055-10MG
Materials for investigative techniques and kits		
Protein LOBind tube 1.5mL	Eppendorf ™	022431081
1,4-Dithio-DL-thriethol (DTT) 98%	Alfa Aesar	A15797.06
Trifluoroacetic Acid (TFA) for synthesis	Biochem Chemopharma	301920100
Acetonitrile (ACN)		200122500
Silver nitrate	Sigma Aldrich	209139

Sodium Thiosulphate		1603121000
Nuclear Fast Red		6409-77-4
Aluminium Sulphate		7784-31-8
Oil-red-o powder		OD625
Alcian Blue powder		A5268
NP-40		(IGEPAL CA-630)
Endoproteinase Lys-C (sequencing grade)		11420429001
Iodoacetamide (IAA)		144-48-9
SOLu-Trypsin dimethylated		EMS0005-100UG
Ammonium Hydrogen Bicarbonate	AnalaR ®	21219.292
Sodium Dodecyl Sulphate (SDS)		108073J
Thick Filter Papers (2.45mm, 8.6x13.5)	BIO-RAD Bio-Rad	1703967
4X Laemmli Sample Buffer		L004133A
1000bp molecular ruler		170-8204
Quick Start™ Bradford Protein Assay		5000205
iScript Reverse Transcription Supermix		1708840/1
FIREPol EvaGreen qPCR supermix	Solis BioDyne	08-36-00001
1.1X ReddyMix PCR Master Mix	Thermofisher Scientific	12951258
SeeBlue plus2 Pre-stained Standard protein marker		LC5925
RNeasy ® Mini Kit	Qiagen	74104, 74106
Dopamine ELISA Kit	Labor Diagnostika	BA E-5300R
Dual Mini Slab Electrophoresis Kit	Atto	AE-6450
Human MSC Functional Identification Kit	R&D systems	SC006
StemXVivo Oesteogenic/Adipogenic Base Media		CCM007
Asymmetric Di-methyl Arginine Motif Rabbit mAb	Cell Signalling	13522S
Symmetric Di-Methyl Arginine Motif Rabbit mAb		13222S
Tri-Methyl Lysine Motif Rabbit mAb		14680S
Mono-Methyl Lysine Rabbit mAb		14679S
Di-Methyl Lysine Rabbit mAb		14117S
Mono-Methyl Arginine Rabbit mAb		8015S
Beta Actin		3700T

Table 2.1. The materials used in this study, grouped by cell culture and treatments as well as investigative techniques and kits.

2.2. Experimental Design

Tissue explant culture from umbilical cord (UC) was used to establish a healthy population of MSCs in culture. MSCs were characterised for trilineage differentiation according to ISCT recommendations. Both cord extraction and characterisation of MSCs were conducted by other researchers in the laboratory since these techniques do not fall within the scope of this project. A neural induction treatment strategy has been devised using a protocol that was previously investigated as an undergraduate research project. The protocol was updated, and several other small molecules have been adopted into the treatment strategy after researching current literature. The small molecule transdifferentiation treatment was composed of 3 treatment stages, each with different small molecule combinations (Section 2.3.1.3. defines such stages and their composition). Treated cells were collected at various stages along their neural induction for indication of the success of the treatment strategy via their extent of neuronal differentiation (Fig. 2.1).

PCR was employed as a quantitative technique to assess changes in expression of a panel of neural markers that are significant along the differentiation process. This involved Ribonucleic Acid (RNA) extraction and complimentary DNA (cDNA) production from differentiated cells. MS was selected as a technique to further investigate the success of the small molecule transdifferentiation treatment strategy. The proteins that were expressed in the induced neuronal cells (Stage 3), vs the starting cells (MSCs) were investigated as an indicator of transdifferentiation success in the cells as brought about by the devised protocol. Proteins were extracted from treated and untreated cells, processed for MS and then sent abroad for identification of the main proteins within samples. An ELISA was another technique utilised for assessment of neural induction efficacy. The ELISA assessed the levels of dopamine released by the neuronally-induced

cells, as an indication of the function and maturation extent of the final cells. Thus, deductions on the success of cellular treatments are based on changes in cellular morphology and characteristics towards those of neurons, including expression of neuronal proteins. Western blotting was used as another method to explore changes occurring in the cells along their treatment, in terms of PTM changes. This involved protein extraction from differentiated and untreated cells, separation of extracted proteins using Polyacrylamide Gel Electrophoresis (PAGE), electroblotting, and incubation with methylation antibodies.

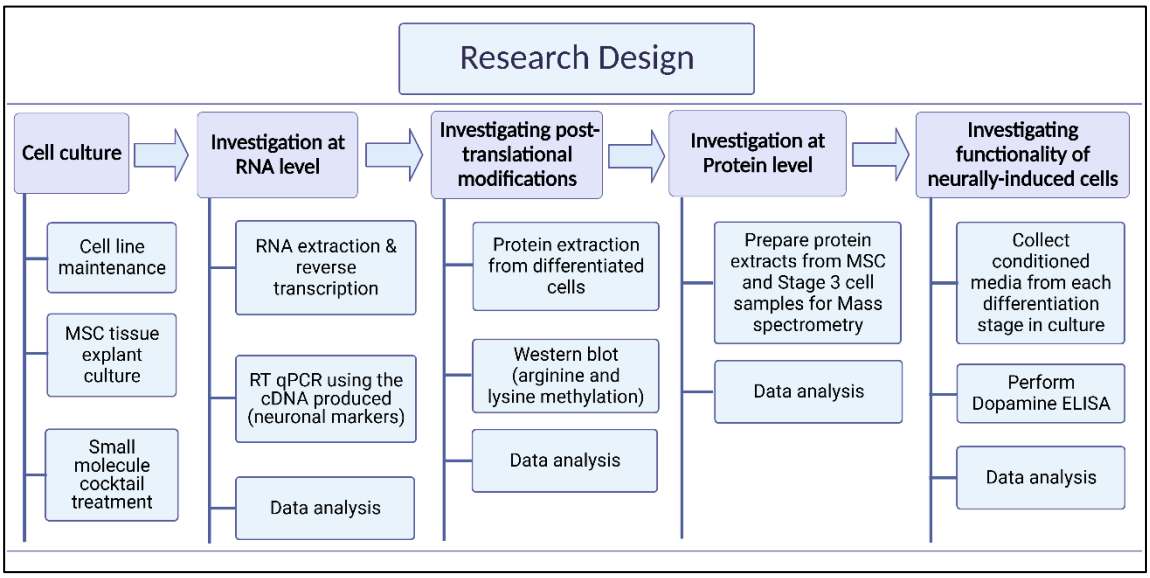

Figure 2.1. A flowchart illustrating the research design of this project. The main objectives can be found within purple boxes. For each, the main steps can be found within blue boxes.

2.3. Cell Culture

2.3.1. Media Preparation

2.3.1.1. Basal Media

1 L of basal cell culture medium was first prepared and then used in aliquots for individual cell treatment experiments. Dulbecco's Modified Eagle Medium:F-12 (DMEM:F-12) was used as the culture medium. All medium preparations were conducted in a Class II safety cabinet (SafeFAST Elite, Faster S.r.l.), under aseptic conditions. The

medium was reconstituted from lyophilised constituents by diluting 12 g of DMEM:F-12 powder and 1.2 g of $NaHCO_3$ in 1 L of sterile distilled water. This mixture was then thoroughly stirred and passed through a 0.2 μm filter. Stock medium was stored at 4 ºC until required. The MSC/induced cells basal media constituted 20 % human plasma (200 μL/ml); PenStrep (1:100 dilution or 10 μL/ml); 1x B27 (1:50 dilution or 20 μL/ml); 1x N2 (1:100 dilution or 10 μL/ml); 1x Glutamax (1:100 dilution or 10 μL/ml); 10 μM Y27632 (1:1000 dilution or 1 μL/ml) in an aliquot of DMEM:F-12.

2.3.1.2. Human Plasma Collection and Preparation

The basal medium was also supplemented with 10 % cryo poor plasma (CPP). This was prepared using human plasma obtained from the National Blood Transfusion Services Malta (see Appendices, ethics Ref. no. 90/2016). Human plasma was used as a replacement serum instead of Foetal Bovine serum to enable xeno-free cell culture conditions whilst still providing the necessary nutrients for cells in culture. Under aseptic conditions, 2 mg/ml of calcium chloride ($CaCl_2$) was added to a given plasma bag, gently mixed and then this was placed in a Transfer Bag and incubated at 37 ºC for 3 hour minimum. The application of $CaCl_2$ and heat was used to promote coagulation and precipitation of factors contained in the plasma. The resulting portion of uncoagulated plasma was poured into several 50 mL centrifuge tubes and stored at -20 ºC. When needed, a tube was taken out of storage and thawed at 37 ºC and then centrifuged for 10 minutes at 1000XG.

2.3.1.2. Small Molecule Stock solutions

Stock solutions were prepared for all media supplements and small molecules used for treatments. Such stock solutions were prepared keeping in mind the final working concentrations that were needed for treatments. When preparing cell treatments, an appropriate volume of each stock solution was added to a volume of DMEM:F12 in order

to produce the final working concentration for each additive. Stock solutions were prepared as follows.

Composite	Stock
A8301	2.5 mM stock solution – 1.05 mg per mL of DMSO
Activin A	0.76 nm stock solution – 20 µg per 1 mL of sterile deionised water
B27 supplement	50X stock solution
BDNF	3.57 nM stock solution – 0.1 mg per mL of sterile deionised water
CHIR99021	2 mM stock solution – 0.931 mg per mL of DMSO
DAPT	10 mM stock – 10 mg per mL of sterile deionised water
db-cAMP	500 mM stock solution – 246 mg per mL of sterile deionised water
FGF8	0.1 mg per mL of sterile deionised water
FSK	50 mM stock solution – 20.53 mg per mL of absolute ethanol
GDNF	3.3 nM stock solution – 0.1 mg per mL of sterile deionised water
Glutamax	left as a 100X stock solution
N2 supplement	left as a 100X stock solution
Purmorphamine	2 mM stock solution – 1 mg per mL DMSO
SB431542	2.5 mM stock solution – 0.96 mg per mL of absolute ethanol
SHH	0.1 mg per mL of sterile deionised water
TGF-β3	0.04 nM stock solution – 1 µg per mL of acetic acid in sterile deionised water
Y27632	10 mM stock solution – 3.2 mg per mL of sterile deionised water.

Table 2.2. Showing how stock solutions for each media composite were prepared. The stock solution concentration is shown, along with the amount of each composite per mL diluent.

2.3.1.3. Complete Media

Small aliquots of complete medium were prepared prior to treating cells in culture. The chosen volume to prepare depended on how many wells of MSCs or neurally-induced cells were to be treated (i.e., 5 mL if 5 wells were to be treated so that 1 mL was added per well). Complete media was composed of the basal medium (as shown below; DMEM:F12 with several additional supplements), together with the addition of small

molecules or proteins depending on the stage of neural treatment. The volume of each additional ingredient was decided upon based on the dilution factors required to achieve the final concentration from the small molecule stock solutions. Such small aliquots were freshly prepared prior to each cell culture treatment. The media components and concentrations of each composite for each stage of treatment are defined below:

Basal Medium

1. DMEM:F12
2. N2 – 1:100
3. B27 – 1:50
4. GlutaMAX – 1:100
5. PenStrep – 1:100
6. Ampicillin – 1:100
7. Heparin – 1:1000
8. Human serum (cryo-poor plasma) – 1:10

Proliferation and Induction Medium (days 1-7)

1. SHH – 250 ng/ml
2. Y27632 – 10 µM
3. CHIR99021 – 2 µM
4. SB431542 – 2.5 µM

Differentiation Medium (days 7-14)

1. FSK – 50 µM
2. SHH – 250 ng/ml or Purmorphamine – 2 µM
3. FGF8 – 100 ng/mL
4. Activin A – 20 µg/ml
5. DAPT – 10µM

6. db-cAMP – 500µM

Maturation Medium (days 14-28)

1. BDNF – 20ng/ml
2. GDNF – 20ng/ml
3. TGF-β3 – 1ng/ml
4. db-cAMP – 500µM
5. DAPT – 10µM
7. Activin A – 20µg/ml

2.3.2. Mesenchymal Stem Cells

2.3.2.1. Sample Collection

Primary MSC cell cultures were generated by tissue explant culture from UC tissue. A UC sample was collected from a healthy donor after delivery by caesarean-section and transported to the laboratory in a sterile PBS solution. The cords were obtained from donors within the Obstetrics and Gynaecology Department at Mater Dei Hospital, Malta. These samples were obtained by researchers conducting a different study in which informed consent was obtained from pregnant donors prior to sample collection. A copy of the ethics declaration (Ref no. 90/2016) for the mentioned study has been included in the appendices.

2.3.2.2. MSC Extraction and Culture Initiation

Once at the lab, operating inside a laminar flow hood, the UC was taken out from the PBS solution and washed thoroughly with 70 % ethanol solution to remove residual blood. Ethanol was removed after washing briefly for one minute since its prolonged exposure could cause a loss of cell viability. The cord was washed again with PBS three times over to ensure that any traces of debris or alcohol would be removed. The vascular and endothelial tissue components were removed from the Wharton's jelly (WJ) which

was retained. The WJ was subsequently divided, using a scalpel, into small pieces around 1.5 cm in length. Each tissue piece was individually rewashed carefully using forceps to squeeze and discard blood within the blood vessels in the WJ. Each piece was then transferred into its own well in a 12-well plate. The ability for MSCs to migrate enables them to exit from the tissue and establish themselves on the cell culture flask or well surface. The tissue pieces were allowed to stand for 10 minutes to enable them to adhere to the new surface. Approximately 1.5 mL of media was added to each well and then the plate was placed in an incubator at 37 ^{o}C in a 5 % CO_2 humidified atmosphere for MSCs to expand in their new environment. The cell culture medium was composed of DMEM:F12, N2 1:100, B27 1:50, GlutaMAX 1:100, Penstrep 1:100, Amphotericin 1:100, and 10 % cryo-poor plasma obtained from human plasma.

The first media change was carried out one week later, when only half of the media was removed and replaced so that some growth factors that are released by the tissue are retained, whilst still replenishing media nutrients and removing cell debris. This was repeated once a week for 3-4 weeks, until cells reached their confluency. After the first week, the ROCK inhibitor Y27632 was added to the media to prevent cell apoptosis and enhance cell viability. Morphological appearance of MSCs was assessed and followed using the laboratory microscope.

2.3.2.3. Trilineage differentiation

Multipotency of MSCs in culture was assessed by trilineage differentiation, carried out using the Human MSC Functional Identification Kit. Adipogenic and osteogenic media were composed of StemXVivo osteogenic or adipogenic base media, 1% PenStrep, and either osteogenic or adipogenic supplement at a 1:20 dilution. Chondrogenic medium was composed of DMEM:F12, 1 % PenStrep, 1 % ITS supplement and 1 % chondrogenic supplement. The MSCs were cultured until they appeared to reach a confluency of around

40 %, and then 6 individual wells (2 wells per cell differentiation type) were treated using osteogenic, adipogenic and chondrogenic differentiation medium. MSC differentiation medium was changed every 4 or 5 days, and for 21 days the cells were incubated at 37 ºC and 5 % CO_2. After the 21 days had elapsed, all wells were washed with 500 µL PBS and fixed with 500 µL Tokuda-Baron Fixative (Tokuda *et al.*, 2018). After 15 minutes with the fixative, the cells were washed twice over with another 500 µL PBS. Then, the von Kossa staining method was used to detect calcification matrices formed in osteocytes in culture, Oil-red-O staining was used to detect lipid vacuoles in the adipocytes, and Alcian Blue staining for detection of glycosaminoglycans in cartilage within chondrocytes.

2.3.2.3.1. Von Kossa staining

Several solutions were prepared before starting. First, a 1 % silver nitrate solution which contained 1 g silver nitrate powder in 100 mL distilled water; a 5 % sodium thiosulphate solution which was composed of 5 g sodium thiosulphate in 100 mL distilled water; and a 1 % Nuclear Fast Red solution which contained 0.1 g nuclear fast red and 5 g aluminium sulphate in 100 mL distilled water. Cells were stained using 500 µL of 1 % silver nitrate solution and kept under ultraviolet light for 20 minutes. Next, cells were washed using 500 µL distilled water 3 times over, and then treated with 500 µL of 5 % sodium thiosulphate for 5 minutes to expel any excess silver. The cells were washed for another 3 times with distilled water and then stained with 1 % Nuclear Fast Red solution for 5 minutes and then rinsed again. Finally, 500 mL distilled water was added to the wells and cells were viewed under the microscope to visualise calcium deposits that were stained brown-black.

2.3.2.3.2. Oil-Red-O staining

Before beginning the staining, a stock solution of 3 % oil-red-o was made to contain 0.30 g oil-red-o powder in 100 ml 2-propanol. For staining cells, this was further diluted

with distilled water at a ratio of 6:4 and filtered with a 0.2 µm filter. Next, cells were stained using 500 µL of diluted oil-red-o for 15 minutes. Then the oil-red-o was removed, and wells were washed with 500 µL distilled water. To view cells under the microscope, another 500 µL of distilled water was added on top of the cells, and they were examined for the presence of red lipid vacuoles.

2.3.2.3.3. Alcian Blue Staining

A stock solution of Alcain blue was prepared to contain 100 mg Alcian Blue powder in 60 mL ethanol and 40 mL acetic acid. This was diluted in distilled water at a ratio of 1:3 and 500 µL was added on top of the cells and left to stain for 15 minutes, after which the wells were washed with distilled water. 500 µL of distilled water were added to the cells and they were examined under the microscope for glycosaminoglycans.

2.3.2.4. Sub-culturing of MSCs

Sub-culturing is used to replenish used growth medium so that cells in culture are provided with an optimal environment and are enabled to grow and propagate further. Since MSCs are adherent cells, they cannot grow properly when the cell culture surface is densely occupied. Hence, sub-culturing is a pertinent aspect of their cultivation, since it allows for the cells to grow at their optimal density, with sufficient space and growth media for them to proliferate in their culture.

Cell culture work was always carried out in a laminar flow hood, and each solution and piece of equipment used was sterilised using 70 % ethanol. Each week, half of the media was removed from the culture and discarded, and then half of the media was replenished with fresh media. The MSCs were first subject to a pre-wash using their old media. In cases where a lot of debris had collected over the week, the cells were instead washed with PBS.

Usually within 3-4 weeks MSCs would have grown substantially, and colonies can be seen under the microscope. Once the required confluence (minimum 50 %) was achieved, tissue pieces were removed from the individual flasks and MSCs were sub-cultured as follows. The pre-wash fluid was discarded and approximately 2 mL of TrypLE was added to the culture to detach the cells. TrypLE was used in preference to trypsin since it is a less potent form of trypsin and MSCs are highly sensitive to stress. The plate was left in the incubator for 3 minutes with TrypLE at 37 ^{o}C and 5 % CO2. Cells were again visualised under the microscope to assess whether they had successfully detached. Once they detached, 4 mL of complete medium was added, and the cells were redistributed by re-aspiration of media over the entire culture surface. The suspended cells were then transferred to 15 mL conical tubes and centrifuged at 1200 rpm for 5 minutes. The resulting supernatant was removed, and 3-4 mL of fresh complete medium was added to the tube and the cell pellet was again resuspended. The resuspended cells within the tube were then removed and added to the original MSC well. If cells were highly confluent, after centrifugation, half of the suspension was returned to the original well and half placed in a new well.

2.4. Treatment of MSCs with small molecules

When MSCs in culture reached a confluency of at least 50 % the cells were ready to be treated with small molecules. In Fig. 2.2, the small molecules treatment is illustrated. This treatment was divided into 3 individual media stages, each having a unique combination of small molecules. Small molecule concentrations can be found in Section 2.3.1.3. As can be seen in Fig. 2.2., the first stage was applied to the MSCs on days 1-7 and served as a Reprogramming and Induction Media to promote the progression of MSCs towards the neuroectoderm and to increase cell numbers. Next, the Differentiation Media was applied from days 7-14 and served to push NSCs further along the neuronal

lineage and towards an immature neuronal stage. Finally, the Maturation Media was added on days 14-28 and served to push the induced immature neurons towards maturity. Throughout the small molecule induction treatment, the media was changed every 3-4 days and included basal media components (Section 2.3.1.3) as well as the small molecules specific to each stage.

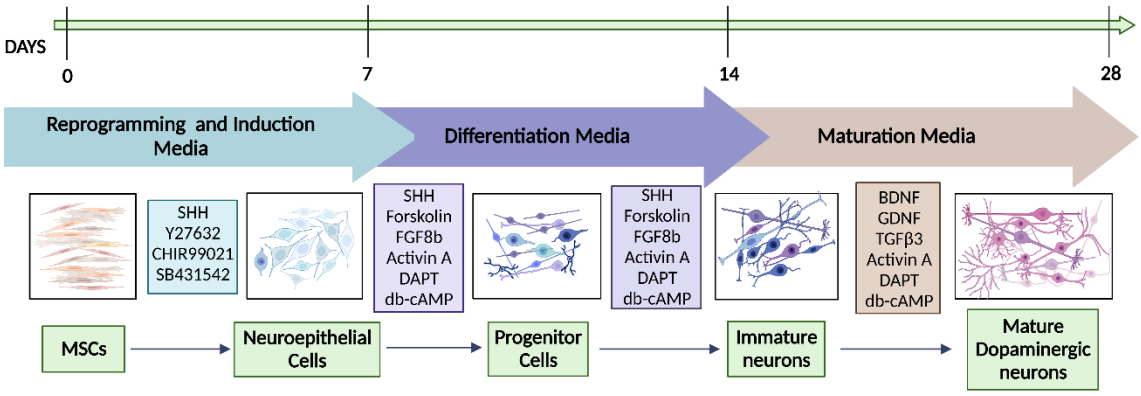

Figure 2.2. A flowchart depicting the 3 stages of the small molecule treatment. The purpose and title of each stage media can be found within the arrows, whilst the composites making up each stage media can be found within boxes. Blue represents Stage 1, purple represents Stage 2, and brown represents Stage 3. The boxes in green define the differentiation stages that cells were expected to reach and go through with each stage of treatment. Above, a timeline showing the days elapsed for each stage can be seen, with a total of 28 days.

2.4.1. Cell collections and freezing for storage

Stages 1, 2 and 3 cells were dislodged from the culture flask surface with 2 mL of 2 mM EDTA in PBS, and allowed 3 minutes, tapping the plate gently to encourage the cells to dislodge. The cells were then neutralised with 2 mL complete DMEM, collected and transferred into a 1.5 mL microcentrifuge tube, after which they were centrifuged at 250 XG for 5 minutes. The supernatant was discarded, and the cell pellet resuspended in 1 mL of PBS. The cells were centrifuged again at 250 XG for another 5 minutes (to ensure no residual EDTA solution would remain), and just as before, the supernatant was discarded. The cell pellets were then stored at -20 ^{o}C until they were needed for PCR, MS

or Western blotting experiments. For MSCs, the same procedure was used, except that TrypLE was used instead of EDTA.

2.5. Microscopy

Cells were observed under the microscope continuously throughout their neural induction. This was done to ensure that cells were healthy and viable along their treatment, to assess confluency of the cells, and importantly, to visualise changes in the morphology of the cells as they progress towards neurons. Cells were visualised using the Nikon Eclipse Ti-2u Inverted Microscope at a magnification of x100 and x200 (x10 eyepiece and x10/x20 lens). Photos of the cells were captured at each media change (every 3 days) so that any subtle changes on cell morphology were documented for examination.

2.6. PCR

2.6.1. RNA extraction from cells

RNA extraction was carried out using the Qiagen RNeasy Mini Kit. The cells used for RNA extraction included MSCs, and induced cells from stages 1, 2, and 3. First, the cells were taken out of storage and thawed at room temperature (RT). The cells were washed with PBS and then cell lysis was performed by adding 300 µL of the RNA Lysis Buffer RLT to the cells, and the pellet was dislodged. The mixture was vortexed and then passed through a 20-gauge needle (0.9 mm diameter) attached to an RNase-free syringe 5 times over to ensure proper sample disruption and homogenisation.

Next, 1 volume of 70 % ethanol was added to the lysate and mixed. The mixture was transferred to the RNeasy spin column contained within a 2 mL collection tube. This was then centrifuged at 8000 XG for 15 seconds. The flow-through liquid was discarded and 700 µL of the Buffer RW1 was added to the spin column. This was centrifuged again at 8000 XG for 15 seconds. The flow-through liquid was discarded again. Next, 500 µL

of Buffer RPE was added to the spin column. This was centrifuged again at 8000 XG for another 15 seconds. Another 500 µL of Buffer RPE were added to the spin column, and this was centrifuged again at 8000 XG for a period of 2 minutes. The spin column was retrieved and placed in a new 1.5 mL collection tube. 40 µL of RNase-free water was then added directly to the spin column membrane, and this was centrifuged at 8000 XG for 1 minute to elute the RNA. The eluate was reused and added to the spin column membrane, and the centrifugation step was repeated to ensure that all the RNA had eluted. Resulting mRNA concentrations were measured using the Eppendorf BioPhotometer (Eppendorf®, Germany). A 1:50 dilution of the RNA extract was prepared by diluting 2 µL mRNA in 98 µL sterile deionised water, and absorbance at 260 nm was measured. Knowing the RNA concentration was necessary to determine the ratios of reaction components for reverse transcription.

2.6.2. Reverse Transcription of RNA and cDNA production

cDNA synthesis was carried out using the iScript Reverse Transcription Supermix Kit. The kit was stored at -20 ^{o}C until needed, when all kit components were thawed at RT and RNA thawed on ice. Total RNA concentration was checked using the Bioanalyser to determine what volume of RNA template would be needed in the reaction so that it was within the recommended concentrations of 1 µg-1 pg. Next, 16 µL of RNA template were added to a labelled reaction tube with 4 µL of iScript Supermix for a total of 20 µL. This was the complete reaction mix and was thus incubated in the thermocycler according to the followed protocol: priming occurred at 25 ^{o}C for 5 minutes, reverse transcription at 46 ^{o}C for 20 minutes, and RT inactivation at 95 ^{o}C for 1 minute.

2.6.3. Primer Design

Primers used for both end-point PCR and RT-qPCR were already available in the lab. These were previously designed in-house and used for related research. For their design, the recommended primer criteria were followed. These include: (1) each primer is an average length of 18-24 bases, (2) the primer G/C content is between 40-60 %, (3) primers start with 1-2 G/C pairs, (4) their melting temperatures (Tm) fall between 50-60 ^{o}C, (5) primer Tms fall within 5 ^{o}C of each other, and lastly (6) primer pairs do not have complimentary sequences (Addgene Inc., 2018)

2.6.4. End-point PCR procedure for CD markers

End-point PCR was used to determine characteristic CD marker expression in MSCs, and to investigate whether CD markers expression was retained as the cells proceeded along the neural treatment. First, a PCR reagent mix was prepared in a PCR tube for each of the 3 CD markers, and contained 9 µL of the PCR Reddy Mix, 0.25 µL of 10 µM reverse primer, and 0.25 µL of 10 µM forward primer. Next, 0.5 µL of the template cDNA was added to the PCR reagent mix, giving a total volume of 10 µL.

The tubes were placed in the Eppendorf Mastercycler (Eppendorf®, Germany) thermocycler with pre-programmed conditions. The initial denaturation step (performed once at the beginning) was set at a temperature of 95 ^{o}C for 5 minutes, the denaturation step was set at 95 ^{o}C for 15 seconds, the annealing step set at 50 ^{o}C for 30 seconds, and the extension step was set at 72 ^{o}C for 30 seconds. The PCR was set to cycle for 35 times. A final extension step was conducted at 72 ^{o}C for 1 minute. Once the procedure was completed, the PCR tube was retrieved, and the sample was used to perform gel electrophoresis to visualise and determine which CD markers were expressed in each of the cell extracts.

Gene Name	Primer Sequence 5' to 3'	Tm in ºC
CD90	F: TGCTCTTTGGCACTGTGG R: AGAGGGAGAGCAGGAGCAG	F: 55.7ºC R: 58.7ºC
CD105	F: GGGGTCAACACCACAGAG R: CAGGACCCTCAGGATGTG	F: 55.5ºC R: 54.8ºC
CD166	F: AGGAAATGGACCCAGTGAC R: CCCCTTCTTTGATGGCA	F: 54.5 ºC R: 52.2 ºC

Table 2.3. Showing the primer sequences and melting temperatures for the CD markers tested with end-point PCR. Both forward and reverse primer sequences are shown for each, and their respective primer Tms (in ºC).

2.6.5. Gel Electrophoresis

After end-point PCR the amplified DNA fragments were separated using gel electrophoresis. A 1 % gel was used to confirm the presence or absence of DNA fragments pertaining to 3 CD markers in cell samples. First, 0.5 g of agarose was dissolved in 50 mL 1x Tris-acetate-EDTA (TAE) buffer prepared from 10x TAE Buffer (40 mM Tris, 20 mM acetate, 2 mM EDTA, pH 8.1). After dissolution, 1 µL ethidium bromide was added to this mixture, and mixed further. This was then poured into the mould and the well comb fixed on top. Once the gel had solidified, the comb was removed and the mould with the gel was placed inside the electrophoresis tank. Next 1x TAE buffer was poured into the tank until the gel was completely covered. A1000 bp molecular weight marker was loaded into the first lane of the gel, and 5 µL of each PCR product were loaded, each in an individual well. The electrophoresis chamber was closed, and the power supply was set at a voltage of 50 V and current of 200 mA. This was left to run for approximately 20 minutes. Once completed the gel was removed from the tank and viewed on a transilluminator to visualise the bands of the PCR products.

2.6.6. Reverse transcription quantitative Polymerase Chain Reaction for stemness and neural markers

Before beginning anything, the PCR set-up was prepared on excel to determine how many genes and samples would be run. Next, the template cDNA, primers and 5X EvaGreen qPCR Supermix were taken out of storage (-20 ºC) and thawed at RT.

PCR tubes were prepared for each gene for each sample tested with appropriate labels. Next, a Master Mix reaction tube was prepared for each gene, to contain the total amount needed for 10 reactions (for 8 cell samples). For each gene, 2.0 µL of EvaGreen qPCR Supermix, 0.5 µL of both forward and reverse primers for the given gene, and 6.0 µL nuclease-free water were added to the respective tube (with each component x10 per gene reaction mix). Next, 9.0 µL of each gene reaction mix were added to the appropriate PCR tube (1 for each cell sample type for each gene), and then 1.0 µL cDNA was added for a total of 10.0 µL. Each qPCR mix was set up for every gene marker in duplicate and with 1 No Template Control (NTC, made up to 20 µL without cDNA) mix for each gene. Next, the PCR tubes were vortexed briefly (Whirli Mixer – SGP-202-010J), and then placed into the Rotor-Gene Q (Qiagen, Netherlands). The program was set for an initial denaturation at 95 ºC for 15 minutes, followed by a repeated denaturation (94 ºC for 20 seconds), annealing (50 ºC for 20 seconds) and elongation (71 ºC for 30 seconds) program for 40 cycles. This was followed by a high-resolution melt (HRM) increasing at 1 ºC/0.5 s from 50-90 ºC.

Gene Name	Primer Sequence 5' to 3'	Tm in ºC
SOX2	F: CAAGATGCACAACTCGGAGA R: GGGCAGCGTGTACTTATCCT	F: 54.9 ºC R: 56.9 ºC
MASH1	F: GAACTGATGCGCTGCAAACG R: CATGCTCGTCCAGCAGCTGC	F: 57.7 ºC R: 61.6 ºC
TUBB3	F: GGAGATCGTGCACATCCAG R: TCGAGGCACGTACTTGTGAG	F: 55.6 ºC R: 56.8 ºC
NEUROD1	F: TAAATTGAGACGCATGAAGG R: GGTGGTGGGTTGGGATAAGC	F: 50.4 ºC R: 58.4 ºC
NEUN	F: TGTACACACCAGCACAGACC R: CGAACATTTGCCGCAAGTCG	F: 57.2 ºC R: 57.6 ºC
MAP2	F: ATACAGGGAGGATGAAGAGG R: GGAGAAGGAGGCAGATTAGC	F: 53.0 ºC R: 54.9 ºC
TH	F: GTTCATTGGGCGCAGG R: CTAGATGGTGGATTTTGGCT	F: 54.4 ºC R: 52.3 ºC

Table 2.4. Showing the primer sequences and melting temperatures for the neural markers tested with RT-qPCR. Both forward and reverse primer sequences are shown for each, and their respective primer melting temperatures (in ºC).

2.7. Polyacrylamide Gel Electrophoresis and Western Blotting

Prior to beginning any steps of the Western blotting experiments, several reagent solutions were prepared.

Buffer/Reagent	Composition
10% Ammonium persulfate (APS)	0.1 g APS powder in 1.0 mL sterile deionised water
5% Blocking Buffer	2.5 g sodium caseinate salt in 50.0 mL of 1X Tris Buffered Saline (TBS)
1M Tris Base	18.2 g Trizma ® Base powder in 100.0 mL sterile deionised water, with pH adjusted to 8.8
10X Running Buffer	30.0 g Tris Base, 144.0 g Glycine, 10.0 g SDS in 1.0 L of sterile deionised water

10X Transfer (Towbin) Buffer	3.0 g Trizma base powder, 14.4 g glycine, 100.0 mL methanol in 1.0 L sterile deionised water and adjusted to a pH of 8.3
10X TBS	24.0 g Tris Base, 88.0 g NaCl, dissolved in 1.0 L sterile deionised water. The pH was adjusted to 7.6
1X RIPA Lysis Buffer	1.5 mL 5 M NaCl, 0.5 mL 0.5 M EDTA (pH 8.0), 2.5 mL 1 M Tris (pH 7.4), 0.5 mL NP-40, 2.5 mL 10% sodium deoxycholate, 0.5 mL 10% SDS, 42 mL deionised water

Table 2.5. Showing the composition and concentrations of various reagents used for PAGE.

2.7.1. Protein Extraction

Cells that had been collected from MSC cultures, small molecules stages 1, 2, and 3 (SM1, SM2 and SM3) as per section 2.4.1., were used for protein analysis. The cells were first allowed to thaw and then they were lysed using the RIPA buffer. First, 1X RIPA buffer was added to the cell pellet at a concentration of 10 µL per µg mass of cells. The cell pellet was dislodged, and the contents were mixed by pipetting, and vortexed briefly. Samples were then placed in refrigeration at 4 ^{o}C for 20 minutes and then sonicated at 50 Amps for 10 seconds (Q55 Probe Sonicator – Qsonica 4422). Samples were then centrifuged at 20,000 XG for 10 minutes. The supernatant was transferred to a fresh tube to quantify the protein concentration using the Bradford Assay (Section 2.7.2.).

2.7.2. Bradford Assay

The Bradford Assay was used to generate a standard calibration curve for Bovine serum albumin (BSA) to quantify protein extract concentrations. The 1X Bradford Reagent was retrieved from refrigeration and left to stand at RT for 5 minutes. A 1:4 dilution was made by adding 200 µL of 1X Bradford Reagent to 800 µL of sterile deionised water. A BSA solution was prepared using 2 mg BSA in 1 mL sterile deionised water. The BSA solution was then used to prepare 3 dilutions for the standard calibration

curve. These included 0 µg/µL, 2 µg/µL, and 4 µg/µL dilutions made by adding 0 µL, 1 µL, and 2 µL of the 2 mg/mL BSA solution in 2 µL, 1 µL, and 0 µL of sterile deionised water, respectively.

Cell lysate solutions were prepared for spectrophotometry by adding 2 µL of protein extract into 0.5 mL microcentrifuge tubes with 98 µL of the diluted Bradford Reagent (1:50 dilutions). A blank sample was prepared to contain 2 µL Urea Lysis Buffer in 98 µL of diluted 1X Bradford Reagent. Diluted protein samples were left at RT for 10 minutes, then vortexed briefly and transferred to plastic cuvettes. The spectrophotometer was blanked, the absorbance of each BSA dilution and sample were measured against the black at a wavelength of 595 nm. A standard calibration curve was formulated by plotting the absorbance values on the y-axis against their respective BSA concentrations on the x-axis. The line of best fit as constructed with its intercept at 0 and the line equation generated for the standard curve was used to calculate protein concentrations for the protein extracts. The volume of protein loaded for each well was calculated using the determined protein concentrations, when 25 µg was the desired protein mass. This was calculated by dividing 25 µg by the resulting protein concentration.

2.7.3. Polyacrylamide Gel Electrophoresis

First, two glass plates were clamped within the casting stands and then an 8 % resolving gel was prepared in a centrifuge tube according to Table 2.6.

8 % Resolving gel		**6 % Stacking gel**	
Reagent	**Volume**	**Reagent**	**Volume**
Deionised water	3.1 mL	Deionised water	3.51 mL
1.0 M Tris-HCl pH 8.8	3.0 mL	1.0 M Tris-HCl pH 6.8	0.75 mL
40 % (w/v) acrylamide	1.6 mL	40 % (w/v) acrylamide	0.63 mL

10 % (w/v) SDS	80.0 µL	10 % (w/v) SDS	50.0 µL
10 % (w/v) APS	80.0 µL	10 % (w/v) APS	50.0 µL
TEMED	10.0 µL	TEMED	5.0 µL

Table 2.6. Showing the composition of the 8 % resolving and 6 % stacking gel. The reagents found within each gel are shown, along with the respective volumes needed.

An appropriate amount of resolving gel solution was added to fill the gap between the glass plates. Approximately 200 µL of butanol were added on top of the resolving gel to avoid formation of air bubbles. The resolving gel was allowed 20 minutes to polymerise. The butanol was decanted, the gel surface was washed using a pipette with deionised water, and filter paper was used to remove any residue. A 6 % stacking gel solution was then prepared in a centrifuge tube as specified in Table 2.6.

The stacking gel was pipetted above the resolving gel. The 14-well-forming comb was inserted into the fresh stacking gel, acting cautiously to avoid trapping air under the teeth. This was left for 20 minutes to polymerise. This time was used to prepare the samples and sample buffer for electrophoresis. Then, 25 µg of each protein extract were added to an Eppendorf® tube according to the volume that was previously determined with spectrophotometry, together with 5 µL of Laemmli sample buffer and made up to 20 µl with deionised water. Depending on the experimental conditions and the number of antibodies being tested, each protein sample was prepared a different number of times. For example, for the lysine methylation expression tests, 3 protein samples were prepared for 3 blots. The samples were placed in a heating block at 95 ^{o}C for 5 minutes and then micro-centrifuged briefly to collect them at the bottom of the tubes.

Once the stacking gel had polymerised, the glass plates were removed from the casting frame and placed in the electrophoresis chamber. The well-forming comb was removed and the 1X Running buffer (produced by 1:10 dilution of the 10X stock, Table

2.5.) was poured into the electrophoresis chamber to reach its level marking. Blank solutions were then prepared to contain 5 µL 4X Laemmli Buffer in 20 µL deionised water. 2 µL of SeeBlue 2 Pre-stained protein marker along with blank samples and prepared protein samples were loaded into appropriate lanes of the stacking gel. Leads were then connected, and electrophoresis was set to run at 200 V for 1 hour. When done, the gel was removed from the chamber and the stacking gel detached and discarded. The resolving gel was then placed in 1X Transfer buffer on a rocker shaker for several minutes.

2.7.4. Electroblotting

Before beginning immunoblotting, the filter papers (4.5 mm) and PVDF membrane were cut, and the membrane was soaked in methanol for 2 minutes. Furthermore, a solution which contained 10 mL 10X Transfer buffer (Table 2.5.), 10 mL methanol and 80 mL deionised water was prepared. The filter papers and membrane were then placed inside this solution on a rocker shaker for 5-10 minutes. Then, 1 of the pre-cut filter papers was placed on the electroblotter (Amersham Pharmacia Biotech) and the PVDF membrane on top of it. The resolving gel was placed on top of the membrane, with the other filter paper on top it. This was covered and the electroblotter was set to run at 100 mA for 1 hour.

When this was done, the membrane was retrieved and separated from filter papers and the gel. The gel was discarded, and the membrane placed in a petri dish with 0.1 % Ponceau S solution to shake for 5 minutes. The membrane was checked for successful protein transfer and then Ponceau S solution was removed through rinsing several times with 1X TBS solution (Table 2.5.). The membrane was placed on the rocker shaker, in a 50 mL centrifuge tube with 20 mL Blocking buffer (Table 2.5.) for 30 minutes. When the time was up, the buffer was discarded, and the membrane washed with 1X TBS for 5

minutes. The membrane was then cut into 2 or 3 pieces depending on how many antibodies were being tested in that experiment. The membranes were placed in individual tubes covered in foil for primary antibody incubation.

2.7.5. Western Blotting

Western blotting was performed on MSC, SM1, SM2, and SM3 cells for methylation antibodies (asymmetrical and symmetrical di-methylated arginine, mono-methylated arginine, mono/di/tri-methylated lysine). Loading controls included alpha-tubulin, beta-actin, and HSP90.

Firstly, 500 mL 1X TBS (antibody diluent solution) was prepared using 50 mL 10X TBS in 450 mL deionised water. For each primary antibody, 0.5 g BSA or caseinate (depending on manufacturing instructions) were dissolved in 10 mL of the diluent solution. Then dilutions of each primary antibody were prepared using 5 µL antibody in 5 mL diluent solution (1:1000), 10 µL antibody in 5 mL diluent solution (1:500), or 25 µL antibody in 5mL diluent solution (1:200) following manufacturer's suggestions. Membranes were retrieved, and 5 mL of diluted primary antibody solution was added to membrane in its tube and incubated at 4 ^{o}C overnight. Once time had elapsed, the membrane was washed 3 times with 1X TBS for 5 minutes whilst shaking. The secondary antibody was prepared as before using 1 µL antibody in 10 mL diluent solution (1:10000) and then 5 mL were added to the membrane tubes and left rolling for an hour at RT. When time was up the membranes were washed several times with 1X TBS. Detection of protein bands was carried out using the Odyssey Infrared Imaging System. The software was set to scan at 800 nm, intensity 5. Most often, membranes were used for re-incubation with the loading control antibodies, incubated overnight and then with their appropriate secondary antibody. Blots were then visualised again using the same settings.

2.8. Mass spectrometry

Protein was extracted from MSC and SM3 cell samples using the PTS lysis buffer and then protein concentration was measured with Bradford assay (as in Section 2.7.2.). Extracted proteins were kept in low binding tubes upon lysis and for the duration of MS sample preparation. Several reagents were prepared prior to the start of the experiment, according to the table below.

Reagent	Contents
0.1 M DTT	15.43 g in 1000 mL deionised water
0.55 M IAA	101.73 g in 1000 mL deionised water
50 mM ABC buffer	3.95 g NH_4HCO_3 in 1000 mL deionised water
10 % TFA	TFA (1:10) in deionised water
Buffer A	0.1 % TFA in deionised water
Buffer B	0.1 % TFA, 80 % Acetonitrile, in deionised water
Buffer E	2 % Acetonitrile, 0.1 % TFA, in deionised water
PTS lysis buffer	100 µL 120 mM SDC, 100 µL 120 mM SLS, 100 µL 1 M Tris (pH 9.0) in 670 µL deionised water for a total of 1 mL

Table 2.7. The composition of several reagents used for MS sample preparation.

First, 20 µL of 0.1 M DTT was added to each tube (incubated for 30 min at 37 °C). Next, 20 µL of 0.55 M IAA were added and the tube was covered to avoid exposure to light (samples incubated again for 30 min at 37 °C). The tubes were retrieved and 800 µL of 50 mM ABC buffer was added. Next, the Lys-C reagent was added to a ratio of 1:100 µg (Lys-C:protein). This was then incubated at 37 °C for 3 hours.

Samples were retrieved and a calculated volume of Trypsin was added to a ratio of 1:100 µg (Trypsin:Protein). Samples were incubated overnight (12 hours, 37 °C). The next morning, 1000 µL of ethyl acetate was added as an equivalent amount of sample in its respective tube. 100 µL of 10 % TFA was added to each sample for a 0.5% TFA final concentration. Each tube was vortexed for 2 minutes, and then centrifuged for 5 min at

10,000 XG. Samples were retrieved, and the upper layer (containing ethyl acetate and detergents) were removed by pipetting, whilst making sure the visible ring between the 2 layers was not removed. The samples were then covered and placed in the SpeedVac (aqueous, no heating, vacuum on) for 4-5 hours, until all liquid had evaporated. During this time, the sample tips were prepared to contain 2 layers of the polystyrenedivinylbenzene (SDB-XC) extraction disk at the lower end of the tip. This was carried out using a special cleaving tool for cutting out small circular bits from the membrane, and using a 1-gauge needle, the disks were pushed into the lower end of a pipette tip. Once the samples were dry, they were retrieved from the SpeedVac and 200 µL of Buffer A was added to dissolve the dried sample and vortexed briefly. Samples were then centrifuged (10,000 XG, 2 minutes).

The next steps involved the desalting of the sample. First 20 µL of Buffer B was added on top of the disks within the tip to activate the membrane. The tip was placed in a microcentrifuge tube and spun (1000 XG, 2 minutes) and the elute was discarded. Next, 20 µL Buffer A was added on top of the tip and this was centrifuged again (1000 XG, 2 minutes) and the elute discarded. Finally, the dissolved sample was added (200 µL) on top of the membrane disks and centrifuged (500 XG, 5 minutes) and the elute was re-aspirated and set aside. Next 20 µL Buffer A was added on top of the membrane disks as a wash step and centrifuged (1000 XG, 2 minutes). Then, 20 µL Buffer B was added as an elution step and this was centrifuged (500 XG, 5 minutes then again at 2000 XG, 2 minutes), and the elute discarded. As a precaution, the dissolved sample elute that was previously set aside, was used again and added on top of the membrane disks, and the washing and eluting steps were repeated in the same order.

2.9. Enzyme-linked immunosorbent assay

The amount of dopamine released by the induced neuronal cells at their final stage of differentiation was investigated by means of ELISA. The kit used was the Dopamine Research ELISA kit produced by Labor Diagnostika. The assay was a competitive ELISA. When the small molecule treated cells had reached the end of the final induction stage, the media supernatant was collected for the last two media changes and stored in a microcentrifuge tube at 4 ^{o}C.

First several reagents were prepared. The Wash Buffer was prepared by diluting 20 mL of the concentrate with deionised water to a total of 1000 mL. Then the Enzyme Solution was prepared by reconstituting the Enzyme powder with 1 mL deionised water, then adding 0.30 mL Coenzyme and 0.70 mL Adjustment Buffer. Next the standards, controls and samples were prepared in the Extraction Plate. The 6 standards and 2 controls were run in duplicate to take up a total of 16 wells. 10 µL of each standard or control were added to an individual well made up to 500 µL using deionised water. As for the samples, 250 µL of sample were added and made up to 500 µL with deionised water and run in duplicate for a total of 16 wells (2 MSC, 4 SM1, 4 SM2, 6 SM3). Next, 25 µL TE Buffer were added to all wells. The plate was covered and placed on a shaker (Eppendorf thermomixer comfort) at 600 rpm for 1 hour at RT.

Once the hour elapsed, the plate was emptied and blotted dry. 1 mL of Wash Buffer was added to all wells, and the plate was again shaken (600 rpm, 5 minutes, RT). The plate was again inverted and blotted dry. This washing step was repeated once more. Next 150 µL of Acylation Buffer was pipetted into all wells, followed by 25 µL of Acylation Reagent. The plate was again shaken (600 rpm, 20 minutes, RT). The plate was emptied and blotted dry, then 1 mL of Wash Buffer was added to all wells. The plate was again shaken (600 rpm, 5 minutes, RT) and then emptied. This washing step was repeated once

more. Next, 100 µL of HCl was added to each well. The plate was covered and shaken (600 rpm, 10 minutes, RT).

90 µL of the extracted samples, controls and standards were transferred into wells of the Microtiter Plate and 25 µL of Enzyme Solution was added on top. The plate was shaken (600 rpm, 1 minute, RT) and then incubated for 2 hours at 37 ^{o}C. After the time elapsed, 100 µL of each standard, control and sample were transferred into wells within the Enzyme Plate containing the pre-coated Dopamine Microtiter Strips. Next, 50 µL of Dopamine Antiserum was added into each well. The plate was covered, shaken (600 rpm, 1 minute, RT) and then incubated overnight for 15 hours at 4 ^{o}C. The next morning, the plate was inverted, and contents discarded. The wells were washed 4 times over by addition of 300 µL Wash Buffer, then discarding it from wells and blotting dry. Next, 100 µL of Enzyme Conjugate were added into all wells and the plate was shaken (600 rpm, 30 minutes, RT). The plate was retrieved, and contents were discarded. Wells were washed 4 times over as done previously. Then 100 µL of Substrate was added to each well and the plate was incubated on a shaker (600 rpm, 20 minutes, RT) whilst avoiding exposure to sunlight. Next 100 µL of Stop Solution was added to each well. Finally, the absorbance of each solution was read at 450 nm and reference wavelength at 620-650 nm (Berthold Mithras LB 940).

2.10. Data Treatment and Statistics

2.10.1. Reverse transcription quantitative Polymerase Chain Reaction

The ΔΔCt method was employed to process RT-qPCR data. Both RT-qPCR sets were processed separately. Briefly, mean Ct values were first calculated by taking an average of the two Ct values resulting for each gene per individual cellular treatment stage. The mean Ct of the target gene was normalised to the Ct of the housekeeping gene

glyceraldehyde-3-phosphate dehydrogenase (GAPDH), by subtracting the average housekeeping gene Ct (for that cell type in question, i.e., MSC, SM1, SM2 or SM3) from the average target gene Ct for each target gene. This gave the ΔCt values for each target gene, which were used for the next step. The ΔΔCt values for each target gene were then calculated by subtracting the control group ΔCt values from the target gene ΔCt values, for each target gene. The MSCs were the untreated, starting cells, thus they were used as the control group and baseline for comparison. Each ΔΔCt value was calculated using target gene ΔCt and the control sample ΔCt values pertaining to the same target gene, but different cell samples. Finally, the fold difference in expression between treated samples' target genes and the control sample's target genes was obtained by computing 2 to the power of the negative ΔΔCt values for each experimental gene ($2^{-\Delta\Delta Ct}$).

2.10.2. Enzyme-linked immunosorbent assay

Using the Assayfit Pro add-in on Excel, the ELISA standard curve was generated and sample concentrations were determined. The add-in was opened on Excel and the ELISA option was selected from the ribbon under the Assayfit tab. Data for standards, controls (absorbance values and concentrations) and samples (absorbance values) were added to the relevant boxes. A 4-paramater logistic curve was then plotted according to manufacturer's instructions.

2.10.3. Neurite growth

The significance of changes in the average neurite lengths for each cellular differentiation stage were assessed by performing a one-way analysis of variance (ANOVA). This was done using Excel data analysis.

2.11. IMAGEJ software analysis

2.11.1. Neurite outgrowth measurement

The Fiji package (Schindelin *et al.*, 2012; Rueden *et al.*, 2017) was downloaded from the Fiji website. The Fiji program was opened and the ImageScience plugin (with NeuronJ) was installed onto the application by adding it to the update list.

For calculating changes in neurite outgrowth along the neural differentiation of cells, 3 microscopy images were selected for each differentiation stage. Images were selected based on several characteristics. Primarily, the images had to have cells containing neurites that were visible and not covered with debris or other cells. All cells in a field of view, and more so, the cells which had neurites, had to be seen clearly. Moreover, the images had to be an average representation of all images taken for that stage. Once an image was opened on the Fiji application, importantly, image distances were calibrated by creating a line of known distance and setting the scale appropriately (1 cm = 100 µm). Images were adjusted for brightness/contrast to make cells and neurites better visible for calculation. Finally, neurite tracing was performed using the NeuronJ plugin. Tracings were done manually by tracing lines over each visible neurite. These were then labelled as primary, secondary, or tertiary depending on whether they appeared to be directly coming out of the cell body or out of another neurite linked to a cell body. Measurements were then computed on ImageJ for each image and saved as an excel document.

2.11.2. Integrated density measurements (western blots, end-point PCR gels)

Scans were colour-inverted which made it easier to recognise bands. The program was set to measure integrated density. From the gel analyser options, the option for inverted peaks was ticked, so that light bands were shown as inverted peaks. Each scan

was loaded onto the program and each lane was set in its own individual box. This way it was easier to identify which peak corresponded to the band being measured. Peaks were closed off using the line draw tool and then measured using the wand tool. Individual blots/gels with several lanes were assigned different lanes (boxes) on the program which were measured at once, together. This was done to ensure that the resulting peaks corresponded to the density of each band in comparison to the others in that blot.

The loading control (actin) bands were also assessed for integrated density to confirm equal loading. The experimental band values were not normalised to the loading control, since different blots did not need to be compared to one another. Rather the analysis requires the comparison of different amounts of protein methylation between different cell stages. In fact, where bands were present for different cell stages within the same blot, the integrated densities were used to compute a ratio of the higher value to the lower value. The ratio indicates the fold increase in protein methylation as compared to the lesser value.

Chapter 3 Results

3.1. Microscopy

3.1.1. Trilineage differentiation

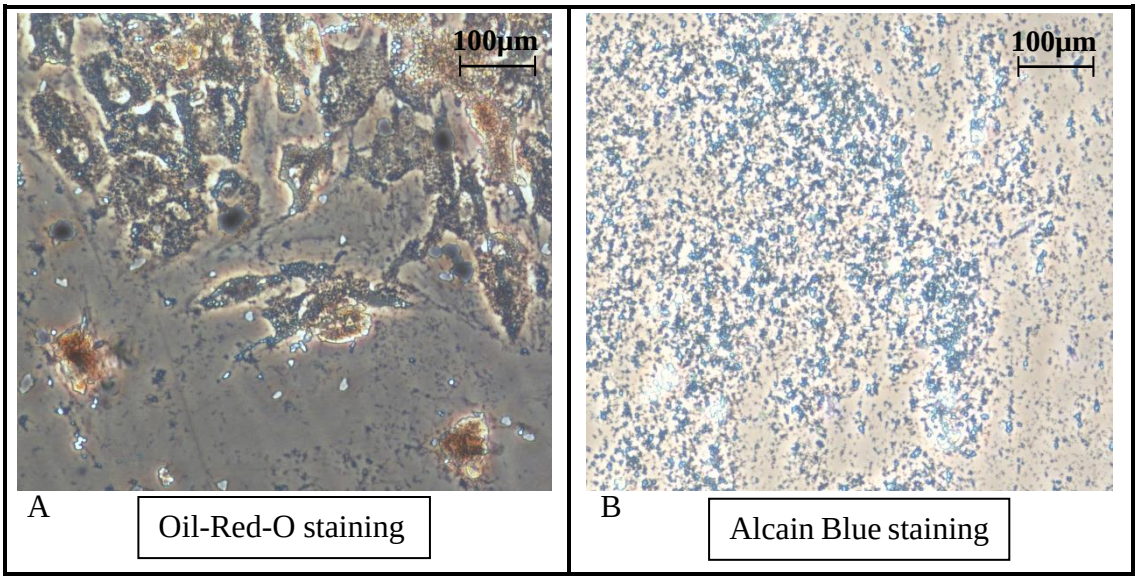

Table 3.1. MSC trilineage differentiation. Microscope images showing MSCs that were treated with adipogenic (A) and Chondrogenic (B) media. These differentiated cells were then stained with Oil-Red-O (A) and Alcain Blue (B) staining for adipocyte lipid vacuoles, seen as red clumps in A, and glycosaminoglycans, seen as blue clumps in B. Images were produced at 100X magnification (scale bar equal to 100 µm).

The microscopy images shown in Table 3.1 illustrate the successful formation of adipocytes and chondrocytes from MSCs. Upon Oil-red-O staining, MSCs that were treated with adipogenic media appeared to have a red colour tint. In the image on the left, there are several small red structures that can be seen within the cells, thus giving cells an overall red appearance. These red structures were adipocyte lipid vacuoles and thus indicate the successful differentiation of MSCs into adipocytes. On the other hand, upon Alcain Blue staining, the MSCs that were treated with chondrogenic media appeared to produce a multitude of small blue structures through the culture well. This can be seen in the image on the right, where the appearance of numerous small blue structures, denotes

the presence of glycosaminoglycans in the culture. This indicates that MSCs were successfully differentiated into chondrocytes.

As established by the ISTC, MSCs should possess the ability to be differentiated into adipocytes, chondrocytes, and osteoblasts (Dominici *et al.*, 2006). Thus, these results demonstrate that the starting cells were authentic MSCs.

3.1.2. Neural Induction

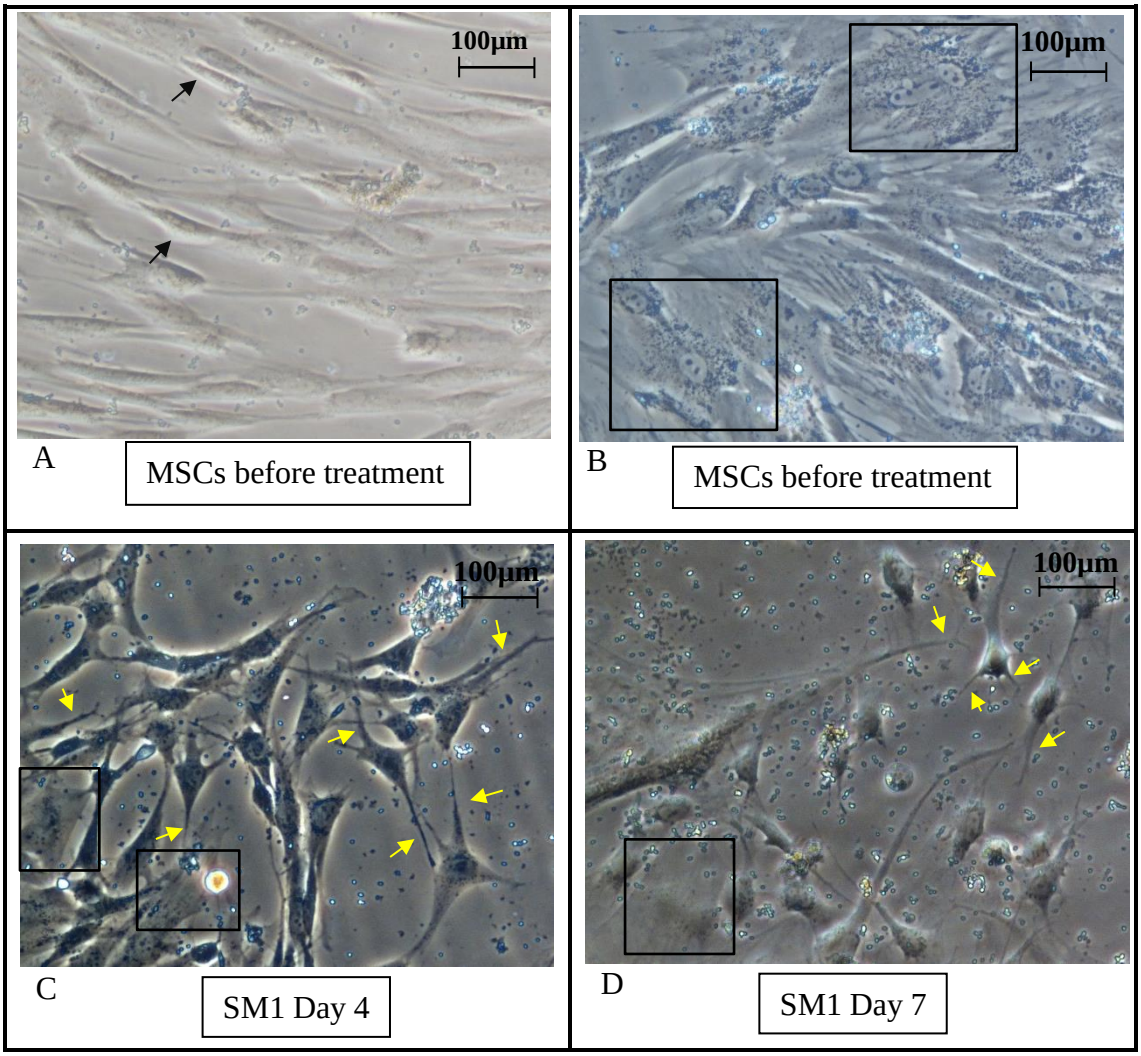

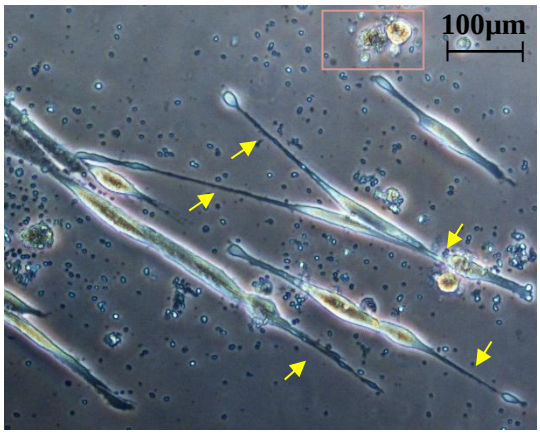

E

SM2 Day 7

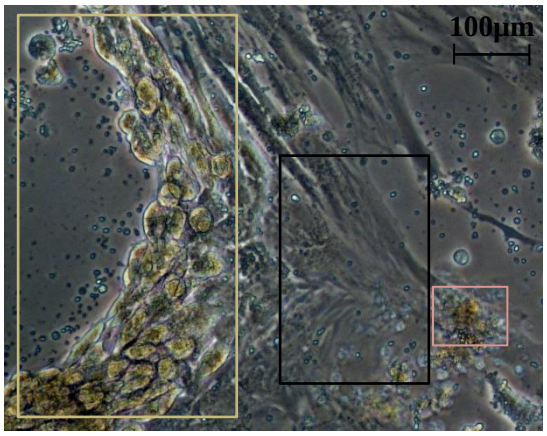

F

SM2 Day 7

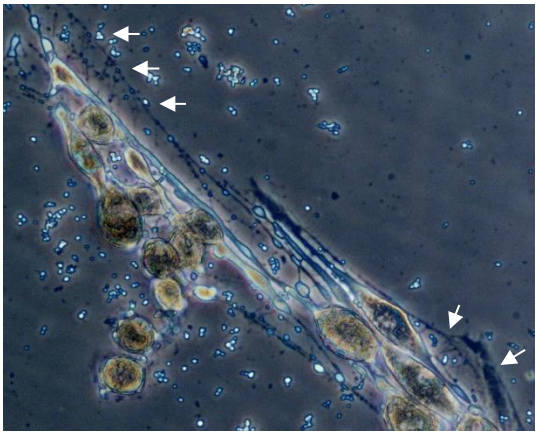

G

SM2 Day 10

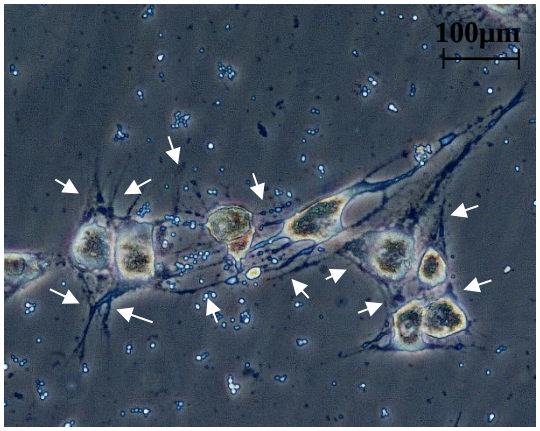

H

SM2 Day 10

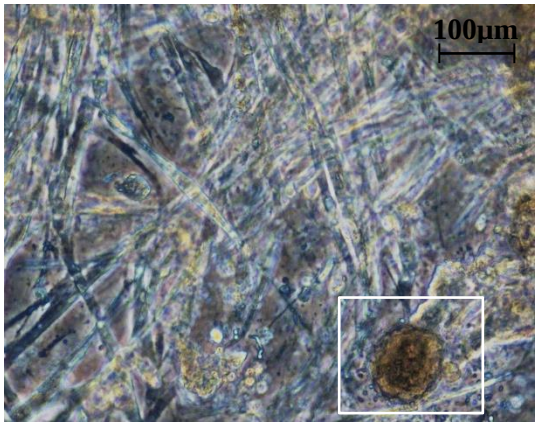

I

SM3 Day 4

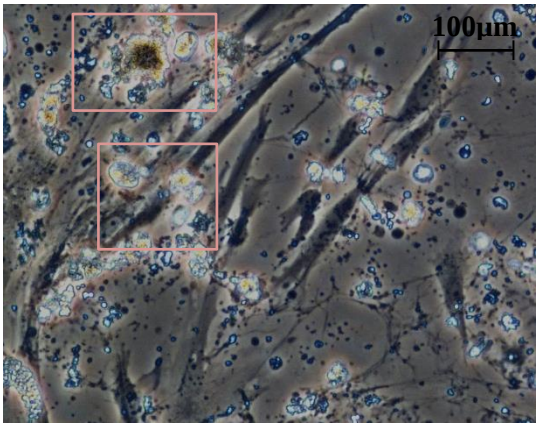

J

SM3 Day 6

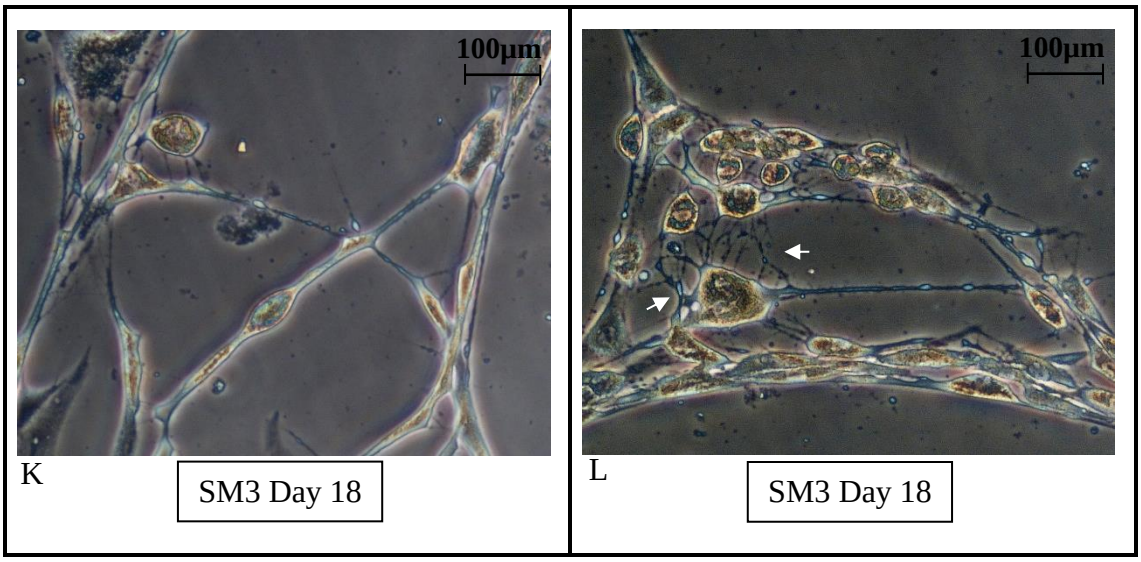

Table 3.2. MSC Neural Induction: a display of microscopy images for each stage of differentiation treatment. SM1/2/3 stands for small molecules treatment stages 1, 2 or 3. A box beneath each image denotes at which stage of treatment the cells were in when the image was captured, followed by the number of days that elapsed for the cells within that stage of treatment. Briefly: images A, B - MSCs before treatment; image C, D – Stage 1; image E-H – Stage 2; images I-L – Stage 3. All images were captured at 100X magnification (scale bar equal to 100 µm). A number of arrows or boxes of various colours have been included within these images to emphasise several aspects of the culture that were observed. These are as follows: black arrows indicate spindle-shaped MSCs (image A); yellow arrows indicate neurite outgrowths (images C, D and E); the yellow box indicates neural networks appearing as rounded cell structures in close contact with one other (image F); black boxes indicate cells with a flattened morphology (images B, C, D and F); the white box indicates a neurosphere-like structure (image I); pink boxes indicate cellular debris appearing like burst neuronally-induced cells (images E, F and J); white arrows indicate dendritic arborisation (images G, H and K).

In Table 3.2, a clear progression in cellular morphology can be seen on going from image A through L. As can be seen in image A and B, the starting cells were flat and spindle-shaped, as is characteristic of MSC morphology. Some MSCs had more of a flattened morphology and appeared as though they were stretched out on the well surface. These more flattened out MSCs can be seen in image B. These MSCs had their nuclei visible within their flattened morphology. This is normal for MSC cultures, since these cells tend to be a heterogeneous cell population (Haasters *et al.,* 2009). Their cellular morphology can be either one of the following: small, elongated and spindle-shaped (black arrows, image 10A), or else large, cuboidal and flattened (black boxes, image

10B). Importantly, no neurites were seen growing out of the starting cells prior to treatments (Image A, B).

Along each stage of differentiation media, there were significant changes in the cells' morphology towards that characteristic of neurons in culture. In image C, cells can be seen 4 days into Small Molecules Stage 1 (SM1) treatment (Reprogramming and Induction media). At this point, cells were already retracting inwards, they had a more spherical appearance and were less flattened. Additionally, they were shorter and smaller as compared to the starting cells, and neurite-like structures (yellow arrows) started to grow out of some of the cells in multiple directions. Some flattened cells were still present (black boxes in images C, and D).

In the second stage (Differentiation media) cells further developed their neuronal morphology. Many cells had developed very distinct cell bodies, as can be seen in image E. At this point the cells started to appear brighter, indicating that they were adopting more of a 3-dimensional morphology. On day 7 of Small Molecules Stage 2 (SM2) (image E) cells appeared to have longer and more developed neurite structures growing from either end of the cell body (yellow arrows). Cells that had started to develop a typical neuronal morphology began forming neural clusters or networks. This aspect of their culture can be seen in image F. On the left half of the image, one can observe a multitude of rounded cell structures in close contact with or even stacked on one other (yellow box). Again, cells with a flattened appearance (black box) can be seen amidst the more developed cells (image F). In images G and H (SM2 treatment extended for 10 days), more developed, brighter and distinct cell bodies can be seen. Here were the first signs of dendritic arborisation surrounding cell body-like structures, seen as secondary and tertiary neurites (white arrows).

By Day 4 of the third stage (Maturation media), parts of the culture had very dense and thick neurite connections growing out of cells in all directions (image I). Cell bodies and axonal structures are hard to make out in this image, due to the layering of induced neuronal cells growing out neurites in all directions. Interestingly, in Small Molecules Stage 3 (SM3) culture, induced neuronal cells appeared to be forming neurosphere-like structures as can be seen on the bottom right corner of image I (white box). In both SM2 and SM3 cultures, one could note the occurrence of some debris that appeared like burst cells with surrounding neurites (pink boxes in images E, F and J).

At day 18 of SM3 (extended past 14 days), distinct and spherical cell bodies were observed (image K, L). Neurite projections were thicker and more complex in terms of connections to neighbouring cells. In image L, a great degree of dendritic arborisation can be seen surrounding several cell bodies (white arrows). Additionally, axonal processes appeared to be growing longer and thicker, with a bright appearance, suggesting the occurrence of axonal transport. These changes indicate that increased neuronal maturation and function occurred by Stage 3. Fig. 3.1 illustrates a structure that was found in several SM2 and more so in SM3 cultures. Cells that had acquired a neuron-like morphology, appeared to be more likely to form clusters of neural networks with other morphologically-similar cells. Under the microscope, these clusters appeared as clumps of circular cells that caught a lot of the microscope's light. In some neural networks there were neurites growing out of the edges in all directions to meet with neighbouring cells.

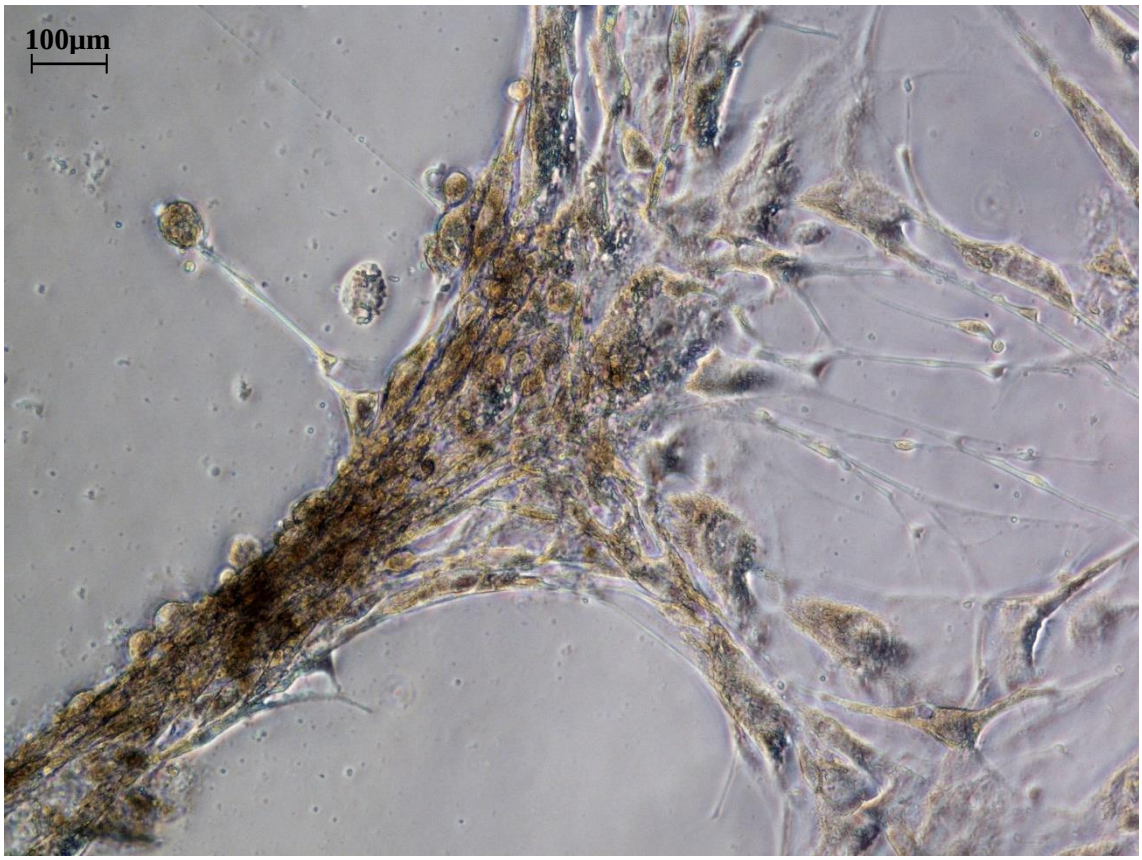

Figure 3.1. Neuronally-induced cells during extended SM3 treatment (day 18). This image demonstrates a structural manifestation of the neuronally-induced cells in culture. Structures similar to this were forming in several SM2 and SM3 cultures. In these stages, cells that had acquired a neuron-like morphology, had a tendency to form clusters of neural networks with other morphologically-similar cells. In the above image, one of these neural structures can be seen. The neural network structure appears as layers of circular cells with several neurites growing out of the cells on its edges to meet with neighbouring cells. This image was captured at 100X magnification (scale bar equal to 100 µm).

As a means by which to assess changes in morphology in a quantifiable manner, the changes in the lengths of neurites in cells of each stage were calculated using ImageJ as described in Section 2.11.1. Results are shown in Table 11 and the average neurite lengths, longest neurite, and total neurite outgrowth data are presented as bar graphs (Fig. 3.2, 3.3 and 3.4 respectively).

The measured values for the mean lengths of neurites growing out of cells were 126.0, 100.6, and 90.0 µm for SM1 (average: 101.7 µm); 141.5, 367.7, and 238 µm for SM2 cells (average: 214.6 µm); and 371.2, 305.9, and 507.7 µm for SM3 cells (average:

374.2 μm). This positive trend is illustrated clearly in Fig. 3.2. The same trend was found for the lengths of the longest neurites measured for each image for each stage (Fig. 3.3.). The range of neurite lengths found for each differentiation stage are as follows: SM1: 14.5 – 522.7 μm; SM2: 28.1 – 909.1 μm; SM3: 23.1 – 1596.0 μm. The total neurite outgrowths found for each stage also reveal significant increases on going from SM1 to SM3 cells, with a range of 6235.6 – 12149.7 μm for SM1; 11186.0 – 15811.5 μm for SM2; and 23385.1 – 39152.4 μm for SM3 cells.

Cell Stage	Count	Min, Max (μm)	Mean length per image (μm)	Mean length of all 3 images (μm)	Total Neurite outgrowth (μm)
SM1	68	28.2, 475.1	126.0	101.7	8566.5
SM1	62	14.5, 409.0	100.6		6235.6
SM1	135	16.2, 522. 7	90.0		12149.7
SM2	105	28.1, 582.2	141.5	214.6	14856.5
SM2	43	97.8, 909.1	367.7		15811.5
SM2	47	55.7, 786.6	238.0		11186.0
SM3	63	80.3, 1236.4	371.2	374.2	23385.1
SM3	128	48.5, 1077.2	305.9		39152.4
SM3	67	23.1, 1596.0	507.7		34014.8

Table 3.3. Showing the data output for the neurite length analysis conducted on 3 microscopy images pertaining to each cellular differentiation stage. From columns left to right, the table denotes the cellular differentiation stage of the cells in the image used to measure neurites; the number of neurites measured; the min and max neurite lengths measured in that image (μm); the average length of all neurites measured within a single image (μm); the average length of all neurites within all 3 images pertaining to an individual differentiation stage (μm); and the total combined lengths of all neurites measured within each of the 3 individual images for each differentiation stage (μm).

A one-way ANOVA at a 99% confidence level was carried out (using Excel) to explore the significance of the differences in the average neurite lengths found for the cells in each differentiation stage. The analysis is as follows.

H_o: $\mu_{SM1} = \mu_{SM2} = \mu_{SM3}$

H_A: At least one mean is different

ANOVA						
Source of Variation	*SS*	*df*	*MS*	*F*	*P-value*	*F crit*
Between Groups	9775040	2	4887520	141.3161	1.92E-52	4.634959
Within Groups	24728789	715	34585.72			
Total	34503829	717				

Table 3.4. Statistical analysis of the significance of differences found in the average neurite lengths of cells in the 3 differentiation stages. This ANOVA table is as produced on Excel and was computed at the 99% confidence level. From the left-hand side is the source of variation (between or within groups and the total); the sum of squares (SS); the degrees of freedom (df); the mean squares (MS); the resulting F statistic for this test (F); the resulting *p* value for this test (*p-value*); and the appropriate critical value as per the degrees of freedom (F crit). This table shows that the resulting F statistic (141.32) is greater than the critical value (4.63) and the resulting *p* value (1.92×10^{-52}) is lesser than the level of significance ($\alpha = .01$). Thus, the null hypothesis was rejected, and the ANOVA indicates significant differences between the average neurite lengths pertaining to each stage of differentiation.

As can be seen in the ANOVA table, the resulting *p* value is lesser than the level of significance ($p < .01$). Thus, the null hypothesis is rejected, and the alternative hypothesis can be accepted. This result indicates that there are highly significant differences between the different cellular differentiation stages in terms of their average neurite lengths.

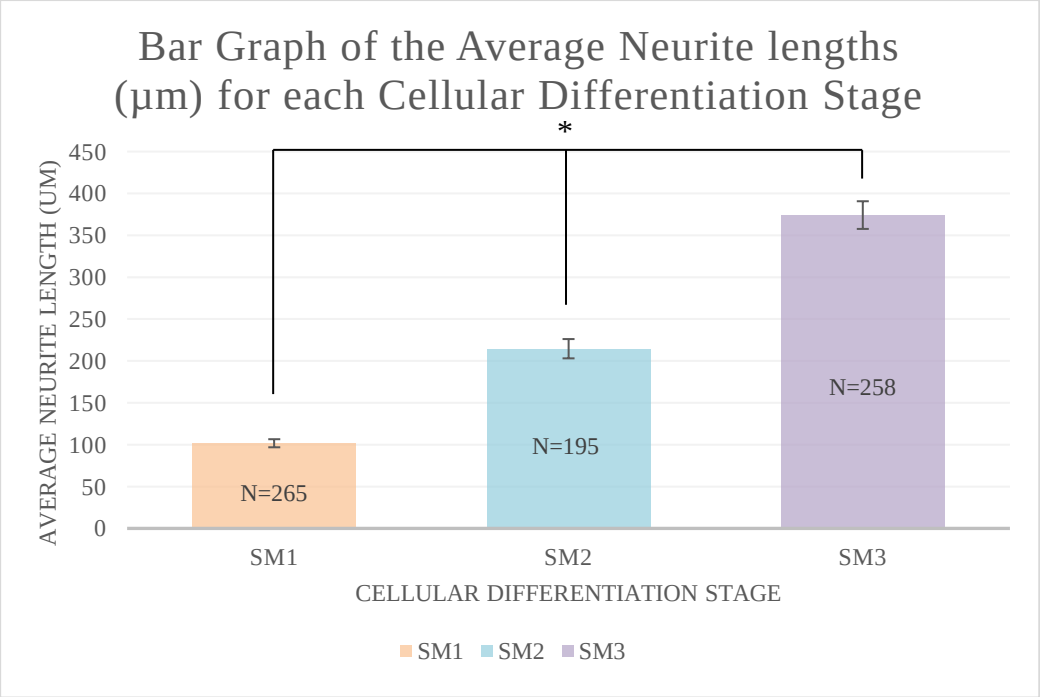

Figure 3.2. Bar graph depicting the changes in average neurite lengths (µm) along neural differentiation. Three bars can be seen, one per stage of differentiation treatment (SM1, SM2, SM3). A colour legend can be found beneath the graph. The y-axis denotes the average neurite lengths in µm, and the x-axis denotes the cellular differentiation stage. Within each bar can be found the number (N) of neurites measured for computation of that average. The neurite counts for each stage are as follows: SM1 - an average of 265 neurites, SM2 - an average of 195 neurites, and SM3 – an average of 258 neurites. Standard error (SE) bars are depicted on top of each bar. These error bars are showing the standard error of the mean (SEM or SE) and these values were computed by calculating the standard deviation (SD) for each set, and then dividing this value by the square root of N (SEM = SD/$\sqrt{n}$). The SEM values for each stage are as follows: SM1 – 4.83; SM2 – 11.51; SM3 – 16.51. It can be inferred that these means are significantly different to each other since none of the SE bars overlap. The asterisk denotes significance of the differences between each of the 3 means ($p < .01$).

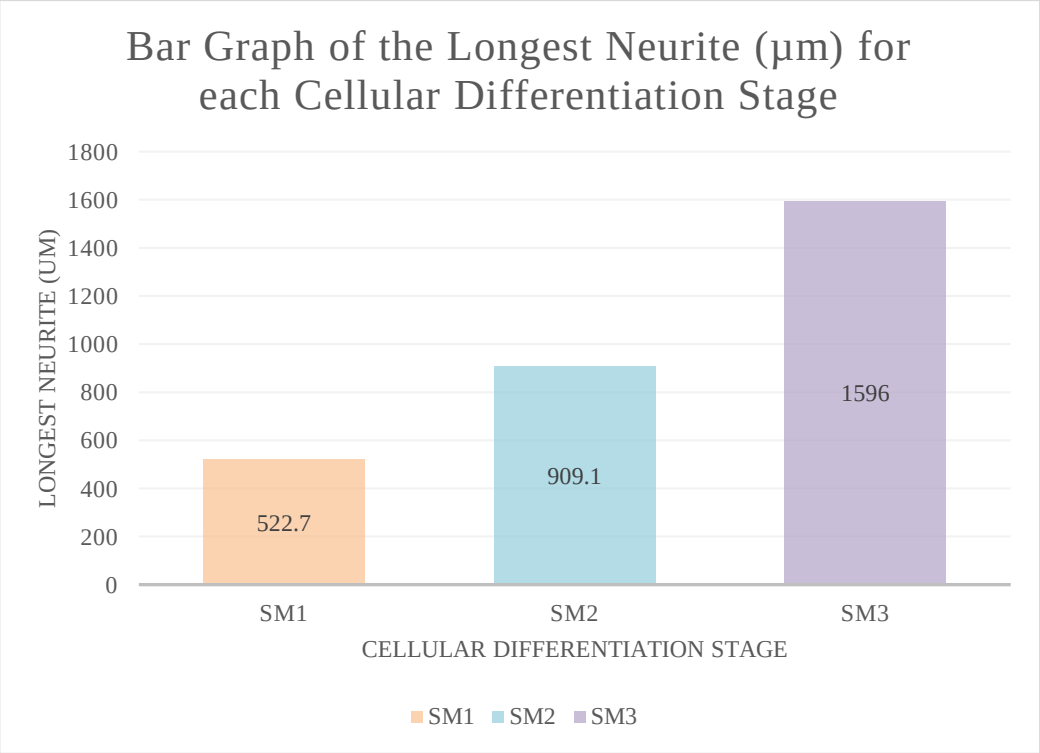

Figure 3.3. Bar graph depicting the measurements of the longest neurites (µm) for each differentiation stage. Three bars can be seen, one per stage of differentiation treatment (SM1, SM2, SM3). The colour legend can be found beneath the graph. The y-axis denotes the longest neurite lengths in µm, and the x-axis denotes the cellular differentiation stage. N=1 for each of these bars since each bar shows the single longest neurite measured for each differentiation stage. At the centre of each bar is the value of the longest neurite pertaining to that differentiation stage.

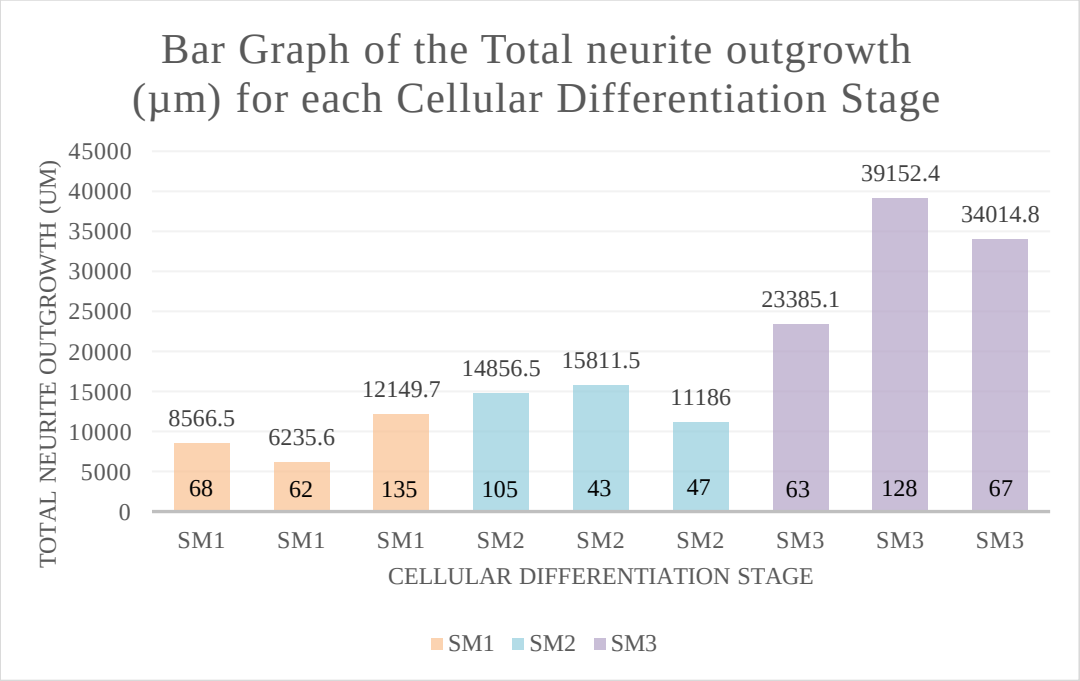

Figure 3.4. Bar graph depicting total neurite lengths (µm) found for 3 microscopy images taken for each neuronal differentiation stage. 9 bars can be seen, with 3 per stage of differentiation treatment (SM1, SM2, SM3) pertaining to 1 of the 3 images measured for that stage. The colour legend can be found beneath the graph. The y-axis denotes the total neurite lengths in µm, and the x-axis denotes the cellular differentiation stage. Within each bar can be found the number of neurites measured for computation of the total neurite lengths for that image. On the top of each bar is the value of the total neurite length pertaining to that image measured for that differentiation stage.

3.2. End-point PCR gel

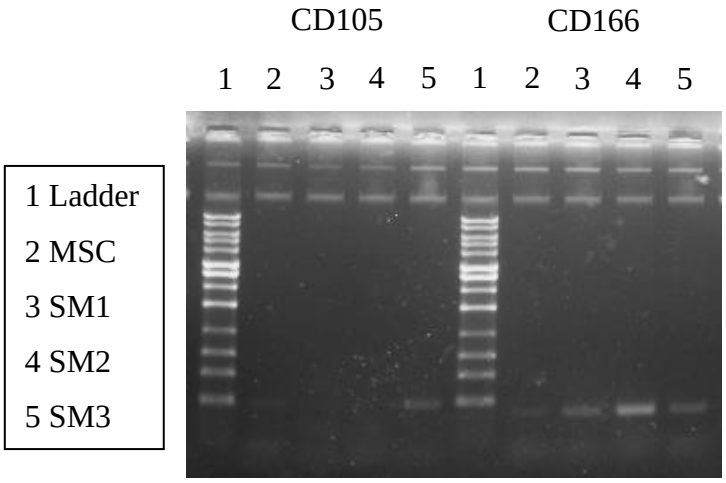

Figure 3.5. The first gel showing bands for CD105 and CD166 expression following amplification by End-point PCR. The cell types pertaining to each lane can be seen as numbers on top of each lane within the blot: 1 – ladder, 2 – MSC, 3 – SM1, 4 – SM2, 5 – SM3. Resulting bands can be seen at the bottom end of the gel. Briefly, a weak band can be seen for CD105 for MSCs and SM3 cells. CD166 expression shows a weak band in MSCs, and bands of greater density in SM1, SM2 and SM3 cells, the densest band being that found for SM2 cells.

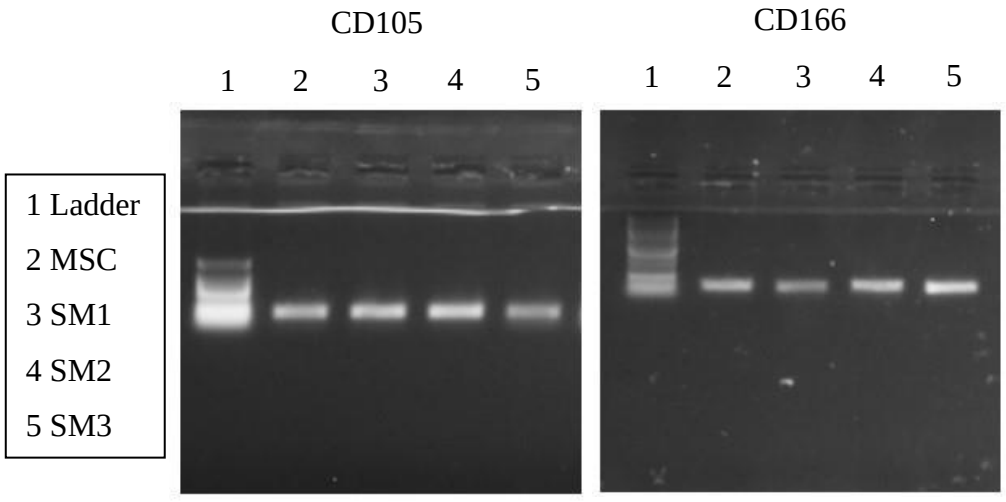

Figure 3.6. The second gel showing bands for CD105 and CD166 expression following amplification by End-point PCR. The cell types pertaining to each lane can be seen as numbers on top of each lane within the blot: 1 – ladder, 2 – MSC, 3 – SM1, 4 – SM2, 5 – SM3. Resulting bands can be seen halfway through the gel. Briefly, a strong band was obtained for each cell type for CD105, all bands of similar intensities. As for CD166, dense bands were found for all cell types, with the lowest density band being that found for SM1 cells.

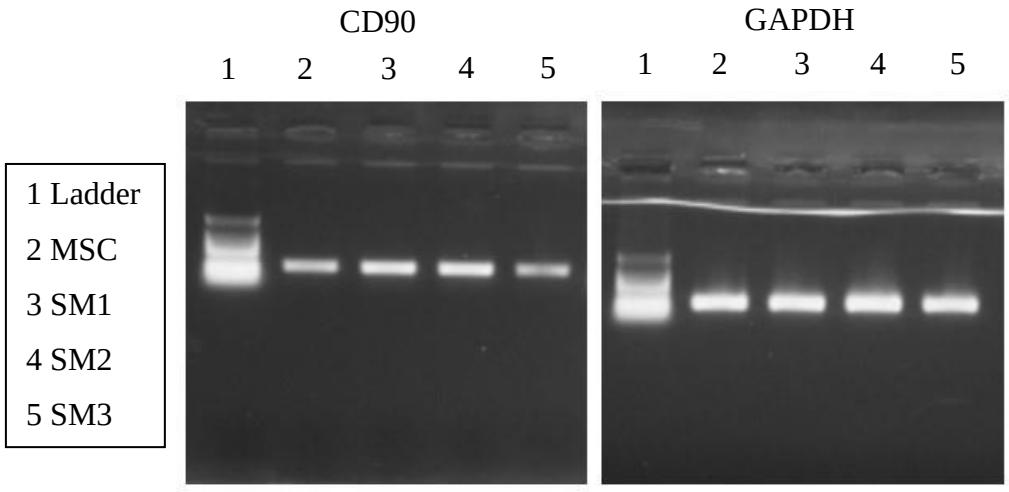

Figure 3.7 Gel showing bands for CD90 and GAPDH expression following amplification by End-point PCR. The cell types pertaining to each lane can be seen as numbers on top of each lane within the blot: 1 – ladder, 2 – MSC, 3 – SM1, 4 – SM2, 5 – SM3. Resulting bands can be seen halfway through the gel. Briefly, CD90 gave strong bands in MSCs and each cellular differentiation stage, with the SM3 band being the weakest. As for the reference gene (GAPDH), this gave bands of very similar intensities, with integrated density ratios of approximately 1 for each differentiation stage in relation to the starting cells. This indicates that there was equal loading of each cell sample in each lane.

Figure number	CD number	Lane/Cell type	Integrated density	Ratio
3.5	CD105	MSC	902	SM3:MSC – 3.5
		SM3	3161	
	CD166	MSC	393	SM1:MSC – 4.6 SM2:MSC – 11.9 SM3:MSC – 3.4
		SM1	1825	
		SM2	4676	
		SM3	1331	
3.6	CD105	MSC	6460	SM1:MSC – 1.2 SM2:MSC – 1.3 SM3:MSC – 0.8
		SM1	7895	
		SM2	8501	
		SM3	5298	
	CD166	MSC	4273	SM1:MSC – 0.7 SM2:MSC – 1.2 SM3:MSC – 1.5
		SM1	2953	
		SM2	5122	
		SM3	6546	
3.7	CD90	MSC	4892	SM1:MSC – 1.5 SM2:MSC – 1.5 SM3:MSC – 0.8
		SM1	7234	
		SM2	7378	
		SM3	3924	
	GAPDH	MSC	9019	SM1:MSC – 1 SM2:MSC – 1.1 SM3:MSC – 0.9
		SM1	9007	
		SM2	10060	
		SM3	8328	

Table 3.5. Showing the integrated density values for observed bands in the presented end-point PCR gels. Integrated density values were calculated using ImageJ. This table includes the figure number where the gel in question can be found, the corresponding CD markers investigated within that gel, the cell type represented in the lanes where bands were observed, and the calculated integrated densities corresponding to the band found within that lane. The last column includes the integrated density ratios computed as differentiated cell type : starting cell. These ratios indicate the fold increase or decrease in integrated density values for a band resulting for the experimental cells vs the starting cells.

The expression of several CD markers was explored in the starting cells and each stage of differentiation treatment. GAPDH was used as a reference gene for this analysis. As can be seen from Table 3.5, the bands that resulted for GAPDH gave very similar integrated density values, with integrated density ratios of approximately 1 for each differentiation stage in relation to the starting cells. This indicates that there was equal loading of each cell sample in each lane. CD markers that were assessed include CD105, CD90 and CD166. CD90 and CD105 are two established MSC markers as published by the ISCT (Dominici *et al.,* 2006). CD166 is expressed in several cellular compartments of neurons in the brain, including axons, dendrites, and the neuronal cell body, and is involved in cell adhesion and migration processes (Kent *et al.,* 2002; Raney *et al.,* 2013).

In both gels where CD166 expression was tested (Fig. 3.5, 3.6), CD166 expression was positive in all lanes, meaning that MSCs, SM1, SM2 and SM3 cells were all found positive for CD166 expression. In the first gel (Fig. 3.5), CD166 expression was very low in MSCs, and this increased greatly in SM1, SM2 and SM3 cells, giving the densest band for SM2 cells, with an integrated density ratio of 11.9 for SM2:MSC. In contrast, in the second gel (Fig. 3.6), dense bands were obtained for all cell types, with the lowest density band for SM1 cells and an integrated density ratio of 1.5 for SM3:MSC. In this gel, the expression did not change as much as the first gel, being in the range of 0.7-1.5-fold that of MSCs. Such a gel would indicate that CD166 expression was more-or-less maintained along the differentiation of the starting cells.

As for CD105 expression, Fig. 3.5, shows a very light band for MSCs and one of greatest density for SM3 cells, where ImageJ analysis indicated an increased integrated density of 3.5-fold for SM3:MSC. On the other hand, Fig. 3.6, shows that the second gel assessing CD105 expression produced bands of similar intensities (integrated density ratios of approximately 1) for each cell stage (MSCs, SM1/2/3). CD90 was found to be

positive in MSCs, but also gave a strong band for each cellular differentiation stage (Fig. 3.7.). Interestingly, its expression seemed to increase by 1.5-fold in SM1 and SM2 cells but was decreased very slightly in SM3 cells.

3.3. Reverse transcription quantitative Polymerase Chain Reaction expression

A panel of neural markers was devised to have markers pertaining to each stage of differentiation. SOX2 expression is found in NECs and radial glia (Abcam, 2016), and it is considered a pluripotency marker involved in neural differentiation (Zhang & Cui, 2014). MASH1 is found in IPCs, TUBB3 and NEUROD1 in immature neurons, and NEUN and MAP2 are mature neuronal markers (Abcam, 2016). TH was chosen as a marker for mature DA neurons. According to the devised protocol and the intended purposes of the 3 media stages, cells from each stage were expected to be expressing several of these markers. A strong positive SOX2 expression was expected in SM1 cells and though this could still be expressed in SM2 cells it was expected to decrease significantly in relation to its expression in SM1 cells. SM2 cells were expected to be at late IPC stages. Thus, they were expected to be expressing MASH1 and maybe show a low TUBB3 and NEUROD1 expression. Finally, the Stage 3 cells were expected to maintain the expression of TUBB3 and NEUROD1. Importantly, SM3 cells were expected to be expressing the mature neural markers NEUN, MAP2 and TH, which would confirm their successful specification towards the DA neuronal fate. The tables below detail the calculated fold-changes in expression for SM1, SM2 and SM3 cells in relation to the starting cells.

	Fold change in expression ($2^{-(\Delta\Delta Ct)}$ values)		
Gene	**SM1**	**SM2**	**SM3**
SOX2	2.75	0.87	0.30
MASH1	2.22	0.10	0.18
NEUROD1	6.66	2.90	5.56
TUBB3	0.36	13.32	0.40
NEUN	1.47	2.60	0.27
MAP2	1.81	5.74	0.19
TH	2.08	2.81	0.87

Table 3.6. Showing the computed values for the fold change in expression for neural markers in SM1, SM2, and SM3 cells for RT-qPCR run 1. Values were computed on Excel using the ΔΔCt method. Values shown in this table correspond to the fold-change in expression pertaining to a single gene for a specific cellular differentiation stage in relation to the starting cells (MSCs). The markers represent the following: SOX2 – a pluripotency marker, MASH1 – an early neural marker, NEUROD1 and TUBB3 – immature neural marker, NEUN and MAP2 – mature neural marker, TH – specific DA neural marker. Briefly, increased expression for SM1 cells was found in SOX2, MASH1, NEUROD1 and a slight increase in TH; increased expression for SM2 cells was found in NEUROD1, TUBB3, NEUN, MAP2 and TH. The output for SM3 cells has been found to be invalid.

	Fold change in expression ($2^{-(\Delta\Delta Ct)}$ values)		
Gene	**SM1**	**SM2**	**SM3**
SOX2	1.31	0.91	0.15
MASH1	2.02	0.42	0.09
NEUROD1	0.83	1.28	0.28
TUBB3	6.11	15.89	0.99
NEUN	1.29	3.84	0.32
MAP2	3.69	7.11	0.12
TH	0.77	1.77	1.41

Table 3.7. Showing the computed values for the fold change in expression for neural markers in SM1, SM2, and SM3 cells for RT-qPCR run 2. Values were computed on Excel using the ΔΔCt method. Values shown in this table correspond to the fold-change in expression pertaining to a single gene for a specific cellular differentiation stage in relation to the starting cells (MSCs). The markers represent the following: SOX2 – a pluripotency marker, MASH1 – an early neural marker, NEUROD1 and TUBB3 –immature neural marker, NEUN and MAP2 – mature neural marker, TH – specific DA

neural marker. Briefly, increased expression for SM1 cells was found in MASH1, TUBB3 and MAP2; increased expression for SM2 cells was found in TUBB3, NEUN, MAP2 and slight increase in TH. The output for SM3 cells has been found to be invalid.

In the first RT-qPCR run (Table 3.6), SM1 cells were found to have increased expression of the stemness marker SOX2 (2.75-fold), the IPC marker MASH1 (2.22-fold), and NEUROD1 (6.66-fold). Additionally, SM1 cells indicated a very slight increase in expression of NEUN (1.47-fold) and MAP2 (1.81-fold), as well as a 2.81-fold increase in TH expression. SM2 cells had decreased SOX2 and MASH1 expression and increased expression of the immature neuronal markers NEUROD1 (2.90-fold) and TUBB3 (13.32-fold) and of both mature neuronal markers NEUN (2.60-fold) and MAP2 (5.74) compared to their expression in SM1 cells. Furthermore, SM2 cells indicated a 2.81-fold increase in TH expression.

In the second RT-qPCR run (Table 3.7), SM1 cells also had increased SOX2 (1.31-fold) and MASH1 (2.02-fold) expression, although this was slightly lesser than that seen in the first run. This time, it was TUBB3 (6.11-fold increase) expression that was increased and not NEUROD1 (0.83-fold decrease). Similarly, to the first run, SM1 cells had slight increases in both NEUN (1.29-fold) and MAP2 expression (3.69-fold). As for the SM2 cells, there was a decreased expression for SOX2 and MASH1 as in the first run. Furthermore, and similarly to the first run, SM2 cells had increased expression of the immature neuronal marker TUBB3 (15.89-fold) and not much of an increase in NEUROD1 expression. TH expression increased less than that found in the first run, with a 1.8-fold change in expression.

Both RT-qPCR runs performed gave an unexpected output for SM3 cells. In Table 3.6, a decreased expression for all markers except NEUROD1 (5.56-fold increase), can be seen for SM3 cells. In the second run (Table 3.7), SM3 cells had no increase in expression for any markers, except a slight increase in TH expression (1.41-fold).

Reasons for such a conflicting output for SM3 cells are suggested in the Discussion. Figs. 3.8 (RT-qPCR run 1) and 3.9 (RT-qPCR run 2) are bar graphs that depict the changes in expression for each of the neural markers tested in each cellular differentiation stage. These bar graphs illustrate the changes delineated in Tables 3.6 and 3.7, respectively. Furthermore, Fig. 3.10, is a bar graph depicting the values of neural markers pertaining to each differentiation stage, averaged for both runs. In this figure, the averaged values for each stage of differentiation illustrate what is shown for both runs in Table 3.6, and 3.7. From this graph it can be noted that SM1 cells have the highest expression of early neural markers in comparison to SM2 and SM3 cells; whilst SM2 cells show large increases in immature and mature neuronal markers in comparison to SM1 cells. The flawed output for SM3 cells is also illustrated effectively – showing a decreased expression of all markers in relation to SM1 cells.

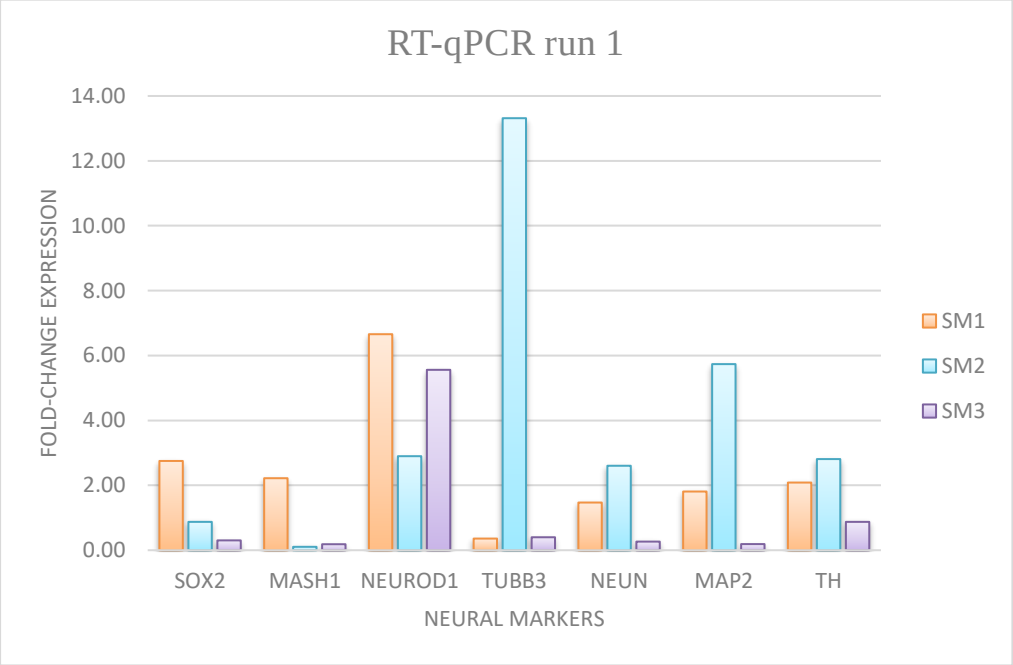

Figure 3.8. Bar graph depicting the changes in expression for neural genes in SM1, SM2 and SM3 cells in relation to MSCs as the starting cells, RT-qPCR run 1. Fold-change in expression is found on the y-axis with the neural markers on the x-axis. Neural markers appear in sequence on going from early to mature markers, making it easier to see a trend in changes in expression on going from stage 1 to stage 3 cells. A legend on the right-hand side of the bar graph indicates which colours pertain to which cellular differentiation stage. Briefly, increased expression for SM1 cells was found in SOX2, MASH1, NEUROD1 and a slight increase in TH and mature neural markers; increased expression for SM2 cells was found in NEUROD1, TUBB3, NEUN, MAP2 and TH. The output for SM3 cells has been found to be invalid – only decreases in gene expression was found for Stage 3 cells tested, except for an increase in NEUROD1.

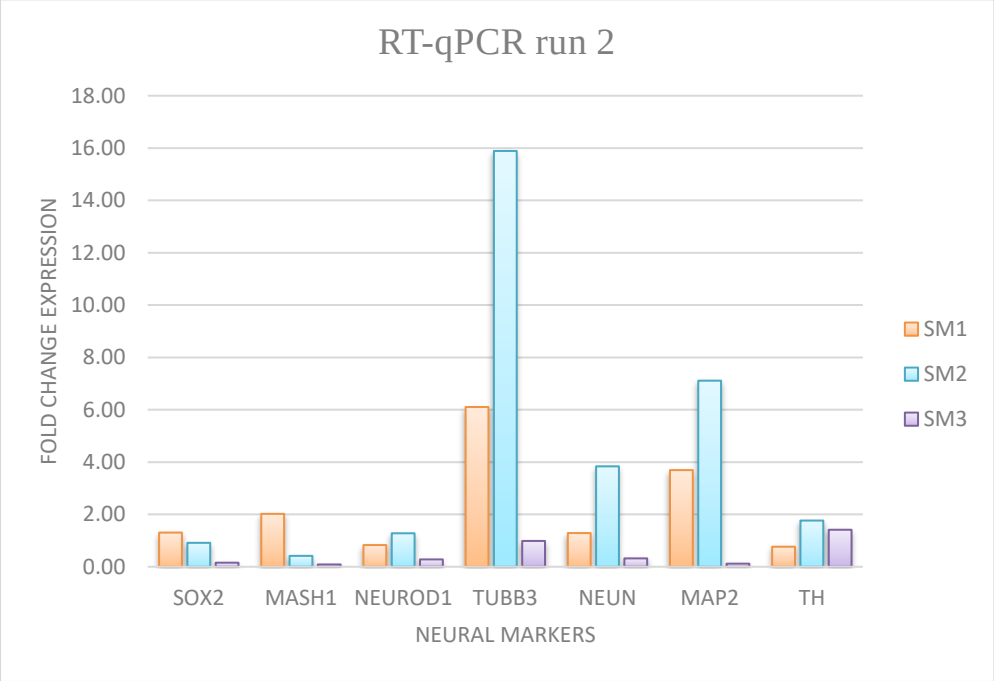

Figure 3.9. Bar graph depicting the changes in expression for neural genes in SM1, SM2 and SM3 cells in relation to MSCs as the starting cells, RT-qPCR run 2. Fold-change in expression is found on the y-axis with the neural markers on the x-axis. Neural markers appear in sequence on going from early to mature markers, making it easier to see a trend in changes in expression on going from stage 1 to stage 3 cells. A legend on the right-hand side of the bar graph indicates which colours pertain to which cellular differentiation stage. Briefly, increased expression for SM1 cells was found in MASH1, TUBB3 and MAP2; increased expression for SM2 cells was found in TUBB3 (large change), NEUN, MAP2 and a slight increase in TH. The output for SM3 cells is considered to be invalid – all neural markers (except TH, 1.4-fold) were found to have decreased in expression in the Stage 3 cells tested.

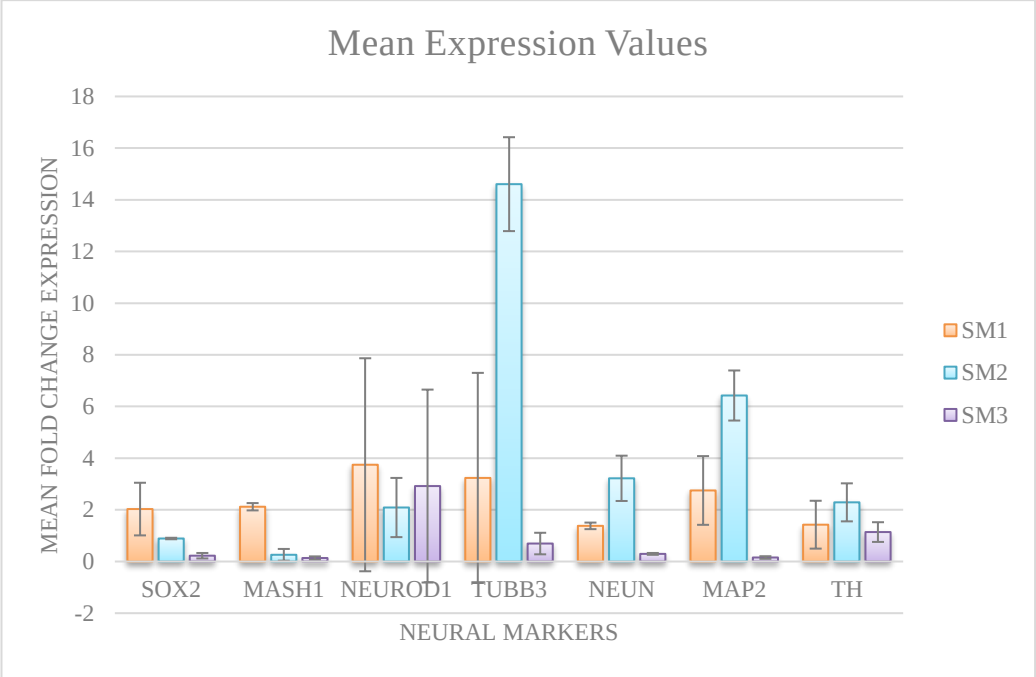

Figure 3.10. Bar graph depicting the mean expression values for neural genes in SM1, SM2 and SM3 cells, with standard deviation (SD) bars. The values for the changes in expression seen here are averages of the values found within the 2 runs. Early neural markers appear first, then immature and later mature neural markers. In this bar graph the overarching expression changes can be deduced. Briefly, SM1 cells show greatest expression of early neural markers in comparison to SM2 and SM3 cells; SM2 cells show large increases in immature and mature neuronal markers in comparison to SM1 cells. The erroneous result for SM3 cells can also be observed in terms of a decreased expression of all markers in relation to SM1 cells.

3.4. Western Blotting

Cell extracts were used for investigation of PTM changes through the use of several methylation antibodies. Table 3.8 displays the calculated integrated densities for each band observed on the presented western blots. Blots in which there was only one band pertaining to one lane/cell type visible were not included in this table and their integrated density values were not calculated considering that they had nothing to be compared to. An appearance of a band in one lane and not in the others is indicative of a change in itself. One example of a blot not included is the di-asymmetric arginine (neither of the 2

blots gave any band). Another blot which was not included is the mono-methylated arginine in Fig. 3.13, since there was only a band for SM1 and nothing for SM3.

Actin was used as a loading control for these Western blotting experiments (Fig. 3.13.). Bands can be seen on the blot in Fig. 3.13, between 35-50 kDa. Actin gave bands of similar intensity for both SM1 and SM3 cells, thus indicating equal protein loading. In Fig. 3.11, scanned images of western blots for lysine mono-, di-, and tri-methylation are shown. On the left, bands for lysine mono-methylation can be seen between 25-50 kDa. As can be seen in Table 3.8 and Fig. 3.11, there was an increase in lysine mono-methylation in SM2 and SM3 cells in comparison to MSCs and SM1 cells. More specifically, no bands occurred for MSCs and SM1 cells, whilst several bands could be seen for SM2 and SM3 cells. The calculated integrated densities of SM2 and SM3 cells were very similar, and thus their lysine mono-methylation changes were found to have occurred to a similar extent. In the blot on the right, lysine di-methylation bands can be seen just below 50 kDa. Di-methylated lysine bands were found to be of lesser intensity in SM1, SM2 and SM3 cells in relation to MSCs. The MSC di-methylated lysine band was found to be 1.6- to 3.2-fold the integrated density of SM1, SM2 and SM3 cells. In the bottom blot, there can be observed bands for lysine tri-methylation, just below 75 kDa. MSCs gave a very light band for tri-methylated lysine residues, SM1 gave no band, and SM2 and SM3 cells had integrated densities of approximately 11-fold greater than MSC.

In Fig. 3.12, are the blots that were incubated with arginine methylation antibodies. Bands can be seen above 75 kDa. Note that these blots that were previously incubated with lysine methylation antibodies and then re-incubated with arginine methylation antibodies. Thus, there are faint bands remaining in the mono- and di-symmetric arginine blots, and the black bands at 75 kDa in the di-asymmetric arginine blot are not pertaining

to arginine but are remaining bands from the previous blot. In Fig. 3.12, the resulting bands showed increased arginine mono-methylation in SM1, SM2 and SM3 cells with no band present for MSCs. These bands were of very similar integrated densities and each of these bands was weak. Bands for di-symmetric methylated arginine were found in all lanes, although this was strongest for MSCs (1343) and SM1 (2373), with SM2 and SM3 cells giving very similar integrated densities (888, and 827 respectively). As for the di-asymmetric arginine, no bands were found for each cell type in both blots performed (Figs. 3.12 and 3.13).

In Fig. 3.13, scanned images show new blots incubated with arginine methylation antibodies. Bands can be seen above 75 kDa. Unfortunately, SM2 cell extracts had run out, so the bands show arginine methylation for SM1 vs SM3 cell extracts. In Fig. 3.13, the SM1 band for di-symmetric methylated arginine was 2.3-fold the integrated density of that found for SM3 cells. In contrast to the first blot, in the second mono-methylated arginine blot, no band was found for SM3 cells, and as before, a weak band was found in the SM1 lane.

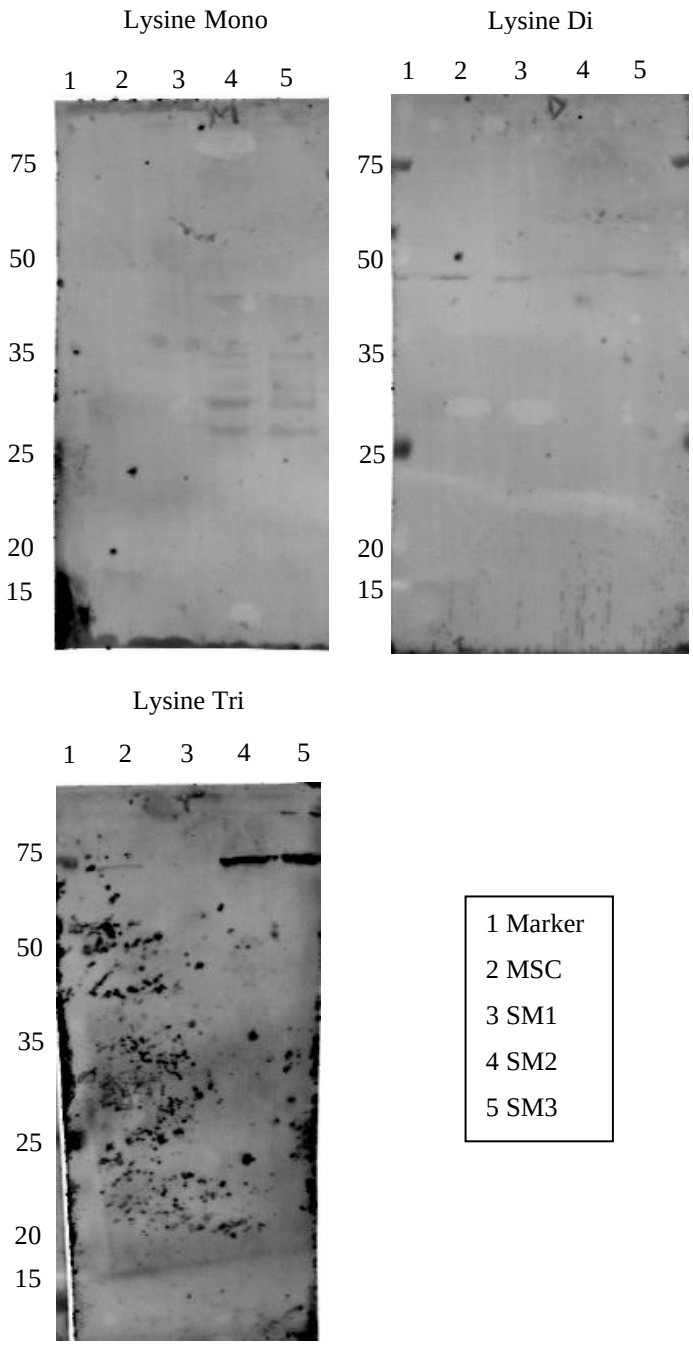

Figure 3.11. Western blot scanned images for Lysine Mono-, Di-, and Tri-methylation. Protein sizes (in kDA) can be found on the left-hand side of each blot. The cell types pertaining to each lane can be seen as numbers on top of each lane within the blot: 1 – protein marker, 2 – MSC, 3 – SM1, 4 – SM2, 5 – SM3. Bands for lysine mono-methylation can be seen between 25-50 kDa. No bands can be observed for MSCs and SM1 cells, whilst several bands could be seen for SM2 and SM3 cells. Di-methylated lysine bands can be seen just below 50 kDa – these bands are of lesser intensity in SM1, SM2 and SM3 cells compared to that for MSCs. Lysine tri-methylation bands can be seen just below 75 kDa. MSCs gave a very light band, SM1 gave no band, and SM2 and SM3 cells had very strong bands.

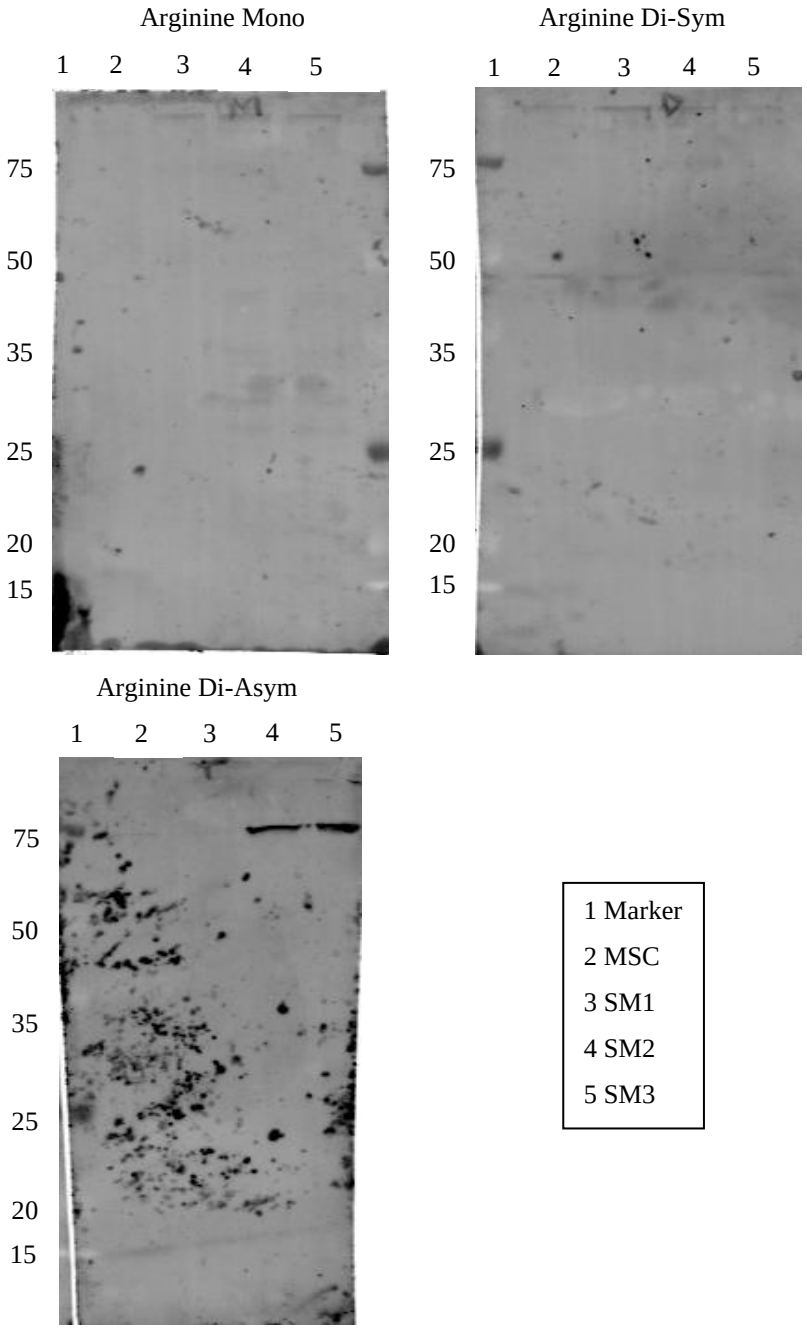

Figure 3.12. Re-incubated blots showing arginine mono-, di-symmetric, and di-asymmetric methylation. Protein sizes (in kDA) can be found on the left-hand side of each blot. The cell types pertaining to each lane can be seen as numbers on top of each lane within the blot: 1 – protein marker, 2 – MSC, 3 – SM1, 4 – SM2, 5 – SM3. Bands can be seen above 75 kDa. The above blots were previously incubated with lysine methylation antibodies and then re-incubated with arginine methylation antibodies. Hence, faint bands can be seen that do not correspond to arginine but are remaining bands from the previous blot. There can be seen weak bands of similar intensities for arginine mono-methylation in SM1, SM2 and SM3 cells with no band present for MSCs. Bands for di-symmetric methylated arginine can be seen in all lanes, the strongest band being that for MSCs and SM1. As for the di-asymmetric arginine, no bands were found for each cell type.

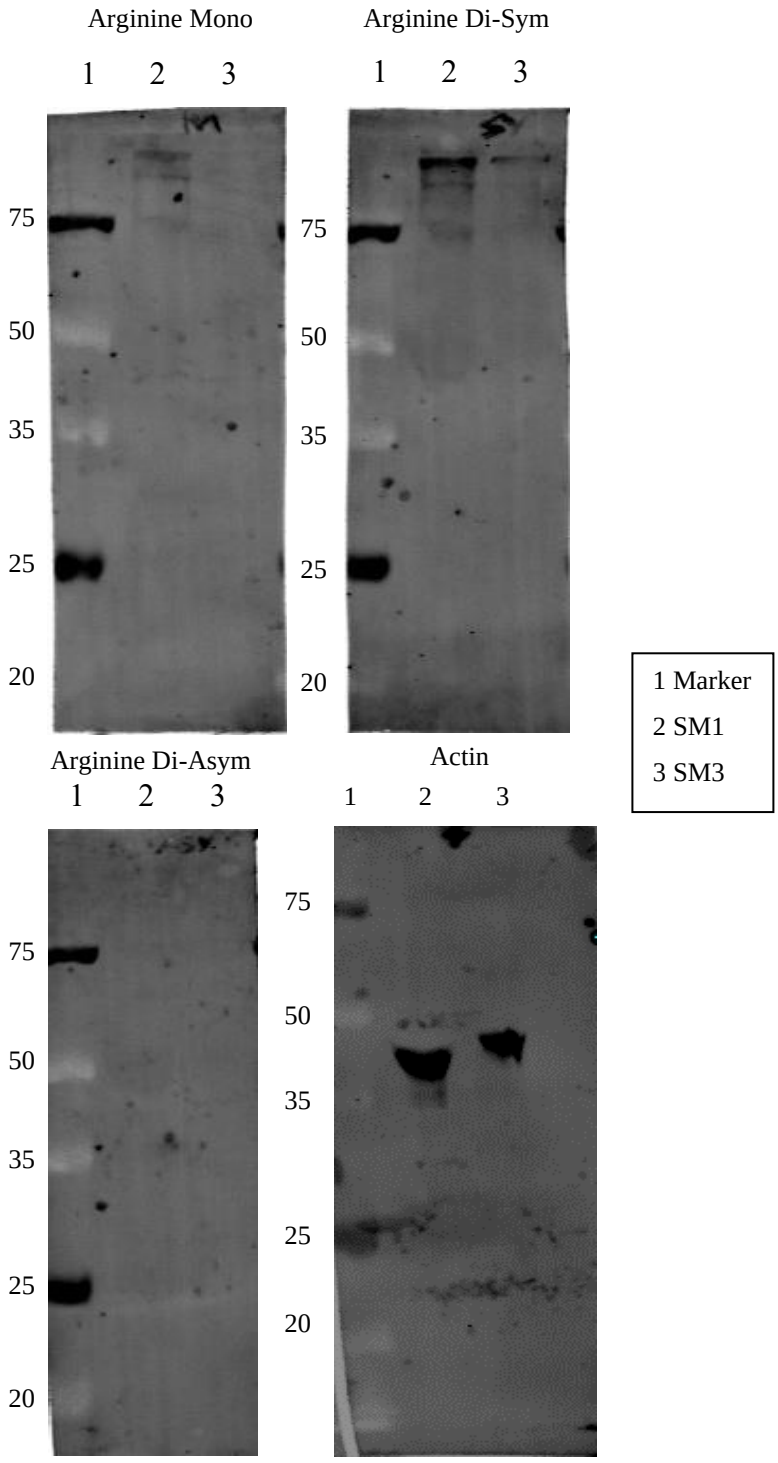

Figure 3.13. Scanned blots showing arginine mono, di-symmetric and di-asymmetric methylation. Protein sizes (in kDA) can be found on the left-hand side of each blot. The cell types pertaining to each lane can be seen as numbers on top of each lane within the blot: 1 – protein marker, 2 – SM1, 3 – SM3. Bands can be seen above 75 kDa. A mono-methylated arginine band was found for SM1, with no band for SM3 cells. A strong SM1 band for di-symmetric methylated arginine was found with a weak band for SM3 cells. As in the previous blot, no bands can be observed for di-asymmetric arginine for each cell type. In the last blot, Actin bands (loading control) can be seen between 35-50 kDa. Actin gave bands of similar intensity for both SM1 and SM3 cells, thus indicating equal protein loading.

Figure number	Antibody	Lane/Cell type	Integrated density	Ratio
3.11	Mono-methylated lysine	MSC	-	*Values are very similar and there are no bands visible for MSC*
		SM1	-	
		SM2	9820	
		SM3	8494	
	Di-methylated lysine	MSC	4015	MSC:SM1 – 1.7 MSC:SM2 – 3.2 MSC:SM3 – 1.6
		SM1	2381	
		SM2	1256	
		SM3	2487	
	Tri-methylated lysine	MSC	438	SM2:MSC – 11 SM3:MSC – 10.7
		SM1	-	
		SM2	4818	
		SM3	4694	
3.12	Mono-methylated arginine	MSC	-	*Values are very similar and no bands visible for MSC*
		SM1	1551	
		SM2	1669	
		SM3	1330	
	Di-symmetric methylated arginine	MSC	1343	SM1:MSC – 1.8 MSC:SM2 – 1.5 MSC:SM3 – 1.6 SM1:SM3 – 2.9
		SM1	2373	
		SM2	888	
		SM3	827	
3.13	Di-symmetric methylated arginine	SM1	6210	SM1:SM3 – 2.3
		SM3	2738	
3.13	Actin	SM1	12307	SM1:SM3 – 1.3
		SM3	9224	

Table 3.8. Showing the measured integrated density values for observed bands in the presented western blots. Integrated density values were calculated using ImageJ. A dash for integrated density means that there was no band visible for that lane in the blot. This table includes the figure number where the blot in question can be found, the corresponding methylation antibodies investigated within that blot, the cell type represented in the lanes where bands were observed, and the calculated

integrated densities corresponding to the band found within that lane. The last column includes the integrated density ratios computed as differentiated cell type : starting cell or the other way around depending on which band had a greater density. These ratios indicate the fold increase or decrease in integrated density values for bands resulting for the experimental cells or the starting cells.

3.5. Dopamine Enzyme Linked Immunosorbent Assay

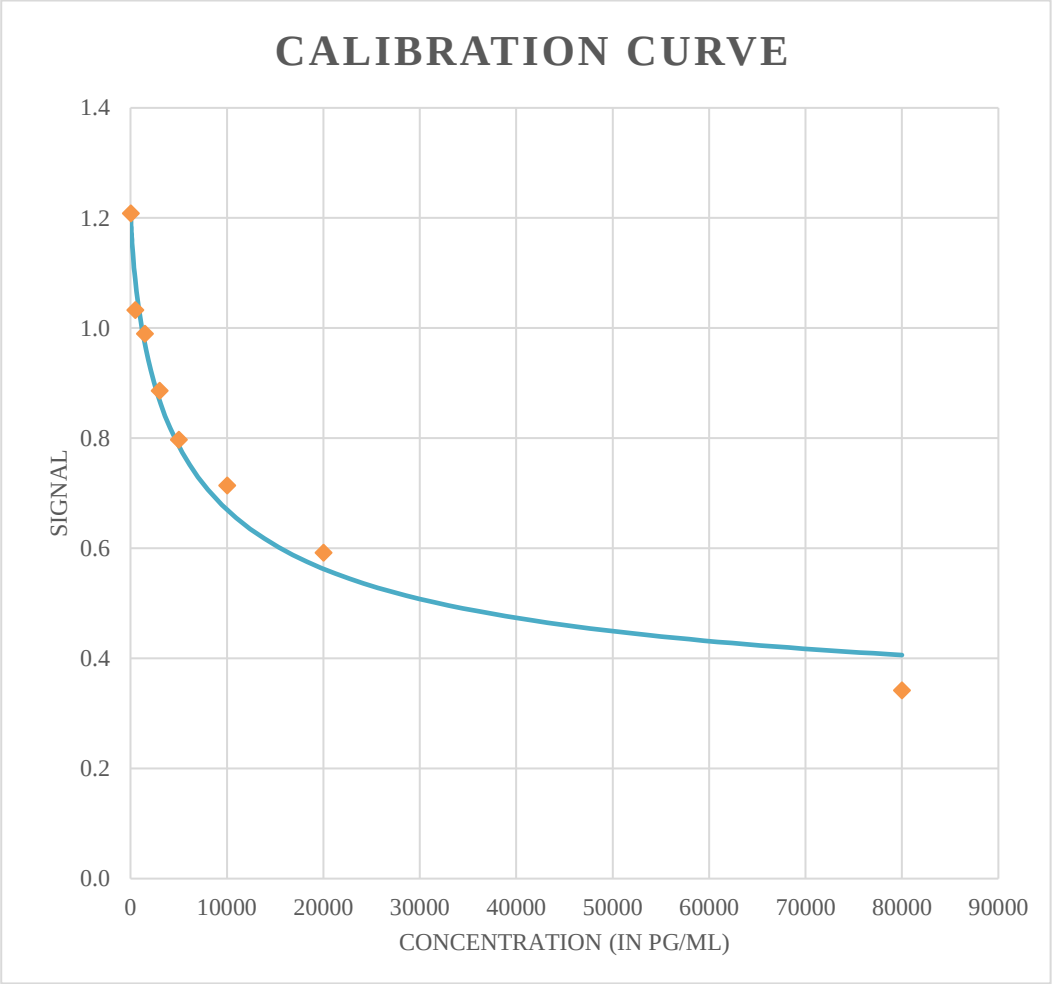

Figure 3.14. The ELISA calibration curve (4-parameter) computed using the AssayFitPro add-in on Excel. The dots on the curve represent the outputs for the standards and control solutions tested in the ELISA. The absorption signal is depicted on the y-axis and the concentrations pertaining to each standard are shown in pg/mL.

The dopamine ELISA was performed as an investigation of the extent of DA differentiation of induced-neuronal cells, and as an assessment of their functionality. Using the AssayFitPro add-in on Microsoft Excel, the calibration curve (Fig. 3.14) was computed using the controls and standards provided by Labor Diagnostika as part of the

dopamine ELISA kit. The standard curve was plotted as a 4-parameter line according to manufacturer's instructions. The function of the standard curve is as follows:

$$y = \left(D + \left(\frac{(A + D)}{(1 + ((x/C)^B))}\right)\right)$$

Where:

A = 1.221

B = 0.708

C = 6332.335

D = 0.271

Furthermore, the inverse function, as solved for x is as follows:

$$x = C\left(\left(\frac{A-D}{y-D}\right) - 1\right)^{\frac{1}{B}}$$

Where A, B, C, and D are the same values as shown above, and Y is the resultant absorbance value and X is the dopamine concentration for a given sample.

The standard curve generated for this analysis produced a coefficient of determination (R^2) value of 0.9797. This indicates that the standard curve produced on AssayFitPro was a good fit for the obtained data, and that results can be considered accurate in terms of their data processing calculations. The concentrations for each cell sample tested were calculated with AssayFitPro add-in using the determined inverse function and standard curve. These concentrations can be seen in Table 3.9 below. This table shows each analytical duplicate's determined concentration, their average, and final concentrations using the appropriate correction factor (amount of standard extracted, divided by amount of sample extracted), and their concentrations in nmol/L. Calculations determined that MSCs and SM1 cells were not releasing any dopamine (0 pg/mL) into their culture media. SM2 samples were found to have released 4.38, 0.73, 4.64, and 5.31 pg/mL of dopamine into their media, with analytical duplicate averages of 2.55 (SM2a)

and 4.98 (SM2b) . SM3 samples were found to have released 0.80, 0.87, 4.90, 0.15, 1.10, and 0.00 pg/mL of dopamine into their media, with analytical duplicate averages of 0.84 (SM3a), 2.52 (SM3b), and 0.55 (SM3c).

	Determined concentrations (pg/mL)				
Sample	**D1**	**D2**	**A**	**Final concentration for D1, D2, A**	**Conversion (nmol/L)**
MSC	0.00	0.00	0.00	0.00	0.00
SM1a	0.00	0.00	0.00	0.00	0.00
SM1b	0.00	0.00	0.00	0.00	0.00
SM2a	109.50	18.20	63.90	4.38, 0.73, 2.55	0.017
SM2b	116.00	132.80	124.40	4.64, 5.31, 4.98	0.032
SM3a	20.00	21.80	20.90	0.80, 0.87, 0.84	0.006
SM3b	122.6	3.7	63.2	4.90, 0.15, 2.52	0.017
SM3c	27.6	0.0	13.8	1.10, 0.00, 0.552	0.004

Table 3.9. Showing the determined dopamine concentrations for duplicate samples of conditioned media obtained from 2 biological replicates of SM1 (SM1a, SM1b) and SM2 cells (SM2a, SM2b), 3 biological replicates of SM3 cells (SM3a, SM3b, SM3c) and 1 sample of MSCs. Within this table are the determined concentrations (in pg/mL) for each analytical duplicate (D1 and D2), their average (A); the final concentrations (pg/mL) determined by multiplying with the appropriate correction factor (0.04); and their concentrations in nmol/L.

3.6. Mass Spectrometry

Main Proteins in MSCs		Main Proteins in Stage 3 Cells	
Q14767	Latent-transforming growth factor beta-binding protein (LTBP) 2/3	O15240	Neurosecretory protein VGF
P23142	Fibulin-1/2	Q16352	Alpha-internexin
P17936	Insulin-like growth factor-binding protein (IGFBP) 2/3	P29762	Cellular retinoic acid-binding protein 1 (CRABP1)

O00468	Agrin	P07196	Neurofilament light (NF-L) polypeptide
P24043	Laminin subunit alpha-2 (LAMA2)	P09172	Dopamine beta-hydroxylase (DBH)
P02751	Fibronectin	Q7L099	Protein RUFY3
Q9HCU0	Endosialin	Q5BJH7	Protein YIF1B
P07996	Thrombospondin-1	P13521	Secretogranin-2
Q13219	Pappalysin-1	P20711	Aromatic-L-amino-acid decarboxylase (AAAD)
P24821	Tenascin-C	Q06787	Synaptic functional regulator FMR1

Table 3.10. Showing the top 10 proteins found within MSCs and those within Stage 3 cells. Protein names are shown alongside their respective MS codes. The functions pertaining to each protein are described below.

The MS analysis specified the expression of 360 unique proteins in MSCs, and a further 650 unique proteins in Stage 3 cells. The top 10 proteins that were expressed in both these cell samples are delineated in Table 3.10. The functions of these proteins found in both cell types are described below.

The 10 main proteins that were found in MSCs used in this study, have been previously found in MSCs in other studies (Ragelle et al., 2017; Mizukami et al. 2019). Their implicated functions are as follows. LTBPs function in the extracellular matrix (ECM) and in the characteristic differentiation of MSCs (Robertson et al., 2015; Singh et al., 2022). Fibulin is an ECM paracrine factor (Won et al., 2020), and IGFBPs serve as carrier proteins for IGFs, whereby they regulate IGF activities, including proliferation, migration and differentiation (Jeon et al., 2017). Agrin has been implicated to function in MSC proliferation and haematopoiesis (Mazzon et al., 2011). LAMA2 serves to regulate characteristic MSC fate commitment (Zhu et al., 2020). Endosialin (CD248) is a C-type lectin-like transmembrane receptor in MSCs that interacts with fibronectin (Kondo et al.,

2021) and other ECM proteins to facilitate cell adhesion and migration (Tomkowicz et al., 2007). Thrombospondin-1 is implicated to play a role in MSC proliferation (Belotti et al., 2016). Pappamysin is a metalloproteinase that interacts with glycosaminoglycans on cell surfaces and functions as a growth promoting enzyme via its effects on IGFs (Oxvig, 2015). Tenascin represents a family of 4 ECM glycoproteins, of which Tenascin-C has been implicated to play a role in neural, skeletal and vascular morphogenesis in development (Tsai et al., 2014).

When it comes to the main 10 proteins found in Stage 3 neuronal cells, these were all different to those found in MSCs. Their neuron-related functions are described below. The Neurosecretory protein VGF is part of the granin family of neuropeptides and functions in regulation of energy, synaptogenesis, and neurogenesis (Quinn et al., 2021). α-Internexin is a type IV neuronal intermediate filament protein (Zhao & Jiang, 2016), and has been implicated to exert various functions, such as in dendritic and axonal growth (Chien et al., 2005; Benson et al., 1996), and post-synaptic signalling (Suzuki et al., 1997). CRABP1 regulates intracellular retinoid activity (Zetterström et al., 1999) to exert various effects on cellular functions in neurons (Nhieu, Lin & Wei, 2022), such as regulation of NSC proliferation, and calcium signalling (Lin et al., 2017). The NF-L polypeptide functions as a principal scaffolding constituent of the axoskeleton (Pogue et al., 2022), and has various roles such as in neurotransmission, and synaptogenesis (Pogue et al., 2022). DBH is an enzyme that catalyses the formation of norepinephrine from dopamine (Gonzalez-Lopez & Vrana, 2019). Protein RUFY3 has been implicated in axonal development and growth (Wei et al., 2014), and neuronal polarity (Wang et al., 2022). Protein YIF1B has been implicated in cargo transport in neurons (Carrel et al., 2008) and serotonin (5-HT) receptor targeting to dendrites (Alterio et al., 2015). Secretogranin II is a member of the secretogranin family (Wen et al., 2021), and has been

implicated to function in promotion of neuronal differentiation and maturation (Kim et al., 2015). AAAD is an enzyme that is critical for the production of catecholamines and indolamines (Hadjiconstantinou & Neff, 2008). Importantly, this enzyme is needed for the generation of dopamine from L-dihydroxyphenylalanine (L-DOPA) (Ren et al., 2017). Lastly, the FMR1 protein is an RNA-binding regulator that functions in synaptic protein synthesis, and formation of axonal and dendritic structures (Smidak et al., 2017).

Chapter 4 Discussion

4.1. Introduction

Neurodegenerative disorders are affecting an ever-growing number of people in today's world and are a leading cause of death (Choudhary, Gupta & Singh, 2020). As aforementioned (Section 1.1), current treatments for such disorders help reduce pain and symptoms but do not work against their cause (Choudhary, Gupta & Singh, 2020). Stem cell therapy has come forth as a possible solution for treatment of neurodegenerative diseases and thus, much research has focussed on the development of specific subtypes of neurons for the regeneration of damaged brain regions (Choudhary, Gupta & Singh, 2020). With more research, stem cell therapy will make it possible to delay neurodegenerative disease progression, and even target the causing factor (Zakrzewski *et al.*, 2019).

In this project, a neural induction protocol for the production of DA neurons was developed from previous research (Warrington, 2021). Considering the issues related to the use of ESCs and iPSCs (as elaborated on in section 1.3.4.), somatic stem cells were chosen as the starting cells (MSCs) to assess the devised protocol. Accordingly, MSCs are void of tumourigenicity, ethical and immunological tolerance issues, and, provided with the right environment for induction, MSCs can be differentiated towards cells of the neuronal lineage (Jiménez-Acosta *et al.*, 2022).

Small molecules for neural induction protocols were chosen based on the pathways that they target. Looking towards the literature that explores *in vivo* DA neurogenesis and differentiation, along with specific morphogens and TFs involved in driving this process, a 3-stage protocol (Fig. 2.2) was devised and tested on Wharton's jelly mesenchymal stem cells (WJ-MSCs). The timely activation/inactivation of 4 pathways and their cross-talk have been heavily implicated in the differentiation of NSCs to mature DA neurons

(Gaggi *et al.,* 2020; Brodski *et al.,* 2019). Such morphogens include SHH, FGF8, WNT, and TGF-β whose interaction bring about expression of multiple TFs crucial to DA neuronal development (Brodski *et al.,* 2019). The 3 stages of the devised protocol are based on the sequential events occurring in mDA neurogenesis, to target the aforementioned morphogens and attempt to mimic events occurring *in vivo.* In the following subsections, the roles of each media stage and the small molecules and proteins within them are defined accordingly.

4.1.1. Stage 1 – Reprogramming and Induction media (days 1-7)

Signalling pathways that influence stem cell quiescence and pluripotency were targeted in this first stage of treatment. The stage 1 media consisted of SHH, Y27632, CHIR99021, and SB431542/A8301. This stage served to encourage the reprogramming of MSCs so that they may be pushed to enter the neuroectoderm lineage. Furthermore, it served to specify MSCs toward a mDA fate.

SHH is central to induction and patterning of the FP and basal plate (Mesman & Smidt, 2020; Blaess & Ang, 2015), and is thus vital for the commitment of NSCs to the mDA fate (Volpicelli *et al.,* 2020). SHH pathway components are expressed very early on in mDA progenitor cells, and these are maintained until cells become differentiated (Brodski *et al.,* 2019). CHIR99021 is a potent WNT signalling inducer (Wang *et al.,* 2020). It is applied to this stage of the protocol to enhance transcription of WNT-activated pluripotency genes thus enhancing pluripotency reprogramming (Qin, Zhao & Fu, 2017). *In vivo,* WNT signalling is specifically involved in development of mDA progenitors and their specific differentiation towards mDA neurons (Brodski *et al.,* 2019). SB431542 was added as an inhibitor of TGF-β family signalling to inhibit endodermal and mesodermal fates, and encourage reprogramming of MSCs so that they may enter the neuroectoderm lineage (Brodski *et al.,* 2019; Galiakberova & Dashinimaev, 2020). Finally, the ROCK

inhibitor Y27632 served to protect cells from cell death during their treatments (Labandeira-Garcia *et al.,* 2019).

4.1.2. Stage 2 – Differentiation media (days 7-14)

Stage 2 served as a means to further specify an mDA neuronal fate and encourage the MSCs' differentiation along this fate. Stage 2 media consisted of SHH, FSK, FGF8, Activin A, DAPT, db-cAMP.

FGF8 is an essential part of the beginning stages of mDA neuronal development (Brodksi *et al.,* 2019) and its expression is specifically induced during development of the isthmus (Mesman & Smidt, 2020). FGF8 signalling is also vital for maintenance of neural progenitor viability (Brodski *et al.,* 2019). *In vitro,* the addition of FGF8 has been found to induce DA neuron differentiation of neural cells. Importantly FGF8 and SHH work concertedly to induce NPCs to acquire an mDA fate (Mesman & Smidt, 2020). Thus, SHH was maintained in this stage of the protocol to sustain promotion of the mDA fate specification. FSK was added to increase intracellular cAMP concentrations, in turn activating MAPK signalling (George *et al.,* 2019). Such an effect enhances neuronal specification and neurite outgrowth (Singh *et al.,* 2020). The Notch inhibitor DAPT served to inhibit glial differentiation and boost neuronal differentiation (Crawford & Roelink, 2007). Activin A has been implicated to serve a neuroprotective role (Tretter *et al.,* 2000) and to enhance neuronal differentiation (Park *et al.,* 2016). Finally, db-cAMP activates PKA signalling and CREB expression (Kim *et al.,* 2011). In this stage it served to promote neuronal differentiation of progenitor cells towards immature neurons.

4.1.3. Stage 3 – Maturation media (days 14-28)

The final stage of small molecules treatment served to promote further differentiation and the final maturation of induced neuronal cells. Stage 3 media consisted of BDNF, GDNF, TGF-B3, Activin A, DAPT, and db-cAMP.

Firstly, Activin A served the same function as it did for Stage 2 media. DAPT has been implicated to play a role in the maturation of neurons during their differentiation, as well as in their electrophysiological development (Rakovic *et al.,* 2022). Its addition fits in well with the purpose of Stage 3 media. In addition to the aforementioned roles, db-cAMP is involved in NT signalling (Kim *et al.,* 2011), thus, its addition with GDNF and BDNF served to further enhance their effects. Moreover, db-cAMP boosts neurite outgrowth and for these reasons it was deemed highly suitable for this stage of the induction protocol.

NTs and NTFs enhance survival of DA neurons (Di Santo & Wildmer, 2018), and are involved in the early survival phase *in vivo* (Jurkowski *et al.,* 2020). Addition of both BDNF and GDNF in this stage served to discourage neuronal cell death and promote their viability in this last stage of treatment. Both these factors served to promote neurite outgrowth and encourage further differentiation, as well as morphological maturation (Leal-Galicia *et al.,* 2021). Finally, TGF-β3 was added to further enhance the effects of GDNF on the induced neuronal cells (Meyers & Kessler, 2017). Furthermore, this factor was added since it specifically serves to promote the survival of DA neurons *in vitro* and encourages neurite outgrowth and morphological maturation (Luo *et al.,* 2016).

4.2. Morphological changes

A clear progression in cellular morphology was found in cells as they progressed through the small molecule treatments (Table 3.2). The starting cells were either flat and cuboidal, or spindle-shaped, as is characteristic of MSC morphology, and had no neurites

growing out of them. Upon the cells' treatment with Stage 1 media (Reprogramming and Induction media), the cells started changing their morphology. By the second stage of treatment (Differentiation media), cells had more distinct cell bodies, with a more 3D morphology and elongating neurites growing from either end of the cell bodies (Image E). During Stages 2 and 3, cultures were observed to present with formation of neural networks composed of many rounded neuron-like cells in close association with one another, thus forming a cluster. Additionally, in Stage 2 cultures, there was the occurrence of dendritic arborisation, and increased neurite complexity, seen as a multitude of secondary and tertiary neurites. During the third stage of treatment (Maturation media), distinct and spherical cell bodies were observed with very dense neurite connections that grew out of cells in all directions (image I). A great degree of dendritic arborisation was observed in Stage 3 induced-neuronal cells (image K, L). Additionally, axonal processes appeared to be growing longer and thicker. This observation suggests the occurrence of axonal transport in the final cells.

By the end of the SM1 treatments (image D), cells seemed to adopt a more neuron-like morphology which suggested that the starting MSCs had been successfully reprogrammed to enter the neuroectoderm lineage with Stage 1 media. Cells at the end of Stage 2 could be said to morphologically resemble IPCs or immature neurons, and the changes in SM3 cells indicated that increased neuronal maturation and function occurred by Stage 3. Moreover, induced neuronal cells appeared to be forming neurosphere-like structures (bottom right corner of image I) and neural networks throughout cultures.

Image J, showing cells on Day 6 of their SM3 treatment, is a good example to illustrate a limitation experienced during neuronal induction treatment of cells in this project. Besides cells undergoing neuronal differentiation changes, there are also areas of the image that show a lot of debris. These debris collections had a shape similar to that of

the transdifferentiated cells, suggesting that they were previously differentiated cells that had died, and their cell contents left behind. Surrounding these bubble-like structures are neurites which formed connections with other cells or neurites of neighbouring cells. Burst cells can also be seen to have started occurring in the SM2 stage (images E, F). Potential reasons for this, and amendments are discussed in later sections.

One thing to note is that in every stage of treatment, there were cells that appeared to be at different stages of differentiation. Some cells appeared as though they had a more MSC-like morphology amongst other cells that seemed to be much more advanced in their differentiation. This could be due to the inherent heterogeneity of cells, and thus of their reactions to treatment. Alternatively, in their study, Nolbrant et al., 2017 suggested that this is common for DA progenitors, since in their experiments, differentiating DA progenitors did not display a typical rosette-forming neuroepithelial morphology. They described an occurrence of cells with different stages of morphology along the treatment, with some cells having a more flattened appearance that does not resemble neuronal cell types. Researchers elaborated further and stated that this was an indication that the cells needed more time for maturation. Their starting cells were iPSCs and this flattened morphology that they described was strikingly similar to that seen in cultures in this study.

An analysis on microscopy images of cells at each stage of differentiation was carried out. As a means by which to quantify changes in neuronal morphology along the cells' differentiation treatment, neurite outgrowth lengths (Table 3.3) were measured on ImageJ (Schindelin *et al.,* 2012; Rueden *et al.,* 2017). This ImageJ analysis of neurite changes depicted a positive trend for the average lengths of neurites growing out of cells, length of the longest neurite measured, and the total neurite outgrowths (μm) on going from SM1 to SM3 cells. Despite the inclusion of many short secondary and tertiary neurites in the quantification of neurites in SM3 images, the average neurite lengths still

increased substantially. Neurite lengths increased by an average of over 100 µm from SM1 to SM2 and SM2 to SM3; a trend that is illustrated in Fig. 3.2. Moreover, there was a significant increase in the length of the longest neurite measured, which was a length of 523 µm in SM1 and 1596 µm in SM3 (Fig. 3.3). Additionally, the lowest value for total neurite outgrowth in SM3 (23385 µm) was almost double the greatest total neurite outgrowth measured in SM1 (12150 µm).

This analysis supports what was implied upon observation of morphological changes by microscopy. Statistical analysis of changes in average neurite outgrowths along the differentiation protocol, further validated these results. The one-way ANOVA indicated that differences between the average neurite lengths measured for each stage were significant, suggesting that morphological changes along the induction and differentiation protocol were considerable.

4.3. Gene Expression

4.3.1. CD Markers

In this study, expression levels of CD166 were found to match those of CD105, an official MSC marker also used in this analysis. Considering the expression of CD166 in several cellular components in neurons, CD166 was intended as a marker that could indicate the differentiation from MSCs, such that a negative expression was expected for MSCs, followed by bands of increasing intensity with increasing differentiation. However, CD166 expression has also recently been found expressed in several types of MSCs isolated from different sources (Brinkhof *et al.*, 2020). This would explain the obtained results for CD166 expression, since a positive expression was found for all stages (MSCs, and SM1/2/3 cells).

No literature could be found to explain a positive expression of CD105 for SM2 and SM3 cells, in terms of its positive expression having been found in neuronal cells. What this can indicate, however, is that there could have been contaminating, undifferentiated MSCs within the SM2 and SM3 cultures. This is quite a plausible explanation, considering that neural transdifferentiation protocols are never 100% efficient, and that cells differentiate in a very heterogenic manner (Wang *et al.*, 2022). Moreover, as aforementioned, cells that resembled the morphology of starting MSCs were found to be present in both SM2 and SM3 cultures.

CD90 was only tested since CD105 expression results were not as expected. Considering these are both established markers for MSCs, their expression, at least in MSCs, should be similar. As expected, CD90 was positive in MSCs, however its expression was maintained throughout the treatment of cells (Fig. 3.7). CD90 expression has been found on the cell surface of many cell types, including in neurons throughout the nervous system (Bradley, Ramirez, & Hagood., 2009; Jósvay *et al.*, 2014). Thus, its expression in starting cells and in cells pertaining to each stage of differentiation can be rationalised based on its expression pattern.

As can be seen from Table 3.5, the bands that resulted for the reference gene (GAPDH) gave very similar integrated density values, implying that equal loading of each cell sample in each lane had occurred. Thus, unequal loading can be ruled out as a reason for changes in band intensities or lack of a band signal. In Fig 3.5, two faint bands were found for MSCs and SM3 cells for CD105 expression. This result did not make much sense, and that is why the second end-point PCR run to check CD105 expression was performed. Fresh cDNA was prepared from different frozen cell collections for the second set of gels shown in Figs. 3.6 and 3.7. Thus, it could be that the sample used for these subsequent end-point PCR runs, had a greater number of contaminating

undifferentiated MSCs in SM1, SM2 and SM3 cultures in comparison to the first samples that were used. Alternatively, it could be that the starting cells used for treatment that resulted in those cell samples, did not have a high expression of CD105 to begin with. This would be due to naturally-occurring endogenous differences in CD marker expression in MSCs.

4.3.2. Neural Markers

In the first RT-qPCR run (Table 3.6), the SM1 cells showed a slight increase (a 2- to 3-fold change compared to MSCs) in pluripotency marker SOX2 and IPC marker MASH1. Note that the starting cells that were used as a baseline for comparison of expression for these neural markers in treated cells, being MSCs, are stem cells and might be expected to have a certain degree of pluripotency marker expression. In fact, MSCs express pluripotency markers OCT4 and SOX2 at low levels at the beginning of their culture (Han *et al.,* 2014). Thus, having increased SOX2 expression in comparison to that in MSCs, indicates that the Stage 1 media served its purpose in causing cells to dedifferentiate to a more primitive state of greater pluripotency. The MASH1 result indicates that the Stage 1 media was able to push cells to enter the neuroectoderm lineage and start expressing markers for cells in IPC stages, such that maybe the Stage 1 media was able to push cells further than was expected. This was decreased in SM2 and SM3 cells, which is as would be expected. However, the MASH1 results are not considered reliable since in each run and for each cell sample, the Ct number was very low, even in MSCs. This suggests that there might have been a problem with the MASH1 primers, and that unspecific annealing might have occurred with these primers.

What was quite unexpected was that SM1 cells in the first run (Table 3.6), showed a 6-fold increase in NEUROD1 expression. No immature neurons were expected to have formed during Stage 1 treatment, and the TUBB3 expression result was conflicting, such

that it showed a decreased expression in relation to MSCs. Although NEUROD1 is generally used as a marker for immature neurons, several papers state that this expression first appears before cells have reached immature stages. In Tutukova, Tarabykin & Hernandez-Miranda (2021), it is stated that the expression of this TF is timely with the transition from primary progenitor cells to intermediate progenitors and is maintained for their terminal neuronal differentiation. Furthermore, in Kempermann, Song & Gage (2015), the authors state that type 2b cells, a kind of IPC in adult neurogenesis, begin to express several neuronal lineage markers including NEUROD1. Thus, the increased expression in SM1 cells could indicate that the cells were in IPC stages approaching immaturity, rather than already immature neurons. Still, this would mean that SM1 media pushed cells a little further than expected. Moreover, there was a very slight increase in expression of the mature neuronal markers NEUN, MAP2 and 2-fold in TH.

In the second run (Table 3.7), SM1 cells showed a slight increase in SOX2 and MASH1 expression, as was expected, although a slightly greater increase in their expression would have been more suitable. In contrast to the first run, TUBB3 expression was increased and NEUROD1 was decreased. Considering that NEUROD1 expression may appear earlier than that of TUBB3, this increased TUBB3 expression cannot mean that cells were in late IPC stages, rather they had reached the stage of immature neurons. Besides, there were also small increases in mature neuronal markers NEUN and MAP2. NEUN was very slightly increased, however MAP2 was increased 3- to 4-fold. This is still a small increase in expression; however, it implies that some cells in this SM1 sample might have already been progressing towards maturity. TH expression was as expected and did not increase.

SM2 cells in the first run (Table 3.6) had decreased pluripotency marker SOX2 expression, and MASH1 expression, indicating that cells were past progenitor stages.

TUBB3 expression was greatly increased (13-fold) in comparison to the starting cells, which would suggest that there were cells in an IPC stage. Interestingly, NEUROD1 expression was increased almost 3-fold, however this was half the increase seen for this IPC/immature neural marker in SM1 cells. Considering that NEUROD1 can be seen earlier than TUBB3, it makes sense that TUBB3 expression is much greater than that of NEUROD1. This suggests that these SM2 cells were mostly immature neuronal cells rather than IPCs. As expected, there was an increase in both mature neural markers NEUN and MAP2. NEUN showed a 2.6-fold increase in expression, and MAP2 a 5.7-fold increase. This results suggests that some of the cells within this SM2 sample tested here, had progressed further and were in a mature neuronal state of differentiation. Some degree of heterogeneity within the cells in the various differentiation cultures was expected, since there is an inherent heterogeneity in cells during their *in vivo* neurogenesis, where some cells are always maintained as proliferating progenitors whilst others differentiate further (Zhang & Jiao, 2015). Hence, it would make sense that some cells in this SM2 sample were still progressing towards maturity, whilst others had already started to mature. Considering the values that resulted for their fold-change in expression (Table 3.6), it can be suggested that most cells were in immature stages still progressing towards maturity. However, an almost a 6-fold increase in MAP2 indicates that a good number of cells had reached maturity. Importantly, the TH expression showed a 2.8-fold increase, indicating that some of these induced neuronal cells had begun expressing TH. This suggests that the small molecules protocol had successfully specified a DA neuronal fate in at least some of the cells in culture.

As in the first run, SM2 cells had decreased SOX2 and MASH1 expression in the second run (Table 3.7). Also, similarly to the first run, SM2 cells showed a great increase in TUBB3 expression, indicating that cells were in an immature neuronal state. However,

NEUROD1 did not increase at all, indicating that these cells were past IPC stages, rather at a stage of late immaturity. In fact, both mature neuronal markers were increased. NEUN increased almost 4-fold, and MAP2 increased 7-fold. The SM2 results in both RT-qPCR runs were quite congruent, and both indicated that cells in SM2 had successfully reached immaturity and even started maturing. In the first run SM2 cells showed a 2.8-fold increase in TH expression, which is enough to indicate that the cells had started progressing towards a DA neuronal fate. However, in this second run, the SM2 cells gave only a slight increase in TH expression (1.8-fold).

Unfortunately, when it came to the SM3 cell sample, both runs gave an odd result. In the first run, all markers showed a decreased expression, except for NEUROD1 which was increased by 5.5-fold. This increase in NEUROD1 expression suggests that cells here were lesser differentiated than cells in SM2. However, explanation for the lack of expression for all other markers cannot be based solely on the cells being in a lesser differentiated state. The same was found in the second run. SM3 cells showed no increases in expression in any markers, but a very slight increase in TH expression. Something went wrong in the RT-qPCR of this SM3 sample and reasons for this are expanded on in the Limitations and Improvements Section (4.7).

Overall, excluding SM3, these results indicated that the small molecules protocol was successful at pushing MSCs to dedifferentiate out of their mesenchymal lineage and start differentiating within that of the neuroectoderm. Changes in expression were not exactly as expected for SM1 and SM2, however, they imply that the media stages pushed cells even further than they were meant to. Specification of the DA neuronal fate might have occurred, however without well-grounded SM3 results, this could not be reliably inferred.

4.4. Western Blotting

4.4.1. Methylation Changes

PTMs on histones within chromatin are varied and complex (Shimomura & Hashino, 2013). Chemical modifications include methylation, acetylation, phosphorylation, sumoylation, and ubiquitination amongst others. However, histone methylation and acetylation are considered the most extensive in terms of having an effect on biological processes during neural differentiation (Shimomura & Hashino, 2013). Histone methylation is performed by histone methyltransferases (HMTs) and removed by histone demethylases (HDMs), and predominantly transpires at lysine and arginine residues on histone tails (Ren *et al.*, 2020).

Methylation at these residues has been linked to both transcriptional repression and activation (Shimomura & Hashimo, 2013). Which effect is conveyed depends upon which residue is methylated. For example, methylations on histone (H) 3 lysine (K) 9 (H3K9), H3K27, and H4K20 have been associated with gene silencing, whereas methylations on H3K4, H3K36 and H3K79 have been shown to activate gene transcription (Shimomura & Hashimo, 2013). Moreover, lysine residues can be mono-, di-, or tri-methylated, which influences the degree of transcriptional activation or repression, and these bring about different outcomes.

Histone demethylation has been linked to regulating proliferation and differentiation of stem cells (Zhou *et al.*, 2018). Both Lysine-specific demethylase 1 (LSD1) and JmjC histone lysine demethylases have been found to be involved in regulating differentiation of stem cells. Inhibition of LSD1 activity has been found to result in a decreased proliferation of NSCs (Sun *et al.*, 2010). Moreover, LSD1 was found to be involved in transcriptional inactivation of multiple developmental genes in hESCs through regulating methylation of lysine residues on histone 3 (Zhou *et al.*, 2018). Such

studies demonstrate the involvement of histone modifications in activating and promoting neural differentiation of NSCs. However, these changes and their mechanisms are still largely not understood.

Histone modification of lysine residues has been implicated in activating or repressing transcription of genes for TFs involved in early lineage commitment in ESCs (Huang & Jiang, 2015). Specifically, H3K27 tri-methylation (repressive) and H3K4 tri-methylation (activating) modifications have been implicated for TFs such as SOX, FOX, and PAX gene family members. Enhancer of Zeste homology 2, an HMT with H3K27 trimethylation specificity has been found to have an inhibitory effect on the neuronal transdifferentiation of MSCs both *in vitro* and *in vivo* (Yu *et al.,* 2011; Ren *et al.,* 2020).

In ESCs, the promoters of pluripotency genes such as OCT4 and Nanog have been demonstrated to be trimethylated at H3K4 residues, that is strongly linked with transcriptional activation (Azuara *et al.*, 2006; Bernstein *et al.,* 2006). On the other hand, genes that lead to neuronal differentiation, are kept in a transcriptionally competent yet inactive state by combined histone modifications that are both activating (H3K4 trimethylation) and inhibiting (H3K27 trimethylation). This is referred to as bivalent histone methylation, and is found in the promoters of pro-neural genes such as neurogenins, *PAX6,* and *MASH1* in undifferentiated ESCs (Mikkelsen *et al.,* 2007). This bivalent histone modification is controlled by Polycomb-group (PcG) and Trithorax-group (TrxG) proteins, which are responsible for repression (H3K27) and activation (H3K4) respectively (Shimomura & Hashimo, 2013). Furthermore, other repressive histone modifications have been discovered to play a role in neuronal differentiation. A study found that during their differentiation, ESCs experienced continuous increases in chromatin silencing via H3K9 methylation (Meshorer *et al.,* 2006). It has thus been suggested that these repressive H3K9 methylation modifications contribute to acquiring

an appropriate neuronal gene expression profile in response to extracellular signals (Song & Ghosh, 2004). In another study they discovered that BIX-01294, a G9a HMT inhibitor, induces expression of neuronal genes such as *Nestin* and *Musashi* by downregulating *G9a* and H3K9 dimethylation in repressor regions of these genes (Kim, Jeong & Cho, 2016).

Such methylation modifications at histone residues were expected to occur between the different cellular differentiation stages in this study. However, whether an increase or a decrease in such modifications was expected could not be determined, since trimethylation of lysine residues seems to occur for both gene activation and silencing. In addition, there would be the inactivation of pluripotency genes, and activation of pro-neural and neuronal genes occurring as the cells differentiate along the neuroctoderm lineage. Thus, there would be different degrees of increases or decreases in lysine trimethylation, depending upon what needs to be activated or repressed at that point in the differentiation timeline for those cells. Furthermore, since histone methylation and demethylation at different histone residues have different effects in terms of activation or repression of genes, then methylation changes explored by Western Blotting are not enough to specifically conclude on what these changes mean. However, having big differences in bands indicating large alterations in methylation patterns, strongly indicates that the neuronal differentiation protocol has epigenetically modified the cells along their treatment. Such protein methylation changes correspond to gene expression changes, and thus signify a lot in terms of the altered phenotypes of the cells along their neural induction treatment.

As can be seen in Table 3.8, there was a big change in lysine mono-methylation in SM2 and SM3 cells in comparison to MSCs and SM1 cells. In fact, no band even occurred in MSCs and SM1 cells, whereas around 6 bands in sequence occurred in SM2 and SM3 lanes. On the contrary, there seemed to be a decrease in lysine di-methylated proteins in

SM1, SM2 and SM3 cells when compared to the starting cells, where the band in the MSC lane was between 1.6- to 3.2-fold the intensity of bands in the lanes corresponding to treated cells. Highly significant changes were found for lysine tri-methylation (Fig 3.11). MSCs gave a very faint band (integrated density: 438), SM1 cells gave no band whatsoever, and SM2 and SM3 cells gave bands that were found to be more than 10-fold more intense than the MSC band. Such drastic changes indicate that epigenetically, the induced cells were very different to the starting cells. Considering the literature on lysine tri-methylation's involvement in neuronal differentiation, these changes might have occurred to repress pluripotency genes, and activate neuronal genes in response to the signals dictated by the small molecule treatments.

When it comes to arginine methylation changes, not much literature could be found regarding its involvement in neuronal differentiation. Two blots for each of the 3 arginine methylation antibodies were carried out. The first was only a reincubation of the lysine blots, and that is why a second arginine methylation blot was performed. In the first blots (Figs. 3.12), resulting bands suggested an increased arginine mono-methylation in SM1, SM2 and SM3 cells when there was no band for MSCs, though these were all weak bands. Additionally, bands for di-symmetric methylated arginine were present in all lanes. However, there was a slight increased signal for SM1 cells, and decreased signals for both SM2 and SM3 in comparison to MSCs (where the MSC band was around 1.5 times the density of both SM2 and SM3 bands). Finally, there were no resulting bands for any lane in the di-asymmetric methylated arginine blot. The same was seen in the second set of blots (Fig. 3.13) for both di-symmetric methylated and di-asymmetric methylated arginine (second and third blots respectively). More specifically, there were no bands in the arginine di-asymmetric methylation blot, and the SM1 di-symmetric methylated arginine band was between 2-3 times denser than the band for SM3. These results

indicated that there were no changes in arginine di-asymmetric methylation occurring on proteins in cells along their progression in the neural induction protocol. However, there were changes in their di-symmetric arginine protein methylation levels, with a general decrease as cells progressed further along the treatment protocol.

Finally, when it came to the second mono-methylated arginine blot, no band resulted for SM3 cells, which is a different result to that found with the previous blot. However, in the first blot, the bands were very faint altogether, with that for SM3 cells being the faintest. In any case, both blots indicated a change in arginine mono-methylation. This was either a change in mono-methylation levels from MSCs to the treated cells (no band vs positive signal), or decreased levels (weak band for SM1 cells vs no band for SM3 cells) for Figs. 3.12 and 3.13 respectively.

Actin, which was used as a loading control, gave bands of more-or-less equal intensities for SM1 and SM3 cells. Although these were slightly different, the SM1 band, which was the stronger one, was only 1.3 times the intensity of the SM3 band. This suggested that the lanes were loaded equally and that unequal protein loading for each lane was not a source of variation in these blots. Unfortunately, when the incubation of blots with Actin antibodies was finally successful and gave a good signal, this was on the SM1 vs SM3 blot. Thus, the equal protein loading for all 4 lanes cannot be assured. An issue was experienced whereby blots kept drying up very quickly after being incubated only once or twice, and fresh blots had to be made each time for antibodies to bind properly to result in good and reliable signals. Additionally, there was an issue in getting bands for Actin since the Actin isoform expressed in these cells seems to change along their treatment.

These results suggest that significant changes in protein methylation patterns at lysine and arginine residues have occurred on going from MSCs through each stage of

differentiation. These results can be supported by the literature elaborated on above, which advocates the success of the devised small molecules treatment protocol in pushing cells to transdifferentiate within the neural lineage. Taken together with changes in morphology, and neural marker expression in SM1 and SM2 cells, these results further suggest that changes in the transcriptome, proteome, and thus phenotype of cells must have occurred along the treatment of cells. These results, however, are not specific, and only indicate general changes in methylation patterns as epigenetic changes occurring while the cells undergo treatment. Hence, conclusions on what they mean exactly cannot be made. Ideally, these results would be further explored by means of MS analysis of protein methylation sites. In this way, the histones and other proteins on which lysine and arginine methylation occurred could be identified, which would paint a better picture regarding the success of this transdifferentiation protocol.

4.5. Dopamine Enzyme Linked Immunosorbent Assay

An essential characteristic of the function of DA neurons is their ability to synthesise and release dopamine in response to membrane depolarisation (Yang *et al.*, 2016). The dopamine ELISA was used as another means to explore the differentiation extent of induced neuronal cells, as well as the success of the protocol in specifying a DA neuronal fate.

Table 3.9 shows the determined concentrations for duplicate samples of conditioned media obtained from 2 biological replicates of SM1 and SM2 cells, 3 biological replicates of SM3 samples and 1 sample of MSCs. The resulting determined concentrations were in the range of approximately 0.0-5.3 pg/mL. As expected, calculations showed that MSCs released 0 pg/mL of DA into the media, and the same was found for SM1 cell samples. SM2 samples were found to have released between 0.73 and 5.31 pg/mL of dopamine into their media. SM3 samples were found to have released between 0.00 and 4.90 pg/mL

of dopamine into their media. It seems odd that SM2 samples gave 3 out of 4 tests greater than 4 pg/mL, when SM3 samples gave only 1 out of 6 tests that were greater than 4 pg/mL, with 4 out of 6 being less than 1 pg/mL. There could be multiple reasons attributed to this. Firstly, it could simply be an accurate representation of the dopamine levels induced by the different stages of the media, although this is unlikely considering that SM3 cells had been in differentiation media for longer. It could also be due to variations in the way the differentiation culture was followed between experimental wells (elaborated on in further sections), variations in the number of cells within the wells out of which media was collected, or variations in the number of viable or non-viable cells, since non-viable induced cells would not likely be releasing dopamine. Reasons could also be the presence of chemicals that degraded the dopamine in the sample, pipetting errors, and improper mixing of the sample after it had been thawed, amongst others.

The standard curve produced gave a coefficient of determination (R^2) value of 0.9797. This indicates that the standard curve produced on AssayFitPro was a good fit for the obtained data, and that results can be considered accurate, at least in terms of their data processing calculations. Some of the determined duplicate concentrations might seem very distant from each other, however these are measurements found in picograms, so large differences are in fact quite small. Additionally, the competitive ELISA used here gives absorbances that are very similar to each other but translate to large differences in concentrations. An example of this is the small difference in the average absorbance readings for 2 of the lower standards. The 500 pg/mL standard had readings of 1.033 when the 1500 pg/mL standard had readings of around 0.99. This shows that very small fluctuations in absorbance readings in this assay resulted in large differences in the output sample concentrations. One aspect of the ELISA that could have resulted in such large variations within samples of the same type could be the fact that standard concentration

samples are given in ng/mL and not pg/mL, and thus they are not accurate within the picogram range.

When looking to the literature, several different papers were found in which a dopamine ELISA was also used for quantification of dopamine released by their neuronally-induced cells. Some reported dopamine concentrations are: 5-20 pg/mL (Yang *et al.,* 2019), 0.36-10.3 pg in 1-2 x10^5 cells (Chabrat *et al.,* 2019), or 400 pg/mL (Trzaska *et al.,* 2007), 10 ng/well (Lim *et al.,* 2015), 1.3 ng/mL (Kim *et al.,* 2017), 20-100 ug/million cells (Yang *et al.,* 2016), and 4.5-6 ng/mL (Singh *et al.,* 2020). However, it is worthy to note that the results reported in all of them except for Yang *et al.,* 2019 were found after the induced-cells were instigated to release dopamine by depolarisation of cells using elevated K^+ solutions, or the addition of L-DOPA (in Chabrat *et al.,* 2019), and cells were also sometimes treated with a DAT inhibitor (in the study by Trzaska *et al.,* 2007). Such additions to cells must have substantially influenced their results. Additionally, the fact that some measurements were given in per million cells, rather than in pg/mL makes it quite difficult to compare. Lim *et al.,* (2015) gave their dopamine measurement in ng/well. Since they used 6-well plates, their culture media volume was in the range of 1-3 mL, and thus their reported dopamine concentrations can be converted to approximately 3-10 ng/mL.

The only paper which reported dopamine release without it being evoked by membrane depolarisation was Yang *et al.,* 2019, and their values were quite comparable to those obtained for induced cells in this study. However, the values reported for the induced cells in this study are on the lower side of what Yang *et al.,* reported. Yang *et al.,* used the same dopamine ELISA kit, which makes comparison more reliable. However, they processed their collected spent media samples, filtered out debris and concentrated them, mixing several media collections into one, before they analysed them with the

ELISA. Concentrating their media samples with reduced volumes would have increased their resulting dopamine concentrations in a way that the samples in this study weren't. Spent media samples tested in this study were collected individually and ELISA experiments were not performed on pooled media concentrated from different collections. This could have decreased the dopamine potency in media samples for this study in relation to those tested in Yang *et al.,* (2019). All this being considered, it could be said that the dopamine release concentrations found for induced neuronal cells in this study, was comparable to that found in one study with similar experimental conditions, despite their samples being concentrated.

Additionally, dopamine release concentrations found in this study were within the same range that was found in a study conducted by Chabrat *et al.,* (2019). The dopamine concentrations they obtained in their study were for a lesser number of cells compared to other studies. It could be that the number of cells in culture when spent media was collected for the ELISA in this project, was similar to the number of cells used for their dopamine measurements in Chabrat *et al.,* (2019). The researchers in this study stated that dopamine synthesis was found to increase significantly when L-DOPA was added to the cell culture media. However, they did not state whether the dopamine values they listed for their induced cells were those obtained with or without such treatment. Unfortunately, other studies had evoked dopamine release in their cells, and thus comparison with their results would not be ideal. In addition, most of these papers do not specify how the dopamine concentration was calculated from their absorbance measurements, or the volume of sample they used for extraction of dopamine. Such things may vary the final concentrations obtained.

The fact that there was a general increase in the amount of dopamine released by the more induced-cells in relation to the starting MSCs, indicates that the protocol did

successfully specify cells to be induced neuronally, and towards a DA fate. Although the determined dopamine concentrations were not as high as the values reported in other studies, their values could be representing a much greater number of cells than that in cultures in this study. Nevertheless, these results are not enough to confirm that fully-mature DA neurons were present in those cultures. The determined concentrations in this study might suggest that the treated cells required further maturation in culture. Additional runs, with a few modifications might give a better idea on the dopamine-releasing ability of the induced cells. It would have been ideal to count the cells in the wells that media was collected from, however this is very difficult since cells tend to detach as clusters. Knowing a rough estimate for the number of cells that the dopamine amount pertains to would paint a clearer picture. Cells were kept in 12-well plates, thus there can only be a maximum of 0.5 $x10^6$ cells in one well. Considering that cells were not at a confluency of 100% but most probably between 60-70% at any point, cells must have been between 3.0 - 3.5 $x10^5$. On top of that, not all cells in culture were at their final stage and those cells were not releasing dopamine, dropping the number further. Thus, the reported dopamine release values in this study, was for a number of cells similar to that reported by Chabrat *et al.,* (2019).

Importantly, all technical replicates had coefficient of variation values of less than 10% indicating good confidence in pipetting precision and thus the results. This suggests that the different results amongst biological replicates most likely came about due to other reasons. One such reason could be that conditioned media samples were collected on different days and at different time points. Generally, the media was left a few days and collected once it was found to have changed colour. However, it was not always collected after the same amount of time. Additionally, some of the media samples would have been the first collected so maybe the cells had matured more and released more dopamine by

the last time the media had been collected. This further highlights how collecting the media for the same stage and concentrating it as one sample would have been advantageous.

4.6. Mass Spectrometry

The MS analysis revealed many different and unique proteins on going from the starting cells to the end-stage cells. This was already an indication that the final cells were drastically different to the starting cells. In addition, the top 10 proteins that were expressed in both these cell samples were all different (Table 3.10 in Section 3.6.).

In a recent study, Ragelle *et al.,* (2017), investigated the protein composition of ECM proteins produced *in vitro* from BM-MSCs amongst other cells. A BM-MSC protein signature was developed, and the main proteins found within at least 3-5 donors were revealed. Their results included 5 of the main proteins found for MSCs in the MS analysis in this research project: Fibulin-1/2, LTBPs, Fibronectin, Thrombospondin-1, Tenascin C (Ragelle *et al.,* 2017). Thus, having been identified in several BM-MSC samples in Ragelle *et al.,* the occurrence of these 5 proteins in the MSC samples used in this study, can be supported. Although the source of MSCs is different, they are still the same kind of stem cell, and thus they would be expected to share a similar protein expression signature.

In another study, MS was used to identify and quantify the global protein expression within conditioned media of UC-MSCs, from 3 different donors (Mizukami *et al.,* 2019). The research group found each of the main 10 proteins shown for MSCs in Table 3.10, within their MSC samples. More specifically, Fibulin-1/2, LTBP2/3, IGFBP 2/3, Agrin, LAMA2, Fibronectin, Endosialin, Thrombospondin-1, Pappalysin-1, and Tenascin were all found to be present in their MSC samples. In their study, Fibronectin was found to be the most highly expressed within all MSC samples, and Thrombospondin-1 was within

their top 10 proteins, whereas the rest of the aforementioned proteins were found in each of their MSC donor samples, except for Tenascin, which was found in 2 out of the 3 donor samples they investigated (Mizukami *et al.,* 2019). Thus, the results of Ragelle *et al.,* (2017) and Mizukami *et al.,* (2019) corroborated the MS findings in this study, since the major 10 proteins found in our MSCs have also been found in other similar proteomic investigations. This suggests that the occurrence of these proteins is typical of MSCs.

The LTBPs are critical players in the ECM, where they interact with fibrillin microfibrils to exert different effects (Robertson *et al.,* 2015). LTBPs have been found to serve important functions in TGF-β regulation, stabilisation of microfibril bundles and elastic fibre assembly. Importantly, different LTBPs have been found to work together during various phases of MSC differentiation to osteoblasts (Koli, Ryynänen & Keski-Oja, 2008). Recently, LTBP3 was also found to be involved in adipogenesis of MSCs (Singh *et al.,* 2022). Thus, the occurrence of this protein as one of the main proteins in MSC samples is greatly justified.

As for the other major proteins found in MSCs, briefly other studies are cited below for the expression of such proteins within MSCs. In a recent study, a different isoform of Fibulin has been implicated as a major ECM paracrine factor secreted from WJ-MSCs (Won *et al.,* 2020). IGFBPs function as transport proteins for IGFs and regulate their bioavailability and effects (Ding & Wu, 2018). These carrier proteins are also involved in cell growth, adhesion, migration and apoptosis (Ding & Wu, 2018). Several members of the IGFBP family have been found to be secreted by MSCs (Park *et al.,* 2010). Agrin is expressed in BM-MSCs both intracellularly and at the cell surface and was also found to be important for *in vitro* MSC haematopoiesis (Mazzon *et al.,* 2011). LAMA2 has been shown to be a crucial regulator of MSC fate commitment towards osteogenic and adipogenic fates (Zhu *et al.,* 2020).

Endosialin or CD248, is a marker of MSCs and is commonly expressed in MSCs found in developing embryos (Naylor *et al.,* 2014). Its expression is diminished in adults; however, it is upregulated in pathological circumstances such as during fibrosis or inflammation. In their study, Naylor *et al.,* found that Endosialin acted as a negative regulator of bone formation in mice (2014). Thrombospondin-1 has been found to be a major regulator of MSC proliferation (Belotti *et al.,* 2016). Pappamysin is a secreted metalloprotease that functions to increase IGF availability via cleavage of IGFBPs (Mohrin *et al.,* 2021). In their study, MSCs were found to be the principal source of Pappamysin production in bone marrow (Mohrin *et al.,* 2021). Finally, Tenascin-C expression is found in connective tissues, tendon, muscle and stem cell niches (Murdamoothoo *et al.,* 2018). This ECM protein serves various roles such as in tissue repair, pathological inflammatory or fibrotic processes, immunity and angiogenesis (Murdamoothoo *et al.,* 2018). Thus, the expression of these main 10 proteins in MSCs in this research project can be supported by the results from several studies, and from this it can be inferred that these proteins are characteristically indicating the presence of MSCs.

When it comes to the major proteins found for SM3 cells, these included Neurosecretory protein VGF (also secretogranin VII), α-internexin, CRABP1, NF-L polypeptide, DBH, protein RUFY3, protein YIF1B, secretogranin-2, AAAD (also dopa decarboxylase), and synaptic functional regulator FMR1. Neurosecretory protein VGF expression may be upregulated in cortical and hippocampal neurons in response to NGF and other NTFs, such as BDNF. Neurosecretory protein VGF and its peptides are crucial modulators of energy, synaptogenesis, and neurogenesis, as well as learning and memory (Quinn *et al.,* 2021). α-Internexin is a type IV neuronal intermediate filament protein found in most neurons of the CNS (Zhao & Liem, 2016). Its expression is tissue specific, and developmentally-regulated. It is highly expressed at the start of neuronal

differentiation, appearing before the expression of NF-M and NF-L (Zhao & Liem, 2016). This NF has been implicated to play a role in axonal growth (Chien *et al.,* 2005), in the formation and maintenance of dendrites (Benson *et al.,* 1996), and post-synaptic signalling (Suzuki *et al.,* 1997).

CRABP1 regulates intracellular retinoid activity (Zetterström *et al.,* 1999) and is postulated to exert its effects by forming several RA-regulated signalling protein complexes that influence certain cellular functions (Nhieu, Lin & Wei, 2022). In their study, Lin *et al.,* found that CRABP1 is involved in modulation of the NSC pool in the adult hippocampus, whereby it exerts its effects on the cell cycle, slowing down NSC proliferation (2017). CRABP1 has also been found to be involved in modulation of calcium signalling in neurons, and through this, its role has been suggested to act as a protective factor in neurons (Nhieu, Lin & Wei, 2022). The NF-L polypeptide is a highly abundant NF in neurons, that functions as a principal scaffolding constituent of the axoskeleton (Pogue *et al.,* 2022). This NF supports neuronal structure, neurotransmission, synaptogenesis, and inter-neuronal signalling through its interaction with numerous synaptic-phosphoproteins (Pogue *et al.,* 2022). DBH is an enzyme that catalyses the formation of norepinephrine from dopamine (Gonzalez-Lopez & Vrana, 2019). In the brain, DBH is highly expressed in noradrenergic cells of the Locus Coeruleus.

Protein RUFY3 is a RUN domain-containing protein expressed specifically in neurons where it interacts with Actin filaments (Wei *et al.,* 2014). This protein has been implicated in axonal development and growth. Moreover, this protein is an adaptor protein of a GTPase protein family, that also functions to support neuronal polarity (Wang *et al.,* 2022). Protein YIF1B forms part of the Yip1 domain family of proteins that are abundant in the Golgi apparatus (Shaik *et al.,* 2019). This protein has been implicated to be involved in cargo transport in neurons (Carrel *et al.,* 2008) and serotonin 5-HT receptor

targeting to dendrites (Alterio *et al.,* 2015). Its functions are yet to be fully elucidated, however its transmembrane structure suggests that it might serve as a channel, transporter or transmembrane receptor (Shaik *et al.,* 2019). Secretogranin II is a member of the secretogranin family, which are acidic secretory proteins that are highly expressed on secretory granules (Wen *et al.,* 2021). Expression of secretogranin proteins is found throughout the nervous system (Li, Hung & Porter, 2008). In vesicles, secretogranin II is cleaved to produce several small peptides such as secretoneurin, which has been implicated in neurotransmission and neuronal differentiation. The majority of proteolytic processing of secretogranin II occurs in the brain (Li, Hung & Porter, 2008). In a study by Kim *et al.,* 2015, secretogranin II was found to be a target of RE-1 silencing TF, whose concerted interactions were found to promote neuronal differentiation of progenitors, and their maturation towards functional neurons.

AAAD is an enzyme that is critical for the production of catecholamines, and indolamines (Hadjiconstantinou & Neff, 2008). More specifically, AAAD is required for conversion of 5-hydroxytryptophan to serotonin, and L-DOPA to dopamine (Ren *et al.,* 2017). Expression of this enzyme is specifically found in both DA and serotonergic neurons. The FMR1 protein is an RNA-binding regulator highly expressed in the brain (Smidak *et al.,* 2017). This protein is involved in synaptic protein synthesis, formation of axonal and dendritic structures, and has been implicated to play a role in synaptic plasticity.

Although only two of the major 10 proteins found in Stage 3 cells is specific to dopamine neuronal metabolism and function, these main proteins were in fact all neuron-specific proteins. Thus, this result suggests that the final cells were indeed reprogrammed neuronal cells that had reached maturity in terms of their expression of proteins involved in neuronal differentiation and maturation, neuronal structure, neuritic processes and

synaptogenesis. Furthermore, the Stage 3 induced-neuronal cells were found to no longer be expressing the major 10 proteins found within MSCs. Finally, having dopa decarboxylase as one of the major 10 proteins found expressed in Stage 3 cells, might suggest that the induced neuronal cells were of a DA neuronal subtype.

4.7. Limitations and Improvements

4.7.1. Cell culture and treatments

A significant limitation that delayed research progress throughout this study was a problem with a lack of MSCs from UC samples. UC samples are available only once every few weeks, and this potential number of MSCs is reduced further by the variation in cord quality (contamination, incorrect UC storage, variations in cell numbers and the cells' chemotaxis ability). Furthermore, the number of potentially-available MSC samples is further reduced since several other ongoing research projects at the Centre for Molecular Medicine and Biobanking use these cells for their research. Unfortunately, sometimes the cord was not of a good enough quality, thus the stem cells would not establish well, and most of them would die off. Additionally, these cells take a long time to settle in their new environment, so that there is around 3-4 weeks waiting to start cell treatments each time a sample arrives. Cell death of MSCs during their small molecule treatments, occurred a few times due to infection of the sample, or intoxication with small molecules. Intoxication with small molecules occurred once when within the cell culture media, some crystal-like structures were observed surrounding cells and the cells were no longer viable, even after changing media.

It was for these reasons that the number of experimental runs (small molecule treatments) conducted were only enough to produce data for 2 RT-qPCR runs, several gels and Western blots and 1 MS analysis. The primary aim of this study was to produce

an optimised DA neuronal differentiation protocol that may be used for research and therapeutic purposes. Hence, it was necessary to have a good amount of experimental treatment runs performed on MSCs in order to be able to fully-optimise the protocol, the timing and concentrations of small molecule additions, and the ideal duration per stage of treatment.

If cells numbers had permitted it, several preliminary optimisation experiments for the small molecule treatments would have been conducted. Ideally, these runs would be carried out at the beginning, whereby the success of each treatment stage is assessed with RT-qPCR to determine which version of that given stage would be ideal for the purpose of producing DA neurons. Once this aspect was done, again having enough starting cells to conduct at least 2 RT-qPCR experiments for each stage, would be essential. This would be needed to show that the protocol has truly been optimised at every level. These experimental runs would amount to having at least 5 runs in total for each stage (having pilot optimisation runs that are different to each other, and then final runs to prove the optimisation of the protocol with one chosen version of each stage).

Thus, there is a clear issue when it comes to the starting cells being used for these experiments. For reasons that have previously been addressed in the Literature Review, MSCs are an ideal stem cell source for the purposes of this study and its intended applications. Unfortunately, however, not enough MSCs are being obtained from UC WJ samples. Hence, a possible improvement regarding this issue with a low number of starting cells would be using the MSCs from the whole of the UC, that is using both the cord blood MSCs and those from WJ. This would have been ideal considering that more MSCs would be obtained from the same exact biological sample. A further improvement could be sourcing MSCs from adipose tissue (AT). Adipose is a great source considering the ease of access, MSC abundance, and having an easy procedure for isolating MSCs

from AT (Wu *et al.,* 2017). There are no apparent disadvantages to using AT-MSCs in terms of the purposes of this research (Choudhary, Gupta & Singh, 2020). Appropriately, a study found that AT-MSCs have the potential to differentiate into both cholinergic and DA neurons (Marei *et al.,* 2018). If MSCs from adipose tissue were also obtained as starting cells, this would have provided a lot more cells to conduct optimisation experiments. Additionally, the use of this MSC source could have been explored, and which source, whether adipose, WJ, or UC blood, would be more amenable to this research could have been determined. All things considered, however, these additional sources of MSCs may have their own limitations. Whether UC blood and adipose would be a viable source with a good yield of MSCs, is not known. This would depend upon the availability of samples from hospital and the success of sample processing.

An alternative stem cell source is urine-derived stem cells (USCs) – a recent and upcoming source of somatic stem cells for regenerative medicine research (Bento *et al.,* 2020; Zhou *et al.,* 2022). These cells are biologically-similar to MSCs and manifest several similar properties that make them a good source as the starting cells for reprogramming and transdifferentiation research. USCs possess a high self-renewal capacity and multilineage differentiation potential, they are of a similar immunophenotype, and also induce therapeutic effects by paracrine mechanisms (Zhou *et al.,* 2022). USCs are easily isolated from urine by centrifugation and inoculation into culture media. Their isolation is non-invasive, economical, and straightforward. Importantly, USCs can also be used autologously for cellular regenerative transplantation (Zhou *et al.,* 2022). These cells have been recently demonstrated as amenable to their successful neuronal transdifferentiation (Liu *et al.,* 2020; Xu *et al.,* 2019).

One inherent drawback in the research design of this project, is that the cells used for comparison of differentiation extent and changes brought about by each stage of the

treatment, are not the same set of cells. More specifically, the cells used for SM1, SM2, and SM3 analysis with various techniques (PCR, Western Blot, MS) were not the same cells. Not only were the cell samples for different treatment stages tested all from different wells/plates, the cells for analysis of the same differentiation stage were also from different wells. Thus, the comparison between the different stages of treatment with different cell groups is not an accurate and fair comparison. There must be added systematic differences amongst these groups of cells, that would result in variations in their levels of outcome measures (changes in mRNA levels and protein expression), in their responses to the small molecules, and their changes over time. Therefore, correlating outcomes of different stages between these different groups of cells, is likely to experience some misestimation of the true effects of the protocol.

This limitation can be seen to have affected the results gathered in this study. There was clearly a very varied neural marker expression in the induced-neuronal cells. As was discussed in greater length in Section 4.3.2, in RT-qPCR results, SM2 cells seemed to be more progressed than the SM3 cells. There was some factor causing great variation in the differentiation extents of cells in SM1, SM2 and SM3 stages. This could have been caused by the fact that individual runs were not conducted in the exact same manner. The duration of treatment of each stage given to cells depended upon a number of factors, such as the number of cells present in the wells, and the morphology of the cells in that given well. If cells appeared to be resistant to morphological changes, or were very low in number, they were treated with Stage 1 media for longer than 7 days.

Another aspect that could have further perpetuated this variation, was that by the time cells were being treated with SM3 media, quite often, a large fraction of cells would peel off the plate surface and begin to float as a sphere. When this occurred, the cells were collected and frozen for data collection. This was done knowing that many of the cells,

especially those on the inner region of the cell clumps, would probably not have any access to media components, would starve and die off. For these reasons, sometimes SM3 cells were collected before the 14 days of SM3 treatment had elapsed. These differences could cause significant variation in the expression of neural markers when comparing different treatment stages.

To improve upon these issues, the protocol must allow for cells to be taken for data collection and the treatment on them to continue still. Unfortunately, MSCs are very sensitive cells, and therefore, cell samples coming from different wells had to be used for comparative analyses. It would be a risk to dislodge cells from the plate surface, to collect half of them and then to re-plate the other half for continued differentiation. In addition, a good number of cells were required to conduct RT-qPCR or Western Blotting. This aspect of the research design (different cell groups used for comparison of different treatment stages) would already create variation in the results between different stages. On top of this, since different wells were treated slightly differently, this introduced more variation.

These variations in the treatment of different cell groups, brought about variations in the resulting differentiation extent of cells as indicated by their RNA transcript levels for neural markers. This points to the need for further optimisation of the protocol, in which maintaining cells for longer or shorter durations of all stages of treatment would be suggested. In this way, comparisons could be made to be able to determine the optimal range of days needed for each stage of differentiation. In a study published by Nolbrant *et al.*, researchers provided a protocol with the optimal range of days for each stage of differentiation media (2017). They too would decide how long to treat cells depending on their appearance, and they even suggested performing a protein or RNA experiment to determine cellular differentiation extent before proceeding. Their protocol was also

specific on the number of cells that should be added per well for each stage of differentiation. Thus, their treated cells were detached from the flask surface and replated between each differentiation stage. They did this to remove dead cells, for assessment of their differentiation extent or DA fate specification, and to ensure the right number of cells were within each well. Though their starting cells were ESCs, their treated cells were digested using accutase (gentle action) and investigating whether this would work well on MSCs would be worth the while. In any case, once the first stage of treatment is done, cells are no longer MSCs, and this should work in the same way. If this were successful, samples for each stage of differentiation with the same cells could be taken, and comparisons between different stages would be more accurate. In addition, the effects of different variations of the protocol would be found for each stage of differentiation and could be considered in the final cells.

For optimisation of the neural transdifferentiation protocol, several improvements to the protocol and the way it is executed can be made. Firstly, media could be changed more often in the beginning stages to encourage cells to transform more effectively. Another aspect is optimisation of small molecule concentrations. A constraint to the efficacy of this protocol could be that the concentrations used here were found from protocols used on different cells. This introduces the possibility of having some small molecules with too strong an effect, or too little. It could be that the MSCs might have required higher or lower concentrations for their efficacious differentiation towards DA neurons. It is evident from what was discussed in the Literature Review that a delicate balance between SHH / Purmorphamine and WNT signalling is involved in specification of the DA fate. In the study by Nolbrant *et al.,* the researchers explain how the right concentrations of WNT-activating small molecules (CHIR99021 in this study) are needed to interact with SHH in order to specify the midbrain (DA neurons) (2017). Furthermore,

they stated that the wrong concentrations could easily contaminate the cultures with progenitors induced towards different fates. This specific CHIR99021 concentration is different for all stem cell types, and therefore its concentration must be optimised for the cells being treated. Additionally, they also emphasised that the SHH signal at this early stage must be very strong, and thus very often a combination of SHH and Purmorphamine is required (Nolbrant *et al.,* 2017).

These points emphasise the necessity for this protocol to be properly and completely optimised for MSCs. Optimisation in terms of which SMs might interact together, which are not necessary in combination with others, and, whether any combinations could be pushing cells to move towards different fates, would also be needed. These aspects could be fulfilled through conducting different combinatorial experiments on several groups of cells, which again emphasises a previously discussed limitation – all this optimisation would only be possible once enough starting cells are available.

Another observation that should be taken into account for optimisation is something discussed in Section 4.2. In several of the experimental wells (as can be seen in microscopy images), many dead or dying cells could be observed. The cells that appeared to be dying were those that were adopting a proper neuronal morphology and not those that still looked similar to MSCs. The debris that was seen in high quantities in the cell cultures, commonly had the appearance of a burst, rounded cell body with fading neurites surrounding it. For these reasons, it is suspected that a good amount of successfully-induced neuronal cells were in fact dying.

This was not experienced in the previously-investigated protocol, the main difference between the 2 being the extended duration of the protocol for this project (other than the addition of several SMs and altered combinations). In this project, the protocol

was maintained for a much longer period (28 days vs 14 days total), and sometimes the cells were kept in early stages for longer than what was planned. Mature neuronal cells have a finite lifespan and are thus expected to undergo cell death at some point, unlike MSCs which are proliferating cells. However, considering the issue of differentiating cells appearing to detach from the flask surface and forming clumps during their treatment, finding a way to help cells attach more effectively would be worth exploring, as a means to deter neuronal cell death. Plates can be coated using an appropriate material such as laminin, fibronectin or poly-ornithine. This would promote the better attachment of neuronal cells, so that they may undergo treatment more effectively. Detaching cells at points during induction protocols and re-plating them on freshly-coated plates, upon their adoption of a neuronal morphology, is a common strategy (Gaggi *et al.,* 2020; Nolbrant *et al.,* 2017, Gantner *et al.,* 2020). Nolbrant *et al.,* even suggested adding a double dose of laminin on plates when culturing cells at their later stages of treatment (2017).

In terms of microscopy, there were several limitations that affected the suitability of images for neurite analysis. MSCs in culture often grow on top of each other. During their treatment, as they change shape, they also grow and cover one another. This made it hard to distinguish cell bodies from each other, and with neurites growing in several directions it was sometimes hard to identify which cells they were coming from. Moreover, positions of the same exact cells cannot be found with the microscope, and thus changes in average neurite length were calculated on different cells. Additionally, the consistent increases in cellular debris sometimes made it difficult to keep track of morphological changes in cells.

4.7.2. Limitations in PCR experiments

Both RT-qPCR runs were conducted using biological replicates from the same original treated cell material. In fact, results between the 2 runs match up quite well. When it comes to the SM3 cells, the results were quite odd. As discussed in Section 4.3.2., the first run suggested that SM3 cells were less differentiated than SM2 cells, when their only positive expression was for NEUROD1. In the second run, SM3 cells showed a decreased expression for all markers, only with a minimal increase in TH. These results suggest that something went wrong with the SM3 cell sample. Several things could have happened, such as maybe that the cDNA sample had somehow been contaminated with endonucleases. RNA degradation of the original sample is also a potential reason for this result. When looking back to cell treatment experiments, the possibility of RNA degradation in one of the collected SM3 samples becomes apparent.

One of the SM3 cell samples that was collected, was one in which the cells had been maintained in culture for very long (SM3 treatment for 39 days). These cells were maintained for this long in order to push cells as far close to maturity as possible. In published neuronal differentiation protocols, cells are often maintained for long in maturation media to achieve cells with a mature state (Gantner *et al.*, 2020 ; Nolbrant *et al.,* 2017). In fact, cells had progressed very well, and appeared to adopt a very mature neuronal morphology. However, by day 39, the culture started to die off and cells were no longer looking viable. The culture was collected and still processed for analyses. Although RNA concentration was measured before cDNA synthesis, its integrity was not taken into account. It is probable that the RNA in this sample collection could have been damaged since in the last few days of their culture, the cells could have begun the process of degrading their resident mRNA. An image of these cells at this point in which they appeared to be dying can be found in the Appendices. Such reasons have been proposed,

since it cannot be that cells had successfully reached an immature neuronal state by the end of Stage 2, only to de-differentiate during SM3 treatments. Additionally, even if they did somehow de-differentiate, then their pluripotency marker should have been high and not decreased. Evidently, there was some error that resulted in a faulty lack of amplification of cDNA transcripts. Considering these reasons, along with the fact that different cell cultures were treated slightly differently, reliable conclusions on the differentiation extent of SM3 cells cannot be drawn from these results. Additional runs are needed to be able to draw reliable conclusions, and to be able to negate such possible reasons for the results shown here.

Briefly, another point regarding a possible improvement for RT-qPCR can be proposed. Ideally, the most optimal reference gene for the MSCs used and for their changes along the neuronal transdifferentiation protocol, must be determined experimentally. In order to do this, comparison of transcriptional variation of several housekeeping genes as cells are progressing along the treatment can be performed. In this way the gene showing the least variation between treatments and starting cells could be selected. This was not done in this project, rather changes in expression in cells were normalised to one reference gene (GAPDH). This was chosen based on the assessment and comparison of GAPDH, Ribosomal Protein Lateral Stalk Subunit P0 (RPLP0) and Peptidylprolyl Isomerase A (PPIA) in previous projects undertaken at the Centre for Molecular Medicine and Biobanking. In a study by He *et al*., (2015) they found that Ribosomal Protein L13a (RPL13A) alone or the combination of cyclin A (CYCA) and PPIA were the most stable reference genes for RT-qPCR in differentiating MSCs. Thus, it would be a good idea to assess these other genes and compare them with GAPDH for the nature of experiments in this study.

Another aspect of this study that can be improved upon is related to confirming cell fate specification. The only DA neuron marker tested for was TH, which occurs during maturation. If markers for TFs important during DA neuronal differentiation (such as EN1, FOXA2, LMX1A/B, NURR1, PITX3, DAT) at earlier stages were tested, this would have given a better idea on the success of the protocol, and its individual stages in specifying the right fate from the start. If cells had not reached maturity and were not yet expressing TH, with these markers it would have been possible to tell if they were at least successfully acquiring a DA neuronal fate.

4.7.3. Enzyme Linked Immunosorbent Assay

When it comes to the ELISA experiment, this was also similarly affected by aforementioned limitations. The ELISA data came from spent media that was collected from independent experiments, since the cells were in different phases and media was collected at the same time. It would have been better to use samples from 2 different experiments but with the media always coming from the same set of cells, and collected only on the last day of each stage of differentiation. In this way, comparison between each stage would be more accurate and reliable, since data for dopamine concentrations would pertain to that released by the same cells at their different differentiation stages.

A primary improvement for dopamine ELISA experiments is one already revealed when discussing the results, in Section 4.5. Considering that in most papers the release of dopamine was evoked in cells prior to spent media collections, if this were also done in this study, comparing the results to other studies would have been fairer and more accurate. Moreover, concentrating the media samples collected, as was done in Yang *et al.*, (2019), would have removed some contaminating proteins or factors and thus reduced matrix interference. This improvement would surely result in much higher outputs.

There are other potential limitations that might have affected ELISA outcomes. Seeing that samples in this study gave DA concentrations no larger than 130 pg/mL (before multiplying with the correction factor), and the standards for the assay were in the range of 10-80,000 pg/mL, it might be worth running the assay again using standards that are diluted within the 10-500 pg range as the standards for making the graph. This would allow for the standards to be more accurate for the samples' concentration range. Moreover, this assay has an analytical sensitivity of 3.3 pg/mL in 750 µL of undiluted sample (in this study sample volumes of 250 µL diluted 1:2 were used). Thus, it would have been better if a larger volume of sample was used for extraction for the ELISA analysis. Additionally, the assay provides all standard concentration values in ng/mL even though the analytical sensitivity is 3.3 pg/mL. Should these values had been given accurately in pg/mL, maybe this would have been more suitable for curve fitting.

To further reiterate the validity of this limitation, the manufacturer of the dopamine ELISA kit, suggests performing a *proof of principle* experiment prior to testing samples. Such an experiment would entail spiking the native sample matrix with small amounts of dopamine to check the dopamine recovery levels of the samples to be tested. They suggested that higher volumes should be used to increase the test's sensitivity, and even trying out different volumes of sample prior to the experiment to determine the ideal volume. Conducting this prior optimisation might have produced better results with stronger signals. Moreover, the manufacturer suggested having collected samples with EDTA or sodium metabisulfite added, to avoid the degradation of dopamine. Thus, it could be that there was a degree of dopamine degradation in the collected media samples.

Chapter 5 Conclusions and Recommendations

When considering all limitations discussed, it can be said that the primary aim of this study was partly fulfilled. A DA neuronal differentiation protocol was defined, and its effects on MSCs were investigated. However, it cannot be stated that this protocol is fully-characterised. Looking towards the literature for current research on neurogenesis, neuronal differentiation, and the pathways involved in such a process, a protocol for developing DA neurons from MSCs was devised and tested. However, this protocol was not sufficiently explored and optimised due to several limitations that were discussed in Section 4.7. For the full-characterisation of the devised protocol, the ideal durations for each differentiation stage, and different concentrations for each small molecule would need to be explored for their optimisation. Thus, it cannot be concluded that this DA neuronal differentiation protocol is ready to be used for research and therapeutic purposes.

That being said, it does not mean that this protocol does not have the potential to be used for research and therapeutic purposes. On the contrary, despite the limitations that occurred, the outcomes of this study are highly relevant to this area of research, and furthermore, would be highly amenable for its continued investigation. In fulfilment of the primary aim, the results suggest that the devised protocol is proficient in the neuronal transdifferentiation of MSCs. The devised protocol brought about drastic changes in cell structure, with cells in their final differentiation stages adopting neuronal morphologies. The small molecule treatments also brought about significant changes in neural marker RNA expression in differentiation Stage 1 and Stage 2 cells. These results indicated that Stage 2 cells had reached a differentiation extent akin to immature neurons. Unfortunately, the RT-qPCR output for Stage 3 cells was concluded to be unreliable, and

thus the differentiation extent (in terms of RNA expression) of the cells at their final stage of small molecules treatment cannot be concluded on.

The MS analysis uncovered considerable differences in the proteome of Stage 3 DA neurons compared to that of the starting cells. Hundreds of unique MSC proteins have been identified between MSCs and the Stage 3 DA neurons, confirming the biochemical differentiation of the former into the latter. In fulfilment of the objective pertaining to the second aim, Western blotting results for PTMs occurring within cells along their differentiation progress were successfully carried out. These results suggested that significant epigenetic changes occurred within the cells along their treatments. Importantly, these results implied the success of the differentiation protocol in terms of inducing changes in the genetic expression of the cells, since the PTMs explored are responsible for gene silencing and activation.

Investigating the functionality of the final cells was also within the primary aim of this study. This was investigated by assessing changes in their release of dopamine within different stages of differentiation treatment. The ELISA experiment revealed changes in dopamine release in differentiating cells in comparison to the starting cells. Both differentiation Stage 2 and 3 neuronal cells had increased levels of dopamine released in their culture. However, more significant changes in dopamine release were expected. Thus, it can be concluded that the neural treatment protocol was successful at specifying a DA fate, however the results suggest that cells might further maturation in culture.

The limitations experienced in this project might have influenced the results that demonstrate proteome and transcriptome changes, as well as the changes in dopamine release. Therefore, more experiments would be required to conclude on the cells' differentiation extent and their functionality. It can be said that the results obtained for this study revealed certain limitations; bringing them to light so that they may be

addressed. The constraining factors along the way limited progress, however they revealed several faults in the experimental design, and ways in which these can be mitigated.

5.1. Further work

Further work for this study can be categorised into two. First, in relation to cell treatments and secondly, relating to the investigation of differentiation extent or changes brought about by the treatments. This section will be divided accordingly.

5.1.1. Cell treatments

An unfulfilled aspect of this study that should be addressed in further work, is for the small molecule protocol to be optimised properly – both in terms of the optimal small molecule concentrations, and the duration of each stage of differentiation media. The three differentiation media stages can be set up as several different iterations of the protocol, with each one either having increased or decreased concentrations of one of the small molecules, applying a stage for a shorter or longer time, and even adding or removing one or two components. These similar versions of the devised protocol would all be conducted on the starting cells whilst noting changes in morphology. Out of all protocols tested, those in which cells appear to be effectively adopting a neuronal-like morphology, can then be assessed for their DA neuron specification ability. Thus, the next step would be exploring the expression changes in a large panel of at least 10 genes essential for DA neuron development *in vivo*. This analysis could be used to rule out the lesser effective protocols, and then the best ones can be chosen and used to further determine which of them is the most effective.

As further work related to the devised protocol, there are several potential new additions that may be explored. In section 4.4., the relevance of epigenetic modifications

occurring along neural differentiation was revealed in terms of research studies that found such changes. Thus, the addition of small molecules that affect histone modifications might hold great potential in terms of enhancing the effects of small molecule combinations on treated cells. Several histone deacetylase inhibitors such as Trichostatin A, and valproic acid (Ren *et al.,* 2020) or DNA methylation inhibitors such as RG-108 have been found to promote neural induction of MSCs (Jiménez-Acosta *et al.,* 2022). The addition of a few of these small molecules could be explored during the optimisation experiments of the protocol. Their value as additional components can be explored by looking for changes in the effects of the protocol stages with and without their addition. Furthermore, the effects of other WNT pathway activators, such as WNT1 or WNT5a proteins, can be explored as a part of the protocol, assessing its effects in replacement of CHIR99021 and in combination with it.

Direct neuronal reprogramming strategies elicit metabolic shifts in the cells that may result in increased intracellular levels of oxidative products (Wang *et al.,* 2022). This build-up might discourage reprogramming in cells and even result in their death. Hence, another potentially-valuable addition to the protocol is a small molecule that can inhibit oxidative stress in cells. A small molecule with this purpose might protect cells during their treatment, in turn making the treatment more effective. One example of such a small molecule that has previously been tested is SP600125, a JNK pathway inhibitor used to decrease stress-induced apoptosis during neuronal transdifferentiation of somatic cells (Liu *et al.,* 2020).

An interesting neuronal induction strategy is the use of Conditioned Media (CM) coming from specific neural cell lines to treat stem cells. CM is essentially spent media obtained from cells in culture and is thus composed of the cell secretome (Dowling & Clynes, 2011). Thus, CM contains proteins having a signal peptide that are secreted from

cells, proteins shed from cell surfaces and even intracellular proteins released through exosomes. These proteins encompass enzymes, growth factors, cytokines, and hormones, amongst other signalling mediators (Dowling & Clynes, 2011). They have pertinent functions in cell growth, differentiation, and angiogenesis via modulation of cell interactions with other cells and the extracellular matrix. CM is an unusual but highly germane neuronal differentiation strategy, since such media simulate the natural neural tissue microenvironment surrounding neurons and stem cells during their development and maintenance (Lo Furno *et al.,* 2018). Thus, the idea behind using CM is to alter the stem cells' surrounding environment akin to that occurring physiologically, as a strategy to induce them to enter the neuroectoderm lineage and progress within it.

In the previous research project, SH-SY5Y cell CM was used to treat MSCs in replacement of the first stage of small molecule treatment. To further investigate the use of CM as a neural induction strategy, Lund Human Mesencephalic (LUHMES) cells appear to be a suitable cell line for the specific neural induction of DA neurons. LUHMES cells derive from the mesencephalon region of an 8-week-old human's brain (Tüshaus *et al.,* 2020). These cells can exist in more than one state. In their non-differentiated state, they are tumour-like, and have a high rate of proliferation. However, non-differentiated LUHMES cells can be differentiated into post-mitotic (mature) DA-like neurons. Hence, differentiated LUHMES cells are frequently employed for research on PD and other neurodegenerative diseases (Tüshaus *et al.,* 2020). To date, there is no literature on the effects of their spent media on neural induction of stem cells. Their spent media would be expected to specifically induce cells towards a DA neuronal fate.

There are some aspects regarding the culture of cells during their differentiation that may be addressed as further work. The ECM serves not only as a support to neural cells, but also promotes neural proliferation and differentiation through its signalling

interactions (Vieira *et al.,* 2018). The ECM is also involved in neuronal cell adhesion and delivers autocrine and paracrine factors pertaining to various differentiation stages. Simulating the natural environment that surrounds NECs as they progress through their neural differentiation, might prove to be highly influential as a neuronal differentiation strategy. A possible idea for further work is to simulate the ECM through use of ECM material or an artificial scaffolding (Hong & Do, 2019). MaxGel is a commercially-available ECM made from ECM components such as collagens, laminins, fibronectins and others (Sigma Aldrich, 2022). In a recent study, the effects of decellularized brain tissue coming from rats was explored for its capacity to simulate the neuronal microenvironment and aid in development of neuronal networks (Lam *et al.,* 2019). In their study, the decellularized brain ECM was compared to MaxGel and poly-D-lysine in terms of their effects on long-term culture of neurons and glia. Investigating various options to simulate the environment of differentiating neurons during treatment of cells (such as fibronectin, polymer plate coatings, or MaxGel) holds potential as further work. This, and its effects on the induced-neuronal cells in culture, can only be explored after all aspects of the protocol have been refined.

5.1.2. Investigation of changes brought about by cell treatment strategies

Once the most effective method has been determined, the efficacy of this protocol should be explored thoroughly. Several further analyses can be done and would be essential in order to assert use of these induced neuronal cells for research and therapeutic purposes. Firstly, a detailed analysis to assess the acquisition of a DA transcriptomic signature must be conducted. This would entail transcriptome analysis of a large panel of 20 genes pertaining to a DA neuronal signature. Once the complete and fully-optimised protocol amongst multiple iterations has been deduced, then its neuronal determination efficacy can be compared with that of a commercial kit on the same cells.

As a means by which to characterise the extent of the effects of the induction treatments, findings in induced DA neurons can be compared and confirmed with the genetic and phenotypic characteristics of *in vivo* real DA neurons. Similar or differential transcriptomic expression between induced neurons and a neuronal cell line can be used to determine how close the induced neurons are to mimicking the authentic corresponding *in vivo* cells. This is essential in determining whether these induced neurons have the capability of fulfilling all that is promised with regenerative cell therapy. Furthermore, it is vital to determine the electrophysiological properties of induced neurons in order for their clinical value to be affirmed (Wang *et al.*, 2020). Thus, further work that is essential to this aspect of evaluation, would be the use of electrophysiology patch clamp recordings to look for the occurrence of spontaneous postsynaptic currents would confirm the maturity of induced neuronal cells (Wang *et al.*, 2020). To further evaluate electrophysiological maturity, testing for the expression of proteins involved in neuron synaptogenesis, such as synaptophysin or postsynaptic density protein 95 (PSD95). To evaluate the DA maturation of induced cells, protein expression of not only TH, but also that of dopa decarboxylase, and the DAT protein can be explored by western blot. Additionally, another technique by which to measure dopamine release from induced neurons that can be used for further work is high-performance liquid chromatography.

An unusual aspect of cellular differentiation that may be addressed as further work are changes in the expression of cell-cycle proteins, such as proteins specifically involved in G1-S phase progression and those involved in G2-M progression (Trzaska *et al.*, 2007). Expression changes in these proteins might indicate whether cells have stopped proliferating and if they have successfully become postmitotic, as mature neurons *in vivo* do. Moreover, MS can be used to explore the PTMs occurring on proteins during the neuronal transdifferentiation of cells. In this study, western blot results demonstrated

significant changes in protein lysine and arginine methylation. Thus, both methylation and acetylation changes, and to which histones and proteins these modifications have occurred during cellular transdifferentiation, can be investigated to define the epigenetic changes that were detected in this study.

Once these methods have all corroborated each other in terms of supporting the clinical use of the induced neurons, these cells can be used for transplantation experiments in an animal model such as a PD mouse model. This way the clinical value of the induced neuronal cells can be explored *in vivo.*

References

Abcam plc [Internet]. [place unknown]: Abcam plc. c1998-2022. Neural Markers; 2021 Mar 18 [cited 2022 Sep 12]; [about 5 screens]. Available from: https://www.abcam.com/neuroscience/neural-markers-guide

Abranches E, Silva M, Pradier L, Schulz H, Hummel O, Henrique D, Bekman E. Neural differentiation of embryonic stem cells in vitro: a road map to neurogenesis in the embryo. PLoS One. 2009 Jul 21;4(7):e6286. doi: 10.1371/journal.pone.0006286. PMID: 19621087; PMCID: PMC2709448.

Ahn S, Joyner AL. In vivo analysis of quiescent adult neural stem cells responding to Sonic hedgehog. Nature. 2005 Oct 6;437(7060):894-7. doi: 10.1038/nature03994. PMID: 16208373.

Alterio J, Masson J, Diaz J, Chachlaki K, Salman H, Areias J, Al Awabdh S, Emerit MB, Darmon M. Yif1B Is Involved in the Anterograde Traffic Pathway and the Golgi Architecture. Traffic. 2015 Sep;16(9):978-93. doi: 10.1111/tra.12306. Epub 2015 Jul 7. PMID: 26077767.

Alvarez-Fischer D, Fuchs J, Castagner F, Stettler O, Massiani-Beaudoin O, Moya KL, Bouillot C, Oertel WH, Lombès A, Faigle W, Joshi RL, Hartmann A, Prochiantz A. Engrailed protects mouse midbrain dopaminergic neurons against mitochondrial complex I insults. Nat Neurosci. 2011 Sep 4;14(10):1260-6. doi: 10.1038/nn.2916. PMID: 21892157.

Arenas E, Denham M, Villaescusa JC. How to make a midbrain dopaminergic neuron. Development. 2015 Jun 1;142(11):1918-36. doi: 10.1242/dev.097394. PMID: 26015536.

Azuara V, Perry P, Sauer S, Spivakov M, Jørgensen HF, John RM, Gouti M, Casanova M, Warnes G, Merkenschlager M, Fisher AG. Chromatin signatures of pluripotent cell lines. Nat Cell Biol. 2006 May;8(5):532-8. doi: 10.1038/ncb1403. Epub 2006 Mar 29. PMID: 16570078.

Badurek S, Griguoli M, Asif-Malik A, Zonta B, Guo F, Middei S, Lagostena L, Jurado-Parras MT, Gillingwater TH, Gruart A, Delgado-García JM, Cherubini E, Minichiello L. Immature Dentate Granule Cells Require Ntrk2/Trkb for the Formation of Functional Hippocampal Circuitry. iScience. 2020 May 22;23(5):101078. doi: 10.1016/j.isci.2020.101078. Epub 2020 Apr 18. PMID: 32361506; PMCID: PMC7200316.

Badurek S, Griguoli M, Asif-Malik A, Zonta B, Guo F, Middei S, Lagostena L, Jurado-Parras MT, Gillingwater TH, Gruart A, Delgado-García JM, Cherubini E, Minichiello L. Immature Dentate Granule Cells Require Ntrk2/Trkb for the Formation of Functional Hippocampal Circuitry. iScience. 2020 May 22;23(5):101078. doi: 10.1016/j.isci.2020.101078. Epub 2020 Apr 18. PMID: 32361506; PMCID: PMC7200316.

Belmonte-Mateos C, Pujades C. From Cell States to Cell Fates: How Cell Proliferation and Neuronal Differentiation Are Coordinated During Embryonic Development. Front Neurosci. 2022 Jan 3;15:781160. doi: 10.3389/fnins.2021.781160. PMID: 35046768; PMCID: PMC8761814.

Belotti D, Capelli C, Resovi A, Introna M, Taraboletti G. Thrombospondin-1 promotes mesenchymal stromal cell functions via TGFβ and in cooperation with PDGF. Matrix Biol. 2016 Sep;55:106-116. doi: 10.1016/j.matbio.2016.03.003. Epub 2016 Mar 16. PMID: 26992552.

Benson DL, Mandell JW, Shaw G, Banker G. Compartmentation of alpha-internexin and neurofilament triplet proteins in cultured hippocampal neurons. J Neurocytol. 1996 Mar;25(3):181-96. doi: 10.1007/BF02284795. PMID: 8737171.

Bento G, Shafigullina AK, Rizvanov AA, Sardão VA, Macedo MP, Oliveira PJ. Urine-Derived Stem Cells: Applications in Regenerative and Predictive Medicine. Cells. 2020 Feb 28;9(3):573. doi: 10.3390/cells9030573. PMID: 32121221; PMCID: PMC7140531.

Bernstein BE, Mikkelsen TS, Xie X, Kamal M, Huebert DJ, Cuff J, Fry B, Meissner A, Wernig M, Plath K, Jaenisch R, Wagschal A, Feil R, Schreiber SL, Lander ES. A bivalent chromatin structure marks key developmental genes in embryonic stem cells. Cell. 2006 Apr 21;125(2):315-26. doi: 10.1016/j.cell.2006.02.041. PMID: 16630819.

Blaess S, Ang SL. Genetic control of midbrain dopaminergic neuron development. Wiley Interdiscip Rev Dev Biol. 2015 Mar-Apr;4(2):113-34. doi: 10.1002/wdev.169. Epub 2015 Jan 6. PMID: 25565353.

Blaess S, Corrales JD, Joyner AL. Sonic hedgehog regulates Gli activator and repressor functions with spatial and temporal precision in the mid/hindbrain region. Development. 2006 May;133(9):1799-809. doi: 10.1242/dev.02339. Epub 2006 Mar 29. PMID: 16571630.

Bodea GO, Blaess S. Establishing diversity in the dopaminergic system. FEBS Lett [Internet]. 2015 Sep 30 [cited 2022 Sep 12]; 580(24): 3773. Available from: https://febs.onlinelibrary.wiley.com/doi/10.1016/j.febslet.2015.09.016

Bonafina A, Trinchero MF, Ríos AS, Bekinschtein P, Schinder AF, Paratcha G, Ledda F. GDNF and GFRα1 Are Required for Proper Integration of Adult-Born Hippocampal

Neurons. Cell Rep. 2019 Dec 24;29(13):4308-4319.e4. doi: 10.1016/j.celrep.2019.11.100. PMID: 31875542.

Bonafina A, Trinchero MF, Ríos AS, Bekinschtein P, Schinder AF, Paratcha G, Ledda F. GDNF and GFRα1 Are Required for Proper Integration of Adult-Born Hippocampal Neurons. Cell Rep. 2019 Dec 24;29(13):4308-4319.e4. doi: 10.1016/j.celrep.2019.11.100. PMID: 31875542.

Bond AM, Bhalala OG, Kessler JA. The dynamic role of bone morphogenetic proteins in neural stem cell fate and maturation. Dev Neurobiol. 2012 Jul;72(7):1068-84. doi: 10.1002/dneu.22022. PMID: 22489086; PMCID: PMC3773925.

Bond AM, Ming GL, Song H. Adult Mammalian Neural Stem Cells and Neurogenesis: Five Decades Later. Cell Stem Cell. 2015 Oct 1;17(4):385-95. doi: 10.1016/j.stem.2015.09.003. PMID: 26431181; PMCID: PMC4683085.

Borghese L, Dolezalova D, Opitz T, Haupt S, Leinhaas A, Steinfarz B, Koch P, Edenhofer F, Hampl A, Brüstle O. Inhibition of notch signaling in human embryonic stem cell-derived neural stem cells delays G1/S phase transition and accelerates neuronal differentiation in vitro and in vivo. Stem Cells. 2010 May;28(5):955-64. doi: 10.1002/stem.408. PMID: 20235098.

Botticelli L, Micioni Di Bonaventura E, Del Bello F, Giorgioni G, Piergentili A, Romano A, Quaglia W, Cifani C, Micioni Di Bonaventura MV. Underlying Susceptibility to Eating Disorders and Drug Abuse: Genetic and Pharmacological Aspects of Dopamine D4 Receptors. Nutrients. 2020 Jul 30;12(8):2288. doi: 10.3390/nu12082288. PMID: 32751662; PMCID: PMC7468707.

Bradley JE, Ramirez G, Hagood JS. Roles and regulation of Thy-1, a context-dependent modulator of cell phenotype. Biofactors. 2009 May-Jun;35(3):258-65. doi: 10.1002/biof.41. PMID: 19422052; PMCID: PMC5675016.

Brinkhof B, Zhang B, Cui Z, Ye H, Wang H. ALCAM (CD166) as a gene expression marker for human mesenchymal stromal cell characterisation. Gene [Internet]. 2020 Dec [cited 2022 Sep 12]; 763:100031. Available from https://www.sciencedirect.com/science/article/pii/S259015832030005X?via%3Dihub

Brisch R, Saniotis A, Wolf R, Bielau H, Bernstein HG, Steiner J, Bogerts B, Braun K, Jankowski Z, Kumaratilake J, Henneberg M, Gos T. The role of dopamine in schizophrenia from a neurobiological and evolutionary perspective: old fashioned, but still in vogue. Front Psychiatry. 2014 May 19;5:47. doi: 10.3389/fpsyt.2014.00047. Erratum in: Front Psychiatry. 2014;5:110. Braun, Anna Katharina [corrected to Braun, Katharina]; Kumaritlake, Jaliya [corrected to Kumaratilake, Jaliya]. PMID: 24904434; PMCID: PMC4032934.

Brodski C, Blaess S, Partanen J, Prakash N. Crosstalk of Intercellular Signaling Pathways in the Generation of Midbrain Dopaminergic Neurons In Vivo and from Stem Cells. J Dev Biol. 2019 Jan 15;7(1):3. doi: 10.3390/jdb7010003. PMID: 30650592; PMCID: PMC6473842.

Bryja V, Andersson ER, Schambony A, Esner M, Bryjová L, Biris KK, Hall AC, Kraft B, Cajanek L, Yamaguchi TP, Buckingham M, Arenas E. The extracellular domain of Lrp5/6 inhibits noncanonical Wnt signaling in vivo. Mol Biol Cell. 2009 Feb;20(3):924-36. doi: 10.1091/mbc.e08-07-0711. Epub 2008 Dec 3. PMID: 19056682; PMCID: PMC2633404.

Carrel D, Masson J, Al Awabdh S, Capra CB, Lenkei Z, Hamon M, Emerit MB, Darmon M. Targeting of the 5-HT1A serotonin receptor to neuronal dendrites is mediated by Yif1B. J Neurosci. 2008 Aug 6;28(32):8063-73. doi: 10.1523/JNEUROSCI.4487-07.2008. PMID: 18685031; PMCID: PMC6670764.

Castelo-Branco G, Andersson ER, Minina E, Sousa KM, Ribeiro D, Kokubu C, Imai K, Prakash N, Wurst W, Arenas E. Delayed dopaminergic neuron differentiation in Lrp6 mutant mice. Dev Dyn. 2010 Jan;239(1):211-21. doi: 10.1002/dvdy.22094. PMID: 19795519.

Castelo-Branco G, Wagner J, Rodriguez FJ, Kele J, Sousa K, Rawal N, Pasolli HA, Fuchs E, Kitajewski J, Arenas E. Differential regulation of midbrain dopaminergic neuron development by Wnt-1, Wnt-3a, and Wnt-5a. Proc Natl Acad Sci U S A. 2003 Oct 28;100(22):12747-52. doi: 10.1073/pnas.1534900100. Epub 2003 Oct 13. Erratum in: Proc Natl Acad Sci U S A. 2004 Nov 16;101(46):16390. PMID: 14557550; PMCID: PMC240689.

Cell Signalling Technology [Internet]. [Massachusetts, USA]. Cell Signalling Technology. c2022. Neuronal and Glial Cell Marker Atlas: Cell type markers; 2018 Sep [cited 2022 Sep 12]; [about 5 screens]. Available from: https://www.cellsignal.com/pathways/neuronal-and-glial-cell-markers

Chabrat A, Lacassagne E, Billiras R, Landron S, Pontisso-Mahout A, Darville H, Dupront A, Coge F, Schenker E, Piwnica D, Nivet E, Féron F, Mannoury la Cour C. Pharmacological Transdifferentiation of Human Nasal Olfactory Stem Cells into Dopaminergic Neurons. Stem Cells Int. 2019 May 19;2019:2945435. doi: 10.1155/2019/2945435. PMID: 31236114; PMCID: PMC6545791.

Chambers SM, Fasano CA, Papapetrou EP, Tomishima M, Sadelain M, Studer L. Highly efficient neural conversion of human ES and iPS cells by dual inhibition of SMAD signaling. Nat Biotechnol. 2009 Mar;27(3):275-80. doi: 10.1038/nbt.1529. Epub 2009 Mar 1. Erratum in: Nat Biotechnol. 2009 May;27(5):485. PMID: 19252484; PMCID: PMC2756723.

Charitos IA, Ballini A, Cantore S, Boccellino M, Di Domenico M, Borsani E, Nocini R, Di Cosola M, Santacroce L, Bottalico L. Stem Cells: A Historical Review about Biological, Religious, and Ethical Issues. Stem Cells Int. 2021 Apr 29;2021:9978837. doi: 10.1155/2021/9978837. PMID: 34012469; PMCID: PMC8105090.

Chen CW, Liu CS, Chiu IM, Shen SC, Pan HC, Lee KH, Lin SZ, Su HL. The signals of FGFs on the neurogenesis of embryonic stem cells. J Biomed Sci. 2010 Apr 29;17(1):33. doi: 10.1186/1423-0127-17-33. PMID: 20429889; PMCID: PMC2873938.

Chi CL, Martinez S, Wurst W, Martin GR. The isthmic organizer signal FGF8 is required for cell survival in the prospective midbrain and cerebellum. Development. 2003 Jun;130(12):2633-44. doi: 10.1242/dev.00487. PMID: 12736208.

Chien CL, Liu TC, Ho CL, Lu KS. Overexpression of neuronal intermediate filament protein alpha-internexin in PC12 cells. J Neurosci Res. 2005 Jun 1;80(5):693-706. doi: 10.1002/jnr.20506. PMID: 15880430.

Choudhary P, Gupta A, Singh S. Therapeutic Advancement in Neuronal Transdifferentiation of Mesenchymal Stromal Cells for Neurological Disorders. J Mol Neurosci. 2021 May;71(5):889-901. doi: 10.1007/s12031-020-01714-5. Epub 2020 Oct 13. PMID: 33047251.

Chuang JH, Tung LC, Lin Y. Neural differentiation from embryonic stem cells in vitro: An overview of the signaling pathways. World J Stem Cells. 2015 Mar 26;7(2):437-47. doi: 10.4252/wjsc.v7.i2.437. PMID: 25815127; PMCID: PMC4369499.

Compagnucci C, Barresi S, Petrini S, Billuart P, Piccini G, Chiurazzi P, Alfieri P, Bertini E, Zanni G. Rho Kinase Inhibition Is Essential During In Vitro Neurogenesis and Promotes Phenotypic Rescue of Human Induced Pluripotent Stem Cell-Derived Neurons With Oligophrenin-1 Loss of Function. Stem Cells Transl Med. 2016 Jul;5(7):860-9. doi: 10.5966/sctm.2015-0303. Epub 2016 May 9. PMID: 27160703; PMCID: PMC4922854.

Crawford TQ, Roelink H. The notch response inhibitor DAPT enhances neuronal differentiation in embryonic stem cell-derived embryoid bodies independently of sonic hedgehog signaling. Dev Dyn. 2007 Mar;236(3):886-92. doi: 10.1002/dvdy.21083. PMID: 17295317.

Das D, Lanner F, Main H, Andersson ER, Bergmann O, Sahlgren C, Heldring N, Hermanson O, Hansson EM, Lendahl U. Notch induces cyclin-D1-dependent proliferation during a specific temporal window of neural differentiation in ES cells. Dev Biol. 2010 Dec 15;348(2):153-66. doi: 10.1016/j.ydbio.2010.09.018. Epub 2010 Sep 29. PMID: 20887720.

de Araújo Farias V, Carrillo-Gálvez AB, Martín F, Anderson P. TGF-β and mesenchymal stromal cells in regenerative medicine, autoimmunity and cancer. Cytokine Growth Factor Rev. 2018 Oct;43:25-37. doi: 10.1016/j.cytogfr.2018.06.002. Epub 2018 Jun 13. PMID: 29954665.

Delgado-Garcia LM, Amorim RM. Adult Brain Neurogenesis, Neural Stem Cells and Neurogenic Niches. Int J Stem Cell Res Ther 2016;3(2):039. doi: 10.23937/2469-570X/1410039

Di Santo S, Widmer HR. Neurotrophic factor-based strategies to enhance survival and differentiation of neural progenitor cells toward the dopaminergic phenotype. Brain Circ. 2018 Jul-Sep;4(3):139-141. doi: 10.4103/bc.bc_23_18. Epub 2018 Oct 9. PMID: 30450422; PMCID: PMC6187939.

Ding H, Wu T. Insulin-Like Growth Factor Binding Proteins in Autoimmune Diseases. Front Endocrinol (Lausanne). 2018 Aug 30;9:499. doi: 10.3389/fendo.2018.00499. PMID: 30214426; PMCID: PMC6125368.

Domanskyi A, Alter H, Vogt MA, Gass P, Vinnikov IA. Transcription factors Foxa1 and Foxa2 are required for adult dopamine neurons maintenance. Front Cell Neurosci. 2014 Sep 9;8:275. doi: 10.3389/fncel.2014.00275. PMID: 25249938; PMCID: PMC4158790.

Dominici M, Le Blanc K, Mueller I, Slaper-Cortenbach I, Marini F, Krause D, Deans R, Keating A, Prockop Dj, Horwitz E. Minimal criteria for defining multipotent mesenchymal stromal cells. The International Society for Cellular Therapy position statement. Cytotherapy. 2006;8(4):315-7. doi: 10.1080/14653240600855905. PMID: 16923606.

Dowling P, Clynes M. Conditioned media from cell lines: a complementary model to clinical specimens for the discovery of disease-specific biomarkers. Proteomics. 2011 Feb;11(4):794-804. doi: 10.1002/pmic.201000530. Epub 2011 Jan 13. PMID: 21229588.

Dworkin S, Mantamadiotis T. Targeting CREB signalling in neurogenesis. Expert Opin Ther Targets. 2010 Aug;14(8):869-79. doi: 10.1517/14728222.2010.501332. PMID: 20569094.

Elkabetz Y, Panagiotakos G, Al Shamy G, Socci ND, Tabar V, Studer L. Human ES cell-derived neural rosettes reveal a functionally distinct early neural stem cell stage. Genes Dev. 2008 Jan 15;22(2):152-65. doi: 10.1101/gad.1616208. Erratum in: Genes Dev. 2008 May 1;22(9):1257. PMID: 18198334; PMCID: PMC2192751.

Ericson J, Muhr J, Placzek M, Lints T, Jessell TM, Edlund T. Sonic hedgehog induces the differentiation of ventral forebrain neurons: a common signal for ventral patterning within the neural tube. Cell. 1995 Jun 2;81(5):747-56. doi: 10.1016/0092-8674(95)90536-7. Erratum in: Cell 1995 Jul 14;82(1):following 165. PMID: 7774016.

Faigle R, Song H. Signaling mechanisms regulating adult neural stem cells and neurogenesis. Biochim Biophys Acta. 2013 Feb;1830(2):2435-48. doi: 10.1016/j.bbagen.2012.09.002. Epub 2012 Sep 12. PMID: 22982587; PMCID: PMC3541438.

Fang L, Wang YN, Cui XL, Fang SY, Ge JY, Sun Y, Liu ZH. The role and mechanism of action of activin A in neurite outgrowth of chicken embryonic dorsal root ganglia. J Cell Sci. 2012 Mar 15;125(Pt 6):1500-7. doi: 10.1242/jcs.094151. Epub 2012 Jan 24. PMID: 22275431.

Ferri AL, Lin W, Mavromatakis YE, Wang JC, Sasaki H, Whitsett JA, Ang SL. Foxa1 and Foxa2 regulate multiple phases of midbrain dopaminergic neuron development in a dosage-dependent manner. Development. 2007 Aug;134(15):2761-9. doi: 10.1242/dev.000141. Epub 2007 Jun 27. PMID: 17596284.

Friling S, Andersson E, Thompson LH, Jönsson ME, Hebsgaard JB, Nanou E, Alekseenko Z, Marklund U, Kjellander S, Volakakis N, Hovatta O, El Manira A, Björklund A, Perlmann T, Ericson J. Efficient production of mesencephalic dopamine neurons by Lmx1a expression in embryonic stem cells. Proc Natl Acad Sci U S A. 2009 May 5;106(18):7613-8. doi: 10.1073/pnas.0902396106. Epub 2009 Apr 21. Erratum in: Proc Natl Acad Sci U S A. 2010 Dec 7;107(49):21229. PMID: 19383789; PMCID: PMC2671325.

Fu YS, Shih YT, Cheng YC, Min MY. Transformation of human umbilical mesenchymal cells into neurons in vitro. J Biomed Sci. 2004 Sep-Oct;11(5):652-60. doi: 10.1007/BF02256131. PMID: 15316141.

Fujioka T, Fujioka A, Duman RS. Activation of cAMP signaling facilitates the morphological maturation of newborn neurons in adult hippocampus. J Neurosci. 2004 Jan 14;24(2):319-28. doi: 10.1523/JNEUROSCI.1065.03.2004. PMID: 14724230; PMCID: PMC6729999.

G7 National Academies. The challenge of neurodegenerative diseases in an aging population. In: G7 Academies' Joint Statements 2017 [Internet]; 2017 May 26-27; Taormina. [publisher unknown]; [cited 2022 Sep 12]. [2 p.]. Available from: https://www.lincei.it/sites/default/files/documenti/Relazioni_Int/2017_2_Aging_population.pdf

Gaggi G, Di Credico A, Izzicupo P, Alviano F, Di Mauro M, Di Baldassarre A, Ghinassi B. Human Mesenchymal Stromal Cells Unveil an Unexpected Differentiation Potential toward the Dopaminergic Neuronal Lineage. Int J Mol Sci. 2020 Sep 9;21(18):6589. doi: 10.3390/ijms21186589. PMID: 32916865; PMCID: PMC7555006.

Galiakberova AA, Dashinimaev EB. Neural Stem Cells and Methods for Their Generation From Induced Pluripotent Stem Cells in vitro. Front Cell Dev Biol. 2020 Oct 8;8:815. doi: 10.3389/fcell.2020.00815. PMID: 33117792; PMCID: PMC7578226.

Galleguillos D, Fuentealba JA, Gómez LM, Saver M, Gómez A, Nash K, Burger C, Gysling K, Andrés ME. Nurr1 regulates RET expression in dopamine neurons of adult rat midbrain. J Neurochem. 2010 Aug;114(4):1158-67. doi: 10.1111/j.1471-4159.2010.06841.x. Epub 2010 Jun 1. PMID: 20533997.

Gantner CW, Cota-Coronado A, Thompson LH, Parish CL. An Optimized Protocol for the Generation of Midbrain Dopamine Neurons under Defined Conditions. STAR Protoc. 2020 Jul 15;1(2):100065. doi: 10.1016/j.xpro.2020.100065. PMID: 33111103; PMCID: PMC7580226.

George S, Hamblin MR, Abrahamse H. Differentiation of Mesenchymal Stem Cells to Neuroglia: in the Context of Cell Signalling. Stem Cell Rev Rep. 2019 Dec;15(6):814-826. doi: 10.1007/s12015-019-09917-z. PMID: 31515658; PMCID: PMC6925073.

Ghosh HS. Adult Neurogenesis and the Promise of Adult Neural Stem Cells. J Exp Neurosci. 2019 Jun 27;13:1179069519856876. doi: 10.1177/1179069519856876. PMID: 31285654; PMCID: PMC6600486.

Gonzalez-Lopez E, Vrana KE. Dopamine beta-hydroxylase and its genetic variants in human health and disease. J Neurochem. 2020 Jan;152(2):157-181. doi: 10.1111/jnc.14893. Epub 2019 Oct 31. PMID: 31613389.

Haasters F, Prall WC, Anz D, Bourquin C, Pautke C, Endres S, Mutschler W, Docheva D, Schieker M. Morphological and immunocytochemical characteristics indicate the yield of early progenitors and represent a quality control for human mesenchymal stem

cell culturing. J Anat. 2009 May;214(5):759-67. doi: 10.1111/j.1469-7580.2009.01065.x. PMID: 19438770; PMCID: PMC2707099.

Hadjiconstantinou M, Neff NH. Enhancing aromatic L-amino acid decarboxylase activity: implications for L-DOPA treatment in Parkinson's disease. CNS Neurosci Ther. 2008 Winter;14(4):340-51. doi: 10.1111/j.1755-5949.2008.00058.x. PMID: 19040557; PMCID: PMC6494005.

Hallett PJ, Cooper O, Sadi D, Robertson H, Mendez I, Isacson O. Long-term health of dopaminergic neuron transplants in Parkinson's disease patients. Cell Rep. 2014 Jun 26;7(6):1755-61. doi: 10.1016/j.celrep.2014.05.027. Epub 2014 Jun 6. PMID: 24910427; PMCID: PMC4105701.

Han SM, Han SH, Coh YR, Jang G, Chan Ra J, Kang SK, Lee HW, Youn HY. Enhanced proliferation and differentiation of Oct4- and SOX2-overexpressing human adipose tissue mesenchymal stem cells. Exp Mol Med. 2014 Jun 20;46(6):e101. doi: 10.1038/emm.2014.28. PMID: 24946789; PMCID: PMC4081551.

Han Y, Li X, Zhang Y, Han Y, Chang F, Ding J. Mesenchymal Stem Cells for Regenerative Medicine. Cells. 2019 Aug 13;8(8):886. doi: 10.3390/cells8080886. PMID: 31412678; PMCID: PMC6721852.

Hauser RA, Freeman TB, Snow BJ, Nauert M, Gauger L, Kordower JH, Olanow CW. Long-term evaluation of bilateral fetal nigral transplantation in Parkinson disease. Arch Neurol. 1999 Feb;56(2):179-87. doi: 10.1001/archneur.56.2.179. PMID: 10025423.

He YX, Zhang Y, Yang Q, Wang C, Su G. Selection of suitable reference genes for reverse transcription-quantitative polymerase chain reaction analysis of neuronal cells

differentiated from bone mesenchymal stem cells. Mol Med Rep. 2015 Aug;12(2):2291-300. doi: 10.3892/mmr.2015.3671. Epub 2015 Apr 23. PMID: 25936423.

Hong YJ, Do JT. Neural Lineage Differentiation From Pluripotent Stem Cells to Mimic Human Brain Tissues. Front Bioeng Biotechnol. 2019 Dec 6;7:400. doi: 10.3389/fbioe.2019.00400. PMID: 31867324; PMCID: PMC6908493.

Hourigan B, Balay SD, Yee G, Saloni S, Quimin T. Capicua regulates the development of adult-born neurons in the hippocampus. Sci Rep [Internet]. 2021 Jun. [cited 2022 Sep 12]; 11: 11725. Available from https://www.nature.com/articles/s41598-021-91168-5

Huang B, Li G, Jiang XH. Fate determination in mesenchymal stem cells: a perspective from histone-modifying enzymes. Stem Cell Res Ther. 2015 Mar 19;6(1):35. doi: 10.1186/s13287-015-0018-0. PMID: 25890062; PMCID: PMC4365520.

Hulley P, Hartikka J, Lübbert H. Cyclic AMP promotes the survival of dopaminergic neurons in vitro and protects them from the toxic effects of MPP+. J Neural Transm Suppl. 1995;46:217-28. PMID: 8821058.

Iarkov A, Barreto GE, Grizzell JA, Echeverria V. Strategies for the Treatment of Parkinson's Disease: Beyond Dopamine. Front Aging Neurosci. 2020 Jan 31;12:4. doi: 10.3389/fnagi.2020.00004. PMID: 32076403; PMCID: PMC7006457.

Imayoshi I, Sakamoto M, Yamaguchi M, Mori K, Kageyama R. Essential roles of Notch signaling in maintenance of neural stem cells in developing and adult brains. J Neurosci. 2010 Mar 3;30(9):3489-98. doi: 10.1523/JNEUROSCI.4987-09.2010. PMID: 20203209; PMCID: PMC6634119.

Imayoshi I, Shimojo H, Sakamoto M, Ohtsuka T, Kageyama R. Genetic visualization of notch signaling in mammalian neurogenesis. Cell Mol Life Sci. 2013 Jun;70(12):2045-57. doi: 10.1007/s00018-012-1151-x. Epub 2012 Sep 13. PMID: 22971775; PMCID: PMC3663255.

Iwahori Y, Saito H, Torii K, Nishiyama N. Activin exerts a neurotrophic effect on cultured hippocampal neurons. Brain Res. 1997 Jun 20;760(1-2):52-8. doi: 10.1016/s0006-8993(97)00275-8. PMID: 9237517.

Jacobs FM, van Erp S, van der Linden AJ, von Oerthel L, Burbach JP, Smidt MP. Pitx3 potentiates Nurr1 in dopamine neuron terminal differentiation through release of SMRT-mediated repression. Development. 2009 Feb;136(4):531-40. doi: 10.1242/dev.029769. Epub 2009 Jan 14. PMID: 19144721.

Jaeger I, Arber C, Risner-Janiczek JR, Kuechler J, Pritzsche D, Chen IC, Naveenan T, Ungless MA, Li M. Temporally controlled modulation of FGF/ERK signaling directs midbrain dopaminergic neural progenitor fate in mouse and human pluripotent stem cells. Development. 2011 Oct;138(20):4363-74. doi: 10.1242/dev.066746. Epub 2011 Aug 31. PMID: 21880784; PMCID: PMC3177308.

Jagasia R, Steib K, Englberger E, Herold S, Faus-Kessler T, Saxe M, Gage FH, Song H, Lie DC. GABA-cAMP response element-binding protein signaling regulates maturation and survival of newly generated neurons in the adult hippocampus. J Neurosci. 2009 Jun 24;29(25):7966-77. doi: 10.1523/JNEUROSCI.1054-09.2009. PMID: 19553437; PMCID: PMC2776747.

Jeon HJ, Park J, Shin JH, Chang MS. Insulin-like growth factor binding protein-6 released from human mesenchymal stem cells confers neuronal protection through IGF-1R-

mediated signaling. Int J Mol Med. 2017 Dec;40(6):1860-1868. doi: 10.3892/ijmm.2017.3173. Epub 2017 Oct 5. PMID: 29039467; PMCID: PMC5716453.

Jia XF, Ye F, Wang YB, Feng DX. ROCK inhibition enhances neurite outgrowth in neural stem cells by upregulating YAP expression in vitro. Neural Regen Res. 2016 Jun;11(6):983-7. doi: 10.4103/1673-5374.184499. PMID: 27482229; PMCID: PMC4962598.

Jiménez-Acosta MA, Hernández LJR, Cristerna MLP, Tapia-Ramírez J, Meraz-Ríos MA. Review: Neuronal Differentiation Protocols of Mesenchymal Stem Cells. Advances in Bioscience and Biotechnology. 2022 [cited 2022 Sep 11];13:15-71. Available from: https://www.scirp.org/journal/paperinformation.aspx?paperid=114996.

Joksimovic M, Yun BA, Kittappa R, Anderegg AM, Chang WW, Taketo MM, McKay RD, Awatramani RB. Wnt antagonism of Shh facilitates midbrain floor plate neurogenesis. Nat Neurosci. 2009 Feb;12(2):125-31. doi: 10.1038/nn.2243. Epub 2009 Jan 4. PMID: 19122665.

Jósvay K, Winter Z, Katona RL, Pecze L, Marton A, Buhala A, Szakonyi G, Oláh Z, Vizler C. Besides neuro-imaging, the Thy1-YFP mouse could serve for visualizing experimental tumours, inflammation and wound-healing. Sci Rep. 2014 Oct 27;4:6776. doi: 10.1038/srep06776. PMID: 25345415; PMCID: PMC4209462.

Jovanovic VM, Salti A, Tilleman H, Zega K, Jukic MM, Zou H, Friedel RH, Prakash N, Blaess S, Edenhofer F, Brodski C. BMP/SMAD Pathway Promotes Neurogenesis of Midbrain Dopaminergic Neurons In Vivo and in Human Induced Pluripotent and Neural Stem Cells. J Neurosci. 2018 Feb 14;38(7):1662-1676. doi: 10.1523/JNEUROSCI.1540-17.2018. Epub 2018 Jan 10. PMID: 29321139; PMCID: PMC5815451.

Joyner AL, Liu A, Millet S. Otx2, Gbx2 and Fgf8 interact to position and maintain a mid-hindbrain organizer. Curr Opin Cell Biol. 2000 Dec;12(6):736-41. doi: 10.1016/s0955-0674(00)00161-7. PMID: 11063941.

Jurkowski MP, Bettio L, K Woo E, Patten A, Yau SY, Gil-Mohapel J. Beyond the Hippocampus and the SVZ: Adult Neurogenesis Throughout the Brain. Front Cell Neurosci. 2020 Sep 29;14:576444. doi: 10.3389/fncel.2020.576444. PMID: 33132848; PMCID: PMC7550688.

Kageyama R, Shimojo H, Imayoshi I. Dynamic expression and roles of Hes factors in neural development. Cell Tissue Res. 2015 Jan;359(1):125-33. doi: 10.1007/s00441-014-1888-7. Epub 2014 May 22. PMID: 24850276.

Kawasaki H, Mizuseki K, Nishikawa S, Kaneko S, Kuwana Y, Nakanishi S, Nishikawa SI, Sasai Y. Induction of midbrain dopaminergic neurons from ES cells by stromal cell-derived inducing activity. Neuron. 2000 Oct;28(1):31-40. doi: 10.1016/s0896-6273(00)00083-0. PMID: 11086981.

Kempermann G, Song H, Gage FH. Neurogenesis in the Adult Hippocampus. Cold Spring Harb Perspect Biol. 2015 Sep 1;7(9):a018812. doi: 10.1101/cshperspect.a018812. PMID: 26330519; PMCID: PMC4563705.

Kent WJ, Sugnet CW, Furey TS, Roskin KM, Pringle TH, Zahler AM, Haussler D. The human genome browser at UCSC. Genome Res. 2002 Jun;12(6):996-1006. doi: 10.1101/gr.229102. PMID: 12045153; PMCID: PMC186604.

Kim H, Zahir T, Tator CH, Shoichet MS. Effects of dibutyryl cyclic-AMP on survival and neuronal differentiation of neural stem/progenitor cells transplanted into spinal cord

injured rats. PLoS One. 2011;6(6):e21744. doi: 10.1371/journal.pone.0021744. Epub 2011 Jun 30. PMID: 21738784; PMCID: PMC3128087.

Kim HJ, Denli AM, Wright R, Baul TD, Clemenson GD, Morcos AS, Zhao C, Schafer ST, Gage FH, Kagalwala MN. REST Regulates Non-Cell-Autonomous Neuronal Differentiation and Maturation of Neural Progenitor Cells via Secretogranin II. J Neurosci. 2015 Nov 4;35(44):14872-84. doi: 10.1523/JNEUROSCI.4286-14.2015. PMID: 26538656; PMCID: PMC4635134.

Kim HT, Jeong SG, Cho GW. G9a inhibition promotes neuronal differentiation of human bone marrow mesenchymal stem cells through the transcriptional induction of RE-1 containing neuronal specific genes. Neurochem Int. 2016 Jun;96:77-83. doi: 10.1016/j.neuint.2016.03.002. Epub 2016 Mar 4. PMID: 26952575.

Kim J, Su SC, Wang H, Cheng AW, Cassady JP, Lodato MA, Lengner CJ, Chung CY, Dawlaty MM, Tsai LH, Jaenisch R. Functional integration of dopaminergic neurons directly converted from mouse fibroblasts. Cell Stem Cell. 2011 Nov 4;9(5):413-9. doi: 10.1016/j.stem.2011.09.011. Epub 2011 Oct 20. PMID: 22019014; PMCID: PMC3210333.

Kim T, Song JJ, Puspita L, Valiulahi P, Shim JW, Lee SH. In vitro generation of mature midbrain-type dopamine neurons by adjusting exogenous Nurr1 and Foxa2 expressions to their physiologic patterns. Exp Mol Med. 2017 Mar 10;49(3):e300. doi: 10.1038/emm.2016.163. PMID: 28280264; PMCID: PMC5382556.

Kim Y, Jeong J, Choi D. Small-molecule-mediated reprogramming: a silver lining for regenerative medicine. Exp Mol Med. 2020 Feb;52(2):213-226. doi: 10.1038/s12276-020-0383-3. Epub 2020 Feb 20. PMID: 32080339; PMCID: PMC7062739.

Kimbrel EA, Lanza R. Next-generation stem cells - ushering in a new era of cell-based therapies. Nat Rev Drug Discov. 2020 Jul;19(7):463-479. doi: 10.1038/s41573-020-0064-x. Epub 2020 Apr 6. PMID: 32612263.

Kirkeby A, Grealish S, Wolf DA, Nelander J, Wood J, Lundblad M, Lindvall O, Parmar M. Generation of regionally specified neural progenitors and functional neurons from human embryonic stem cells under defined conditions. Cell Rep. 2012 Jun 28;1(6):703-14. doi: 10.1016/j.celrep.2012.04.009. Epub 2012 May 26. PMID: 22813745.

Kirkeby A, Nolbrant S, Tiklova K, Heuer A, Kee N, Cardoso T, Ottosson DR, Lelos MJ, Rifes P, Dunnett SB, Grealish S, Perlmann T, Parmar M. Predictive Markers Guide Differentiation to Improve Graft Outcome in Clinical Translation of hESC-Based Therapy for Parkinson's Disease. Cell Stem Cell. 2017 Jan 5;20(1):135-148. doi: 10.1016/j.stem.2016.09.004. Epub 2016 Oct 27. PMID: 28094017; PMCID: PMC5222722.

Koli K, Ryynänen MJ, Keski-Oja J. Latent TGF-beta binding proteins (LTBPs)-1 and -3 coordinate proliferation and osteogenic differentiation of human mesenchymal stem cells. Bone. 2008 Oct;43(4):679-88. doi: 10.1016/j.bone.2008.06.016. Epub 2008 Jul 11. PMID: 18672106.

Kondo Y, Honoki K, Kishi S, Mori S, Fujiwara-Tani R, Tsukamoto S, Fujii H, Kuniyasu H, Tanaka Y. Endosialin/CD248 may be a potential therapeutic target to prevent the invasion and metastasis in osteosarcoma. Oncol Lett. 2022 Feb;23(2):42. doi: 10.3892/ol.2021.13160. Epub 2021 Dec 6. PMID: 34976154; PMCID: PMC8674875.

Kordower JH, Goetz CG, Chu Y, Halliday GM, Nicholson DA, Musial TF, Marmion DJ, Stoessl AJ, Sossi V, Freeman TB, Olanow CW. Robust graft survival and normalized

dopaminergic innervation do not obligate recovery in a Parkinson disease patient. Ann Neurol. 2017 Jan;81(1):46-57. doi: 10.1002/ana.24820. Epub 2017 Jan 6. PMID: 27900791; PMCID: PMC5890810.

Kovalevich J, Langford D. Considerations for the use of SH-SY5Y neuroblastoma cells in neurobiology. Methods Mol Biol. 2013;1078:9-21. doi: 10.1007/978-1-62703-640-5_2. PMID: 23975817; PMCID: PMC5127451.

Krabbe C, Zimmer J, Meyer M. Neural transdifferentiation of mesenchymal stem cells--a critical review. APMIS. 2005 Nov-Dec;113(11-12):831-44. doi: 10.1111/j.1600-0463.2005.apm_3061.x. PMID: 16480453.

Krashia P, Nobili A, D'Amelio M. Unifying Hypothesis of Dopamine Neuron Loss in Neurodegenerative Diseases: Focusing on Alzheimer's Disease. Front Mol Neurosci. 2019 May 17;12:123. doi: 10.3389/fnmol.2019.00123. PMID: 31156387; PMCID: PMC6534044.

Krashia P, Nobili A, D'Amelio M. Unifying Hypothesis of Dopamine Neuron Loss in Neurodegenerative Diseases: Focusing on Alzheimer's Disease. Front Mol Neurosci. 2019 May 17;12:123. doi: 10.3389/fnmol.2019.00123. PMID: 31156387; PMCID: PMC6534044.

Krieglstein K, Unsicker K. Transforming growth factor-b promotes survival of midbrain dopaminergic neurons and protects them against N-methyl-4-phenylpyridinium ion toxicity. Neuroscience [Internet]. 1994 Dec [cited 2022 Sep 12];63:1189–96. Available from https://www.sciencedirect.com/science/article/abs/pii/0306452294905835

Kriks S, Shim JW, Piao J, Ganat YM, Wakeman DR, Xie Z, Carrillo-Reid L, Auyeung G, Antonacci C, Buch A, Yang L, Beal MF, Surmeier DJ, Kordower JH, Tabar V, Studer

L. Dopamine neurons derived from human ES cells efficiently engraft in animal models of Parkinson's disease. Nature. 2011 Nov 6;480(7378):547-51. doi: 10.1038/nature10648. PMID: 22056989; PMCID: PMC3245796.

Kume T, Kawato Y, Osakada F, Izumi Y, Katsuki H, Nakagawa T, Kaneko S, Niidome T, Takada-Takatori Y, Akaike A. Dibutyryl cyclic AMP induces differentiation of human neuroblastoma SH-SY5Y cells into a noradrenergic phenotype. Neurosci Lett. 2008 Oct 10;443(3):199-203. doi: 10.1016/j.neulet.2008.07.079. Epub 2008 Aug 5. PMID: 18691633.

Kunath T, Saba-El-Leil MK, Almousailleakh M, Wray J, Meloche S, Smith A. FGF stimulation of the Erk1/2 signalling cascade triggers transition of pluripotent embryonic stem cells from self-renewal to lineage commitment. Development. 2007 Aug;134(16):2895-902. doi: 10.1242/dev.02880. PMID: 17660198.

Labandeira-Garcia JL, Rodríguez-Perez AI, Villar-Cheda B, Borrajo A, Dominguez-Meijide A, Guerra MJ. Rho Kinase and Dopaminergic Degeneration: A Promising Therapeutic Target for Parkinson's Disease. Neuroscientist. 2015 Dec;21(6):616-29. doi: 10.1177/1073858414554954. Epub 2014 Oct 16. PMID: 25323761.

Ladewig J, Mertens J, Kesavan J, Doerr J, Poppe D, Glaue F, Herms S, Wernet P, Kögler G, Müller FJ, Koch P, Brüstle O. Small molecules enable highly efficient neuronal conversion of human fibroblasts. Nat Methods. 2012 Jun;9(6):575-8. doi: 10.1038/nmeth.1972. Epub 2012 Apr 8. PMID: 22484851.

Lahti L, Saarimäki-Vire J, Rita H, Partanen J. FGF signaling gradient maintains symmetrical proliferative divisions of midbrain neuronal progenitors. Dev Biol. 2011 Jan

15;349(2):270-82. doi: 10.1016/j.ydbio.2010.11.008. Epub 2010 Nov 11. Erratum in: Dev Biol. 2011 Aug 15;356(2):608. PMID: 21074523.

Lai K, Kaspar BK, Gage FH, Schaffer DV. Sonic hedgehog regulates adult neural progenitor proliferation in vitro and in vivo. Nat Neurosci. 2003 Jan;6(1):21-7. doi: 10.1038/nn983. Erratum in: Nat Neurosci. 2003 Jun;6(6):645. PMID: 12469128.

Lam D, Enright HA, Cadena J, Peters SKG, Sales AP, Osburn JJ, Soscia DA, Kulp KS, Wheeler EK, Fischer NO. Tissue-specific extracellular matrix accelerates the formation of neural networks and communities in a neuron-glia co-culture on a multi-electrode array. Scientific Reports [Internet]. 2019 Mar 11 [cited 2022 Sep 12];9:4159. https://www.nature.com/articles/s41598-019-40128-1#Abs1.

Le Foll B, Gallo A, Le Strat Y, Lu L, Gorwood P. Genetics of dopamine receptors and drug addiction: a comprehensive review. Behav Pharmacol. 2009 Feb;20(1):1-17. doi: 10.1097/FBP.0b013e3283242f05. PMID: 19179847.

Leal-Galicia P, Chávez-Hernández ME, Mata F, Mata-Luévanos J, Rodríguez-Serrano LM, Tapia-de-Jesús A, Buenrostro-Jáuregui MH. Adult Neurogenesis: A Story Ranging from Controversial New Neurogenic Areas and Human Adult Neurogenesis to Molecular Regulation. Int J Mol Sci. 2021 Oct 25;22(21):11489. doi: 10.3390/ijms222111489. PMID: 34768919; PMCID: PMC8584254.

Lepski G, Jannes CE, Nikkhah G, Bischofberger J. cAMP promotes the differentiation of neural progenitors in vitro via modulation of voltage-gated calcium channels. Front Cell Neurosci. 2013 Sep 19;7:155. doi: 10.3389/fncel.2013.00155. PMID: 24065885. PMCID: PMC3777016.

Li L, Hung AC, Porter AG. Secretogranin II: a key AP-1-regulated protein that mediates neuronal differentiation and protection from nitric oxide-induced apoptosis of neuroblastoma cells. Cell Death Differ. 2008 May;15(5):879-88. doi: 10.1038/cdd.2008.8. Epub 2008 Feb 1. PMID: 18239671.

Li Z, Theus MH, Wei L. Role of ERK 1/2 signaling in neuronal differentiation of cultured embryonic stem cells. Dev Growth Differ. 2006 Oct;48(8):513-23. doi: 10.1111/j.1440-169X.2006.00889.x. PMID: 17026715.

Lim MS, Chang MY, Kim SM, Yi SH, Suh-Kim H, Jung SJ, Kim MJ, Kim JH, Lee YS, Lee SY, Kim DW, Lee SH, Park CH. Generation of Dopamine Neurons from Rodent Fibroblasts through the Expandable Neural Precursor Cell Stage. J Biol Chem. 2015 Jul 10;290(28):17401-14. doi: 10.1074/jbc.M114.629808. Epub 2015 May 28. PMID: 26023233; PMCID: PMC4498077.

Lin LF, Doherty DH, Lile JD, Bektesh S, Collins F. GDNF: a glial cell line-derived neurotrophic factor for midbrain dopaminergic neurons. Science. 1993 May 21;260(5111):1130-2. doi: 10.1126/science.8493557. PMID: 8493557.

Lin YL, Persaud SD, Nhieu J, Wei LN. Cellular Retinoic Acid-Binding Protein 1 Modulates Stem Cell Proliferation to Affect Learning and Memory in Male Mice. Endocrinology. 2017 Sep 1;158(9):3004-3014. doi: 10.1210/en.2017-00353. PMID: 28911165; PMCID: PMC5659671.

Liu D, Pavathuparambil Abdul Manaph N, Al-Hawwas M, Zhou XF, Liao H. Small Molecules for Neural Stem Cell Induction. Stem Cells Dev. 2018 Mar 1;27(5):297-312. doi: 10.1089/scd.2017.0282. Epub 2018 Feb 21. PMID: 29343174.

Liu D, Rychkov G, Al-Hawwas M, Manaph NPA, Zhou F, Bobrovskaya L, Liao H, Zhou XF. Conversion of human urine-derived cells into neuron-like cells by small molecules. Mol Biol Rep. 2020 Apr;47(4):2713-2722. doi: 10.1007/s11033-020-05370-1. Epub 2020 Mar 17. PMID: 32185687.

Liu D, Rychkov G, Al-Hawwas M, Manaph NPA, Zhou F, Bobrovskaya L, Liao H, Zhou XF. Conversion of human urine-derived cells into neuron-like cells by small molecules. Mol Biol Rep. 2020 Apr;47(4):2713-2722. doi: 10.1007/s11033-020-05370-1. Epub 2020 Mar 17. PMID: 32185687.

Lo Furno D, Mannino G, Pellitteri R, Zappalà A, Parenti R, Gili E, Vancheri C, Giuffrida R. Conditioned Media From Glial Cells Promote a Neural-Like Connexin Expression in Human Adipose-Derived Mesenchymal Stem Cells. Front Physiol. 2018 Nov 29;9:1742. doi: 10.3389/fphys.2018.01742. PMID: 30555356; PMCID: PMC6282092.

Logan CY, Nusse R. The Wnt signaling pathway in development and disease. Annu Rev Cell Dev Biol. 2004;20:781-810. doi: 10.1146/annurev.cellbio.20.010403.113126. PMID: 15473860.

Luo SX, Timbang L, Kim JI, Shang Y, Sandoval K, Tang AA, Whistler JL, Ding JB, Huang EJ. TGF-β Signaling in Dopaminergic Neurons Regulates Dendritic Growth, Excitatory-Inhibitory Synaptic Balance, and Reversal Learning. Cell Rep. 2016 Dec 20;17(12):3233-3245. doi: 10.1016/j.celrep.2016.11.068. PMID: 28009292; PMCID: PMC5312261.

MacDonald BT, Tamai K, He X. Wnt/beta-catenin signaling: components, mechanisms, and diseases. Dev Cell. 2009 Jul;17(1):9-26. doi: 10.1016/j.devcel.2009.06.016. PMID: 19619488; PMCID: PMC2861485.

Madhu V, Dighe AS, Cui Q, Deal DN. Dual Inhibition of Activin/Nodal/TGF-β and BMP Signaling Pathways by SB431542 and Dorsomorphin Induces Neuronal Differentiation of Human Adipose Derived Stem Cells. Stem Cells Int. 2016;2016:1035374. doi: 10.1155/2016/1035374. Epub 2015 Dec 20. PMID: 26798350; PMCID: PMC4699250.

Mannino G, Cristaldi M, Giurdanella G, Perrotta RE, Lo Furno D, Giuffrida R, Rusciano D. ARPE-19 conditioned medium promotes neural differentiation of adipose-derived mesenchymal stem cells. World J Stem Cells. 2021 Nov 26;13(11):1783-1796. doi: 10.4252/wjsc.v13.i11.1783. PMID: 34909123; PMCID: PMC8641022.

Marei HES, El-Gamal A, Althani A, Afifi N, Abd-Elmaksoud A, Farag A, Cenciarelli C, Thomas C, Anwarul H. Cholinergic and dopaminergic neuronal differentiation of human adipose tissue derived mesenchymal stem cells. J Cell Physiol. 2018 Feb;233(2):936-945. doi: 10.1002/jcp.25937. Epub 2017 Jun 22. Erratum in: J Cell Physiol. 2019 Jul;234(7):12088. PMID: 28369825.

Martynoga B, Drechsel D, Guillemot F. Molecular control of neurogenesis: a view from the mammalian cerebral cortex. Cold Spring Harb Perspect Biol. 2012 Oct 1;4(10):a008359. doi: 10.1101/cshperspect.a008359. PMID: 23028117; PMCID: PMC3475166.

Maxwell SL, Ho HY, Kuehner E, Zhao S, Li M. Pitx3 regulates tyrosine hydroxylase expression in the substantia nigra and identifies a subgroup of mesencephalic dopaminergic progenitor neurons during mouse development. Dev Biol. 2005 Jun 15;282(2):467-79. doi: 10.1016/j.ydbio.2005.03.028. PMID: 15950611.

Mazzon C, Anselmo A, Cibella J, Soldani C, Destro A, Kim N, Roncalli M, Burden SJ, Dustin ML, Sarukhan A, Viola A. The critical role of agrin in the hematopoietic stem cell

niche. Blood. 2011 Sep 8;118(10):2733-42. doi: 10.1182/blood-2011-01-331272. Epub 2011 Jun 7. PMID: 21653324; PMCID: PMC3172792.

McGowan LD, Alaama RA, Striedter GF. FGF2 delays tectal neurogenesis, increases tectal cell numbers, and alters tectal lamination in embryonic chicks. PLoS One. 2013 Nov 12;8(11):e79949. doi: 10.1371/journal.pone.0079949. PMID: 24265789; PMCID: PMC3827156.

Memorial Sloan Kettering Cancer Center [Internet]. [place unknown]: Memorial Sloan Kettering Centre. c2022. SH-SY5Y: Human Neuroblastoma Cell Line (ATCC CRL-2266); 2022 [cited 2022 Sep 12]; [about 1 screen]. Available from: https://www.mskcc.org/research-advantage/support/technology/tangible-material/human-neuroblastoma-cell-line-sh-sy5y#:~:text=SH%2DSY5Y%20is%20a%20thrice,the%20addition%20of%20specific%20compounds.

Mena MA, Casarejos MJ, Bonin A, Ramos JA, García Yébenes J. Effects of dibutyryl cyclic AMP and retinoic acid on the differentiation of dopamine neurons: prevention of cell death by dibutyryl cyclic AMP. J Neurochem. 1995 Dec;65(6):2612-20. doi: 10.1046/j.1471-4159.1995.65062612.x. PMID: 7595558.

Merz K, Herold S, Lie DC. CREB in adult neurogenesis--master and partner in the development of adult-born neurons? Eur J Neurosci. 2011 Mar;33(6):1078-86. doi: 10.1111/j.1460-9568.2011.07606.x. PMID: 21395851.

Meshorer E, Yellajoshula D, George E, Scambler PJ, Brown DT, Misteli T. Hyperdynamic plasticity of chromatin proteins in pluripotent embryonic stem cells. Dev

Cell. 2006 Jan;10(1):105-16. doi: 10.1016/j.devcel.2005.10.017. Erratum in: Dev Cell. Jan 17;22(1):233-4. PMID: 16399082; PMCID: PMC1868458.

Mesman S, Smidt MP. Acquisition of the Midbrain Dopaminergic Neuronal Identity. Int J Mol Sci. 2020 Jun 30;21(13):4638. doi: 10.3390/ijms21134638. PMID: 32629812; PMCID: PMC7369932.

Mesman S, von Oerthel L, Smidt MP. Mesodiencephalic dopaminergic neuronal differentiation does not involve GLI2A-mediated SHH-signaling and is under the direct influence of canonical WNT signaling. PLoS One. 2014 May 27;9(5):e97926. doi: 10.1371/journal.pone.0097926. PMID: 24865218; PMCID: PMC4035267.

Meyers EA, Kessler JA. TGF-β Family Signaling in Neural and Neuronal Differentiation, Development, and Function. Cold Spring Harb Perspect Biol. 2017 Aug 1;9(8):a022244. doi: 10.1101/cshperspect.a022244. PMID: 28130363; PMCID: PMC5538418.

Mikkelsen TS, Ku M, Jaffe DB, Issac B, Lieberman E, Giannoukos G, Alvarez P, Brockman W, Kim TK, Koche RP, Lee W, Mendenhall E, O'Donovan A, Presser A, Russ C, Xie X, Meissner A, Wernig M, Jaenisch R, Nusbaum C, Lander ES, Bernstein BE. Genome-wide maps of chromatin state in pluripotent and lineage-committed cells. Nature. 2007 Aug 2;448(7153):553-60. doi: 10.1038/nature06008. Epub 2007 Jul 1. PMID: 17603471; PMCID: PMC2921165.

Mizukami A, Thomé CH, Ferreira GA, Lanfredi GP, Covas DT, Pitteri SJ, Swiech K, Faça VM. Proteomic Identification and Time-Course Monitoring of Secreted Proteins During Expansion of Human Mesenchymal Stem/Stromal in Stirred-Tank Bioreactor. Front Bioeng Biotechnol. 2019 Jun 26;7:154. doi: 10.3389/fbioe.2019.00154. PMID: 31297369; PMCID: PMC6607109.

Mohrin M, Liu J, Zavala-Solorio J, Bhargava S, Maxwell Trumble J, Brito A, Hu D, Brooks D, Koukos G, Alabdulaaly L, Paw JS, Hake K, Kolumam G, Bouxsein ML, Baron R, Kutskova Y, Freund A. Inhibition of longevity regulator PAPP-A modulates tissue homeostasis via restraint of mesenchymal stromal cells. Aging Cell. 2021 Mar;20(3):e13313. doi: 10.1111/acel.13313. Epub 2021 Feb 9. PMID: 33561324; PMCID: PMC7963332.

Mollinari C, Zhao J, Lupacchini L, Garaci E, Merlo D, Pei G. Transdifferentiation: a new promise for neurodegenerative diseases. Cell Death Dis. 2018 Aug 6;9(8):830. doi: 10.1038/s41419-018-0891-4. PMID: 30082779; PMCID: PMC6078988.

Moreno EL, Hachi S, Hemmer K, Trietsch SJ, Baumuratov AS, Hankemeier T, Vulto P, Schwamborn JC, Fleming RM. Differentiation of neuroepithelial stem cells into functional dopaminergic neurons in 3D microfluidic cell culture. Lab Chip. 2015 Jun 7;15(11):2419-28. doi: 10.1039/c5lc00180c. PMID: 25902196.

Morii A, Katayama S, Inazu T. Establishment of a Simple Method for Inducing Neuronal Differentiation of P19 EC Cells without Embryoid Body Formation and Analysis of the Role of Histone Deacetylase 8 Activity in This Differentiation. Biol Pharm Bull. 2020;43(7):1096-1103. doi: 10.1248/bpb.b20-00091. PMID: 32612072.

Mukhtar T, Taylor V. Untangling Cortical Complexity During Development. J Exp Neurosci. 2018 Mar 1;12:1179069518759332. doi: 10.1177/1179069518759332. PMID: 29551911; PMCID: PMC5846925.

Murdamoothoo D, Schwenzer A, Kant J, Rupp T, Marzeda A, Midwood K, Orend G. Investigating cell-type specific functions of tenascin-C. Methods Cell Biol.

2018;143:401-428. doi: 10.1016/bs.mcb.2017.08.023. Epub 2017 Dec 1. PMID: 29310789.

Murphy M, Drago J, Bartlett PF. Fibroblast growth factor stimulates the proliferation and differentiation of neural precursor cells in vitro. J Neurosci Res. 1990 Apr;25(4):463-75. doi: 10.1002/jnr.490250404. PMID: 2112611.

Nadig RR. Stem cell therapy - Hype or hope? A review. J Conserv Dent. 2009 Oct;12(4):131-8. doi: 10.4103/0972-0707.58329. PMID: 20543921; PMCID: PMC2879724.

Navarro Quiroz E, Navarro Quiroz R, Ahmad M, Gomez Escorcia L, Villarreal JL, Fernandez Ponce C, Aroca Martinez G. Cell Signaling in Neuronal Stem Cells. Cells. 2018 Jul 14;7(7):75. doi: 10.3390/cells7070075. PMID: 30011912; PMCID: PMC6070865.

Naylor AJ, Azzam E, Smith S, Croft A, Poyser C, Duffield JS, Huso DL, Gay S, Ospelt C, Cooper MS, Isacke C, Goodyear SR, Rogers MJ, Buckley CD. The mesenchymal stem cell marker CD248 (endosialin) is a negative regulator of bone formation in mice. Arthritis Rheum. 2012 Oct;64(10):3334-43. doi: 10.1002/art.34556. PMID: 22674221; PMCID: PMC4209224.

Neirinckx V, Coste C, Rogister B, Wislet-Gendebien S. Concise review: adult mesenchymal stem cells, adult neural crest stem cells, and therapy of neurological pathologies: a state of play. Stem Cells Transl Med. 2013 Apr;2(4):284-96. doi: 10.5966/sctm.2012-0147. Epub 2013 Mar 13. PMID: 23486833; PMCID: PMC3659839.

Nhieu J, Lin YL, Wei LN. CRABP1 in Non-Canonical Activities of Retinoic Acid in Health and Diseases. Nutrients. 2022 Apr 6;14(7):1528. doi: 10.3390/nu14071528. PMID: 35406141; PMCID: PMC9003107.

Nolbrant S, Heuer A, Parmar M, Kirkeby A. Generation of high-purity human ventral midbrain dopaminergic progenitors for in vitro maturation and intracerebral transplantation. Nat Protoc. 2017 Sep;12(9):1962-1979. doi: 10.1038/nprot.2017.078. Epub 2017 Aug 31. PMID: 28858290.

Nouri N, Patel MJ, Joksimovic M, Poulin JF, Anderegg A, Taketo MM, Ma YC, Awatramani R. Excessive Wnt/beta-catenin signaling promotes midbrain floor plate neurogenesis, but results in vacillating dopamine progenitors. Mol Cell Neurosci. 2015 Sep;68:131-42. doi: 10.1016/j.mcn.2015.07.002. Epub 2015 Jul 9. PMID: 26164566; PMCID: PMC4633300.

Oakes HV, DeVee CE, Farmer B, Allen SA, Hall AN, Ensley T, Medlock K, Hanley A, Pond BB. Neurogenesis within the hippocampus after chronic methylphenidate exposure. J Neural Transm (Vienna). 2019 Feb;126(2):201-209. doi: 10.1007/s00702-018-1949-2. Epub 2018 Oct 28. PMID: 30370451.

Oakes HV, DeVee CE, Farmer B, Allen SA, Hall AN, Ensley T, Medlock K, Hanley A, Pond BB. Neurogenesis within the hippocampus after chronic methylphenidate exposure. J Neural Transm (Vienna). 2019 Feb;126(2):201-209. doi: 10.1007/s00702-018-1949-2. Epub 2018 Oct 28. PMID: 30370451.

Oxvig C. The role of PAPP-A in the IGF system: location, location, location. J Cell Commun Signal. 2015 Jun;9(2):177-87. doi: 10.1007/s12079-015-0259-9. Epub 2015 Jan 25. PMID: 25617049; PMCID: PMC4458251.

Palasz E, Wysocka A, Gasiorowska A, Chalimoniuk M, Niewiadomski W, Niewiadomska G. BDNF as a Promising Therapeutic Agent in Parkinson's Disease. Int J Mol Sci. 2020 Feb 10;21(3):1170. doi: 10.3390/ijms21031170. PMID: 32050617; PMCID: PMC7037114.

Pandey S, Jirásko M, Lochman J, Chvátal A, Chottova Dvorakova M, Kučera R. iPSCs in Neurodegenerative Disorders: A Unique Platform for Clinical Research and Personalized Medicine. J Pers Med. 2022 Sep 10;12(9):1485. doi: 10.3390/jpm12091485. PMID: 36143270; PMCID: PMC9500601.

Paratcha G, Ledda F. GDNF and GFRalpha: a versatile molecular complex for developing neurons. Trends Neurosci. 2008 Aug;31(8):384-91. doi: 10.1016/j.tins.2008.05.003. Epub 2008 Jul 1. PMID: 18597864.

Paratcha G, Ledda F. GDNF and GFRalpha: a versatile molecular complex for developing neurons. Trends Neurosci. 2008 Aug;31(8):384-91. doi: 10.1016/j.tins.2008.05.003. Epub 2008 Jul 1. PMID: 18597864.

Park HW, Lim MJ, Jung H, Lee SP, Paik KS, Chang MS. Human mesenchymal stem cell-derived Schwann cell-like cells exhibit neurotrophic effects, via distinct growth factor production, in a model of spinal cord injury. Glia. 2010 Jul;58(9):1118-32. doi: 10.1002/glia.20992. PMID: 20468053.

Park SE, Lee J, Chang EH, Kim JH, Sung JH, Na DL, Chang JW. Activin A secreted by human mesenchymal stem cells induces neuronal development and neurite outgrowth in an in vitro model of Alzheimer's disease: neurogenesis induced by MSCs via activin A. Arch Pharm Res. 2016 Aug;39(8):1171-9. doi: 10.1007/s12272-016-0799-4. Epub 2016 Aug 11. PMID: 27515053.

Pascual A, Hidalgo-Figueroa M, Piruat JI, Pintado CO, Gómez-Díaz R, López-Barneo J. Absolute requirement of GDNF for adult catecholaminergic neuron survival. Nat Neurosci. 2008 Jul;11(7):755-61. doi: 10.1038/nn.2136. Epub 2008 Jun 8. PMID: 18536709.

Patani R, Compston A, Puddifoot CA, Wyllie DJ, Hardingham GE, Allen ND, Chandran S. Activin/Nodal inhibition alone accelerates highly efficient neural conversion from human embryonic stem cells and imposes a caudal positional identity. PLoS One. 2009 Oct 6;4(10):e7327. doi: 10.1371/journal.pone.0007327. PMID: 19806200; PMCID: PMC2752165.

Peng C, Aron L, Klein R, Li M, Wurst W, Prakash N, Le W. Pitx3 is a critical mediator of GDNF-induced BDNF expression in nigrostriatal dopaminergic neurons. J Neurosci. 2011 Sep 7;31(36):12802-15. doi: 10.1523/JNEUROSCI.0898-11.2011. PMID: 21900559; PMCID: PMC6623418.

Peterziel H, Unsicker K, Krieglstein K. TGFbeta induces GDNF responsiveness in neurons by recruitment of GFRalpha1 to the plasma membrane. J Cell Biol. 2002 Oct 14;159(1):157-67. doi: 10.1083/jcb.200203115. Epub 2002 Oct 7. PMID: 12370242; PMCID: PMC2173495.

Pittenger MF, Discher DE, Péault BM, Phinney DG, Hare JM, Caplan AI. Mesenchymal stem cell perspective: cell biology to clinical progress. NPJ Regen Med. 2019 Dec 2;4:22. doi: 10.1038/s41536-019-0083-6. PMID: 31815001; PMCID: PMC6889290.

Pogue AI, Jaber VR, Sharfman NM, Zhao Y, Lukiw WJ. Downregulation of Neurofilament Light Chain Expression in Human Neuronal-Glial Cell Co-Cultures by a Microbiome-Derived Lipopolysaccharide-Induced miRNA-30b-5p. Front Neurol. 2022

Jun 24;13:900048. doi: 10.3389/fneur.2022.900048. PMID: 35812116; PMCID: PMC9263091.

Poliwoda S, Noor N, Downs E, Schaaf A, Cantwell A, Ganti L, Kaye AD, Mosel LI, Carroll CB, Viswanath O, Urits I. Stem cells: a comprehensive review of origins and emerging clinical roles in medical practice. Orthop Rev (Pavia). 2022 Aug 25;14(3):37498. doi: 10.52965/001c.37498. PMID: 36034728; PMCID: PMC9404248.

Poulsen KT, Armanini MP, Klein RD, Hynes MA, Phillips HS, Rosenthal A. TGF beta 2 and TGF beta 3 are potent survival factors for midbrain dopaminergic neurons. Neuron. 1994 Nov;13(5):1245-52. doi: 10.1016/0896-6273(94)90062-0. PMID: 7946360.

Prakash N, Brodski C, Naserke T, Puelles E, Gogoi R, Hall A, Panhuysen M, Echevarria D, Sussel L, Weisenhorn DM, Martinez S, Arenas E, Simeone A, Wurst W. A Wnt1-regulated genetic network controls the identity and fate of midbrain-dopaminergic progenitors in vivo. Development. 2006 Jan;133(1):89-98. doi: 10.1242/dev.02181. PMID: 16339193.

Puelles E, Annino A, Tuorto F, Usiello A, Acampora D, Czerny T, Brodski C, Ang SL, Wurst W, Simeone A. Otx2 regulates the extent, identity and fate of neuronal progenitor domains in the ventral midbrain. Development. 2004 May;131(9):2037-48. doi: 10.1242/dev.01107. PMID: 15105370.

Qin H, Zhao A, Fu X. Small molecules for reprogramming and transdifferentiation. Cell Mol Life Sci. 2017 Oct;74(19):3553-3575. doi: 10.1007/s00018-017-2586-x. Epub 2017 Jul 11. PMID: 28698932.

Qin H, Zhao AD, Sun ML, Ma K, Fu XB. Direct conversion of human fibroblasts into dopaminergic neuron-like cells using small molecules and protein factors. Mil Med Res.

2020 Nov 1;7(1):52. doi: 10.1186/s40779-020-00284-2. PMID: 33129359; PMCID: PMC7603706.

Quinn JP, Kandigian SE, Trombetta BA, Arnold SE, Carlyle BC. VGF as a biomarker and therapeutic target in neurodegenerative and psychiatric diseases. Brain Commun. 2021 Oct 27;3(4):fcab261. doi: 10.1093/braincomms/fcab261. PMID: 34778762; PMCID: PMC8578498.

Ragelle H, Naba A, Larson BL, Zhou F, Prijić M, Whittaker CA, Del Rosario A, Langer R, Hynes RO, Anderson DG. Comprehensive proteomic characterization of stem cell-derived extracellular matrices. Biomaterials. 2017 Jun;128:147-159. doi: 10.1016/j.biomaterials.2017.03.008. Epub 2017 Mar 7. PMID: 28327460; PMCID: PMC8191742.

Rahhal B, Heermann S, Ferdinand A, Rosenbusch J, Rickmann M, Krieglstein K. In vivo requirement of TGF-beta/GDNF cooperativity in mouse development: focus on the neurotrophic hypothesis. Int J Dev Neurosci. 2009 Feb;27(1):97-102. doi: 10.1016/j.ijdevneu.2008.08.003. Epub 2008 Sep 6. PMID: 18824086.

Rakovic A, Voß D, Vulinovic F, Meier B, Hellberg AK, Nau C, Klein C, Leipold E. Electrophysiological Properties of Induced Pluripotent Stem Cell-Derived Midbrain Dopaminergic Neurons Correlate With Expression of Tyrosine Hydroxylase. Front Cell Neurosci. 2022 Mar 23;16:817198. doi: 10.3389/fncel.2022.817198. PMID: 35401116; PMCID: PMC8983830.

Raney BJ, Dreszer TR, Barber GP, Clawson H, Fujita PA, Wang T, Nguyen N, Paten B, Zweig AS, Karolchik D, Kent WJ. Track data hubs enable visualization of user-defined genome-wide annotations on the UCSC Genome Browser. Bioinformatics. 2014 Apr

1;30(7):1003-5. doi: 10.1093/bioinformatics/btt637. Epub 2013 Nov 13. PMID: 24227676; PMCID: PMC3967101.

Redmond DE Jr, Bjugstad KB, Teng YD, Ourednik V, Ourednik J, Wakeman DR, Parsons XH, Gonzalez R, Blanchard BC, Kim SU, Gu Z, Lipton SA, Markakis EA, Roth RH, Elsworth JD, Sladek JR Jr, Sidman RL, Snyder EY. Behavioral improvement in a primate Parkinson's model is associated with multiple homeostatic effects of human neural stem cells. Proc Natl Acad Sci U S A. 2007 Jul 17;104(29):12175-80. doi: 10.1073/pnas.0704091104. Epub 2007 Jun 22. PMID: 17586681; PMCID: PMC1896134.

Ren J, Huang D, Li R, Wang W, Zhou C. Control of mesenchymal stem cell biology by histone modifications. Cell Biosci. 2020 Feb 3;10:11. doi: 10.1186/s13578-020-0378-8. PMID: 32025282; PMCID: PMC6996187.

Ren LQ, Chen M, Hultborn H, Guo S, Zhang Y, Zhang M. Heterogenic Distribution of Aromatic L-Amino Acid Decarboxylase Neurons in the Rat Spinal Cord. Front Integr Neurosci. 2017 Nov 8;11:31. doi: 10.3389/fnint.2017.00031. PMID: 29225571; PMCID: PMC5706469.

Ribeiro FF, Xapelli S. Intervention of Brain-Derived Neurotrophic Factor and Other Neurotrophins in Adult Neurogenesis. Adv Exp Med Biol. 2021;1331:95-115. doi: 10.1007/978-3-030-74046-7_8. PMID: 34453295.

Robertson IB, Horiguchi M, Zilberberg L, Dabovic B, Hadjiolova K, Rifkin DB. Latent TGF-β-binding proteins. Matrix Biol. 2015 Sep;47:44-53. doi: 10.1016/j.matbio.2015.05.005. Epub 2015 May 8. PMID: 25960419; PMCID: PMC4844006.

Rodríguez-Martínez G, Molina-Hernández A, Velasco I. Activin A promotes neuronal differentiation of cerebrocortical neural progenitor cells. PLoS One. 2012;7(8):e43797. doi: 10.1371/journal.pone.0043797. Epub 2012 Aug 22. PMID: 22928036; PMCID: PMC3425505.

Roelen BA, Dijke Pt. Controlling mesenchymal stem cell differentiation by TGFBeta family members. J Orthop Sci. 2003;8(5):740-8. doi: 10.1007/s00776-003-0702-2. Erratum in: J Orthop Sci. 2004;9(2):220. PMID: 14557946.

Roussa E, Farkas LM, Krieglstein K. TGF-beta promotes survival on mesencephalic dopaminergic neurons in cooperation with Shh and FGF-8. Neurobiol Dis. 2004 Jul;16(2):300-10. doi: 10.1016/j.nbd.2004.03.006. PMID: 15193287.

Roussa E, Oehlke O, Rahhal B, Heermann S, Heidrich S, Wiehle M, Krieglstein K. Transforming Growth Factor β Cooperates with Persephin for Dopaminergic Phenotype Induction. STEM CELLS [Internet]. 2009 Jan 2 [cited 2022 Sep 12];26:1683-94. Available from https://stemcellsjournals.onlinelibrary.wiley.com/doi/full/10.1634/stemcells.2007-0805. doi: https://doi.org/10.1634/stemcells.2007-0805

Roussa E, Wiehle M, Dünker N, Becker-Katins S, Oehlke O, Krieglstein K. Transforming growth factor beta is required for differentiation of mouse mesencephalic progenitors into dopaminergic neurons in vitro and in vivo: ectopic induction in dorsal mesencephalon. Stem Cells. 2006 Sep;24(9):2120-9. doi: 10.1634/stemcells.2005-0514. Epub 2006 Jun 1. PMID: 16741229.

Roybon L, Hjalt T, Christophersen NS, Li JY, Brundin P. Effects on differentiation of embryonic ventral midbrain progenitors by Lmx1a, Msx1, Ngn2, and Pitx3. J Neurosci.

2008 Apr 2;28(14):3644-56. doi: 10.1523/JNEUROSCI.0311-08.2008. PMID: 18385323; PMCID: PMC6671084.

Rueden CT, Schindelin J, Hiner MC, DeZonia BE, Walter AE, Arena ET, Eliceiri KW. ImageJ2: ImageJ for the next generation of scientific image data. BMC Bioinformatics. 2017 Nov 29;18(1):529. doi: 10.1186/s12859-017-1934-z. PMID: 29187165; PMCID: PMC5708080.

Saarimäki-Vire J, Peltopuro P, Lahti L, Naserke T, Blak AA, Vogt Weisenhorn DM, Yu K, Ornitz DM, Wurst W, Partanen J. Fibroblast growth factor receptors cooperate to regulate neural progenitor properties in the developing midbrain and hindbrain. J Neurosci. 2007 Aug 8;27(32):8581-92. doi: 10.1523/JNEUROSCI.0192-07.2007. PMID: 17687036; PMCID: PMC6672929.

Sánchez-Pernaute R, Studer L, Bankiewicz KS, Major EO, McKay RD. In vitro generation and transplantation of precursor-derived human dopamine neurons. J Neurosci Res. 2001 Aug 15;65(4):284-8. doi: 10.1002/jnr.1152. PMID: 11494363.

Sasai Y, Lu B, Steinbeisser H, De Robertis EM. Regulation of neural induction by the Chd and Bmp-4 antagonistic patterning signals in Xenopus. Nature. 1995 Jul 27;376(6538):333-6. doi: 10.1038/376333a0. Erratum in: Nature. 1995 Oct 26;377(6551):757. Erratum in: Nature. 1995 Nov 23;378(6555):419. PMID: 7630399.

Schindelin J, Arganda-Carreras I, Frise E, Kaynig V, Longair M, Pietzsch T, Preibisch S, Rueden C, Saalfeld S, Schmid B, Tinevez JY, White DJ, Hartenstein V, Eliceiri K, Tomancak P, Cardona A. Fiji: an open-source platform for biological-image analysis. Nat Methods. 2012 Jun 28;9(7):676-82. doi: 10.1038/nmeth.2019. PMID: 22743772; PMCID: PMC3855844.

Shaik S, Pandey H, Thirumalasetti SK, Nakamura N. Characteristics and Functions of the Yip1 Domain Family (YIPF), Multi-Span Transmembrane Proteins Mainly Localized to the Golgi Apparatus. Front Cell Dev Biol. 2019 Jul 30;7:130. doi: 10.3389/fcell.2019.00130. PMID: 31417902; PMCID: PMC6682643.

Shimomura A. Hashino E. Epigenetic Regulation of Neural Differentiation from Embryonic Stem Cells [Internet]. In Wislet-Gendebien S, editor. Trends in Cell Signaling Pathways in Neuronal Fate Decision. London:IntechOpen; 2013. Available from https://www.intechopen.com/chapters/43849

Shin WJ, Seo JH, Choi HW, Hong YJ, Lee WJ, Chae JI, Kim SJ, Lee JW, Hong K, Song H, Park C, Do JT. Derivation of primitive neural stem cells from human-induced pluripotent stem cells. J Comp Neurol. 2019 Dec 15;527(18):3023-3033. doi: 10.1002/cne.24727. Epub 2019 Jun 20. PMID: 31173371.

Sigma Aldrich [Internet]. Darmstadt: Merck KGaA. c2022. MaxGel™ ECM Hydrogel: An In Vitro Human Cell Derived Basement Membrane Extract for 3D Cell Culture Applications; 2022 [cited 2022 Sep 12]; [about 5 screens]. Available from: https://www.sigmaaldrich.com/MT/en/technical-documents/technical-article/cell-culture-and-cell-culture-analysis/3d-cell-culture/maxgel-human-ecm

Simeone A. Genetic control of dopaminergic neuron differentiation. Trends Neurosci. 2005 Feb;28(2):62-5; discussion 65-6. doi: 10.1016/j.tins.2004.11.007. PMID: 15667926.

Singh K, Sachan N, Ene T, Dabovic B, Rifkin D. Latent transforming growth factor β binding protein 3 controls adipogenesis. Matrix Biol. 2022 Sep;112:155-170. doi: 10.1016/j.matbio.2022.08.001. Epub 2022 Aug 4. PMID: 35933071.

Singh M, Vaishnav PK, Dinda AK, Mohanty S. Evaluation of Priming Efficiency of Forskolin in Tissue-Specific Human Mesenchymal Stem Cells into Dopaminergic Neurons: An In Vitro Comparative Study. Cells. 2020 Sep 9;9(9):2058. doi: 10.3390/cells9092058. PMID: 32917012; PMCID: PMC7565008.

Smidak R, Sialana FJ, Kristofova M, Stojanovic T, Rajcic D, Malikovic J, Feyissa DD, Korz V, Hoeger H, Wackerlig J, Mechtcheriakova D, Lubec G. Reduced Levels of the Synaptic Functional Regulator FMRP in Dentate Gyrus of the Aging Sprague-Dawley Rat. Front Aging Neurosci. 2017 Nov 23;9:384. doi: 10.3389/fnagi.2017.00384. PMID: 29218006; PMCID: PMC5703695.

Smidt MP, Smits SM, Bouwmeester H, Hamers FP, van der Linden AJ, Hellemons AJ, Graw J, Burbach JP. Early developmental failure of substantia nigra dopamine neurons in mice lacking the homeodomain gene Pitx3. Development. 2004 Mar;131(5):1145-55. doi: 10.1242/dev.01022. PMID: 14973278.

Song MR, Ghosh A. FGF2-induced chromatin remodeling regulates CNTF-mediated gene expression and astrocyte differentiation. Nat Neurosci. 2004 Mar;7(3):229-35. doi: 10.1038/nn1192. Epub 2004 Feb 8. PMID: 14770186.

Sonnenschein SF, Gomes FV, Grace AA. Dysregulation of Midbrain Dopamine System and the Pathophysiology of Schizophrenia. Front Psychiatry. 2020 Jun 30;11:613. doi: 10.3389/fpsyt.2020.00613. PMID: 32719622; PMCID: PMC7350524.

Sousa KM, Villaescusa JC, Cajanek L, Ondr JK, Castelo-Branco G, Hofstra W, Bryja V, Palmberg C, Bergman T, Wainwright B, Lang RA, Arenas E. Wnt2 regulates progenitor proliferation in the developing ventral midbrain. J Biol Chem. 2010 Mar 5;285(10):7246-

53. doi: 10.1074/jbc.M109.079822. Epub 2009 Dec 16. PMID: 20018874; PMCID: PMC2844173.

Sun G, Alzayady K, Stewart R, Ye P, Yang S, Li W, Shi Y. Histone demethylase LSD1 regulates neural stem cell proliferation. Molecular & Cellular Bio [Internet]. 2010 Apr 15 [cited 2022 Sep 12]; 30(8):1997–2005. Available from https://journals.asm.org/doi/10.1128/MCB.01116-09

Sun LN, Qi JS, Gao R. Physical exercise reserved amyloid-beta induced brain dysfunctions by regulating hippocampal neurogenesis and inflammatory response via MAPK signaling. Brain Res. 2018 Oct 15;1697:1-9. doi: 10.1016/j.brainres.2018.04.040. Epub 2018 May 2. PMID: 29729254.

Sun LN, Qi JS, Gao R. Physical exercise reserved amyloid-beta induced brain dysfunctions by regulating hippocampal neurogenesis and inflammatory response via MAPK signaling. Brain Res. 2018 Oct 15;1697:1-9. doi: 10.1016/j.brainres.2018.04.040. Epub 2018 May 2. PMID: 29729254.

Surmeier DJ, Halliday GM, Simuni T. Calcium, mitochondrial dysfunction and slowing the progression of Parkinson's disease. Exp Neurol. 2017 Dec;298(Pt B):202-209. doi: 10.1016/j.expneurol.2017.08.001. Epub 2017 Aug 2. PMID: 28780195; PMCID: PMC6037988.

Suzuki K, Kobayashi T, Funatsu O, Morita A, Ikekita M. Activin A induces neuronal differentiation and survival via ALK4 in a SMAD-independent manner in a subpopulation of human neuroblastomas. Biochem Biophys Res Commun. 2010 Apr 9;394(3):639-45. doi: 10.1016/j.bbrc.2010.03.039. Epub 2010 Mar 10. PMID: 20226172.

Suzuki T, Mitake S, Okumura-Noji K, Shimizu H, Tada T, Fujii T. Excitable membranes and synaptic transmission: postsynaptic mechanisms. Localization of alpha-internexin in the postsynaptic density of the rat brain. Brain Res. 1997 Aug 8;765(1):74-80. doi: 10.1016/s0006-8993(97)00492-7. PMID: 9310396.

Syal C, Seegobin M, Sarma SN, Gouveia A, Hsu K, Niibori Y, He L, Wondisford FE, Frankland PW, Wang J. Ectopic expression of aPKC-mediated phosphorylation in p300 modulates hippocampal neurogenesis, CREB binding and fear memory differently with age. Sci Rep. 2018 Sep 10;8(1):13489. doi: 10.1038/s41598-018-31657-2. PMID: 30201979; PMCID: PMC6131509.

Temple S. The development of neural stem cells. Nature. 2001 Nov 1;414(6859):112-7. doi: 10.1038/35102174. PMID: 11689956.

Timmer J, Chesnutt C, Niswander L. The activin signaling pathway promotes differentiation of dI3 interneurons in the spinal neural tube. Dev Biol. 2005 Sep 1;285(1):1-10. doi: 10.1016/j.ydbio.2005.05.039. PMID: 16039645.

Timmer JR, Wang C, Niswander L. BMP signaling patterns the dorsal and intermediate neural tube via regulation of homeobox and helix-loop-helix transcription factors. Development. 2002 May;129(10):2459-72. doi: 10.1242/dev.129.10.2459. PMID: 11973277.

Tojima T, Kobayashi S, Ito E. Dual role of cyclic AMP-dependent protein kinase in neuritogenesis and synaptogenesis during neuronal differentiation. J Neurosci Res. 2003 Dec 15;74(6):829-37. doi: 10.1002/jnr.10754. PMID: 14648587.

Tokuda K, Baron B, Kuramitsu Y, Kitagawa T, Tokuda N, Morishige N, Kobayashi M, Kimura K, Nakamura K, Sonoda KH. Optimization of fixative solution for retinal

morphology: a comparison with Davidson's fixative and other fixation solutions. Jpn J Ophthalmol. 2018 Jul;62(4):481-490. doi: 10.1007/s10384-018-0592-7. Epub 2018 Apr 24. PMID: 29691783.

Tomkowicz B, Rybinski K, Foley B, Ebel W, Kline B, Routhier E, Sass P, Nicolaides NC, Grasso L, Zhou Y. Interaction of endosialin/TEM1 with extracellular matrix proteins mediates cell adhesion and migration. Proc Natl Acad Sci U S A. 2007 Nov 13;104(46):17965-70. doi: 10.1073/pnas.0705647104. Epub 2007 Nov 6. PMID: 17986615; PMCID: PMC2084280.

Tonge PD, Andrews PW. Retinoic acid directs neuronal differentiation of human pluripotent stem cell lines in a non-cell-autonomous manner. Differentiation. 2010 Jul;80(1):20-30. doi: 10.1016/j.diff.2010.04.001. Epub 2010 Apr 28. PMID: 20427117.

Tönges L, Frank T, Tatenhorst L, Saal KA, Koch JC, Szego ÉM, Bähr M, Weishaupt JH, Lingor P. Inhibition of rho kinase enhances survival of dopaminergic neurons and attenuates axonal loss in a mouse model of Parkinson's disease. Brain. 2012 Nov;135(Pt 11):3355-70. doi: 10.1093/brain/aws254. Epub 2012 Oct 19. PMID: 23087045; PMCID: PMC3501973.

Traiffort E, Charytoniuk DA, Faure H, Ruat M. Regional distribution of Sonic Hedgehog, patched, and smoothened mRNA in the adult rat brain. J Neurochem. 1998 Mar;70(3):1327-30. doi: 10.1046/j.1471-4159.1998.70031327.x. PMID: 9489757.

Tretter YP, Hertel M, Munz B, ten Bruggencate G, Werner S, Alzheimer C. Induction of activin A is essential for the neuroprotective action of basic fibroblast growth factor in vivo. Nat Med. 2000 Jul;6(7):812-5. doi: 10.1038/77548. PMID: 10888932.

Tropepe V, Hitoshi S, Sirard C, Mak TW, Rossant J, van der Kooy D. Direct neural fate specification from embryonic stem cells: a primitive mammalian neural stem cell stage acquired through a default mechanism. Neuron. 2001 Apr;30(1):65-78. doi: 10.1016/s0896-6273(01)00263-x. PMID: 11343645.

Tropepe V, Sibilia M, Ciruna BG, Rossant J, Wagner EF, van der Kooy D. Distinct neural stem cells proliferate in response to EGF and FGF in the developing mouse telencephalon. Dev Biol. 1999 Apr 1;208(1):166-88. doi: 10.1006/dbio.1998.9192. PMID: 10075850.

Trzaska KA, Kuzhikandathil EV, Rameshwar P. Specification of a dopaminergic phenotype from adult human mesenchymal stem cells. Stem Cells. 2007 Nov;25(11):2797-808. doi: 10.1634/stemcells.2007-0212. Epub 2007 Jul 26. PMID: 17656644.

Tsai HL, Chiu WT, Fang CL, Hwang SM, Renshaw PF, Lai WF. Different forms of tenascin-C with tenascin-R regulate neural differentiation in bone marrow-derived human mesenchymal stem cells. Tissue Eng Part A. 2014 Jul;20(13-14):1908-21. doi: 10.1089/ten.TEA.2013.0188. PMID: 24829055; PMCID: PMC4086655.

Tüshaus J, Kataka ES, Zaucha J, Frishman D, Müller SA, Lichtenthaler SF. Neuronal Differentiation of LUHMES Cells Induces Substantial Changes of the Proteome. PROTEOMICS. 2020 Sep 19;21:2000174. Doi: 10.1002/pmic.202000174

Tutukova S, Tarabykin V, Hernandez-Miranda LR. The Role of Neurod Genes in Brain Development, Function, and Disease. Front Mol Neurosci. 2021 Jun 9;14:662774. doi: 10.3389/fnmol.2021.662774. PMID: 34177462; PMCID: PMC8221396.

Ullah I, Subbarao RB, Rho GJ. Human mesenchymal stem cells - current trends and future prospective. Biosci Rep. 2015 Apr 28;35(2):e00191. doi: 10.1042/BSR20150025. PMID: 25797907; PMCID: PMC4413017.

Unsicker K, Meier C, Krieglstein K, Sartor BM, Flanders KC. Expression, localization, and function of transforming growth factor-beta s in embryonic chick spinal cord, hindbrain, and dorsal root ganglia. J Neurobiol. 1996 Feb;29(2):262-76. doi: 10.1002 PMID: 8821181.

Urrutia DN, Caviedes P, Mardones R, Minguell JJ, Vega-Letter AM, Jofre CM. Comparative study of the neural differentiation capacity of mesenchymal stromal cells from different tissue sources: An approach for their use in neural regeneration therapies. PLoS One. 2019 Mar 11;14(3):e0213032. doi: 10.1371/journal.pone.0213032. PMID: 30856179; PMCID: PMC6437714.

Vasan L, Park E, David LA, Fleming T, Schuurmans C. Direct Neuronal Reprogramming: Bridging the Gap Between Basic Science and Clinical Application. Front Cell Dev Biol. 2021 Jul 5;9:681087. doi: 10.3389/fcell.2021.681087. PMID: 34291049; PMCID: PMC8287587.

Veenvliet JV, Dos Santos MT, Kouwenhoven WM, von Oerthel L, Lim JL, van der Linden AJ, Koerkamp MJ, Holstege FC, Smidt MP. Specification of dopaminergic subsets involves interplay of En1 and Pitx3. Development. 2013 Aug;140(16):3373-84. doi: 10.1242/dev.094565. Epub 2013 Jul 17. Erratum in: Development. 2013 Oct;140(19):4116. PMID: 23863478.

Vieira MS, Santos AK, Vasconcellos R, Goulart VAM, Parreira RC, Kihara AH, Ulrich H, Resende RR. Neural stem cell differentiation into mature neurons: Mechanisms of

regulation and biotechnological applications. Biotechnol Adv. 2018 Nov 15;36(7):1946-1970. doi: 10.1016/j.biotechadv.2018.08.002. Epub 2018 Aug 3. PMID: 30077716.

Volpicelli F, Caiazzo M, Greco D, Consales C, Leone L, Perrone-Capano C, Colucci D'Amato L, di Porzio U. Bdnf gene is a downstream target of Nurr1 transcription factor in rat midbrain neurons in vitro. J Neurochem. 2007 Jul;102(2):441-53. doi: 10.1111/j.1471-4159.2007.04494.x. Epub 2007 May 15. PMID: 17506860.

Volpicelli F, Perrone-Capano C, Bellenchi GC, Colucci-D'Amato L, di Porzio U. Molecular Regulation in Dopaminergic Neuron Development. Cues to Unveil Molecular Pathogenesis and Pharmacological Targets of Neurodegeneration. Int J Mol Sci. 2020 Jun 3;21(11):3995. doi: 10.3390/ijms21113995. PMID: 32503161; PMCID: PMC7312927.wang

Wallén A A, Castro DS, Zetterström RH, Karlén M, Olson L, Ericson J, Perlmann T. Orphan nuclear receptor Nurr1 is essential for Ret expression in midbrain dopamine neurons and in the brain stem. Mol Cell Neurosci. 2001 Dec;18(6):649-63. doi: 10.1006/mcne.2001.1057. PMID: 11749040.

Wang J, Chen S, Pan C, Li G, Tang Z. Application of Small Molecules in the Central Nervous System Direct Neuronal Reprogramming. Front Bioeng Biotechnol. 2022 Jul 7;10:799152. doi: 10.3389/fbioe.2022.799152. PMID: 35875485; PMCID: PMC9301571.

Wang M, Ling KH, Tan JJ, Lu CB. Development and Differentiation of Midbrain Dopaminergic Neuron: From Bench to Bedside. Cells. 2020 Jun 18;9(6):1489. doi: 10.3390/cells9061489. PMID: 32570916; PMCID: PMC7349799.

Wang Y, Xu J, You W, Shen H, Li X, Yu Z, Li H, Chen G. Roles of Rufy3 in experimental subarachnoid hemorrhage-induced early brain injury via accelerating neuronal axon repair and synaptic plasticity. Mol Brain. 2022 Apr 23;15(1):35. doi: 10.1186/s13041-022-00919-6. PMID: 35461284; PMCID: PMC9034509.

Warrington D. Neural Induction of Mesenchymal Stem Cells via small molecule cocktail treatment [dissertation]. [Malta]: University of Malta; 2021. 94 p.

Watabe T, Miyazono K. Roles of TGF-beta family signaling in stem cell renewal and differentiation. Cell Res. 2009 Jan;19(1):103-15. doi: 10.1038/cr.2008.323. PMID: 19114993.

Wechsler-Reya RJ, Scott MP. Control of neuronal precursor proliferation in the cerebellum by Sonic Hedgehog. Neuron. 1999 Jan;22(1):103-14. doi: 10.1016/s0896-6273(00)80682-0. PMID: 10027293.

Wei Z, Sun M, Liu X, Zhang J, Jin Y. Rufy3, a protein specifically expressed in neurons, interacts with actin-bundling protein Fascin to control the growth of axons. J Neurochem. 2014 Sep;130(5):678-92. doi: 10.1111/jnc.12740. Epub 2014 May 19. PMID: 24720729.

Wei ZJ, Fan BY, Liu Y, Ding H, Tang HS, Pan DY, Shi JX, Zheng PY, Shi HY, Wu H, Li A, Feng SQ. MicroRNA changes of bone marrow-derived mesenchymal stem cells differentiated into neuronal-like cells by Schwann cell-conditioned medium. Neural Regen Res. 2019 Aug;14(8):1462-1469. doi: 10.4103/1673-5374.253532. PMID: 30964074; PMCID: PMC6524508.

Wen G, Pang H, Wu X, Jiang E, Zhang X, Zhan X. Proteomic characterization of secretory granules in dopaminergic neurons indicates chromogranin/secretogranin-mediated protein processing impairment in Parkinson's disease. Aging (Albany NY).

2021 Aug 21;13(16):20335-20358. doi: 10.18632/aging.203415. Epub 2021 Aug 21. PMID: 34420933; PMCID: PMC8436928.

Wen S, Li H, Liu J. Epigenetic background of neuronal fate determination. Prog Neurobiol. 2009 Feb;87(2):98-117. doi: 10.1016/j.pneurobio.2008.10.002. Epub 2008 Oct 21. PMID: 19007844.

Westerlund U, Moe MC, Varghese M, Berg-Johnsen J, Ohlsson M, Langmoen IA, Svensson M. Stem cells from the adult human brain develop into functional neurons in culture. Exp Cell Res. 2003 Oct 1;289(2):378-83. doi: 10.1016/s0014-4827(03)00291-x. PMID: 14499639.

Widmer HR, Schaller B, Meyer M, Seiler RW. Glial cell line-derived neurotrophic factor stimulates the morphological differentiation of cultured ventral mesencephalic calbindin- and calretinin-expressing neurons. Exp Neurol. 2000 Jul;164(1):71-81. doi: 10.1006/exnr.2000.7418. PMID: 10877917.

Wilson PA, Hemmati-Brivanlou A. Induction of epidermis and inhibition of neural fate by Bmp-4. Nature. 1995 Jul 27;376(6538):331-3. doi: 10.1038/376331a0. PMID: 7630398.

Won SY, Kwon S, Jeong HS, Chung KW, Choi BO, Chang JW, Lee JE. Fibulin 5, a human Wharton's jelly-derived mesenchymal stem cells-secreted paracrine factor, attenuates peripheral nervous system myelination defects through the Integrin-RAC1 signaling axis. Stem Cells. 2020 Oct 27;38(12):1578–93. doi: 10.1002/stem.3287. Epub ahead of print. PMID: 33107705; PMCID: PMC7756588.

Wu Y, Hoogduijn MJ, Baan CC, Korevaar SS, de Kuiper R, Yan L, Wang L, van Besouw NM. Adipose Tissue-Derived Mesenchymal Stem Cells Have a Heterogenic Cytokine

Secretion Profile. Stem Cells Int. 2017;2017:4960831. doi: 10.1155/2017/4960831. Epub 2017 May 31. PMID: 28642794; PMCID: PMC5470019.

Wurst W, Bally-Cuif L. Neural plate patterning: upstream and downstream of the isthmic organizer. Nat Rev Neurosci. 2001 Feb;2(2):99-108. doi: 10.1038/35053516. PMID: 11253000.

Xi J, Liu Y, Liu H, Chen H, Emborg ME, Zhang SC. Specification of midbrain dopamine neurons from primate pluripotent stem cells. Stem Cells. 2012 Aug;30(8):1655-63. doi: 10.1002/stem.1152. PMID: 22696177; PMCID: PMC3405174.

Xu G, Wu F, Gu X, Zhang J, You K, Chen Y, Getachew A, Zhuang Y, Zhong X, Lin Z, Guo D, Yang F, Pan T, Wei H, Li Y. Direct Conversion of Human Urine Cells to Neurons by Small Molecules. Scientific Reports [Internet]. 2019 [cited 2022 Sep 12];9:16707. Available from https://www.nature.com/articles/s41598-019-53007-6.

Yang H, Hao D, Liu C, Huang D, Chen B, Fan H, Liu C, Zhang L, Zhang Q, An J, Zhao J. Generation of functional dopaminergic neurons from human spermatogonial stem cells to rescue parkinsonian phenotypes. Stem Cell Res Ther. 2019 Jun 27;10(1):195. doi: 10.1186/s13287-019-1294-x. PMID: 31248447; PMCID: PMC6598262.

Yang H, Wang J, Wang F, Liu X, Chen H, Duan W, Qu T. Dopaminergic Neuronal Differentiation from the Forebrain-Derived Human Neural Stem Cells Induced in Cultures by Using a Combination of BMP-7 and Pramipexole with Growth Factors. Front Neural Circuits. 2016 Apr 20;10:29. doi: 10.3389/fncir.2016.00029. PMID: 27147976; PMCID: PMC4837145.

Ye W, Shimamura K, Rubenstein JL, Hynes MA, Rosenthal A. FGF and Shh signals control dopaminergic and serotonergic cell fate in the anterior neural plate. Cell. 1998 May 29;93(5):755-66. doi: 10.1016/s0092-8674(00)81437-3. PMID: 9630220.

Yi JJ, Barnes AP, Hand R, Polleux F, Ehlers MD. TGF-beta signaling specifies axons during brain development. Cell. 2010 Jul 9;142(1):144-57. doi: 10.1016/j.cell.2010.06.010. PMID: 20603020; PMCID: PMC2933408.

Ying QL, Stavridis M, Griffiths D, Li M, Smith A. Conversion of embryonic stem cells into neuroectodermal precursors in adherent monoculture. Nat Biotechnol. 2003 Feb;21(2):183-6. doi: 10.1038/nbt780. Epub 2003 Jan 13. PMID: 12524553.

Yu YL, Chou RH, Chen LT, Shyu WC, Hsieh SC, Wu CS, Zeng HJ, Yeh SP, Yang DM, Hung SC, Hung MC. EZH2 regulates neuronal differentiation of mesenchymal stem cells through PIP5K1C-dependent calcium signaling. J Biol Chem. 2011 Mar 18;286(11):9657-67. doi: 10.1074/jbc.M110.185124. Epub 2011 Jan 7. PMID: 21216957; PMCID: PMC3059014.

Zahir T, Chen YF, MacDonald JF, Leipzig N, Tator CH, Shoichet MS. Neural stem/progenitor cells differentiate in vitro to neurons by the combined action of dibutyryl cAMP and interferon-gamma. Stem Cells Dev. 2009 Dec;18(10):1423-32. doi: 10.1089/scd.2008.0412. PMID: 19355840.

Zakrzewski W, Dobrzyński M, Szymonowicz M, Rybak Z. Stem cells: past, present, and future. Stem Cell Res Ther. 2019 Feb 26;10(1):68. doi: 10.1186/s13287-019-1165-5. PMID: 30808416; PMCID: PMC6390367.

Zetterström RH, Lindqvist E, Mata de Urquiza A, Tomac A, Eriksson U, Perlmann T, Olson L. Role of retinoids in the CNS: differential expression of retinoid binding proteins

and receptors and evidence for presence of retinoic acid. Eur J Neurosci. 1999 Feb;11(2):407-16. doi: 10.1046/j.1460-9568.1999.00444.x. PMID: 10051741.

Zhang J, Huang X, Wang H, Liu X, Zhang T, Wang Y, Hu D. The challenges and promises of allogeneic mesenchymal stem cells for use as a cell-based therapy. Stem Cell Res Ther. 2015 Dec 1;6:234. doi: 10.1186/s13287-015-0240-9. PMID: 26620426; PMCID: PMC4665863.

Zhang J, Jiao J. Molecular Biomarkers for Embryonic and Adult Neural Stem Cell and Neurogenesis. Biomed Res Int. 2015;2015:727542. doi: 10.1155/2015/727542. Epub 2015 Sep 1. PMID: 26421301; PMCID: PMC4569757.

Zhang L, Yin JC, Yeh H, Ma NX, Lee G, Chen XA, Wang Y, Lin L, Chen L, Jin P, Wu GY, Chen G. Small Molecules Efficiently Reprogram Human Astroglial Cells into Functional Neurons. Cell Stem Cell. 2015 Dec 3;17(6):735-747. doi: 10.1016/j.stem.2015.09.012. Epub 2015 Oct 17. PMID: 26481520; PMCID: PMC4675726.

Zhang L, Yin JC, Yeh H, Ma NX, Lee G, Chen XA, Wang Y, Lin L, Chen L, Jin P, Wu GY, Chen G. Small Molecules Efficiently Reprogram Human Astroglial Cells into Functional Neurons. Cell Stem Cell. 2015 Dec 3;17(6):735-747. doi: 10.1016/j.stem.2015.09.012. Epub 2015 Oct 17. PMID: 26481520; PMCID: PMC4675726.

Zhang S, Cui W. SOX2, a key factor in the regulation of pluripotency and neural differentiation. World J Stem Cells. 2014 Jul 26;6(3):305-11. doi: 10.4252/wjsc.v6.i3.305. PMID: 25126380; PMCID: PMC4131272.

Zhao J, Liem RK. α-Internexin and Peripherin: Expression, Assembly, Functions, and Roles in Disease. Methods Enzymol. 2016;568:477-507. doi: 10.1016/bs.mie.2015.09.012. Epub 2015 Nov 3. PMID: 26795481.

Zhou H, Wang B, Sun H, Xu X, Wang Y. Epigenetic Regulations in Neural Stem Cells and Neurological Diseases. Stem Cells Int. 2018 Mar 18;2018:6087143. doi: 10.1155/2018/6087143. PMID: 29743892; PMCID: PMC5878882.

Zhou Q, Cheng Y, Sun F, Shen J, Nasser MI, Zhu P, Zhang X, Li Y, Yin G, Wang Y, Wu X, Zhao M. A Comprehensive Review of the Therapeutic Value of Urine-Derived Stem Cells. Front Genet. 2022 Jan 3;12:781597. doi: 10.3389/fgene.2021.781597. PMID: 35047009; PMCID: PMC8762167.

Zhou X, Pace J, Filichia E, Lv T, Davis B, Hoffer B, Selman W, Luo Y. Effect of the sonic hedgehog receptor smoothened on the survival and function of dopaminergic neurons. Exp Neurol. 2016 Sep;283(Pt A):235-45. doi: 10.1016/j.expneurol.2016.06.013. Epub 2016 Jun 15. PMID: 27317298; PMCID: PMC5479305.

Zhu Y, Zhang X, Gu R, Liu X, Wang S, Xia D, Li Z, Lian X, Zhang P, Liu Y, Zhou Y. LAMA2 regulates the fate commitment of mesenchymal stem cells via hedgehog signaling. Stem Cell Res Ther. 2020 Mar 25;11(1):135. doi: 10.1186/s13287-020-01631-9. PMID: 32213190; PMCID: PMC7093965.

Zhu Y, Zhang X, Gu R, Liu X, Wang S, Xia D, Li Z, Lian X, Zhang P, Liu Y, Zhou Y. LAMA2 regulates the fate commitment of mesenchymal stem cells via hedgehog signaling. Stem Cell Res Ther. 2020 Mar 25;11(1):135. doi: 10.1186/s13287-020-01631-9. PMID: 32213190; PMCID: PMC7093965.

Zirra A, Wiethoff S, Patani R. Neural Conversion and Patterning of Human Pluripotent Stem Cells: A Developmental Perspective. Stem Cells Int. 2016;2016:8291260. doi: 10.1155/2016/8291260. Epub 2016 Mar 16. PMID: 27069483; PMCID: PMC4812494.

Appendices

Screenshots of the ELISA data processing on Excel with the AssayFitPro add-in:

ELISA

Input	1	2	3	4	5	6	7	8	9	10	11	12
A	1.230	1.187	1.575	1.530								
B	1.063	1.003	1.461	1.584								
C	0.983	0.996	1.533	1.531								
D	0.826	0.769	1.171	1.207								
E	0.601	0.583	1.169	1.164								
F	0.337	0.347	1.206	1.205								
G	0.932	0.840	1.167	1.217								
H	0.739	0.689	1.202	1.231								

Sample ID

Layout	1	2	3	4	5	6	7	8	9	10	11	12
A	CAL-10	CAL-10	MSC	MSC								
B	CAL-500	CAL-500	SM1a	SM1a								
C	CAL-1500	CAL-1500	SM1b	SM1b								
D	CAL-5000	CAL-5000	SM2a	SM2a								
E	CAL-20000	CAL-20000	SM2b	SM2b								
F	CAL-80000	CAL-80000	SM3a	SM3a								
G	CAL-3000	CAL-3000	SM3b	SM3b								
H	CAL-10000	CAL-10000	SM3c	SM3c								

concentration

Output	1	2	3	4	5	6	7	8	9	10	11	12
A	0.0	62.6	0.0	0.0								
B	655.1	1150.9	0.0	0.0								
C	1354.0	1219.6	0.0	0.0								
D	3927.0	5532.8	109.5	18.2								
E	15436.2	17395.0	116.0	132.8								
F	245803.7	198355.8	20.0	21.8								
G	1976.3	3603.4	122.6	3.7								
H	6612.2	8912.4	27.6	0.0								

Figure 7.1. ELISA input and output.

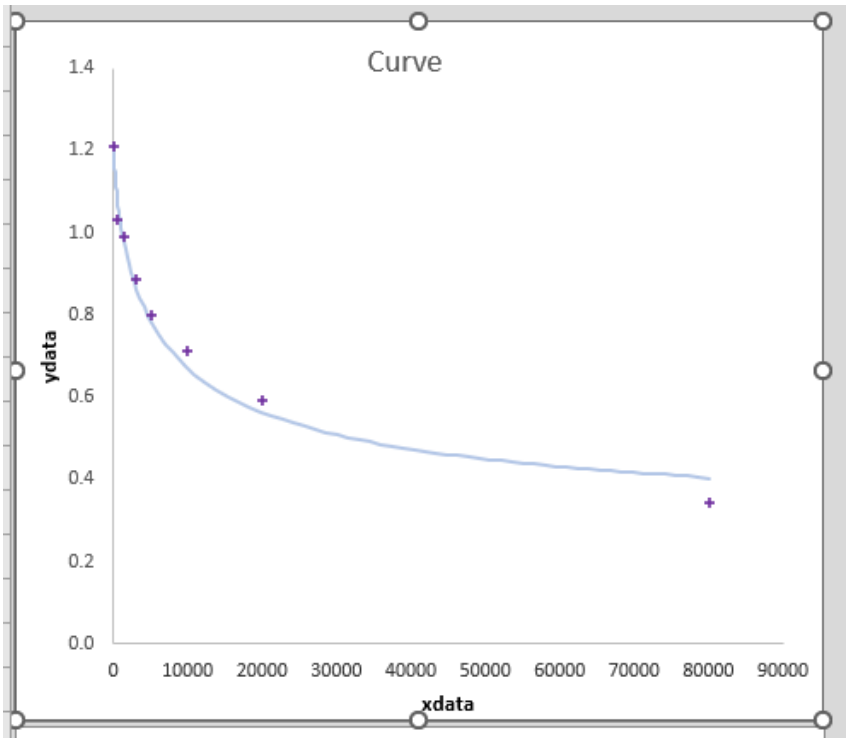

Figure 7.2. Standard curve for ELISA on Excel

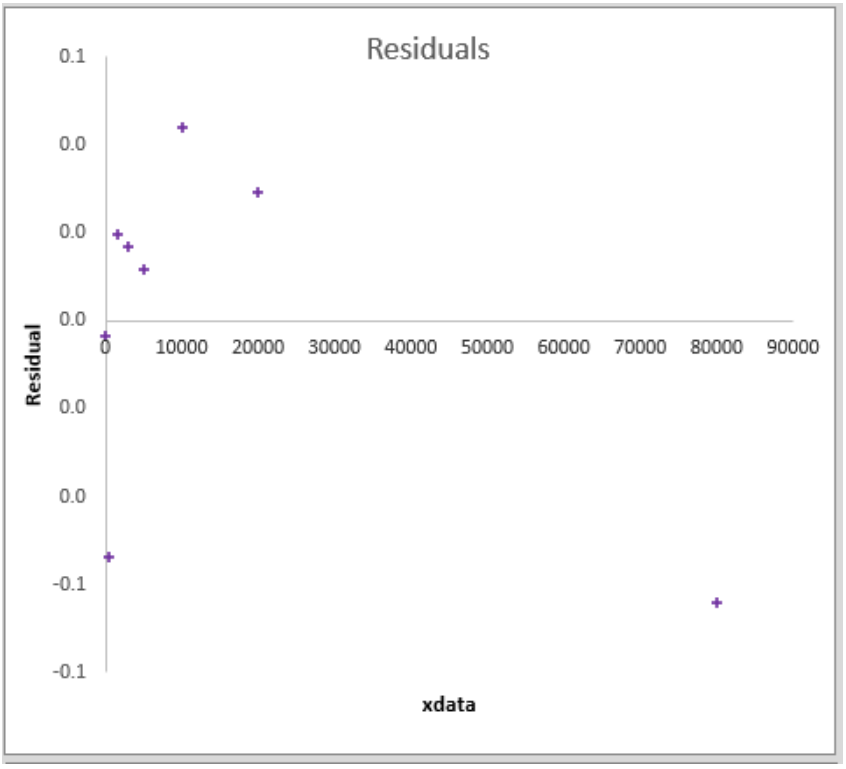

Figure 7.3. Residuals for ELISA on Excel

Report

AssayFit Pro

ELISA result report

Operator	Kit	Units
		pg/mL
Date	**Lot**	**LOQ**
21-Aug-22		

Fit function	Fit parameters	
4 parameter logistic	A	1.222
(D + ((A - D) / (1 + ((x / C) ^ B)))) |4 paran	B	0.708
	C	6332.335
R2 **SSQ**	D	0.271
0.9797 1.06E-02		

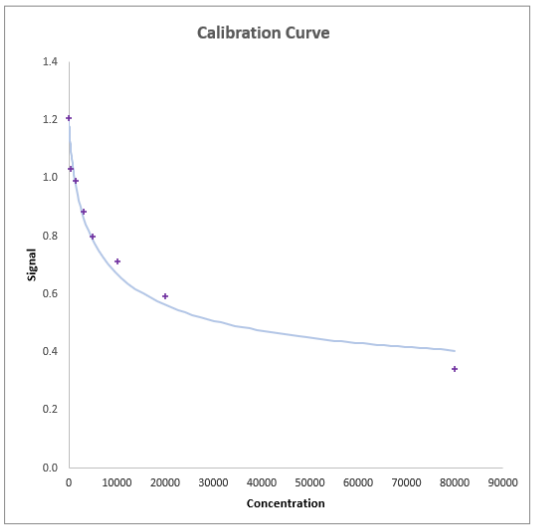

Figure 7.4. ELISA report part 1.

Report

	Signal						Concentration						
ID	Rep1	Rep2	Rep3	Rep av	Rep CV%	ID	Conc1	Conc2	Conc3	Conc Av	Dilution	Conc x Dil	Conc CV%
CAL-10	1.230	1.187		1.209	2.516	CAL-10	0.0	62.6		31.3	50	1566.0	141.4
CAL-500	1.063	1.003		1.033	4.107	CAL-500	655.1	1150.9		903.0	50	45148.4	38.8
CAL-1500	0.983	0.996		0.990	0.929	CAL-1500	1354.0	1219.6		1286.8	50	64341.6	7.4
CAL-3000	0.932	0.840		0.886	7.342	CAL-3000	1976.3	3603.4		2789.8	50	139491.4	41.2
CAL-5000	0.826	0.769		0.798	5.054	CAL-5000	3927.0	5532.8		4729.9	50	236494.7	24.0
CAL-10000	0.739	0.689		0.714	4.952	CAL-10000	6612.2	8912.4		7762.3	50	388116.1	21.0
CAL-20000	0.601	0.583		0.592	2.150	CAL-20000	15436.2	17395.0		16415.6	50	820778.1	8.4
CAL-80000	0.337	0.347		0.342	2.068	CAL-80000	245803.7	198355.8		222079.8	50	11103988.5	15.1
MSC	1.575	1.530		1.553	2.050	MSC	0.0	0.0		0.0	2	0.0	
SM1a	1.461	1.584		1.523	5.713	SM1a	0.0	0.0		0.0	2	0.0	
SM1b	1.533	1.531		1.532	0.092	SM1b	0.0	0.0		0.0	2	0.0	
SM2a	1.171	1.207		1.189	2.141	SM2a	109.5	18.2		63.9	2	127.7	101.1
SM2b	1.169	1.164		1.167	0.303	SM2b	116.0	132.8		124.4	2	248.8	9.6
SM3a	1.206	1.205		1.206	0.059	SM3a	20.0	21.8		20.9	2	41.8	6.2
SM3b	1.167	1.217		1.192	2.966	SM3b	122.6	3.7		63.2	2	126.3	133.2
SM3c	1.202	1.231		1.217	1.686	SM3c	27.6	0.0		13.8	2	27.6	141.4

Figure 7.5. ELISA report part 2

Optimisation blots for neural antibodies

A panel of 5 neuronal proteins were selected to assess for their presence in cellular extracts. The panel consisted of PAX6, EOMES/TBR2, MASH1, NEUROD1 and TH. Upon arrival of these antibodies, several blots were conducted for optimisation purposes. Though these antibodies were tested on more than one neural-related sample, they never gave a positive signal. Samples tested on included SH-SY5Y cells, rat brain lysate, U87 cells, and stocks of small molecule-treated differentiated neuronal cells from the prior project. Several images of these optimisation blots can be found below.

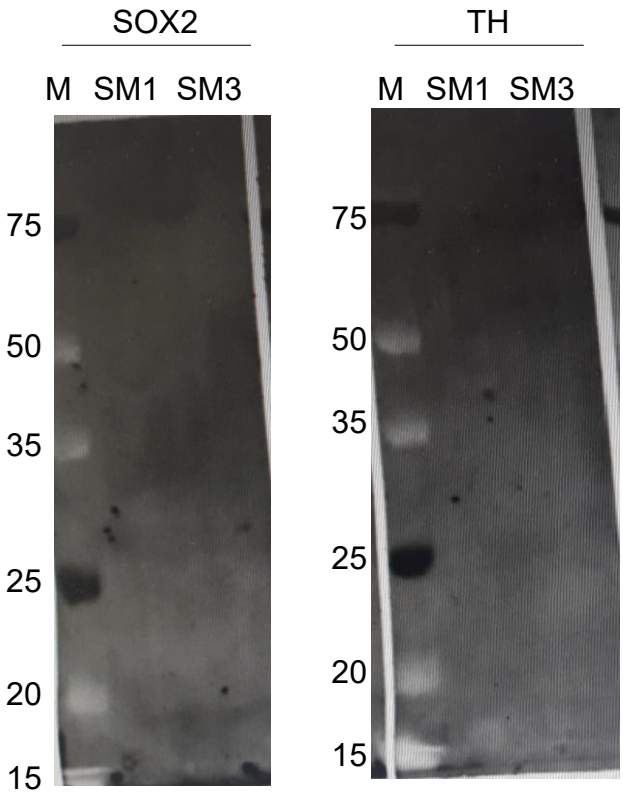

Figure 7.6. SOX2 and TH blots.

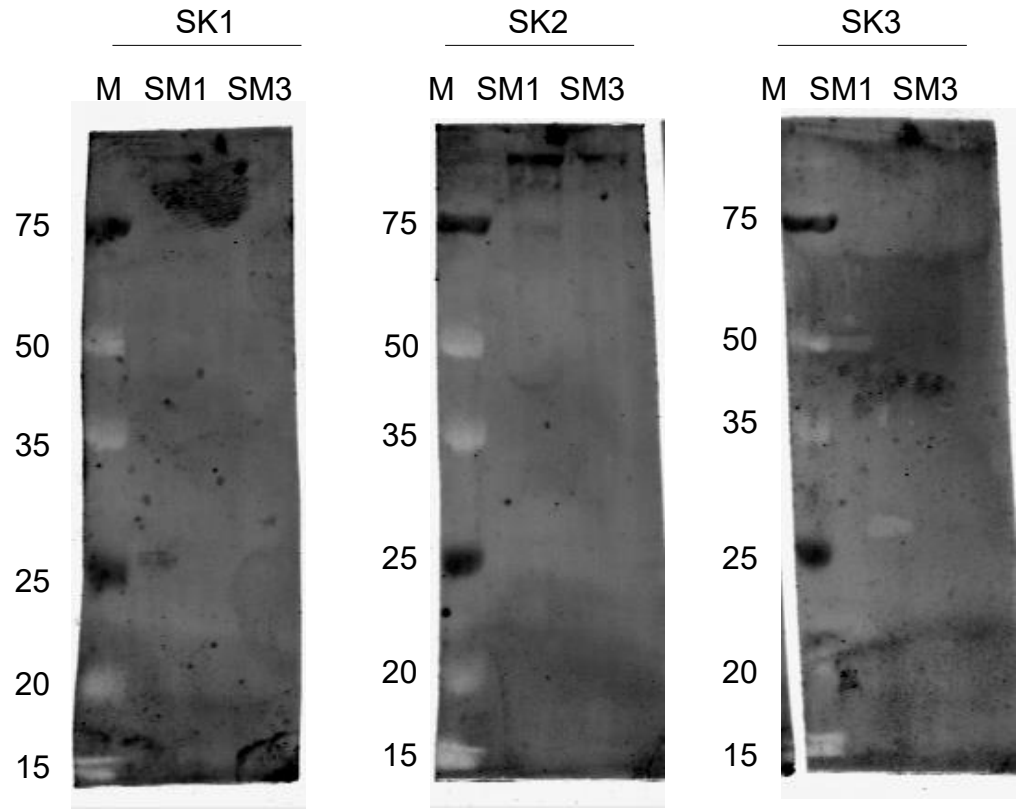

Figure 7.7. SK channel (SK1/2/3) blots.

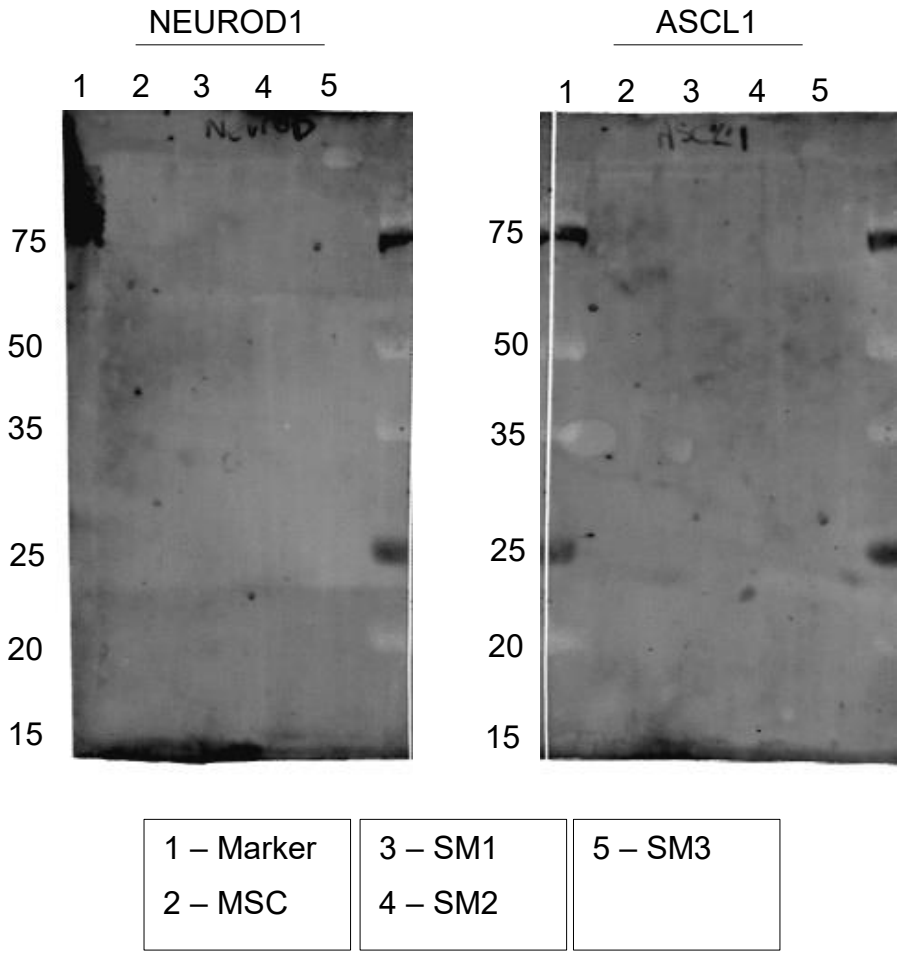

Figure 7.8. NEUROD1 and ASCL1 blots.

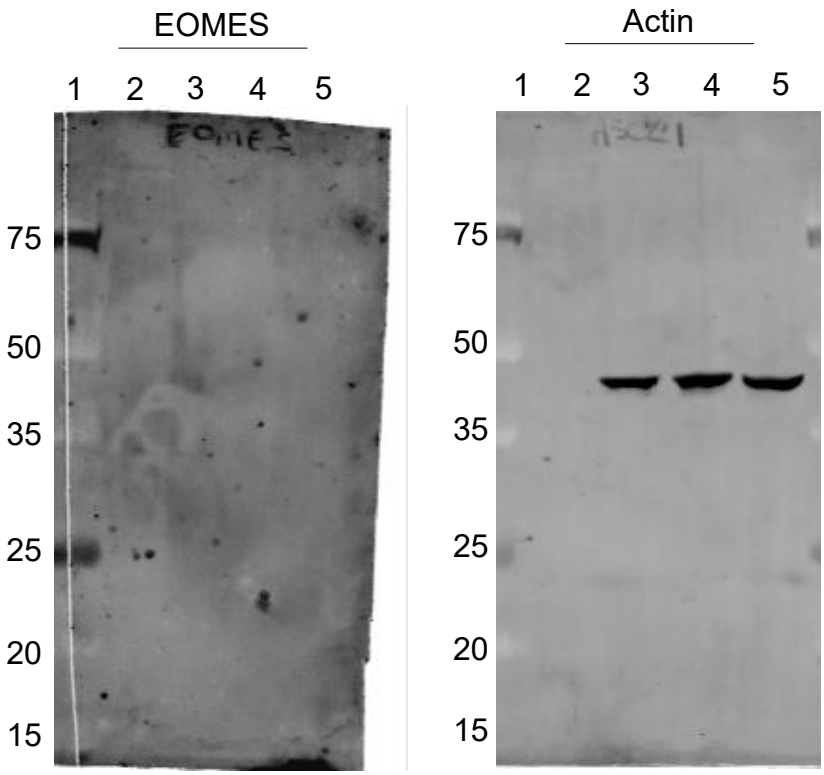

1 – Marker 2 – MSC	3 – SM1 4 – SM2	5 – SM3

Figure 7.9. EOMES and Actin blots.

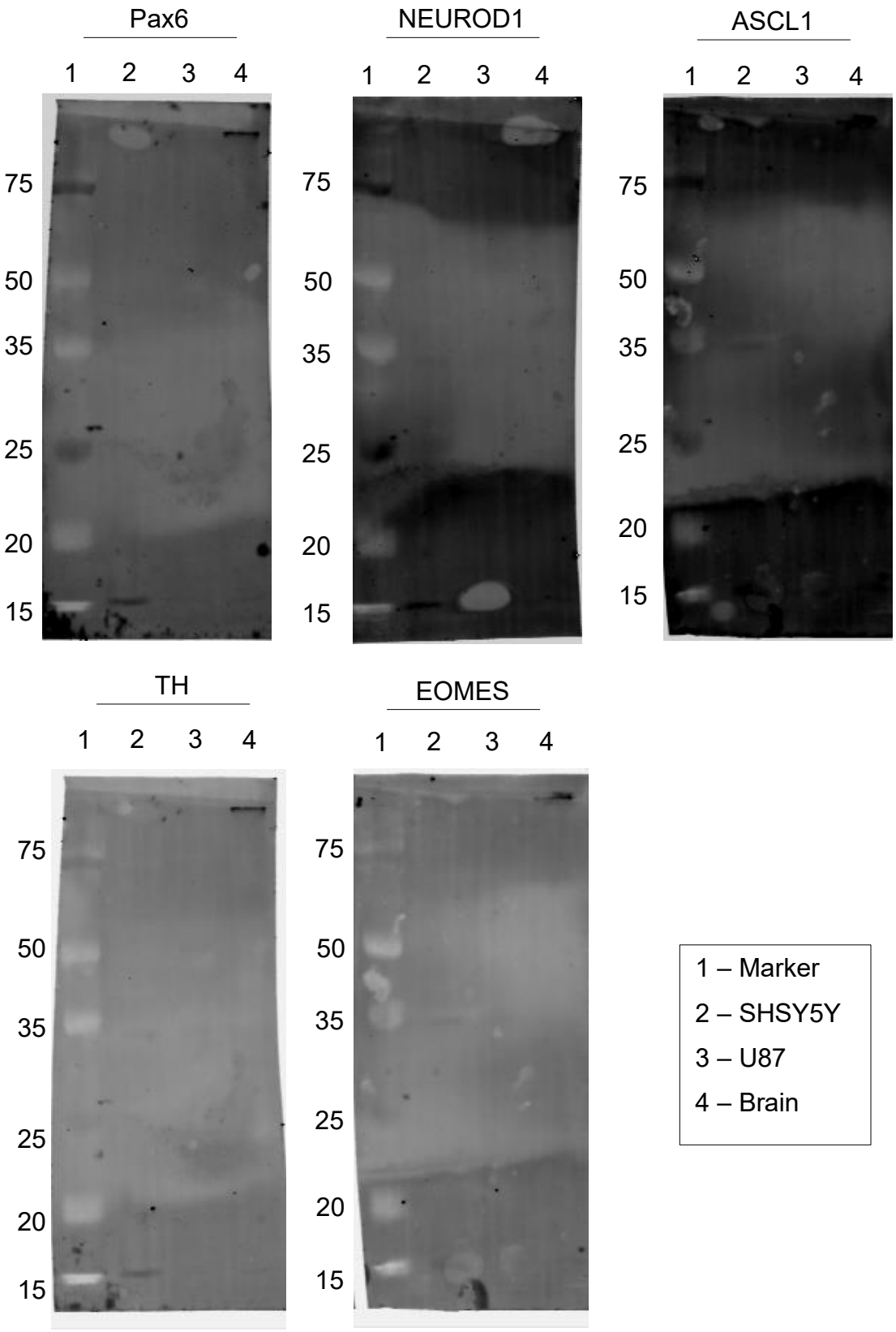

Figure 7.10. PAX6, NEUROD1, ASCL1, TH, EOMES blots.

Ethics approval, ref number 90/2016

L-Università ta' Malta

Faculty of
Medicine & Surgery
University of Malta
Msida MSD 2080, Malta

Tel: +356 2340 1879/1891/1167
umms@um.edu.mt

www.um.edu.mt/ms

Ref No: 90/2016

Monday 17 February 2020

Ms. Vanessa Zammit
85, Reggie Miller Street
Gzira. GZR1541

Dear Ms. Vanessa Zammit,

Please refer to your application submitted to the Faculty Research Ethics Committee in connection with your research entitled:

miRNA influences in mesenchymal stem cell commitment to neuroblast lineage development

The Faculty Research Ethics Committee granted ethical approval for the above mentioned protocol after providing amendments on 12 February 2020 and which study was already ethically approved on 07 February 2017.

Yours sincerely,

Professor Pierre Mallia
Chairman
Research Ethics Committee